# Stereoselectivity and Catalyst Activity in Acrylate Insertion Polymerization

## Dissertation

zur Erlangung des Akademischen Grades eines
Doktors der Naturwissenschaften (Dr. rer. nat.)
dem
Fachbereich Chemie der Universität Konstanz
vorgelegt von

**Boris Neuwald**

aus Bonn

**Konstanz 2013**

Die vorliegende Dissertation entstand in der Zeit von März 2009 bis Februar 2013 unter der Leitung von Herrn Prof. Dr. Stefan Mecking am Fachbereich Chemie der Universität Konstanz.

Einreichungsdatum: 20.02.2013

Tag der mündlichen Prüfung: 05.07.2013

| | |
|---|---|
| Prüfungsvorsitz & mündlicher Prüfer: | Frau Prof. Dr. Karin Hauser |
| Erstgutachter & mündlicher Prüfer: | Herr Prof. Dr. Stefan Mecking |
| Zweitgutachter & mündlicher Prüfer: | Herr Prof. Dr. Rainer Winter |
| Drittgutachterin: | Frau Prof. Dr. Lucia Caporaso |

Für meine Familie

*Sometimes it seems, we'll touch that dream*
*But things come slow or not at all*
*And the ones on top, won't make it stop*
*So convinced that they might fall*
*Let's love ourselves, then we can't fail*
*To make a better situation tomorrow*
*Our seeds will grow, all we need is dedication*

Lauryn Hill

# Acknowledgment / Danksagung

Zunächst möchte ich Prof. Dr. Stefan Mecking für die interessante und fordernde Themenstellung, für die Ideen und Anregungen, und die Freiheiten bei der Erarbeitung der Themen danken.

Herrn Prof. Dr. Rainer Winter danke ich herzlich für die Übernahme des Zweitgutachtens.

Frau Prof. Dr. Karin Hauser danke ich für die Übernahme des Prüfungsvorsitzes.

Der Landesgraduiertenförderung Baden-Württemberg danke ich für die Gewährung eines Stipendiums zur Finanzierung meiner Promotion.

Ich bin dankbar für die großartige und äußerst fruchtbare Zusammenarbeit mit Prof. Dr. Lucia Caporaso von der Universität Salerno in Italien, die sämtliche DFT Rechnungen in dieser Arbeit beigesteuert hat. Ein Dank auch an alle anderen Theoretiker aus Salerno, die in die Projekte involviert waren. Mille grazie, cari amici!

Ich möchte mich ganz herzlich bei meinen Bachelor-Studenten Franz Ölscher (*Labilität von Liganden in Pd(II) Phosphinosulfonat Methyl Komplexen*), Thomas Wiedemann (*Stereoselektivität der Acrylat Insertion*) und Alexander Klaiber (*Insertionsreaktionen Polarer Olefine*) für ihre Mühen, ihre Motivation und ihren Beitrag zu dieser Arbeit bedanken. Ich weiß, es war eine harte Zeit Jungs, aber ich hoffe ihr hatte genauso viel Freude wie ich. Ich zieh meinen Hut vor Euch!

Ein besonderer Dank gebührt Dr. Iñaqui Göttker-Schnetmann für die zahlreichen Diskussionen, Ideen, Anregungen und das Heranführen an die Einkristall-Röntgenstrukturanalyse, sowie dem Lösen einiger früher Röntgenstrukturen in dieser Arbeit. Ich danke Philipp Wucher, Thomas Rünzi, Iñaqui Göttker-Schnetmann, Thomas Wiedemann, Nici Schuster und Christoph Jung für das vollständige oder teilweise Korrekturlesen dieser Arbeit. Ich danke der aktuellen Polar-Monomer Task Force allen voran Thomas Rünzi und Philipp Wucher, aber auch Nicole Schuster und Hannes Leicht, für die zahlreichen Diskussionen und die gute freundschaftliche Zusammenarbeit. Ein großes Dankeschön geht auch an die früheren Mitglieder der Task Force besonders Dr. Damien Guironnet für die Einarbeitung in das Themenfeld und für das erste Projekt, dass wir zusammen gestemmt haben, aber auch an Dr. Samir Chikkali, Tobias Friedberger, Ulrich Tritschler und Dr. Cécile Bouilhac.

Ich danke Anna-Lena Steck für das Messen von HR-ESI-MS Spektren. Allen Serviceabteilungen des Fachbereichs Chemie der Universität Konstanz möchte ich für ihre

erstklassige Arbeit danken. Ein großer Dank gebührt der NMR-Core-Facility-Crew: Ulrich Haunz, Anke Friemel und Prof. Dr. Heiko Möller für ihren unermüdlichen Einsatz, ihr großes Interesse und ihre Kompetenz. Ich danke Lars Bolk für das Messen von GPC und DSC an meinen Polymerproben. Herrn Galetsky möchte ich für das Messen von FAB-Massen Spektren danken.

Robin Kirsten danke ich für das Versorgen mit allem was man so braucht im Labor und Inspirationen was die Frisur angeht. Susan Kyncl danke ich für das ganze Management im Hintergrund und für das Erledigen von all dem unangenehmen Papierkram. Lieben Dank auch an die anderen Permanenten: Dr. Werner Röll und Dr. Marina Krumova.

Meinen Laborkollegen über den ganzen Zeitraum -Dr. Maica Morant, Dr. Johannes Pecher und Christoph Jung- danke ich für die schöne gemeinsame Zeit in L708, wo immer eine warme Sommerbrise weht, wenn der Trockenschrank leise schnurrt.

Ich danke dem ganzen McKing-Team der vergangenen vier Jahre -Stefan, Christoph F., Wuchi, Thomas R., Philipp R., Christoph J., Flo, Anna, Benni, Jussy, Moritz, Frieda, Carla, Alex, Patrick, Franz, Inigo, Werner, Robin, Susan, Marina, Lars, Timo, Nici, Thomas W., Hannes, Tjaard, Johannes P., Doro, Stefan M., Maica, Johannes H., Gitte, Damien, Samir, Fabi, Uli, Tobi, Christoph D., Jörg, Sabrina, Marius, Cécile, Beate- für die angenehme Atmosphäre, die hervorragende Teamarbeit, die gemeinsamen Feierabendbiere und die schöne Zeit in Konstanz.

Schließlich möchte ich meiner Familie und meinen Freunden für die ganze Unterstützung in all den Jahren danken. Ohne Euch wäre es nicht gegangen!

# Publications and Communications

Parts of this thesis have been published

### Manuscripts

- Neuwald, B.; Caporaso, L.; Cavallo, L.; Mecking, S: *J. Am. Chem. Soc.* **2013**, *135*, 1026-1036: „*Concepts for Stereoselective Acrylate Insertion*“
- Neuwald, B.; Ölscher, F.; Göttker-Schnetmann, I.; Mecking, S. *Organometallics* **2012**, *31*, 3128-3137: „*Limits of Activity: Weakly Coordinating Ligands in Arylphosphinesulfonato Palladium(II) Polymerization Catalysts.*“
- Guironnet, D.; Caporaso, L.; Neuwald, B.; Göttker-Schnetmann, I.; Cavallo, L.; Mecking, S. *J. Am. Chem. Soc.* **2010**, *132*, 4418-4426: „*Mechanistic Insights on Acrylate Insertion Polymerization*.“

### Posters

- Neuwald, B.; Ölscher, F.; Göttker-Schnetmann, I.; Mecking, S., *JCF Frühjahrssymposium*, Rostock/Germany, 2012: “*Limits of Activity: Weakly Coordinating Ligands in Arylphosphinesulfonato Palladium(II) Polymerization Catalysts.*“
- Neuwald, B.; Ölscher, F.; Göttker-Schnetmann, I.; Mecking, S., *CaRLa Winter School*, Heidelberg/Germany, 2012: „*Limits of Activity: Weakly Coordinating Ligands in Arylphosphinesulfonato Palladium(II) Polymerization Catalysts.*“
- Neuwald, B.; Rünzi, T.; Tritschler, U.; Caporaso, L.; Guironnet, D.; Göttker-Schnetmann, I.; Wucher, P.; Chikkali, S.; Cavallo, L.; Mecking, S. *Heidelberg Forum of Molecular Catalysis*, Heidelberg/Germany, 2011: „*Insertion Polymerization of Polar Monomers.“*
- Neuwald, B.; Guironnet, D.; Caporaso, L.; Göttker-Schnetmann, I.; Cavallo, L.; Mecking, S. *Gordon Research Conference - Organometallic Chemistry*, Newport/USA, 2010: „*Mechanistic Insights on Acrylate Insertion Polymerization“*
- Neuwald, B.; Guironnet, D.; Rünzi, T.; Göttker-Schnetmann, I.; Mecking, S. *118th BASF International Summer Course*, Ludwigshafen/ Germany, 2009: „*Insertion Polymerization of Acrylates*“

# Abstract / Zusammenfassung

Die vorliegende Arbeit beschäftigt sich mit dem Verständnis und der Weiterentwicklung von neutralen Phosphinsulfonato-Palladium(II)-Komplexen für die katalytische Insertions(co)polymerisation von Ethylen und polaren Olefinen. Bisher ermöglichen ausschließlich Phosphinsulfonato-Pd(II)-Katalysatoren die Copolymerisation solcher Monomere zu linearen Copolymeren. Solche linearen Copolymere aus apolaren und polaren Olefinen haben dabei ein großes Anwendungspotential als vielseitige Materialien in der Kunststoffindustrie sobald grundlegende Anforderungen an die Materialeigenschaften erfüllt werden können.

Die Koordinationsstärke des neutralen, einzähnigen Lewis-Base Ligand L in Phosphinsulfonato-Pd(II)-Komplexen [(P^O)PdMe(L)] (P^O = $(Aryl)_2PC_6H_4SO_3$) beeinflusst die Polymerisationsaktivität entscheidend, da der Ligand L, welcher die Katalysatorvorstufe in der aktiven Spezies stabilisiert, mit dem Monomer um die freie Koordinationsstelle am Metallzentrum konkurriert. Im Rahmen dieser Arbeit werden Phosphinoxide als schwach koordinierende Liganden L für diese Katalysatoren etabliert. Die Koordinationsstärke von diversen Phosphinoxiden wurde im Vergleich zu DMSO quantifiziert und der bisher am schwächsten koordinierte, stabile Komplex [$^{MeO}$(P^O)PdMe($OPPh_3$)] dieser Klasse konnte synthetisiert werden. Es zeigte sich, dass Komplexe mit noch schwächer koordinierenden Liganden L in Lösung nicht stabil sind, da sie durch intermolekulare Koordination der Sulfonatgruppe des Liganden zu unlöslichen Aggregaten verbrücken. Ein alternativer Weg zu hoch aktiven Katalysatoren für die Ethylen/Methylacrylat Copolymerisation wurde in der *in situ* Chlorid-Abstraktion von einfach zugänglichen, Natrium-verbrückten Komplexen [{($^{MeO}$(P^O)Pd(Me)Cl)-μ-Na}$_2$] gefunden. Der *in situ* erzeugte, lösliche Komplex ist frei von signifikant koordinierenden Liganden an der vierten Koordinationsstelle. Mechanistische Untersuchungen mit schwach koordinierten Katalysator-Vorstufen zeigten, dass die Katalysatoraktivität in der Copolymerisation durch die Ausbildung von sehr stabilen 6-gliedrigen κ-*O* koordinierten Chelat-Komplexen [(P^O)Pd{$\kappa^2$-*C*,*O*-*C*H(R)$CH_2$CH(C(*O*)OMe)$CH_2CH_3$}] intrinsisch limitiert ist. Solche Chelate entstehen nach jeder Monomerinsertion die auf eine Acrylatinsertion folgt. Die Koordinationsstärke dieser Chelate im Vergleich zu Ethylen konnte quantifiziert werden und erklärt die deutliche Senkung der Polymerisationsgeschwindigkeit auf Grund der stark gehinderten Chelatöffnung.

Um einen tieferen Einblick in den Zusammenhang zwischen Katalysatorstruktur und erzeugten (Co)Polymeren zu erhalten wurden 15 verschiedene Komplexe mit variierendem

Phosphinsulfonato-Ligandengerüst synthetisiert. Die Reaktivität der Komplexe gegenüber Ethylen und Alkylacrylaten wurde ausführlich in Insertions- und Polymerisationsstudien evaluiert und bestimmte elektronische, und besonders sterische Einflüsse identifiziert. Im Rahmen dieser Arbeit wird ein neues Konzept für eine zielgerichtetere Katalysator-Entwicklung vorgestellt. In Palladiumkomplexen mit asymmetrisch substituierten Phosphinsulfonato-Liganden (P^O = $(X)(Y)PC_6H_4SO_3^-$), können Eigenschaften von zwei symmetrisch substituierten Katalysatoren miteinander vereint werden. Dadurch lassen sich positive Eigenschaften miteinander kombinieren, während einzelne Nachteile ausgeglichen werden können. In der Folge konnten asymmetrische Komplexe synthetisiert werden, die Copolymere mit deutlich erhöhten Molekulargewichten produzieren.

Eine stereokontrollierte Homopolymerisation von Acrylaten ist von höchstem Interesse, da sie Zugang zu völlig neuen Materialien ermöglichen würde. In diesem Zusammenhang wurden die Stereochemie der Insertionspolymerisation und der Mechanismus der Stereokontrolle mit Phosphinsulfonato-Pd(II) Katalysatoren erstmalig untersucht. Zur Analyse der Stereoselektivität der Acrylatinsertion konnte eine NMR-gestützte Methodik entwickelt werden. In Oligomerisationsstudien wurde gezeigt, dass die so ermittelte Stereoselektivität auf die Kettenkonfiguration der Oligomere übertragen werden kann. Studien zur Komplexkonformation zeigten, dass symmetrische Phosphinsulfonato-Komplexe konformationsbedingte intrinsische Stereozentren besitzen. Dynamische NMR-Studien zeigten aber, dass eine Stereokontrolle auf Grund der hohen Flexibilität des Ligandengerüsts erschwert wird, da alle Stereozentren im Vergleich zur Insertion einer schnellen Racemisierung unterliegen. Folglich wurde für die symmetrischen Systeme nur eine geringfügige Stereokontrolle gefunden. In Folge konnte gezeigt werden, dass asymmetrische Katalysatoren mit einem permanenten Stereozentrum am Phosphoratom eine hohe Stereoselektivität für die erste Acrylatinsertion in die Pd-Me Bindung ermöglichen. Die Stereoselektivität für die folgende Acrylatinsertion ist jedoch stark vermindert. Dies weist darauf hin, dass in den untersuchten Systemen Kettenendkontrolle und Katalysatorkontrolle entgegengesetzt wirken. Eine DFT-gestützte Analyse der Übergangszustände zeigt, dass der Ligand der wachsenden Kette ausweicht und dass folglich die Flexibilität des Ligandengerüsts einer Stereokontrolle entgegenwirkt. Eine Reduzierung der Flexibilität durch einen erhöhten sterischen Anspruch des Liganden führt aber gleichzeitig zur einer Inhibierung der Acrylatinsertion, sowie dem Verlust der Regiokontrolle der Insertion. Als zukünftiges Konzept zur Erhöhung der Rigidität bieten sich cyclische Verbindungen an, für welche allerdings zunächst geeignete Synthesen entwickelt werden müssen.

# I. Table of Contents

# II. Annotations

**Abbreviations:**

| | |
|---|---|
| Ar | aryl |
| av | average |
| BA | butyl acrylate |
| BHT | 2,6-di-*tert*-butyl-4-methylphenol |
| BuLi | *n*-butyllithium |
| COD | cyclooctadiene |
| COSY | correlation spectroscopy |
| δ | chemical shift in ppm |
| DMF | dimethylformamide |
| $DP_n$ | degree of polymerization |
| DSC | differential scanning calorimetry |
| DMSO | dimethylsulfoxide |
| Et | ethyl |
| equiv. | equivalent(s) |
| ESI | electron spray ionization |
| GPC | gel permeation chromatography |
| HDPE | high density polyethylene |
| HR-MS | high resolution mass spectrometry |
| *i*Pr | *iso*-propyl |
| *i*PrA | *iso*-propyl acrylate |
| IR | infrared |
| L | neutral ligand, Lewis-base-donor |
| LDPE | low density polyethylene |
| lut | 2,6-lutidine |
| M | metal center, counter ion |
| M | molar, mol $L^{-1}$ |
| MA | methyl acrylate |
| MMA | methyl methacrylate |
| m/z | mass-to-charge ratio |
| Me | methyl |

| | |
|---|---|
| | number average molecular weight |
| $M_n$ | $M_n = \frac{\sum M_i N_i}{\sum N_i}$ |
| | weight average molecular weight |
| $M_w$ | $M_w = \frac{\sum M_i^2 N_i}{\sum M_i N_i}$ |
| MS | mass spectrometry |
| n.o. | not observed |
| n.d. | not detected |
| *n*Bu | *n*-butyl |
| NMR | nuclear magnetic resonance |
| NOE | nuclear Overhauser effect |
| NOESY | nuclear Overhauser effect spectroscopy |
| PE | polyethylene |
| Ph | phenyl |
| PMA | poly(methyl acrylate) |
| PMMA | poly(methyl methacrylate) |
| PP | polypropylene |
| ppm | parts per million |
| PS | polystyrene |
| py | pyridine |
| ROESY | rotating-frame nuclear Overhauser spectroscopy |
| r.t. | room temperature (25 °C) |
| SAN | styrene-acrylonitrile resin |
| *t*Bu | *tert*-butyl |
| THF | tetrahydrofuran |
| $T_m$ | melting temperature |
| tmeda | *N,N,N',N'*-tetramethylethylene-1,2-diamine |
| TOCSY | total correlation spectroscopy |
| TON | turn over number $\frac{\text{mol}_{\text{substrate converted}}}{\text{mol}_{\text{catalyst}}}$ |
| TOF | turn over frequency $\frac{\text{mol}_{\text{substrate converted}}}{\text{mol}_{\text{catalyst}} \cdot \text{h}}$ |
| TS | transition state |

| | |
|---|---|
| vs. | versus |
| (X^Y) | $\kappa^2$-*X*,*Y* coordinated ligand |

**Nomenclature of compounds:**

Compounds discussed in this work are generally marked by bold numbers and letters. Multidentate (free) ligands are denoted by the coordinating atoms in brackets, ligand details are given by superscripted acronyms X, e.g. for phosphinesulfonato ligands: $^{X}$**(P^O)H**

Phosphinesulfonato palladium(II) methyl complexes are numbered **1**, ligand details are given by superscripted acronyms X, and coordinating monodentate ligands at the fourth coordination site of the palladium atom are added by –L, so that [$^{X}$(P^O)PdMe(L)] is abbreviated: $^{X}$**1-L**

Products of a single olefin insertion into the Pd-Me bond are numbered **2**, ligand details are given by superscripted acronyms X, details concerning the insertion are given by subscripted olefin and insertion mode, so that the 2,1-insertion of MA into $^{X}$**1** is abbreviated: $^{X}\mathbf{2}_{\mathbf{MA\text{-}2,1}}$

Products of a consecutive 2,1 methyl acrylate insertion into $^{X}\mathbf{2}_{\mathbf{MA\text{-}2,1}}$ are numbered **3**, ligand details are given by superscripted acronyms X, details concerning the insertion are given by subscripted olefin and stereoconfiguration: meso/rac (if needed), so that the consecutive 2,1-insertion of MA into $^{X}\mathbf{2}_{\mathbf{MA\text{-}2,1}}$ is abbreviated: $^{X}\mathbf{3}_{\mathbf{MA}}$. The rac/meso designation is based on consideration of the stereocenters as part of a growing chain, which emerge from two MA insertions with the same ($^{X}\mathbf{3}_{\mathbf{MA\text{-}meso}}$) or opposite ($^{X}\mathbf{3}_{\mathbf{MA\text{-}rac}}$) stereoselectivity leading to an isotactic or a syndiotactic configuration in a virtual polymer chain, respectively.

Products of a single olefin insertion into the Pd-H bond are numbered **4**, ligand details are given by superscripted acronyms X, details concerning the insertion are given by subscripted olefin and insertion mode, so that the 2,1-insertion of MA into [$^{X}$(P^O)PdH] is abbreviated: $^{X}\mathbf{4}_{\mathbf{MA\text{-}2,1}}$

Products of a consecutive 2,1 methyl acrylate insertion into $^{X}\mathbf{4}_{\mathbf{MA\text{-}2,1}}$ are numbered **5**, ligand details are given by superscripted acronyms X, concerning the insertion are given by subscripted olefin, so that the consecutive 2,1-insertion of MA into $^{X}\mathbf{2}_{\mathbf{MA\text{-}2,1}}$ is abbreviated: $^{X}\mathbf{5}_{\mathbf{MA}}$.

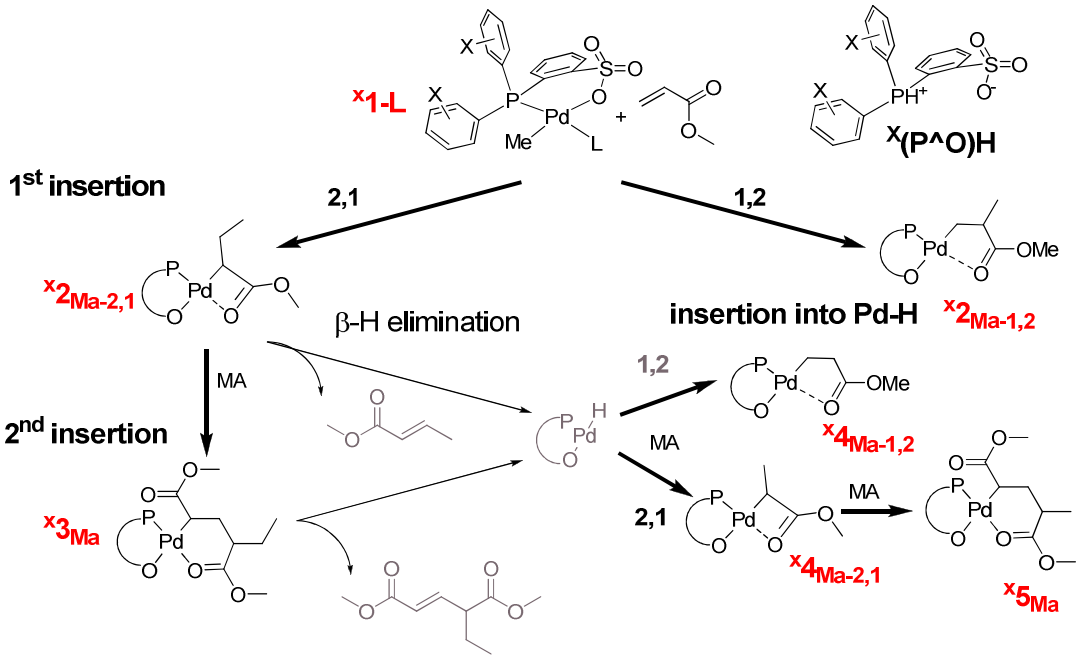


**Scheme II-1.** Nomenclature of compounds discussed in this work.

# III. Index of Complexes

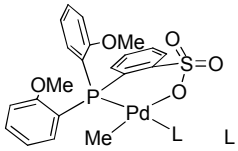


L = dmso, $OPBu_3$, $OPOct_3$, $OPPh_3$

**$^{MeO}$1-L**

---

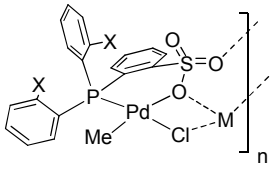


**[{($^{X}$1-Cl)-μ-M}$_n$]**

M = Na, Li

with $^{X}$1 =

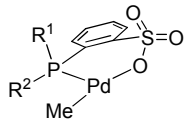


**$^{X}$1**

$R^1 = R^2 =$

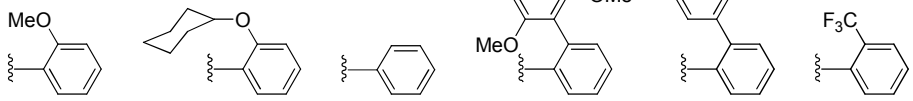


**$^{MeO}$1** **c$^{HexO}$1** **$^{H}$1** **$^{Ar}$1** **$^{Ph}$1** **$^{CF3}$1**

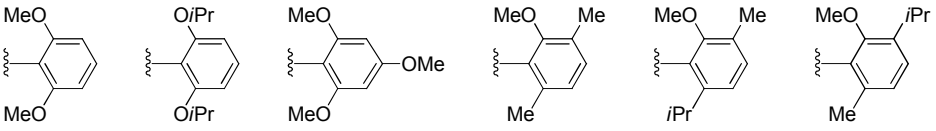


**(MeO)$_2$1** **(*i*PrO)$_2$1** **(MeO)$_3$1** **(MeO;Me2)$_1$** **Car$_1$** **Thy$_1$**

$R^1 =$ $R^2 =$ $R^1 =$ $R^2 =$ $R^1 =$ $R^2 =$

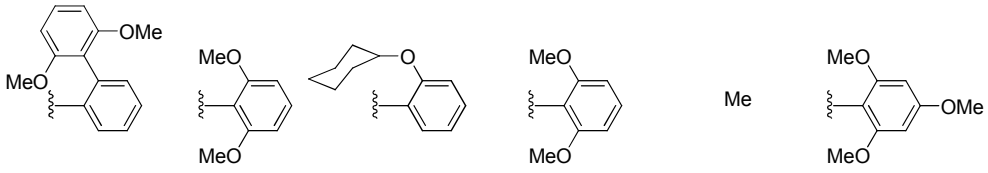


**Ar/(MeO)$_2$1** **c$^{HexO}$/(MeO)$_2$1** **Me*/(MeO)$_3$1**

---

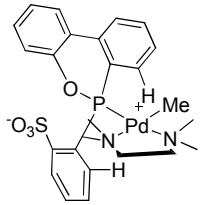


**[$^{oxa}$($^{O}$P^O)PdMe(tmeda)]**

# 1. General Introduction – Copolymerization of Ethylene with Polar Olefins

Functionalized polar olefins like alkyl (meth)acrylates, (meth)acrylic acid, acrylonitrile, or vinyl chloride represent an important (co)monomer class for an immense number of commercially important polymers like poly(methyl methacrylate) (PMMA, *Plexiglas*® - EVONIK, ARKEMA) or styrene-acrylonitrile resins (SAN, *Luran*® - BASF). These (co)polymers are produced by free-radical or ionic pathways. On the other hand catalytic insertion polymerization of ethylene and propylene is employed for the production of more than 70 million tons of non-polar polyolefins annually.[1] Here, the incorporation of functional groups into an otherwise non-polar, linear polymer backbone, like high density polyethylene (HDPE), is highly interesting, since e.g. toughness, adhesion, barrier properties, surface properties (e.g. paintability), or solvent resistance can be controlled.[2] Random copolymers of ethylene with polar monomers are important industrial products as illustrated by the *Amplify*® product family of DOW (ethylene-ethyl acrylate and acrylic acid copolymers, maleic anhydride grafted polyolefins), or the *Lotryl*® product family of ARKEMA (ethylene-acrylic ester copolymers). These materials are used mainly as additives for processing with polyethylene (PE), polypropylene (PP), polystyrene (PS), or polyethylene terephthalate (PET) to adjust materials properties. However, production of these copolymers is accomplished by high pressure free-radical processes similar to those used in LDPE production yielding highly branched, random copolymers.[3,4,5] Hence, linear copolymers with advantageous materials properties are not available by a direct polymerization procedure by these methods.

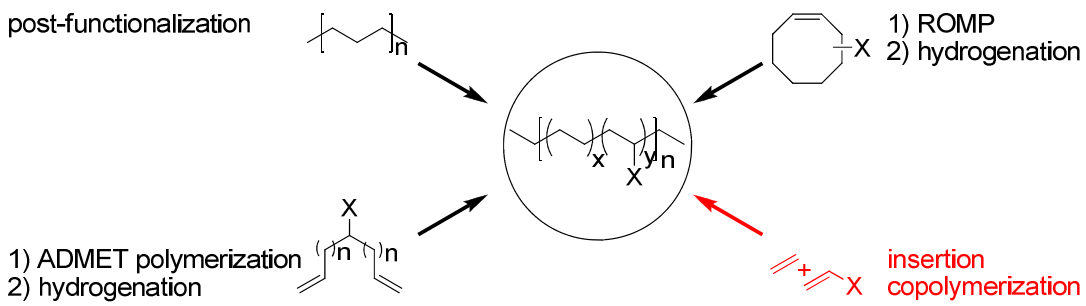


**Scheme 1-1.** Synthetic routes towards functionalized, linear polyethylene.

Such linear copolymers can be synthesized, besides by post functionalization,[6] by ring-opening metathesis polymerization (ROMP) of functionalized cyclooctenes,[7] or by acyclic diene metathesis (ADMET) polymerization of symmetrical substituted α,ω-dienes and

subsequent hydrogenation, respectively (Scheme 1-1).[8] In addition, direct copolymerization of the corresponding olefins by an insertion mechanism is an attractive, route towards these linear copolymers.

Since its discovery by Ziegler[9] and Natta[10] catalytic insertion polymerization has been studied intensively with regard to the mechanistic understanding of the catalytic systems as well as to the properties of the resulting polymeric materials. Chain growth by insertion in polymeryl(R)-olefin complexes [$L_nMR$(olefin)] allows for the control of the regio- and stereoselectivity of the inserted monomer as well as for a sequence control of different monomers in the polymer chain by the catalyst. This enables a control over the polymer microstructure and hence a control over macroscopic materials properties. In stark contrast to the production of PE and PP in a multi-million ton scale the (co)polymerization of polar vinyl monomers like acrylates by an insertion mechanism remains challenging.

Industrial olefin polymerization is mainly accomplished with catalyst based on early transition metals such as Ti, Zr, Cr, or V. The high oxophilicity of these metal centers prevents an application for insertion polymerization of polar substituted olefins since the catalysts are deactivated by heteroatom coordination of the substrate. Notably, Yasuda et al. showed that linear ethylene-(meth)acrylates diblock-copolymers can be obtained with early transition metal complexes. However, this is accompanied by an irreversible switch of the polymerization mechanism from migratory insertion for ethylene to an (anionic) coordination-addition mechanism for (meth)acrylates and requires the primary polymerization of the non-polar olefin.[11] A promising approach is the use of late transition metal based catalysts, which are characterized by a significantly reduced affinity towards polar groups. However, late transition metal alkyl complexes are prone to β-H elimination and hence polymerization catalysts often suffer from inability to form high molecular weight polymers. This feature was the basis for the development of the Shell-Higher-Olefin Process (SHOP), where linear α-olefins are obtained by the nickel catalyzed oligomerization of ethylene. Remarkably, the neutral phosphine-oxygen coordinated nickel(II) complexes used are extremely stable towards polar media, so that the oligomerization process can be carried out in a biphasic system with 1,4-butandiol being the polar catalyst phase (Scheme 1-2).[12-14]

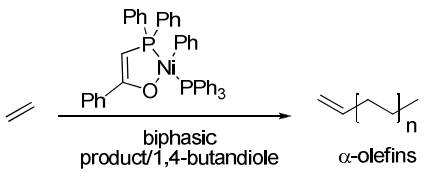


**Scheme 1-2.** Ethylene oligomerization with a SHOP catalyst.

# 1.1 Cationic α-Diimine Catalysts

In the mid 1990s Brookhart et al. discovered that cationic Ni(II) and Pd(II) diimine complexes are capable of an effective polymerization of ethylene with activities of up to $4\times10^6$ mol($C_2H_4$) mol(Ni)$^{-1}$ h$^{-1}$ for the Ni catalysts. Whereas the Pd catalysts produce hyperbranched polymers, the degree of branching is adjustable with the Ni catalysts (ethylene pressure, temperature). The molecular weight can be varied from oligomers to high molecular weight polyethylene. Sterically demanding ligands, blocking the axial position of the metal centers, are essential for the production of high molecular weight polymers, since chain transfer is suppressed.[3,15]

The palladium catalysts enabled the insertion copolymerization of ethylene with acrylates, methyl vinyl ketones[16] and silyl vinyl ethers[17] for the first time. However, other important monomers such as vinyl acetate, acrylonitrile and vinyl chloride were not amenable for copolymerization with these catalysts. Similar to the ethylene homopolymers, the copolymers obtained possess a hyperbranched structure with ca. 100 branches per 1000 carbon atoms (Scheme 1-3).[3,16]

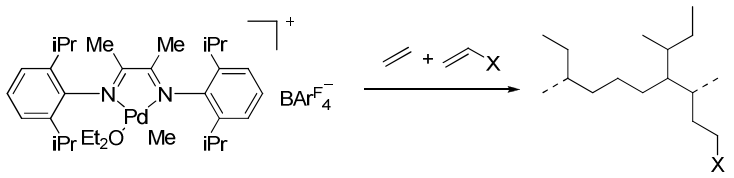


**Scheme 1-3.** Ethylene/polar olefin copolymerization with Pd α-diimine catalyst to highly branched copolymers.

With increasing incorporation ratio of the polar monomer the catalyst activity decreases. The copolymers formed consist of ethylene as the major component (≥ 75%). Here, the incorporated polar monomer is located at the ends of branches predominantly, which is due to the excessive "chain walking" of the catalyst. Due to a series of β-H eliminations and reinsertions the catalyst can move along the polymer chain, thereby creating a high amount of branches and positioning the polar monomer at the chain ends. This mechanistic understanding of the origin of the copolymer microstructure could be provided by in-depth NMR studies of the relevant organometallic species. Acrylate insertion is followed by a series of β-H eliminations and reinsertions leading to a stable six-membered chelate resting state. Insertion of ethylene and additional β-H elimination/reinsertion steps then lead to the formation of branched polyethylene with an ester group at the branch end (Scheme 1-4).[18]

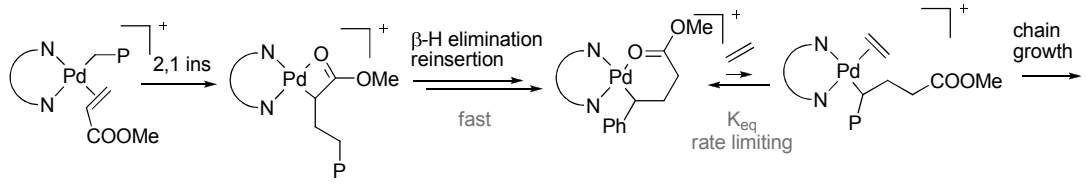


**Scheme 1-4.** Formation of functionalized chain ends in the copolymerization of ethylene with acrylates with Pd(II) diimine catalysts.

# 1.2 Neutral Palladium Phosphinesulfonato Catalysts

In 2002 Drent et al. reported that catalysts generated *in situ* from arylphosphonium sulfonates and Pd(0) precursors like $Pd_2(dba)_3$ are capable of copolymerizing alkyl acrylates and ethylene to linear copolymers with incorporation of up to 10 mol% polar monomer in the polymer backbone (Scheme 1-5).[19] This report initiated manifold studies concerned with this catalyst system. Defined synthesis and catalyst characterization revealed that the active species is based on discrete neutral phosphinesulfonato Pd(II) complexes.[20,21]

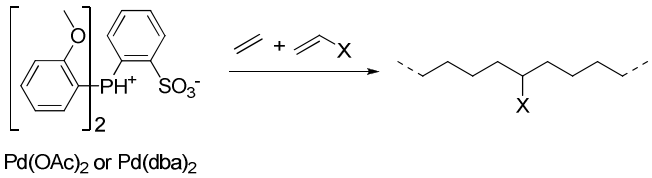


**Scheme 1-5.** Copolymerization of ethylene with polar olefins to linear copolymers with phosphinesulfonato Pd(II) catalysts.

## 1.2.1 Catalyst Modifications

The catalyst synthesis involves the reaction of ortho-lithiated benzenesulfonate derivatives with diorganophosphine chlorides. The lithium salts obtained, (P^O)Li, can either be reacted directly with Pd(II) precursors yielding anionic complexes [(P^O)PdMe(X)]Li, which can be converted to neutral complexes [(P^O)PdMe(L)]. As an alternative, the lithium salts can be protonated to the zwitterionic ligand (P^O)H. The proton is localized at phosphorus due to the low p$K_A$ value of the sulfonic acid (< 3). The reaction of (P^O)H with e.g. [(tmeda)$PdMe_2$] yields neutral complexes [(P^O)PdMe(L)] with a monodentate ligand L situated trans to the phosphine (Scheme 1-6).[22]

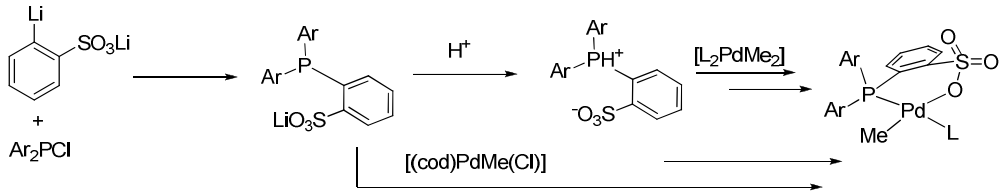


**Scheme 1-6.** Synthesis of defined arylphosphinesulfonato Palladium catalyst precursors.

In recent years multiple variations of the ligand framework have been discussed or appeared in the patent literature (Figure 1-1, Figure 1-2, Figure 1-4, Figure 1-5). Here, variation of the non-chelating aryl moieties of the (P^O)-ligand is a key approach for catalyst modification (Figure 1-1, Figure 1-2).[19,21-38]

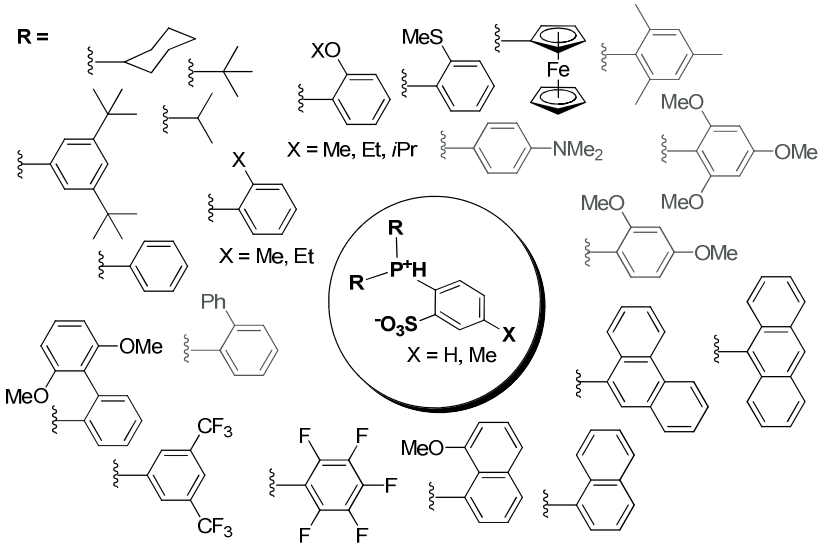


**Figure 1-1.** Symmetric substitution patterns for the non-chelating moieties R of phosphinesulfonato ligands (ligands that only appear in the patent literature are shaded in grey).[19-38]

However, so far no conclusive picture of a structure activity relationship could be drawn for the palladium complexes. In most of the cases no significant improvements in ethylene homo- and copolymerization could be achieved in comparison to the system exhibiting a ligand with two 2-$MeOC_6H_4$ substituted non-chelating aryl moieties, which was already described by Drent in the first publication.[19] Catalysts with modified aryl substituents often either suffer from low catalyst stability, low polymerization activity, decreased polymer molecular weight, low polar monomer incorporation, or a combination thereof. For example, catalysts with ligands bearing the very bulky naphthyl, anthracenyl or phenanthryl moieties showed decreased activity, produced lower molecular weight polymers and were not able to incorporate significant amounts of polar monomers.[28,31] Catalysts with ligands exhibiting *tert*-butyl instead of aryl moieties showed high activity and produced high molecular weight polymers, but decomposed rapidly.[37] An exception are catalysts based on ligands exhibiting the bulky 2-(2,6-$(MeO)_2C_6H_3$)$C_6H_4$ moieties, which show very high activities combined with

good catalyst stability in the ethylene homopolymerization and produce high molecular weight polymers (> 100000 g/mol). This is explained with the capability of this ligand to shield the axial positions at the palladium center and suppress chain transfer. However, the incorporation of polar monomers is drastically reduced, resulting in copolymers with low contents of polar groups.[24]

The synthesis of (P^O) ligands with asymmetric substituted phosphorus atoms has also been described (Figure 1-2).[29,30,37-40] Here, it was reported that the combination of a phenyl substituent with a *tert*-butyl substituent results in catalysts with properties comparable to the initial system with 2-$MeOC_6H_4$ moieties.[37]

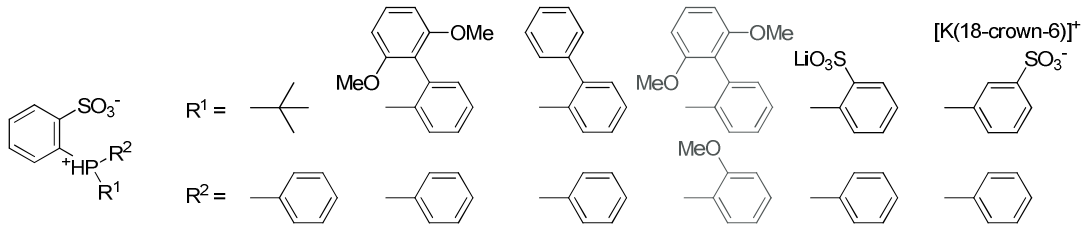


**Figure 1-2.** Asymmetric substitution patterns for the non-chelating moieties R of phosphinesulfonato ligands (ligands that only appear the in patent literature are shaded in grey).[29,30,37- NOTEREF _Ref340485786 \h 40]

Jordan and Rieger et al. reported palladium catalysts based on *ortho*- or *meta*-phosphine-arenesulfonate ligands (M-O*P*^*O*)$^-$ exhibiting two sulfonated aryl moieties.[29,30] For ligands with two ortho-sulfonated aryl moieties the self-assembly of the corresponding palladium complexes to tetranuclear structures bridged by a $Li_4S_4O_{12}$ cage was observed (Figure 1-3). In polymerization studies it turned out that these complexes produce high molecular weight polymers with a broad molecular weight distribution ($M_n$ = 39000, $M_w/M_n$ = 28), if the tetranuclear structures stays intact during polymerization. However, if the multinuclear structure is destructed polymers with low molecular weight are obtained ($M_n$ = 3026, $M_w/M_n$ = 2.6).[29]

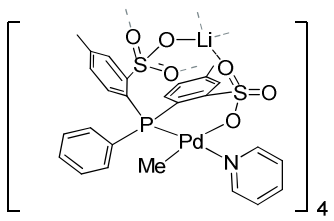


**Figure 1-3.** Tetranuclear *ortho*-phosphine-arenesulfonate Pd(II) complex.[29]

In addition, asymmetric substituted phosphinesulfonato palladium complexes have recently been applied for CO/ethylene copolymerization.[40] Beyond theses studies, complexes

with asymmetric substituted phosphinesulfonato ligands were only reported for nickel,[39] or appeared in the patent literature without additional discussion.[38]

In then non-patent literature only two systems with a variation of the chelating arylsulfonate substituent appeared (Figure 1-4). Piers and Jordan et al. reported a phosphine-trifluoroborate ligand and the formation of a stable (P^F)Pd complexes was observed.[33,34] However, these complexes can only dimerize ethylene to butenes with low activities. Erker et al. reported various *ortho*-diarylphosphinoferrocene sulfonate based palladium catalysts, but so far only the reactivity in CO/ethylene copolymerization was reported.[32]

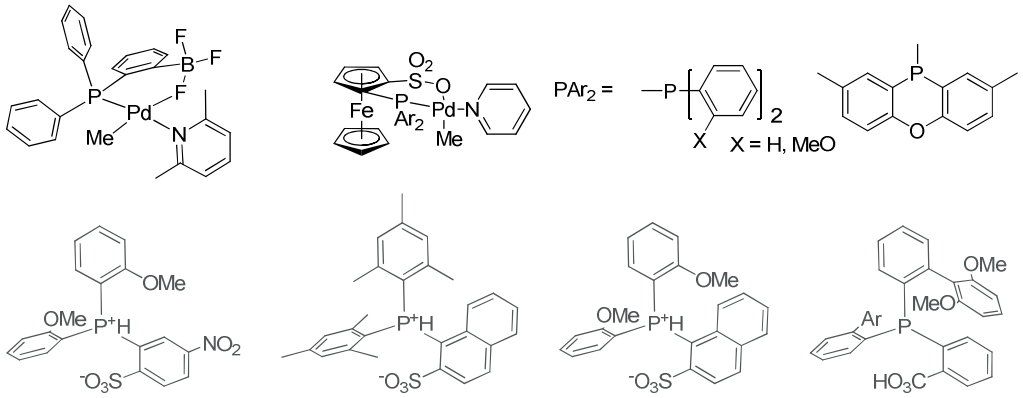


**Figure 1-4.** Variations of the arylsulfonate moiety (compounds only described in patent literature are shaded in grey).[33,34,38]

Jordan and Nozaki et al. reported palladium complexes that contain N-heterocyclic-carbene sulfonate ligands, but these complexes showed no activity in olefin polymerization (Figure 1-5).[27,36] In addition, Göttker-Schnetmann et al. reported the synthesis of sterically demanding diazaphospholidine sulfonato palladium(II) methyl complexes, which showed a moderate reactivity in ethylene homopolymerization.[41,42]

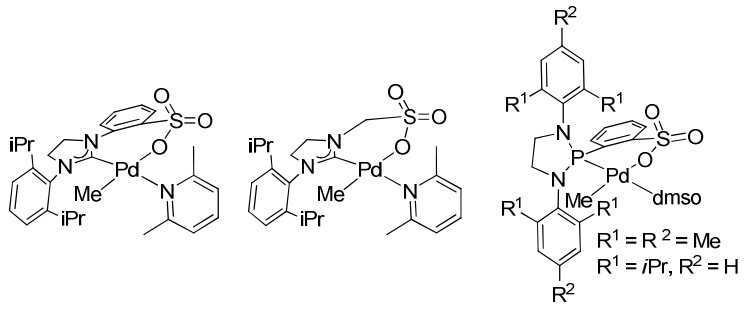


**Figure 1-5.** *N*-heterocyclic-carbene sulfonato and diazaphospholidine sulfonato Pd(II) complexes.[27,36,41,42]

Besides the choice of the chelating (P^O) ligand, catalyst activity is related to the monodentate ligand L occupying the fourth coordination site trans to the phosphine in [(P^O)PdR(L)] catalyst precursors (Scheme 1-7). It has been shown that the activity of the

catalytic system at a given ethylene/methyl acrylate concentration strongly depends on the coordination strength of L, especially for low ethylene pressures.[43] Here, activity is determined by the L/monomer equilibrium, where L competes effectively with the monomer for coordination to the active site, and monomer coordination (cis to the polymeryl species R) is a prerequisite for a chain growth event by a migratory insertion mechanism.

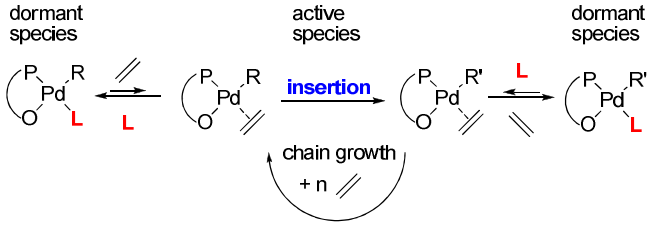


**Scheme 1-7.** Rate determining equilibria in ethylene polymerization with [(P^O)PdR(L)] catalyst precursors.

It was found that substitution the often applied pyridine ligand by weaker coordinating DMSO in $^{MeO}$**1-dmso** lead to a 3.5 fold increase in activity for ethylene homopolymerization at 5 bar ethylene pressure (Scheme 1-8). In copolymerization experiments this enabled the utilization of high MA concentrations and subsequently led to the formation of ethylene MA copolymers with up to 50 mol% MA incorporation. NMR analysis of the copolymers obtained revealed that linear chains were formed which contained even consecutive MA units. Attempts to homopolymerize methyl acrylate with this catalyst led to the isolation of methyl acrylate homooligomers with an average $DP_n$ of ca. five. Here, free-radical pathways could be excluded by appropriate comparative experiments. In consequence this represents the first example of an insertion homopolymerization of polar olefins (Scheme 1-8).[43] An alternative concept for providing weakly coordinated precursors devoid of additional ligands L, is the substitution of L by the O($SO_2$)-donor of another (P^O)Pd fragment to multinuclear species. These compounds can be isolated after abstraction of the monodentate ligand L in [(P^O)PdMe(L)], e.g. pyridine by $B(C_6F_5)_3$.[25,44] However, the isolated compounds suffer from a low solubility in non-coordinating solvents which counteracts an effective homogenous catalysis. Alternatively *in situ* abstractions of L have also been mentioned.[21,45-47]

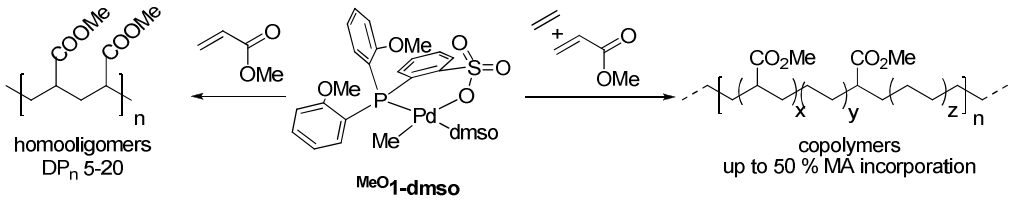


**Scheme 1-8.** Ethene/ MA copolymerization and MA homooligomerization with DMSO coordinated (P^O)PdMe catalyst $^{MeO}$**1-dmso**.

## 1.2.2 Monomer Scope

Phosphinesulfonato Pd(II) catalysts are capable of copolymerizing a large range of polar vinyl monomers with ethylene (Scheme 1-9).[19,22,26,43,45,46,48-60]

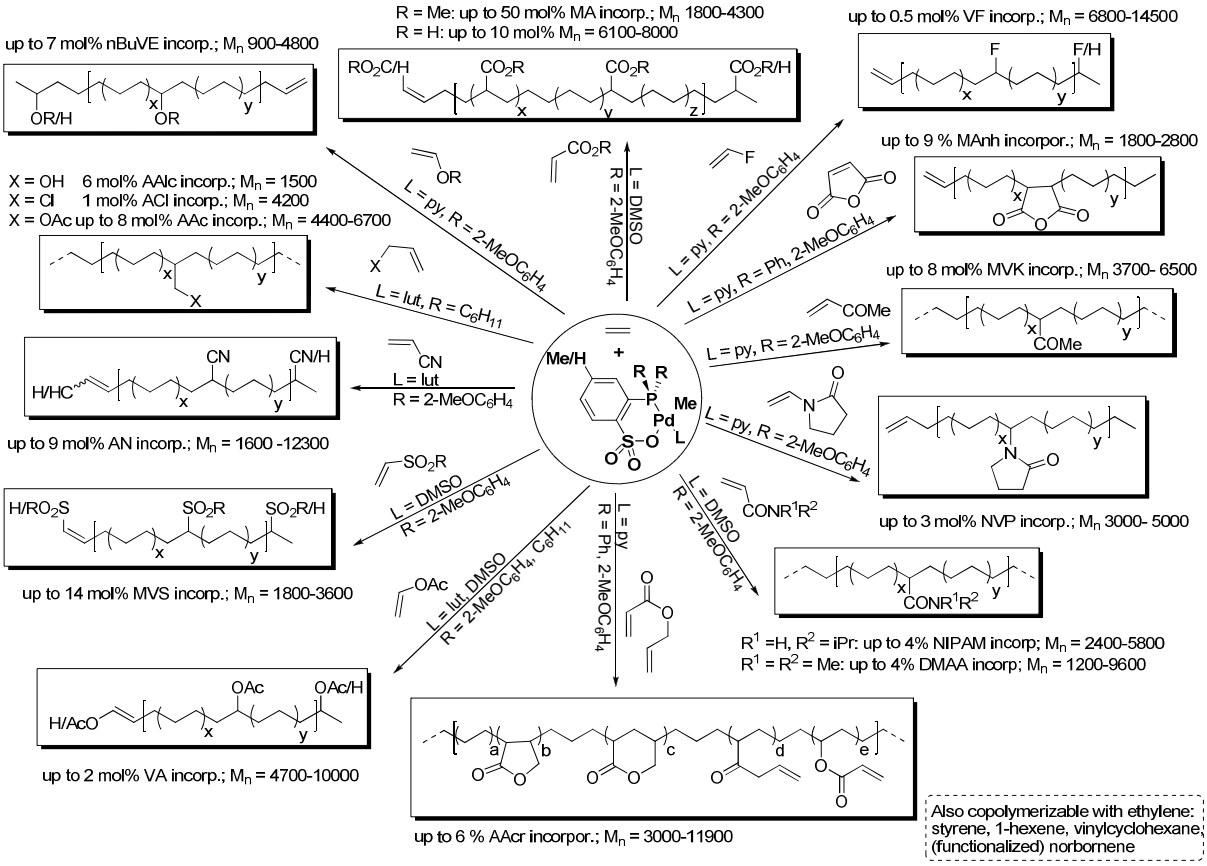


**Scheme 1-9.** Insertion copolymerization of ethylene and polar vinyl monomers with phosphinesulfonato Pd(II) catalysts. [19,22,26,43,45,46,48-60]

Most impressively linear copolymers could be obtained with acrylonitrile,[45] vinyl acetate,[51] vinyl fluoride,[26] and acrylic acid[54] with (P^O)Pd catalysts for the first time. For the incorporation of amide and pyrrolidone based monomers a pronounced effect on surface properties for incorporations of only up to 4 mol% has been reported.[50] Here, the water contact angle for copolymer films with only 2 mol% N-vinylpyrrolidone incorporation could be reduced to 95° in comparison to 121° for neat polyethylene reaching values similar to polystyrene films (92°), a paintable polymer.

In strong contrast to the broad scope of copolymers accessible with phosphinesulfonato Pd(II) catalysts it was shown that a copolymerization of the industrially important monomer methyl methacrylate (MMA) is not possible. The study revealed that MMA is at least $10^2$-fold less amenable to incorporation than MA under polymerization conditions, presumably for steric reasons.[61]

Beside the copolymerization of ethylene with polar monomers, (P^O)Pd catalysts are also capable of the copolymerization of CO with various apolar and polar monomers. In contrast to other catalysts, phosphinesulfonato palladium(II) complexes were reported to catalyze the copolymerization of ethylene with CO in a nonalternating fashion for the first time.[20,23,62-64] The alternating copolymerization of CO with polar monomers with (P^O)Pd catalysts has been reported for vinyl acetate[65] and methyl acrylate.[47,66] For the alternating copolymerization of CO with methyl acrylate even a regio and stereocontrol could be achieved lately, resulting in the production of enantiopure copolymers.[40]

### 1.2.3 Mechanistic Considerations

The mechanisms of ethylene and MA homopolymerization, as well as ethylene/polar monomer copolymerization have been studied in detail for (P^O)Pd catalysts with combined experimental and DFT-methods.[44,67-70] Essential features of the mechanism of ethylene homopolymerization are depicted in Scheme 1-10. In the ground state the growing chain is always placed cis to phosphorus in **1'-E$_{cis}$**, which is due to the high trans influence of the alkyl and the phosphine, respectively, and is in accordance with X-ray structures for (P^O)Pd(alkyl) complexes. Ethylene coordinates cis to the sulfonate group, respectively. The insertion proceeds by a cis/trans isomerization placing the growing chain trans to the phosphine in **1'-E$_{trans}$**. Here, ethylene insertion from **1'-E$_{trans}$** exhibits significantly lower barriers than from **1'-E$_{cis}$**. This can be explained by the enhanced migratory ability of the growing chain from **1'-E$_{trans}$**, due to the strong trans influence of both the phosphine and the methyl group, which are strong σ–donors, while the sulfonate group is considerably less σ–donating. In the resulting insertion product **1''$_{A,cis}$** the phosphine and the alkyl are placed cis to each other again. Simultaneously, the monomer in **1'-E$_{trans}$** experiences an enhanced back-donation from the palladium, as the sulfonate group in trans position is only a weak π-acceptor. Nozaki et al. showed that the C=C bond length of MA in **1'-E$_{trans}$** is significantly longer than in **1'-E$_{cis}$** or in the symmetrical environment of a (P^P)-coordinated dppe(Pd) complex. This should facilitate the conversion from a $sp^2$ to a $sp^3$ carbon during insertion.[66] Thus the stronger back donation activates the olefin. The cis/trans isomerization is predicted to proceed by a concerted Barry-pseudo rotation of the sulfonate group and to be always fast in comparison to the insertion. Finally, the insertion results in the formation of **1''$_{A,cis}$** stabilized by β-agostic interactions. From this intermediate either chain growth or β-H elimination can appear. The overall barriers either for β-H elimination from **1''$_{A,cis}$**, or for isomerization and β-H

elimination via **1''$_{A,trans}$** are calculated to be in the same range as the insertion barriers. This implies that under sufficient ethylene concentration β-H elimination is suppressed.[22,67,69] This is in line with experimental observations that (P^O)Pd catalysts form highly linear polymers, but can isomerize α-olefins in the absence of ethylene under NMR conditions.[25,67] An additional explanation, which does not exclude β-H elimination, is that insertion into primary alkyls is strongly favoured compared to insertion into higher alkyls. This could also explain the formation of partly deuterated PE by polymerization of ethylene in presence of MeOD, due to an H/D exchange of the intermediately formed Pd-H species.[71]

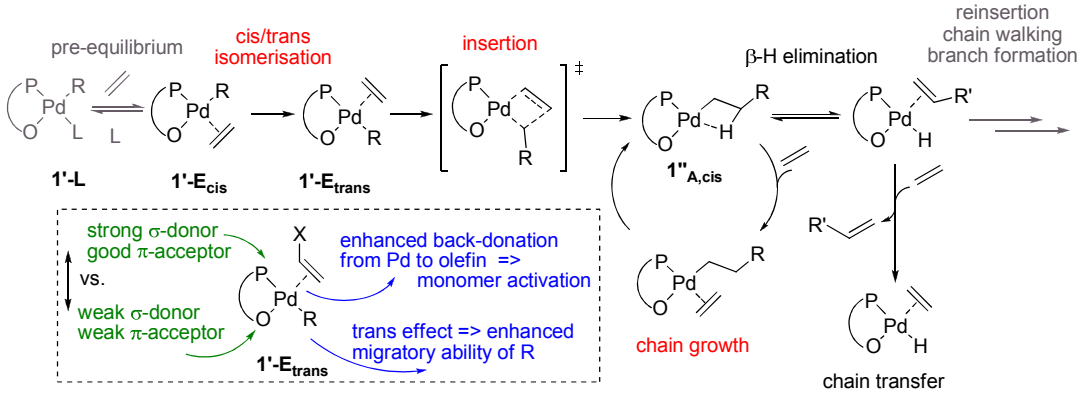


**Scheme 1-10.** Mechanism of ethylene polymerization with (P^O)Pd catalysts.[22,67]

For the copolymerization of ethylene with polar vinyl monomers additional factors have to be considered. The π-coordination of the monomer is a prerequisite for an insertion. For monomers exhibiting a polar group, a κ-*X* coordination competes with the π-coordination (Scheme 1-11).

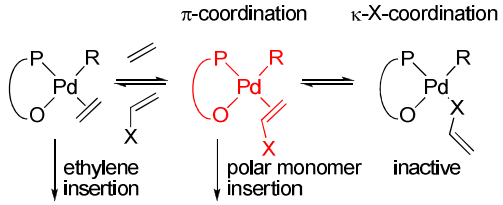


**Scheme 1-11.** Monomer coordination in ethylene/polar monomer copolymerization.

Predominant κ-*X* coordination to Pd(II) centers was found for acrylonitrile. In contrast, π-coordination predominates for methyl acrylate. The coordination mode is strongly influenced by the electronic properties of the metal center. Electron rich metals prefer π-coordination of the monomer, whereas electron poor metal centers tend to κ-*X* coordination. However, κ-*X* coordination of the polar monomer always occurs to a certain degree and the resulting inhibition of the active site is one reason for the decreased activities observed in the copolymerization experiments. In comparison to ethylene, electron deficient monomers

exhibit a reduced π-coordination strength, so that the monomer coordination pre-equilibrium is shifted towards ethylene in the copolymerization. However, this is partly compensated by the lower barriers for the migratory insertion of electron deficient monomers compared to ethylene.[72]

Regarding the regioselectivity of insertion experimentally a clear preference for a 2,1-insertion has been observed for electron deficient monomers like e.g. acrylates,[19,43,45,51] whereas electron rich monomers like e.g. vinyl ethers undergo a 1,2-insertion.[49] However, very bulky ligands may reverse the preference as the ligand interacts with the substituent at the double bond during a 2,1-insertion. This was shown for MA insertion in bulky diazaphospholidine sulfonato palladium(II) methyl species (Figure 1-5), for which the 2,1 regioselectivity is completely inverted to a 1,2-insertion.[41] That also the monomer steric bulk can influence the regioselectivity becomes obvious for MMA insertion into $^{MeO}$**1-dmso**, which proceed in a 1,2-mode to a significant extent in contrast to the completely 2,1-selective insertion of the less bulky MA monomer.[61] The origin of regioselectivity for the insertion of polar monomers has not been fully clarified yet (Scheme 1-12).[22] In principal electronic effects of the monomer are more pronounced for more electron-deficient palladium centers due to higher polarization of the double bond.[73] Concerning the migrating group it has been stated that in the Cossée-Arlman-type insertion step the nucleophilic carbon of the migrating group attacks the more electrophilic carbon of the double bond, which depends on the electron withdrawing or donating substituent. In contrast, a 2,1-insertion is always favoured for steric reasons as the migrating group attacks the less substituted carbon.[73] It should be noted that Svensson et al. found no pronounced differences in charge-separation and orbital coefficients for electron deficient vinyl monomers like MA, whereas for electron rich monomers like e.g. vinyl ether the substituted carbon of the double bond was found to be more positively charged.[74] Concerning the transition state of the insertion Ziegler et al. distinguish three components affecting the regioselectivity during the insertion:[75,76,77] The distortion energy, steric repulsion between migrating group and monomer, and steric repulsion between the ligand and the monomer. In the transition state the bonds around the carbon of the double bond that form the new C-C bond are more bent by angular distortion than the bonds at the other carbon. Here, a C-H bond distortion is always favored compared to other bonds, leading to a preference for a 2,1-insertion with the new bond formed at the non-substituted carbon. Ziegler et al. state that these effects are affected by electronics and that the angular distortion energy is larger for a COOMe-substituent compared to a methyl-substituent. Steric interactions between the substituent at the double bond and the migrating

group occur only in the transition state for the 1,2-insertion, and further favor a 2,1-insertion. In contrast, steric interactions between the substituent of the double bond and the chelating ligand only occur during the 2,1-insertion and favor the 1,2-insertion. The interplay of these three effects controls the regioselectivity. For the MA insertion in bulky diazaphospholidine sulfonato palladium(II) methyl species it has been shown that the steric interactions between the ligand and the monomer during the 2,1-insertion result in a deviation from planarity in the four-membered Cossée-Arlman-type transition state. In contrast, the transition state for the 1,2-insertion is unaffected and has an almost perfectly planar geometry.[41]

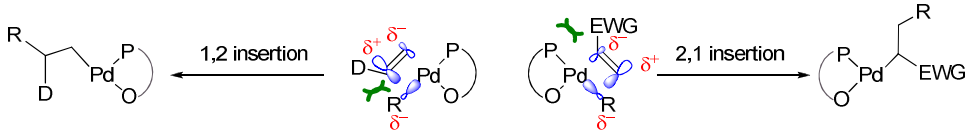


**Scheme 1-12.** Possible influences on regioselectivity for insertion of monomers bearing an electron withdrawing group (EWG) or an electron donating group (D) (green: sterics during insertion TS, blue: orbital coefficient (monomer-LUMO), red: charge).[22]

The mechanism for the insertion of methyl acrylate has also been studied by DFT methods. The 2,1-insertion of MA in the Pd-Me bond proceeds by similar pathways as the ethylene insertion including cis/trans isomerization prior to insertion (Scheme 1-13). The insertion primarily affords the kinetic product $\mathbf{2_{MA\text{-}KP}}$ stabilized by $\alpha$-agostic interactions, similar to the ethylene insertion, but the stable final product $\mathbf{2_{MA\text{-}Ch}}$ features a coordination of the carbonyl group of the inserted monomer to the palladium center forming a four membered chelate complex.

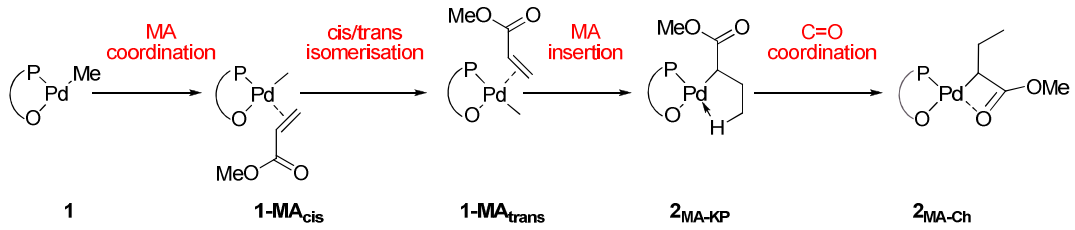


**Scheme 1-13.** Mechanism of acrylate insertion for (P^O)Pd catalysts.[44]

Further insertions proceed by a similar pathway. Differences are found in the ground state now always being a stable chelate complex, which has to be opened by the incoming monomer. In addition, the insertion products resulting from subsequent olefin insertion always form very stable six-membered chelate complexes (Scheme 1-14).[44] The six-membered chelate complexes $\mathbf{3_{MA\text{-}rac/meso}}$ resulting from two consecutive 2,1 MA insertions into the Pd-Me bond could be isolated starting from a 'base-free' multinuclear complex $[(P\text{^}O)PdMe]_n$, and were fully characterized by NMR spectroscopy. The existence of two

stereocenters in $\mathbf{3}_{\mathbf{MA\text{-}rac/meso}}$ introduced by the twofold insertion of the prochiral MA molecule results in the formation of two diastereomers distinguishable by NMR. NMR analysis revealed that the two diastereomers are formed in a 2:1 ratio (Scheme 1-14).

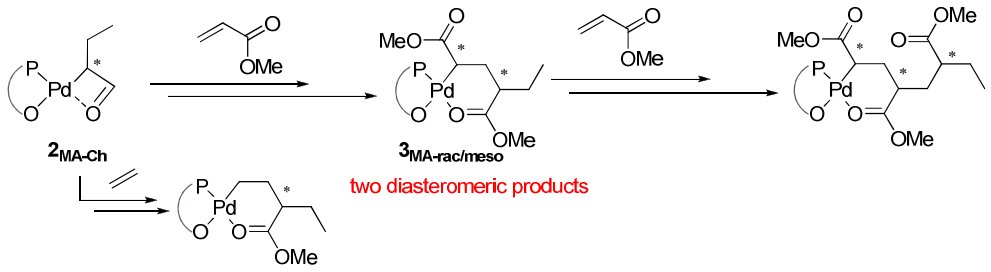


**Scheme 1-14.** Stable resting states in ethylene/MA copolymerization and MA homopolymerization.

Isolable, stable six-membered chelates are formed upon consecutive MA insertion, or upon ethylene insertion after an inserted MA unit. The hindered displacement of the chelating carbonyl moiety by π-coordination of an incoming monomer significantly retards polymerization (Scheme 1-14). Qualitative NMR-studies concerning the chelate stability of $\mathbf{3}_{\mathbf{MA\text{-}rac/meso}}$ showed that the chelate is completely opened by pyridine, but that with ethylene or methyl acrylate no opening could be observed under NMR tube conditions. However, homopolymerization experiments revealed that $\mathbf{3}_{\mathbf{MA\text{-}rac/meso}}$ is a suitable precursor for ethylene homopolymerization and hence the chelate can be opened under polymerization conditions. DFT analysis of the subsequent methyl acrylate insertion into $\mathbf{3}_{\mathbf{MA\text{-}rac/meso}}$ revealed that the insertion into the six-membered chelate is associated with an overall energy barrier of 100 kJ/mol, which is similar to the overall barrier for the insertion of ethylene. This clearly discloses that a homopolymerization of MA is possible, which agrees with the observed homooligomerization of MA with $^{\mathbf{MeO}}$**1-dmso**.[43,44]

Nozaki et al. studied the copolymerization of acrylonitrile with ethylene for (P^O)Pd and other catalysts in detail. An increasing electron rich nature of the palladium center by monoanionic ligands like $(P\text{^}O)^-$ in comparison to neutral diimine or diphosphine ligands leads to an equilibration of the insertion barriers for ethylene and acrylonitrile in neutral palladium(II) complexes, while ethylene insertion is strongly preferred for cationic (N^N)- and (P^P)-complexes. In comparison to neutral imine-phenolato (N^O)Pd systems the barrier for β-H elimination is increased for the (P^O)Pd complexes, which explains why only oligomers are obtained with (N^O)Pd compounds, while (P^O)Pd complexes produce linear copolymers.[68]

## 1.3 Miscellaneous Catalysts

Besides the aforementioned studies of cationic α-diimine palladium(II) catalysts and neutral phosphinesulfonato palladium(II) catalysts, the coordination-insertion copolymerization of ethylene with polar substituted vinyl monomers has not been reported in detail for other systems. A low degree of acrylate incorporation (< 2%) into the polymer backbone of mostly low molecular weight, moderately linear polymers was observed with cationic α-diimine nickel catalysts[78,79] and various other Ni catalysts based on anionic [P^O], [P^N],[79,80] or formal neutral *N*-oxide [N^O] ligands.[81] Gibson et al. reported that (P^O)Ni catalysts can produce low molecular weight PE with MMA derived endgroups.[82] Grubbs et al. reported a class of salicylaldimine derived (N^O)Ni(II) complexes that are capable of copolymerizing ethylene with functionalized monomers. However, in this case the polar group was always well separated from the olefinic double bond.[83] Methyl acrylate was reported to result in complete inhibition of the polymerization reaction.[84]

Most recently Nozaki and Carrow reported cationic bisphosphine monoxide palladium complexes, which allowed for the copolymerization of ethylene with vinyl acetate, acrylonitrile and vinyl ethers to linear copolymers (Figure 1-6). Surprisingly, alkyl acrylates could not be copolymerized with this class of catalysts.[85]

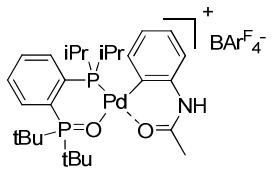


**Figure 1-6.** Bisphosphine monoxide (BPMO) palladium(II) complex.[85]

# 2. Scope of Thesis

The industrial importance of insertion polymerization is reflected in the production of more than 100 million tons of polyolefins by transition metal catalysis annually. In strong contrast, the industrial insertion (co)polymerization of polar vinyl monomers such as acrylates has remained elusive. An insertion polymerization of these monomers is highly attractive, as this mechanism offers unique possibilities for a microstructure control and consequently can give access to new materials with predeterminable properties.

Until now only two catalytic systems effective for the copolymerization of ethylene with polar olefins have been reported. Cationic palladium(II) diimine complexes afford highly branched copolymers with incorporation of the polar olefin preferentially at the chain ends, limiting the scope of materials properties and applications. In contrast, neutral palladium(II) phosphinesulfonato catalysts produce linear copolymers with incorporation of the polar olefin into the main chain. Here, the special importance of weakly coordinated catalyst precursors for highly active catalysts enabling high incorporation ratios of polar monomers and even allowing for a homooligomerization of methyl acrylate has been highlighted.

In this context the role of weakly coordinating monodentate ligands L occupying the fourth coordination site of [(P^O)PdMe(L)] catalyst precursors was studied in detail to evaluate perspectives and (intrinsic) limitations regarding catalyst activity. With the insights obtained, new easily accessible catalyst precursors for highly active catalysts are identified to maximize activity and polar monomer incorporation for a given phosphinesulfonato palladium combination (Chapter 3).

So far the existing catalysts suffer from certain intrinsic limitations e.g. low molecular weight of the copolymers. In order to overcome these limitations a deeper understanding of the relationship between catalyst structure and produced (co)polymer is necessary. For this purpose, electronic and steric effects of the phosphinesulfonato ligands on the catalyst performance were investigated. With the insights gained new concepts for a more directed catalyst design are devised (Chapter 4).

Until now the unique possibilities of an insertion mechanism for a (stereo)controlled polymerization have never been studied for polar olefins. In this context mechanisms of stereocontrol for late transition metal catalyzed insertion reaction should be evaluated and concepts for an effective stereoselective polymerization with phosphinesulfonato palladium(II) catalysts are developed, demonstrated, and applied (Chapter 5).

# 3. Limits of Activity: Weakly Coordinating Ligands in Arylphosphinesulfonato Palladium(II) Polymerization Catalysts[A]

## 3.1 Introduction

The coordination strength of the monodentate ligand L introduced with the catalyst precursors [(P^O)PdMe(L)] (**$^{MeO}$1-L**; P^O = $\kappa^2$-*P,O*-Ar$_2$*P*C$_6$H$_4$SO$_2$*O* with Ar = 2-MeOC$_6$H$_4$) has a major impact on the catalytic activity in homo- and copolymerizations due to the equilibrium (P^O)PdR(L) + monomer ⇆ (P^O)PdR(monomer) + L, which accompanies chain-growth. Thus, stronger coordinating ligands shift the equilibrium towards the dormant species **$^{MeO}$1-L**. So far monodentate ligands, e.g. $PPh_3$, tmeda, pyridine, 2,6-lutidine, DMSO and derivatives thereof have been used (Figure 3-1).[24,25,38,43,45,86] Alternatively, carbon based ligands occupying two coordination sites, e.g. $\eta^3$-allyl or $\eta^1$,$\eta^2$-2-methoxycyclooct-5-enyl are suitable precursors to initiate chain growth.[20,87]

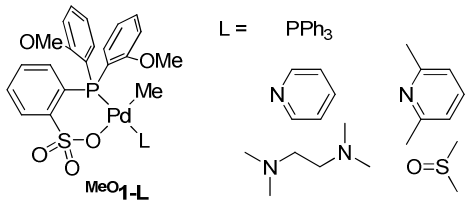


**Figure 3-1.** Reported complexes **$^{MeO}$1-L** with neutral, monodentate ligands L.

By comparison to the aforementioned *N*- and *P*-based ligands dimethylsulfoxide (DMSO) binds less strongly to the metal center and is more readily displaced by olefinic substrates. This enabled homooligomerization of methyl acrylate (MA) and the isolation of ethylene-methyl acrylate copolymers with more than 50 mol% MA incorporation.[43] Here, the weak coordination strength of DMSO permitted polymerization at low ethylene pressures and thus high MA/ethylene ratios. For completeness it should be mentioned that entirely 'base-free' species of the molecular composition [(P^O)PdMe] have been isolated[25,44,49] or synthesized *in situ* by abstraction of L from (P^O)PdMe(L).[21,45-47,87] However, so far no improved polymerization activities in comparison to 'base-coordinated' compounds have

[A] Contribution of Franz Ölscher within his Bachelor Thesis is acknowledged

been reported. For *in situ* activated catalysts this might be due to incomplete activation or side reactions by activation reagents or catalyst precursors.[21,45,87] For isolated material the reported low solubility likely renders part of the catalyst inactive.[44]

The significantly higher activity observed with DMSO- vs. pyridine-coordinated catalyst precursors suggests studies of further weaker coordinating ligands. Phosphine oxides ($O{=}PR_3$) as a ligand class lend themselves for this purpose, as they are easily accessible from the corresponding phosphines and exhibit a defined coordination site at the oxygen atom. Furthermore, a great variety of phosphines is commercially available and allows for electronic and steric fine-tuning. While chelating, hemilabile ligands (X^O; X = N,P,O; O = phosphine oxide), and especially the phosphine-phosphine oxide ligands have attracted much attention in homogeneous catalysis,[88-93] the application of monodentate tertiary phosphine oxides in homogenous catalysis is rare,[94-98] even though coordination towards metal centers is well studied.[99] With respect to ethylene polymerization, Starzewski *et al.* reported a remarkable effect with a catalyst system based on a hemilabile $\kappa^2$-*P,O* ligand, $Ni(cod)_2$ and an additional monodendate ligand. By changing the monodentate ligand from triphenylphosphine to the corresponding phosphine oxide molecular weight of the produced polymer could be significantly increased from low-molecular weight waxes to high molecular weight polyethylene ($M_\eta > 10^6$ g/mol).[97,98]

## 3.2 Results and Discussion

### 3.2.1 Coordination Strength of Phosphine Oxides

Since the coordination strength is influenced by steric as well as electronic properties, both parameters should be varied independently. Here, the cone angle θ and the electronic parameter χ of the corresponding phosphines enable an educated selection of phosphine oxides (χ is defined as the difference between the ν(CO) ($A_1$) absorption in L-Ni(CO)$_3$ and the ν(CO) ($A_1$) absorption in (*t*-Bu)$_3$P-Ni(CO)$_3$).[100] For this study OPBu$_3$, OPOct$_3$, OPPh$_3$, OP(*o*-Tol)$_3$, and OP(*p*-$CF_3C_6H_4$)$_3$,[100,101] for which θ– and χ–parameters have been reported, as well as the even more electron deficient OP(3,5-$(CF_3)_2C_6H_3$)$_3$ were selected (Figure 3-2). For OP(3,5-$CF_3C_6H_3$)$_3$ no parameter data was available, but coordination strength can be expected to be rather low due to increased electron deficiency in comparison to OP(*p*-$CF_3C_6H_4$). Phosphine oxides not available commercially were synthesized by phosphine oxidation with $H_2O_2$ (c.f. Chapter 7.2.1).

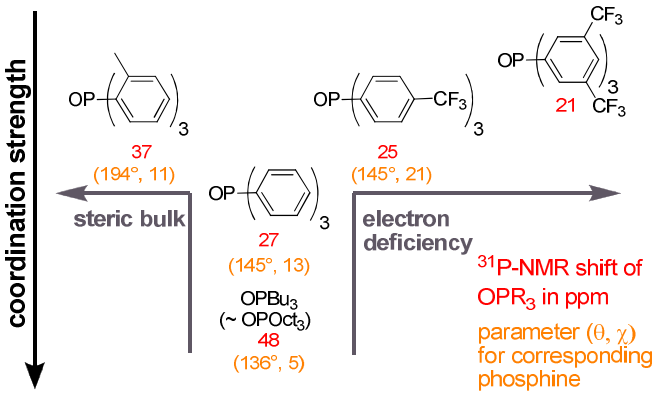


**Figure 3-2.** Coordination strength of phosphine oxides based on parameters θ and χ of the corresponding phosphines.[33,100]

Regarding electronic properties, the comparison of the literature derived electronic parameters with the observed $^{31}$P NMR shifts of the phosphine oxides show a good correlation. With increasing electron deficiency χ increases, while δ decreases. It is important to note that the $^{31}$P NMR shift of phosphine oxides is a reliable measure of the basicity as opposed to the $^{31}$P NMR shift of phosphines which is also influenced by sterics.[102] As expected, the aryl phosphine oxides exhibit a weaker basicity than OPBu$_3$. In comparison to OPPh$_3$, steric bulk is increased by introduction of a methyl group in ortho-position in OP(*o*-Tol)$_3$. It should be noted that the steric influence is lower than indicated by the cone angle of the corresponding phosphine, because the distance between metal center and the aryl groups

is enlarged in comparison to the phosphine. In contrast, the introduction of a $CF_3$-group in *para*-position in OP(*p*-$CF_3C_6H_4)_3$ does not change steric properties but increases electron deficiency. In OP(3,5-$(CF_3)_2C_6H_3)_3$ electron deficiency is further increased while the steric influence is believed to be similar to OP(*p*-$CF_3C_6H_4)_3$ ($\theta$ = 145° vs. ~151° for P(3,5-$Me_2C_6H_3)_3$).[103]

The relative coordination strength of these phosphine oxides compared to DMSO ($K_{OPR3}$) was determined by $^1$H NMR spectroscopy. The $^1$H resonance of DMSO in $CD_2Cl_2$ is downfield shifted from 2.54 ppm (free DMSO) to 2.95 ppm by complexation to the Pd center in $^{MeO}$**1-dmso**. Here, the exact coordination mode of DMSO remains unclear, but for a related complex an *S*-coordination was observed by X-Ray analysis.[43] Partial replacement of DMSO by $OPR_3$ leads to a high field shift due to a fast equilibrium between Pd-bound and uncoordinated DMSO. From the shift difference the ratio between $^{MeO}$**1-dmso** and $^{MeO}$**1-L** and consequently $K_L$ at 25 °C was calculated (cf. Chapter 7.1.10).

**Table 3-1.** $K_L$ for $^{MeO}$**1-dmso** + L ⇆ **1-L** + DMSO.

| entry | Ligand | equiv. L | $\delta_{eq}$ [ppm] | $K_L$ |
|---|---|---|---|---|
| 1-1 | $OPBu_3$ | 1.0 | 2.68 | 3.5 |
| 1-2 | $OPOct_3$ | 1.2 | 2.66 | 3.3 |
| 1-3 | $OPPh_3$ | 9.2 | 2.67 | 0.2 |
| 1-4 | OP(*o*-Tol)$_3$ | 11.3 | 2.78 | 0.03 |
| 1-5 | OP(*p*-$CF_3C_6H_4)_3$ | 10.2 | 2.77 | 0.04 |
| 1-6 | OP(3,5-$(CF_3)_2C_6H_3)_3$ | 9.2 | 2.91[a] | ~0.001[a] |
| 1-7 | MeOH | 9.4 | 2.82 | 0.02 |
| 1-8 | 2.6-lutidine | 1.4 | 2.54 | >>$10^2$ |
| 1-9 | $MeSO_3C_6H_5$ | 38 | 2.93 | <<$10^{-4}$ |

[a] $\Delta\delta$ is low due to limited solubility of $OPR_3$ consequently inaccuracy of $K_L$ is enhanced.

The results are summarized in Table 3-1. Whereas both alkyl phosphine oxides coordinate slightly stronger than DMSO ($K_{OPBu3}$ = 3.5, $K_{OPOct3}$ = 3.3), the more bulky and electron-deficient $OPPh_3$ exhibits $K_{OPPh3}$ = 0.2 for the equilibrium $^{MeO}$**1-dmso** + $OPR_3$ ⇆ $^{MeO}$**1-OPR$_3$** + DMSO. An even weaker coordination is evident for the comparison with OP(*o*-Tol)$_3$ ($K_{OPTol3}$ = 0.03), and OP(*p*-$CF_3C_6H_4)_3$ ($K_{OP(pCF3Ar)3}$ = 0.04, Table 3-1, compare $K_L$ for MeOH and 2,6-lutidine). Hence, coordination strength can be controlled by either steric bulk or electron deficiency over a large range. The introduction of a second electron withdrawing group in OP(3,5-$(CF_3)_2C_6H_3)_3$ further reduces coordination strength significantly ($K_{OP(3,5CF3Ar)3}$ ~ 0.001). Note, that in a related study $K_L$ was determined vs. DMSO for ethyl acetate ($K_{EA}$ < $10^{-2}$), methyl ethyl sulfone ($K_{MES}$ < $10^{-2}$), propionic acid ($K_{PrA}$ < 0.1),

*N,N*-dimethylacetamide ($K_{DMAcA} \approx 0.4$), *N*-methylacetamide ($K_{MAcA} \approx 0.6$) and acrylonitrile ($K_{ACN} \approx 1$).[56]

In order to investigate the influence of the temperature on the coordination equilibrium, $K_{OPPh3}$ was determined in the temperature range between -25 °C and 25 °C. Only minor changes of $K_{OPPh3}$ in this temperature range have been observed (Table 3-2).

**Table 3-2.** $K_L$ at different Temperatures ([$^{MeO}$**1-dmso**] = 0.016 mol $L^{-1}$; equiv. L: 10.3).

| entry | T [°C] | $\delta_{1\text{-dmso}}$ [ppm] | $\delta_{DMSO}$ [ppm] | $\delta_{eq}$ [ppm] | $K_L$ |
|---|---|---|---|---|---|
| 2-1 | 25.5 | 2.951 | 2.558 | 2.658 | 0.23 |
| 2-2 | 14.5 | 2.957 | 2.550 | 2.666 | 0.19 |
| 2-3 | 6.0 | 2.966 | 2.548 | 2.672 | 0.17 |
| 2-4 | -4.5 | 2.974 | 2.549 | 2.681 | 0.16 |
| 2-5 | -15.0 | 2.980 | 2.549 | 2.692 | 0.14 |
| 2-6 | -25.0 | 2.982 | 2.545 | 2.703 | 0.12 |

Plotting the natural logarithm of the equilibrium constants against the temperature in a Van't Hoff analysis allowed for the determination of $\Delta H°_{DMSO/OPPh3}$ = 8 kJ $mol^{-1}$, $\Delta S°_{DMSO/OPPh3}$ = 13 J $mol^{-1}K^{-1}$ (Figure 3-3). Extrapolation to typical polymerization conditions, i.e. 80 °C results in $K_{OPPh3}$(80 °C) = 0.35 which compares to $K_{OPPh3}$(25 °C) = 0.22.

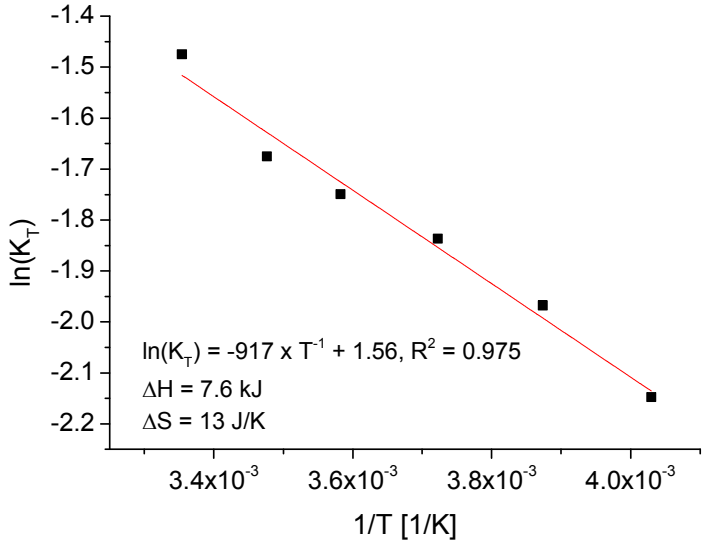


**Figure 3-3.** Van't Hoff plot for the equilibrium $^{MeO}$**1-dmso** + $OPPh_3$ ⇆ $^{MeO}$**1-OPPh$_3$** + DMSO determined by variable temperature $^1$H NMR spectroscopy from T = -25 °C to 25 °C.

It is assumed that a similar small temperature dependence applies to all $K_{OPR3}$ and that $K_{OPR3} < 1$ should result in more active precatalysts $^{MeO}$**1-L**: Since during polymerization monomer can also compete with L for coordination to (P^O)PdR (R = growing chain)

according to the equilibrium [(P^O)PdR(L)] + ethylene ⇆ [(P^O)PdR(ethylene)] + L, complexes $^{MeO}$**1-L** derived from phosphine oxides with a weaker coordination strength than DMSO, i.e. from $OPPh_3$, $OP(o\text{-}Tol)_3$, $OP(p\text{-}CF_3C_6H_4)_3$, and $OP(3,5\text{-}(CF_3)_2C_6H_3)_3$ are expected to exhibit higher turnover frequencies than $^{MeO}$**1-dmso** as long as saturation kinetics are not reached. Consequently, such complexes $^{MeO}$**1-L** represent valuable synthetic targets for highly active single component catalysts.

## 3.2.2 Complex Synthesis and Characterization

For the synthesis of phosphine oxide complexes $^{MeO}$**1-OPR$_3$** standard procedures were not applicable since they are either based on introduction of the ligand with the Pd-precursor as with L = TMEDA from $[(tmeda)PdMe_2]$,[20,24,38,87] or subsequent ligand substitution by a stronger coordinating ligand.[25,38,44,45,62,86] Notably, the weaker coordinating DMSO could be introduced by substitution of TMEDA. This substitution occurs since TMEDA is removed from the equilibrium ½ ($^{MeO}$**1)$_2$-tmeda** + DMSO ⇆ $^{MeO}$**1-dmso** + ½ TMEDA under vacuum due to the considerably higher volatility of TMEDA vs. DMSO.[43] However, an analogous procedure, e.g. solvent evaporation from a mixture of ($^{MeO}$**1)$_2$-tmeda** and phosphine oxide in high boiling solvents, did not result in the isolation of clean products. In an alternative approach, multinuclear 'base-free' palladium alkyl complexes which are accessible e.g. by pyridine or lutidine abstraction with $B(C_6F_5)_3$[25,44] may be suitable precursors for the preparation of phosphine oxide complexes $^{MeO}$**1-OPR$_3$**. However, a more convenient synthesis starts from $[\{(^{MeO}$**1-Cl**$)\text{-}\mu\text{-}Na\}_2)]$[61] and chloride abstraction in the presence of phosphine oxides is expected to generate $^{MeO}$**1-OPR$_3$** if the presence of stronger coordinating ligands is avoided (Scheme 3-1).

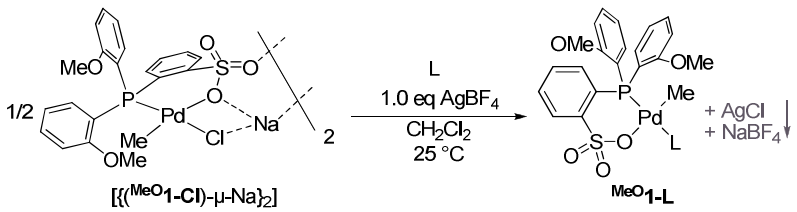


**Scheme 3-1.** Synthesis of $^{MeO}$**1-L**.

The viability of this general route was demonstrated by the synthesis and isolation of $^{MeO}$**1-dmso**. As expected, also the complexes $^{MeO}$**1-OPBu$_3$** and $^{MeO}$**1-OPOct$_3$** with the slightly stronger coordinating alkyl phosphine oxides as compared to DMSO could be isolated by this method. In contrast to stronger coordinating ligands like pyridine, the Pd-C$H_3$-group

exhibits no visible $^{3}J_{PH}$ coupling in the $^{1}H$ NMR spectrum at 25 °C as also observed for $^{MeO}$**1-dmso**.[43] Coordination of the phosphine oxide in solution is further evidenced by a downfield shift of the $OPBu_3$-resonance in the $^{31}P$ NMR spectrum from 48 ppm to 66 ppm (Table 3-3).[104,105,B] In the solid state, coordination of the phosphine oxide is evidenced by the shift of the $\nu$(O=P)-band in the IR-spectrum to lower frequencies from 1154 $cm^{-1}$ to 1113 $cm^{-1}$. This observed frequency decrease can be related to a lowering of the O-P bond order due to coordination.[106] In addition, the molecular connectivity of $^{MeO}$**1-OPBu$_3$** could be established by X-Ray diffraction analysis (Figure 3-5). The analogous complex $^{MeO}$**1-OPOct$_3$** exhibits very similar properties (Table 3-3).

**Table 3-3.** $^{31}P$ NMR shift and O=P-IR band of Pd-coordinated vs. non-coordinated phosphine oxide $OPR_3$.

| entry | R | $\nu(O=P)_{coord}$ [$cm^{-1}$] | $\nu(O=P)_{free}$ [$cm^{-1}$] | $\Delta\nu(O=P)$ [$cm^{-1}$] | $\delta(^{31}P)_{coord}$ [c] [ppm] | $\delta(^{31}P)_{free}$ [ppm] | $\Delta\delta(^{31}P)$ [ppm] |
|---|---|---|---|---|---|---|---|
| 3-1 | Bu | 1113 | 1154 | 41 | 66 | 48 | 18 |
| 3-2 | Oct | 1107 | 1145 | 38 | 65 | 47 | 18 |
| 3-3 | Ph | 1150 | 1189 | 39 | 35 | 27 | 8 |
| 3-4 | *p*-$CF_3C_6H_4$ | n.d.[a] | 1198 | [b] | 29 | 25 | 4 |
| 3-5 | *o*-Tol | n.d.[a] | 1185 | [b] | 40 | 37 | 3 |
| 3-6 | 3,5-$(CF_3)_2C_6H_3$ | n.d.[a] | 1216 | [b] | 21[d] | 21 | 0 |

[a]clear identification of the $\nu(O=P)_{coord}$-band not possible due to weak intensity and numerous overlapping bands; [b]disappearance of the $\nu(O=P)_{free}$-band is observable; [c]from isolated raw material directly after resolution in $CD_2Cl_2$; [d]no clear homogeneous reaction mixture obtained.

The synthesis of $^{MeO}$**1-OPPh$_3$** could also be achieved. Here, coordination is evidenced by a shift in the $^{31}P$ NMR from 27 ppm to 35 ppm (Figure 3-4). A weaker coordination in solution by comparison to the trialkyl phosphine oxide complexes may be reflected in the much lower $^{31}P$-shift ($\Delta\delta$ = 8 ppm for O*P*Ph$_3$ vs. 18 ppm for O*P*Bu$_3$/O*P*Oct$_3$; Table 3-3). In the IR-spectrum again a decrease of the P=O stretching frequency from 1189 $cm^{-1}$ to 1150 $cm^{-1}$ is observed, which agrees with $\nu$(O=P) = 1145 $cm^{-1}$ reported for the complex $[Pd(NO_3)_2(OPPh_3)(PPh_3)]$.[105,107] Suitable crystals for X-Ray analysis were obtained from a $CHCl_3$ solution. As for all reported (P^O)PdMe structures the palladium complex adopts a square planar geometry and the methyl group is situated in the trans-position to the sulfonate group (Figure 3-5).

[B] For an example of $OPPh_3$ and $OPBu_3$ coordination towards lanthanides and resulting changes in $^{31}P$-NMR, IR and X-ray see ref. 105.

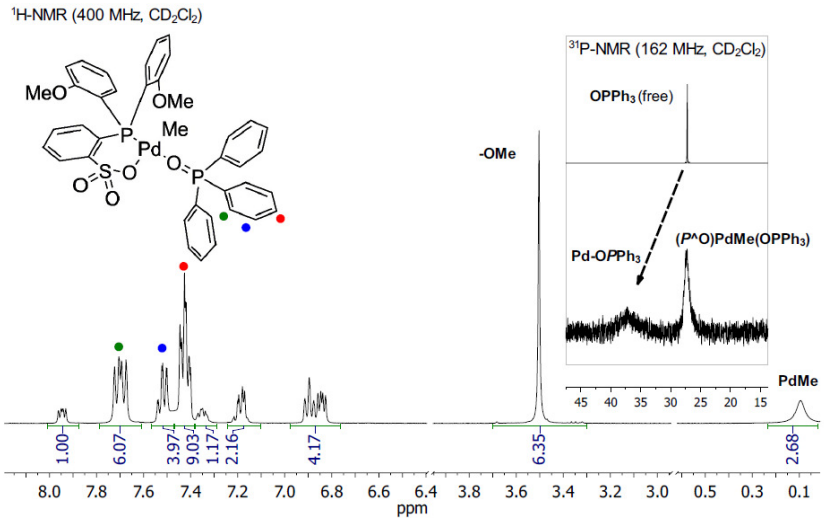


**Figure 3-4.** $^{1}$H NMR spectrum (400 MHz, $CD_2Cl_2$) of $^{MeO}$**1-OPPh$_3$**; Inset: $^{31}$P NMR (162 MHz, $CD_2Cl_2$) spectra of $OPPh_3$ and $^{MeO}$**1-OPPh$_3$**.

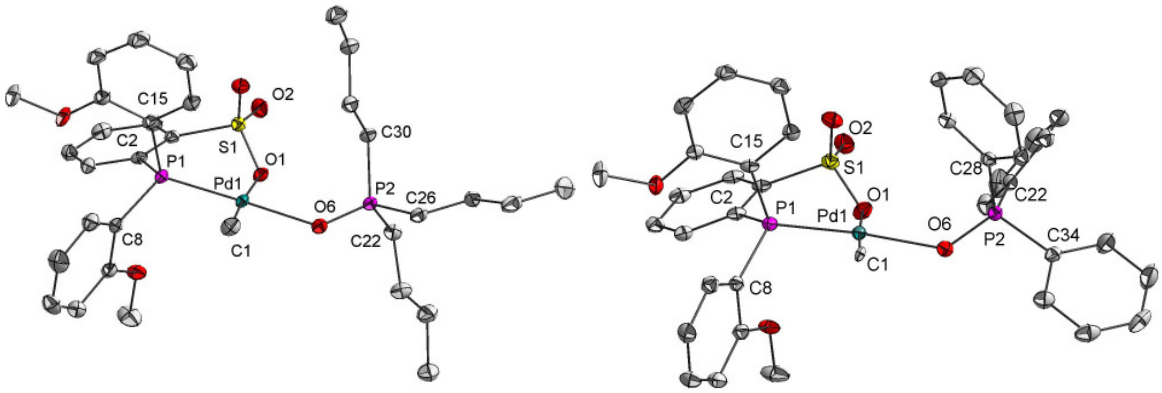


**Figure 3-5.** Molecular structure of $^{MeO}$**1-OPBu$_3$** (left) and $^{MeO}$**1-OPPh$_3$** (right) at 50% probability ellipsoids. All hydrogen atoms are omitted for clarity. Selected bond length [Å] and angles [°] for $^{MeO}$**1-OPBu$_3$:** Pd(1)-P(1) = 2.203(1); Pd(1)-C(1) = 2.010(3); Pd(1)-O(1) = 2.157(2); Pd(1)-O(6) = 2.129(2); O(6)-P(2) = 1.514(2); Pd(1)-O(6)-P(2) = 132.1(1), P(1)-Pd(1)-O(6) = 174.4(1). Selected bond length [Å] and angles [°] for $^{MeO}$**1-OPPh$_3$:** Pd(1)-P(1) = 2.199(1); Pd(1)-C(1) = 2.089(3); Pd(1)-O(1) = 2.150(3); Pd(1)-O(6) = 2.138(3); O(6)-P(2) = 1.503(3); Pd(1)-O(6)-P(2) = 133.5(1), P(1)-Pd(1)-O(6) = 175.2(1).

Coordination of the phosphine oxide leads only to a small elongation of the O-P bond (1.514(2) Å vs. ~1.49 Å[108] in $OPPh_3$),[109,C] which is in accordance with the aforementioned bis(nitrato)-Pd(II) complex (*vide supra*, O-P: 1.501(8) Å)[107] and $OPPh_3$ complexes of other metals for which in general a length change <1% is observed.[104] In comparison to $^{MeO}$**1-OPBu$_3$** the Pd-OP bond length is slightly elongated (2.138(3) Å for $^{MeO}$**1-OPPh$_3$** vs. 2.129(2) Å for $^{MeO}$**1-OPBu$_3$**, Figure 3-5) which is in agreement with the reduced coordination strength of $OPPh_3$. Phosphine oxides are capable of showing a rather wide range of M-O-P bond angles (~180°-140°) while the bonding mode is discussed to be end-on in contrast to

[C] The crystal structure of free $OPPh_3$ has been determined several times for different crystal modifications and at different temperatures resulting in a bond range from 1.46(1) Å to 1.494 Å. For comparison see: Ref. 109.

thio- and seleno-phosphorylic units which show a side-on coordination (<(M-E-P) ~115°-98°).[104] In comparison the M-O-P bond angles for Pd-complexes seem to be at the lower end of the scale independently of the steric bulk at the Pd center created by additional ligands (<(Pd-O-P) = 133.5(1)° ($^{MeO}$**1-OPPh$_3$**), 132.1(1)° ($^{MeO}$**1-OPBu$_3$**), 132.1(4)° [$Pd(NO_3)_2(OPPh_3)(PPh_3)$]).[107]

### 3.2.3 Limitations for Weakly Coordinating Ligands

The isolation of $^{MeO}$**1-OPPh$_3$** already revealed a relatively weak binding of this phosphine oxide to the Pd center, which affects the work up procedure: coordinated $OPPh_3$ can be extracted from the complex by extensive washing with toluene, leading to partly insoluble material. In contrast, $^{MeO}$**1-OP(*o*-Tol)$_3$** and $^{MeO}$**1-OP(*p*-CF$_3$C$_6$H$_4$)$_3$** exhibiting phosphine oxides with further decreased coordination strength (Table 3-1) were only obtained as crude products which are not stable in solution for a prolonged period of time. For the solid raw materials isolated by solvent evaporation after filtration the disappearance of the *v*(PO)-band for uncoordinated $OPR_3$ in the IR-spectra can be observed (the detection of a new band for coordinated $OPR_3$ is hampered by numerous overlapping *v*(P^O) ligand bands, Figure **3-6**), evidencing a Pd-$OPR_3$ interaction. Dissolving the isolated material in $CH_2Cl_2$ yields a clear solution and the $^{31}$P NMR spectra of the dissolved raw material show a further reduced but significant shift for the $OPR_3$ resonances ($\Delta\delta(OP(o\text{-}Tol)_3)$ = 3 ppm; $\Delta\delta(OP(p\text{-}CF_3C_6H_4)_3)$ = 4 ppm). However, within 1-12 hours in solution white precipitates form. Detailed analysis of these precipitates by ATR-IR and NMR spectroscopy in $CD_3OD$ confirmed the decomposition of $^{MeO}$**1-OP(*o*-Tol)$_3$** and $^{MeO}$**1-OP(*p*-CF$_3$C$_6$H$_4$)$_3$** to [{(P^O)PdMe}$_n$] ($^{MeO}$**1$_n$**; Scheme 3-2).[25,44]

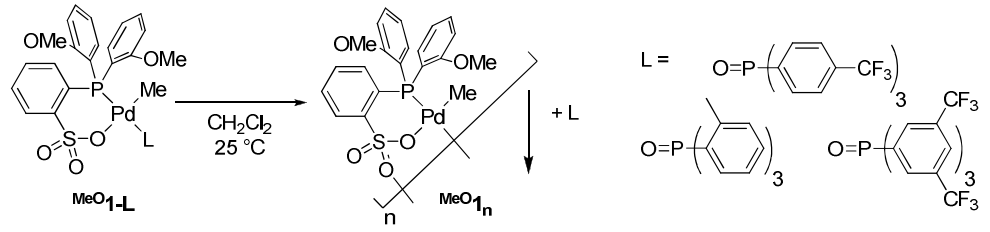


**Scheme 3-2.** Decomposition of $^{MeO}$**1-L**.

It is assumed that $^{MeO}$**1$_n$** is bridged via coordination of multiple Pd centers to the sulfonate groups in analogy to [{$^{MeO}$(P^O)PdCH$_2$SiMe$_3$}$_2$].[25] An extensive IR comparison revealed a further detail. Removal of the coordinating ligand from $^{MeO}$**1-L** and transformation to $^{MeO}$**1$_n$** leads to the disappearance of a strong band at ~1000 cm$^{-1}$ assigned to $\nu_{sym}(SO_3)$ and

growth of a very strong band at ~950 $cm^{-1}$ (Figure 3-6, Figure 3-8, Figure 3-10). Such a frequency shift could be induced after coordination of the $SO_3$-group to a further palladium center, e.g. in $^{MeO}\mathbf{1_n}$. In this context it is important to note that for all other (ligand coordinated) (P^O)PdMe complexes $^{MeO}\mathbf{1\text{-}L}$ described in this work the $\nu_{sym}(SO_3)$-band can always be found at around 1000 $cm^{-1}$ (Figure 3-6), which is in agreement with literature data for Pd-coordinated benzenesulfonic acid.[110] Hence the absence of a strong band around 950 $cm^{-1}$ in the IR-spectra can be seen as a reliable indication for the formation of discrete ligand coordinated (P^O)PdMe species $^{MeO}\mathbf{1\text{-}L}$.

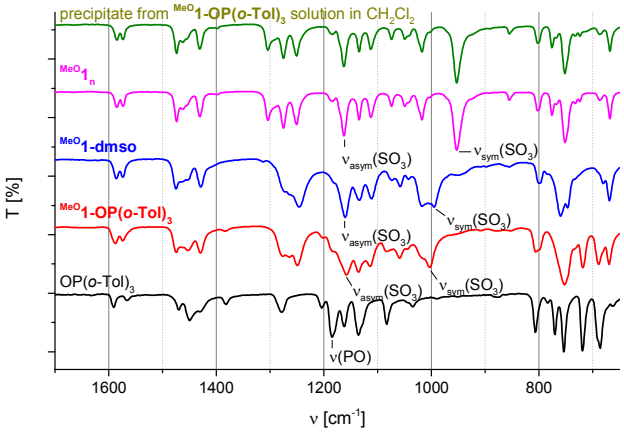


**Figure 3-6.** ATR-IR spectra of OP(*o*-Tol)$_3$, ligated complexes $^{MeO}\mathbf{1\text{-}L}$ (L = OP(*o*-Tol)$_3$, DMSO), the 'base-free' complex $^{MeO}\mathbf{1_n}$ and isolated precipitate from a $^{MeO}\mathbf{1\text{-}OP(o\text{-}Tol)_3}$ solution in $CH_2Cl_2$.

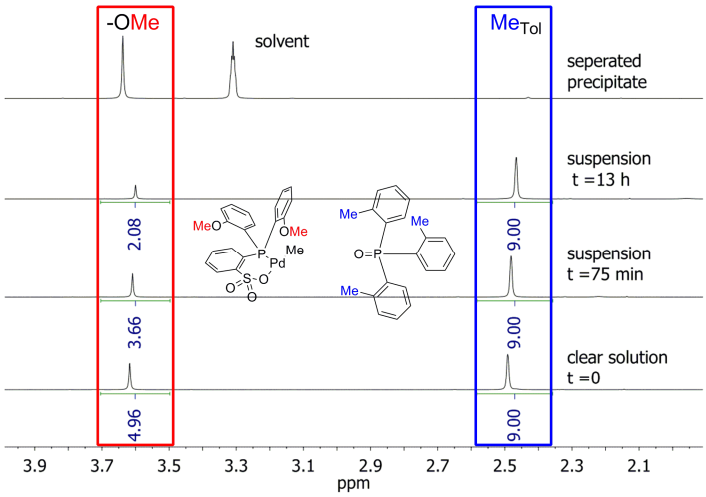


**Figure 3-7.** $^1$H NMR spectra (expansion, 400 MHz, $CD_2Cl_2$) of decomposition of $^{MeO}\mathbf{1\text{-}OP(o\text{-}Tol)_3}$ with time and $^1$H NMR spectrum (400 MHz, MeOD) of the resulting precipitate. Note that the initial $^{(P\text{^}O)}$OMe:OPR$_3$-ratio at t = 0 is 5:9 and deviates from the expected 6:9 ratio. This can be explained by (a) the excess of OPR$_3$ used in synthesis and (b) an already started decomposition process during preparation and handling of the NMR sample.

Decomposition of $^{MeO}$**1-OP(*o*-Tol)$_3$**, and $^{MeO}$**1-OP(*p*-CF$_3$C$_6$H$_4$)$_3$** to free phosphine oxide and $^{MeO}$**1$_n$** can be monitored by $^1$H NMR spectroscopy over the course of several hours as $^{MeO}$**1$_n$** precipitates upon formation which results in diminishing signals for $^{MeO}$**1-OP(*o*-Tol)$_3$**, and $^{MeO}$**1-OP(*p*-CF$_3$C$_6$H$_4$)$_3$**, while OPR$_3$ remains in solution (Figure 3-7).

In the case of the significantly weaker coordinating OP(3,5-(CF$_3$)$_2$C$_6$H$_3$)$_3$ crude $^{MeO}$**1-OP(3,5-(CF$_3$)$_2$C$_6$H$_3$)$_3$** already contains substantial amounts of $^{MeO}$**1$_n$** as evidenced by the IR spectrum, the limited solubility and the intensity ratio of anisyl-methoxy to aromatic 3,5-(CF$_3$)$_2$C$_6$H$_3$ $^1$H NMR resonances (Figure 3-8).

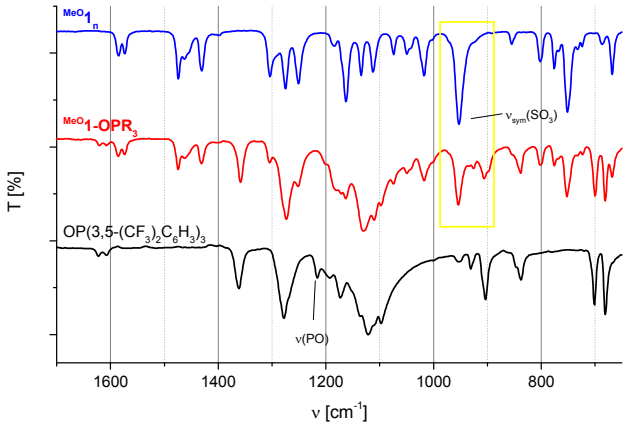


**Figure 3-8.** ATR-IR spectra of crude $^{MeO}$**1-OP(3,5-(CF$_3$)$_2$C$_6$H$_3$)$_3$** in comparison to free OP(3,5-CF$_3$(C$_6$H$_3$))$_3$ and the 'base-free' complex $^{MeO}$**1$_n$**.

The instability of $^{MeO}$**1-OP(*o*-Tol)$_3$** and $^{MeO}$**1-OP(*p*-CF$_3$C$_6$H$_4$)$_3$**, and their decomposition towards $^{MeO}$**1$_n$** and free phosphine oxide as well as the elusive isolation of $^{MeO}$**1-OP(3,5-(CF$_3$)$_2$C$_6$H$_3$)$_3$** clearly points to a coordination strength of palladium coordinated sulfonate which effectively competes with these phosphine oxides. However, attempts to quantify the coordination strength of the sulfonate group by the model substance methyl benzenesulfonate were not successful. The equilibrium experiments reveal that methyl benzenesulfonate coordination to the palladium center is at least four orders of magnitude weaker compared to DMSO (*vide supra*, $K_L << 10^{-4}$, Table 3-1, entry 1-9)

Kinetic control may allow for the isolation of complexes of weakly coordinating ligands such as methanol. While methanol binds less strongly to (P^O)PdMe than OP(*o*-Tol)$_3$ or OP(*p*-CF$_3$C$_6$H$_4$)$_3$ (Table 3-1, entries 1-4 and 1-5 vs. 1-7), $^{MeO}$**1-MeOH** was isolated by crystallization from methanol solution and analyzed by X-ray diffraction analysis at 100 K (Figure 3-9).

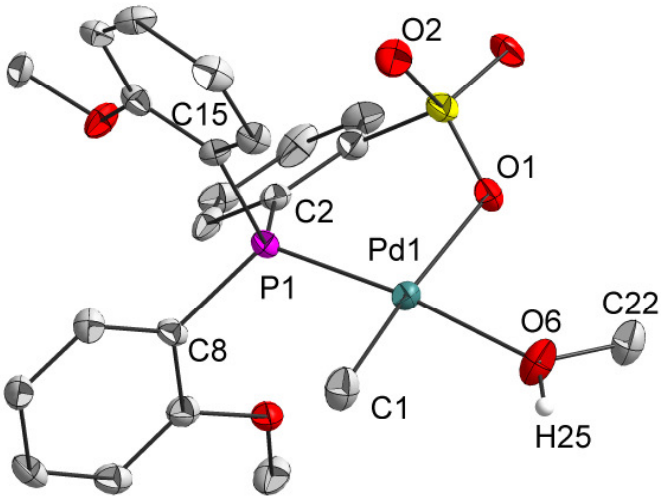


**Figure 3-9.** Molecular structure of $^{MeO}$**1-MeOH** at 50% probability ellipsoids. All solvent molecules and hydrogen atoms -except the hydroxyl hydrogen H25- are omitted for clarity. Selected bond length [Å] and angles [°]: Pd(1)-P(1) = 2.209(2); Pd(1)-C(1) = 2.01(1); Pd(1)-O(1) = 2.177(6); Pd(1)-O(6) = 2.136(6); O(6)-C(22) = 1.46(1); Pd(1)-O(6)-C(22) = 126.0(5), P(1)-Pd(1)-O(6) = 172.2(2).

However, even solid $^{MeO}$**1-MeOH** in the absence of a methanol atmosphere looses methanol within 20 minutes at room temperature and forms $^{MeO}$**1$_n$** as evidenced by ATR-IR spectroscopy (Figure 3-10).

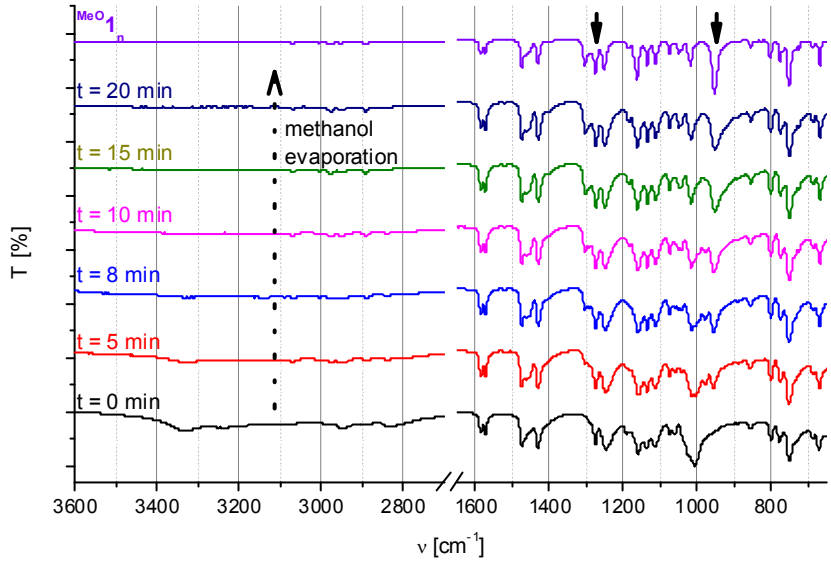


**Figure 3-10.** ATR-IR spectra of the transformation of $^{MeO}$**1-MeOH** (single crystals) to $^{MeO}$**1$_n$** at the air over time.

Phosphine oxides even if stronger coordinating than DMSO can still be interesting ligands as they are rather weak coordinating compared to pyridine, 2,6-lutidine or TMEDA derived ligands, but can influence the solubility of the resulting complexes. As an example $^{MeO}$**1-OPOct$_3$** is soluble in toluene, whereas $^{MeO}$**1-dmso** only dissolves in coordinating or chlorinated solvents. The use of $^{MeO}$**1-OPOct$_3$** as catalyst precursor allows for the

abandonment of chlorinated solvents, usually $CH_2Cl_2$, in the polymerization mixture, while NMR-studies have revealed that presence of chlorinated solvents may contribute to catalyst decomposition towards Pd-Cl species.[67] Another interesting class of complexes would be weakly coordinated water soluble catalyst precursors. So far only water soluble phosphinesulfonato Pd(II) complexes coordinated by phosphines or amines have been reported.[86] For this reason a PEG-substituted, water soluble phosphine oxide $OPPh_3^{PEG}$ based on the promising $OPPh_3$ motif was synthesized (Figure 3-11). However, the coordination strength was found to be too low to form stable complexes $^{MeO}$**1-OPPh$_3^{PEG}$** and decomposition towards $^{MeO}\mathbf{1_n}$ is observed during synthesis. In consideration of the similar basicity of $OPPh_3^{PEG}$ and $OPPh_3$, which is reflected in the similar $^{31}$P NMR shifts for the free phosphine oxides (30 ppm vs. 27 ppm for $OPPh_3$), this has to be explained by the slightly increased steric bulk of $OPPh_3^{PEG}$, due to the PEG-chains. This again reveals that the coordination strength of $OPPh_3$ is exactly at the limit to stabilize mononuclear complexes $^{MeO}$**1-L**.

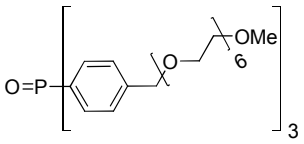


**Figure 3-11.** Water soluble phosphine oxide $OPPh_3^{PEG}$.

### 3.2.4 NMR Studies on the Influence of the Weakly Coordinating Ligand on Monomer Insertion

In order to study the influence of the coordinating ligand on monomer insertion in detail the insertion of ethylene and methyl acrylate were investigated by NMR spectroscopy, respectively. The insertion of ethylene into the Pd-Me bond of $^{MeO}$**1-OPPh$_3$** and of species $^{MeO}$**1** generated by *in situ* chloride abstraction from [{($^{MeO}$**1-Cl**)-μ-Na}$_2$)] with $AgBF_4$ in the absence of additional ligands was monitored at -15 °C (likely, in $^{MeO}$**1** the [(P^O)PdMe] fragment is weakly coordinated by the methylene chloride solvent). The determined first order rate constants (22 equiv. ethylene as compared to palladium) show that at -15 °C $^{MeO}$**1** is consumed slightly faster than $^{MeO}$**1-OPPh$_3$** ($k_{1\text{-OPPh3;ethylene}}$ = 5.7 × $10^{-4}$ $s^{-1}$, $k_{1;ethylene}$ = 7.0 × $10^{-4}$ $s^{-1}$, Figure 3-12).

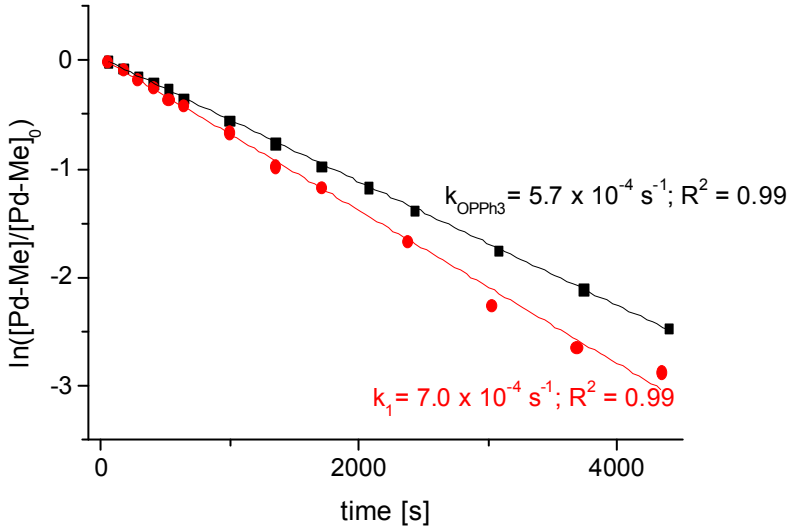


**Figure 3-12.** Pseudo first-order consumption of Pd-Me by insertion of ethylene, [Pd] = 0.0013 mol $L^{-1}$ in $CD_2Cl_2$ at -15 °C.

The analysis of higher ethylene insertions is hampered by the fact that [(P^O)PdR(L)] species precipitate with growing size of the alkyl chain. However, by monitoring the insertion over a period of two hours it becomes obvious that higher insertions into $^{MeO}$**1** are also significantly faster than into $^{MeO}$**1-OPPh$_3$**, because ethylene is consumed more rapidly. Interestingly, not only ethylene-insertion but also β-H elimination is faster with *in situ* generated $^{MeO}$**1** than with $^{MeO}$**1-OPPh$_3$** as evidenced by the increasing signal of vinylic end groups for this sample (Figure 3-13). This is in line with the observation that the polymeryl complex [(P^O)Pd(polymeryl)] resulting from the insertion in $^{MeO}$**1** in $CD_2Cl_2$ solution decomposes significantly faster as the $OPPh_3$ coordinated species at room temperature. This

might be explained by the blocking of the fourth coordination site by the ligand L. Thus the formation of agostic species that are assumed to be crucial intermediates for β-H elimination is hindered.[67] In addition, phosphine oxide coordination might hamper a bimolecular decomposition pathway.

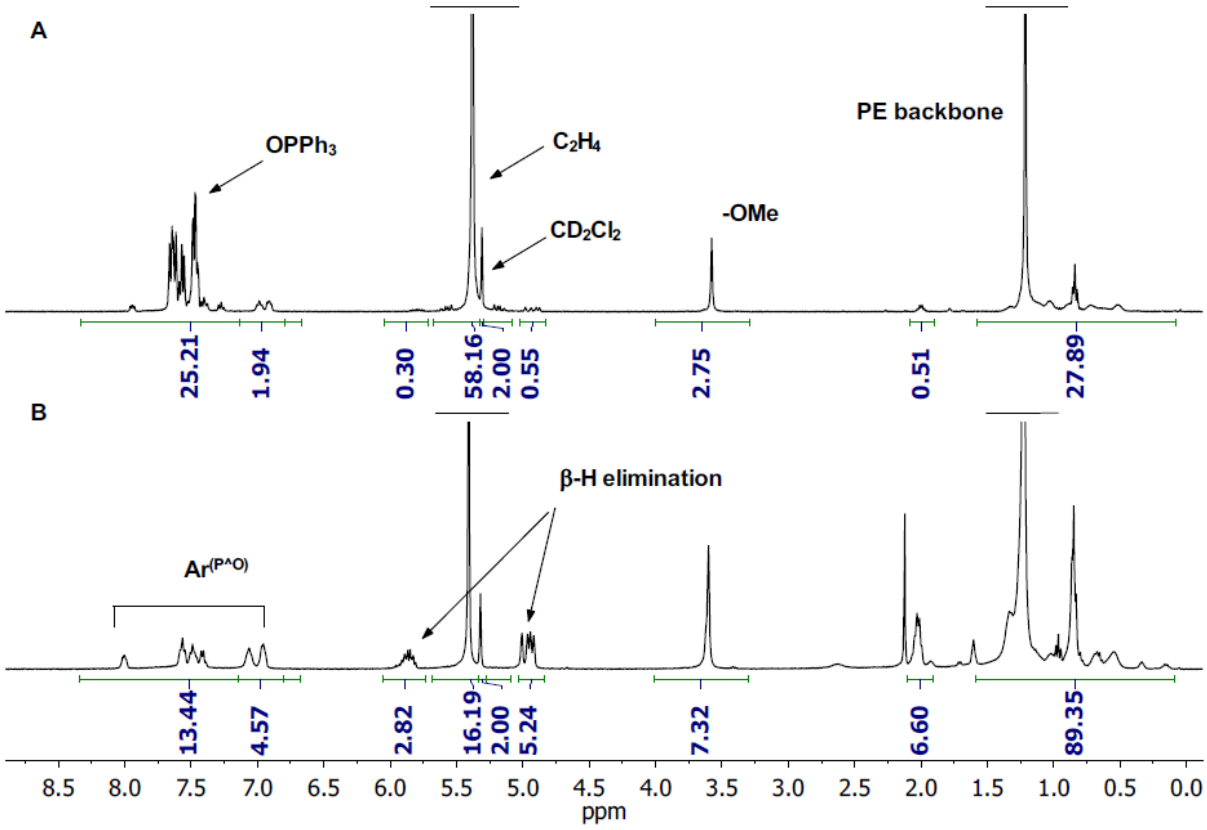


**Figure 3-13.** $^{1}$H NMR spectrum (400 MHz, $CD_2Cl_2$, -15 °C) of ethylene insertion into $^{MeO}$**1-OPPh$_3$** (A) and $^{MeO}$**1** (B) after ~140 minutes.

A similar trend of decreasing insertion rate constants with increasing coordination strength was also observed for the reaction of $^{MeO}$**1-L** and $^{MeO}$**1** with MA. Rate constants at 25 °C for the first insertion $^{1st}k_{1\text{-}L}$ range from 0.6 × $10^{-3}$ $s^{-1}$ for $^{MeO}$**1-OPBu$_3$** to 3.2 × $10^{-3}$ $s^{-1}$ for $^{MeO}$**1** at 0.02 mol $L^{-1}$ palladium and 0.3 mol $L^{-1}$ MA (Figure 3-14). Insertion of MA at 25 °C into the first insertion product [(P^O)Pd*C*H(C(O)OMe)$CH_2$Me] also proceeds fastest for $^{MeO}$**1** ($^{2nd}k_1$ = 9.2 × $10^{-5}$ $s^{-1}$) as compared to $^{MeO}$**1-OPBu$_3$** ($^{2nd}k_{1\text{-}OPBu3}$ = 8.2 × $10^{-6}$ $s^{-1}$; Figure 3-14). Since the rate constants for the second MA-insertion are significantly affected by the applied ligands it can be concluded that coordination strength of DMSO, $OPPh_3$ and $OPBu_3$ exceeds that of the carbonyl group in a possible 4-membered chelate $\kappa^2$-*C,O*-[(P^O)Pd*C*H(C(*O*)OMe)$CH_2$Me] This is in accordance with the isolation of the DMSO coordinated insertion product $\kappa^2$-*C,O*-[(P^O)Pd*C*H(C(O)OMe)$CH_2$Me(dmso)].[43]

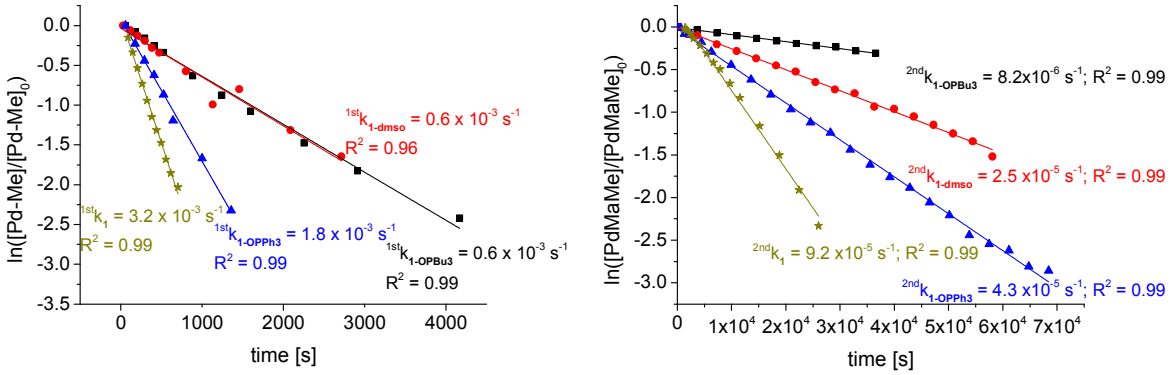


**Figure 3-14.** First-order consumption of Pd-*Me* by insertion of MA, [Pd] = 0.02 mol $L^{-1}$ in $CD_2Cl_2$ (left) and first-order consumption of Pd-CH(C(O)OMe)$CH_2$-*Me* by consecutive insertion of MA, [Pd] = 0.02 mol $L^{-1}$ in $CD_2Cl_2$ (right).

The first MA insertion into the Pd-Me bond of $^{MeO}$**1-OPPh$_3$** under pseudo first-order conditions has been studied in more detail in the temperature range from 5 °C to 34 °C. From an Eyring plot the activation parameters $\Delta H^{\#}$ = 75 kJ $mol^{-1}$ and $\Delta S^{\#}$ = -50 J $mol^{-1}K^{-1}$, were determined and the average free activation enthalpy was calculated to be $\Delta G^{\#}$ = 89 kJ $mol^{-1}$ at 25 °C (Figure 3-15). This can be compared to the parameters determined for MA insertion into $^{MeO}$**1** in the temperature range from -20 °C to 26 °C: $\Delta H^{\#}$ = 49 kJ $mol^{-1}$ and $\Delta S^{\#}$ = -138 J $mol^{-1}K^{-1}$, $\Delta G^{\#}$ = 90 kJ $mol^{-1}$.[61] The comparison reveals that the overall barrier is rather similar, but that $\Delta H^{\#}$ and $\Delta S^{\#}$ vary significantly. However, for insertion studies with $^{MeO}$**1-OPPh$_3$** the activation parameters obtained contain the monomer/$OPPh_3$ pre-equilibrium which can have a pronounced influence on $\Delta H^{\#}$ and especially $\Delta S^{\#}$.

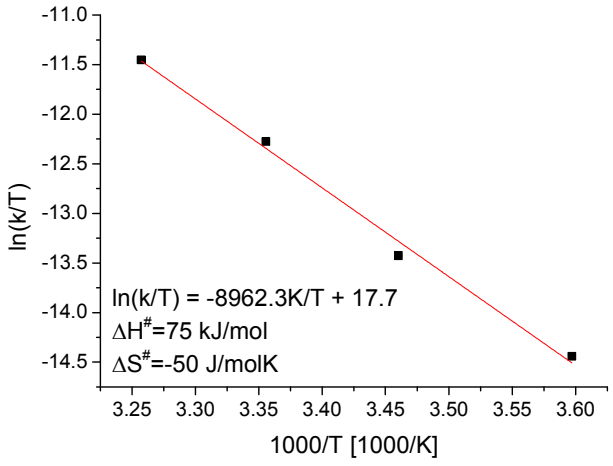


**Figure 3-15.** Eyring plot of MA insertion into Pd-Me bond of $^{MeO}$**1-OPPh$_3$**.

### 3.2.5 Influence of the Weakly Coordinating Ligand on Polymerization Activities

Replacement of pyridine or 2,6-lutidine by significantly weaker coordinating DMSO in catalyst precursors $^{MeO}$**1-L** has resulted in a nearly fourfold activity increase in ethylene homopolymerizations at a pressure of 5 bar. At this low ethylene pressure the equilibrium [(P^O)PdR(L)] + ethylene ⇆ [(P^O)PdR(ethylene)] + L (R = growing chain) is believed to be shifted far to the ethylene complex for L = DMSO, while pyridine or 2,6-lutidine compete much more effectively with ethylene and require higher ethylene concentrations in order to reach saturation kinetic conditions. Arguably, the most promising species to reach saturation kinetic behavior at the lowest possible ethylene concentration is the 'base-free' catalyst precursor (P^O)PdMe ($^{MeO}$**1**). However, the formation of $^{MeO}$**1$_n$** from $^{MeO}$**1** (e.g. after pyridine abstraction from $^{MeO}$**1-py**) and the low solubility of $^{MeO}$**1$_n$** so far prevented higher catalytic activities than observed for $^{MeO}$**1-dmso**.[44] Therefore, $^{MeO}$**1-OPR$_3$** (R = Ph, *o*-Tol, *p*-$CF_3C_6H_4$) described in this work are of interest for achieving saturation kinetic conditions at the lowest possible ethylene pressure. To this end, polymerizations at variable ethylene concentrations with the isolable defined precatalysts $^{MeO}$**1-dmso**, $^{MeO}$**1-OPBu$_3$** and $^{MeO}$**1-OPPh$_3$** were studied (Table 3-4). In addition, the polymerization of ethylene in the presence of $^{MeO}$**1** prepared by *in situ* chloride abstraction from ½ [{(**1-Cl**)-μ-Na}$_2$] with one equivalent of $AgBF_4$ was investigated. Note in this context, that [{($^{MeO}$**1-Cl**)-μ-Na}$_2$] contains up to one equivalent of coordinating solvents such as acetone or diethyl ether per Na depending on the preparative workup.

The analysis of the obtained polyethylenes revealed that under the same conditions all catalysts produce very similar polymers and hence the weakly coordinating ligands L have no pronounced influence on the molecular weight or the degree of branching under polymerization conditions (Table 3-4). As expected, molecular weight, melting point, and crystallinity increase with the ethylene pressure. This is consistent with a DFT study by Nozaki et al., which came to the conclusion that barriers for ethylene insertion and β-H elimination exhibit barriers of similar height and hence the preference of chain growth compared to chain transfer and branch formation increases with the ethylene concentration.[67]

**Table 3-4.** Ethylene Homopolymerization with $^{MeO}$**1-OPBu$_3$**, $^{MeO}$**1-OPPh$_3$**, $^{MeO}$**1-dmso**, and $^{MeO}$**1** at different ethylene pressures.

| entry | catalyst precursor | p [bar] | yield [g] | TOF [× $10^4$]$^a$ | $M_n$$^b$ [$10^3$ g/mol] | $M_w/M_n$$^b$ | $T_m$$^c$ [°C] | cryst.$^c$ [%] |
|---|---|---|---|---|---|---|---|---|
| 4-1 | $^{MeO}$**1-OPBu$_3$** | 10 | 8.2 | 15 | 10.3 | 2.2 | 133 | 73 |
| 4-2 | $^{MeO}$**1-dmso** | 10 | 8.6 | 15 | 11.1 | 2.1 | 134 | 71 |
| 4-3 | $^{MeO}$**1-OPPh$_3$** | 10 | 8.4 | 15 | 10.1 | 2.2 | 133 | 72 |
| 4-4 | $^{MeO}$**1** (*in situ*) | 10 | 7.0 | 13 | 10.8 | 2.1 | 133 | 72 |
| 4-5 | $^{MeO}$ **1-OPBu$_3$** | 5 | 6.0 | 11 | 9.3 | 2.1 | 130 | 71 |
| 4-6 | $^{MeO}$**1-dmso** | 5 | 7.8 | 14 | 8.3 | 2.2 | 130 | 69 |
| 4-7 | $^{MeO}$**1-OPPh$_3$** | 5 | 7.0 | 12 | 8.5 | 2.2 | 130 | 69 |
| 4-8 | $^{MeO}$**1** (*in situ*) | 5 | 9.1 | 17 | - | - | - | - |
| 4-9 | $^{MeO}$**1-OPBu$_3$** | 3.5 | 4.2 | 8 | 7.9 | 2.1 | 128 | 68 |
| 4-10 | $^{MeO}$**1-dmso** | 3.5 | 4.7 | 9 | 6.9 | 2.2 | 128 | 69 |
| 4-11 | $^{MeO}$**1-OPPh$_3$** | 3.5 | 5.2 | 9 | 6.4 | 2.4 | 128 | 66 |
| 4-12 | $^{MeO}$**1** (*in situ*) | 3.5 | 6.7 | 12 | 7.3 | 2.1 | 128 | 69 |
| 4-13 | $^{MeO}$**1-OPBu$_3$** | 2 | 2.6 | 5 | 5.6 | 2.2 | 124 | 64 |
| 4-14 | $^{MeO}$**1-dmso** | 2 | 2.4 | 4 | 5.1 | 2.2 | 123 | 64 |
| 4-15 | $^{MeO}$**1-OPPh$_3$** | 2 | 3.3 | 6 | 5.0 | 2.3 | 123 | 63 |
| 4-16 | $^{MeO}$**1** (*in situ*) | 2 | 2.8 | 5 | 4.9 | 2.1 | 124 | 65 |

Reaction conditions: 100 mL of toluene; [Pd] = 40 µmol $L^{-1}$; 90 °C, 30 minutes polymerization time. $^a$[mol($C_2H_4$) mol(Pd)$^{-1}$ $h^{-1}$];$^b$determined by GPC in 1,2,4-trichlorobenzene at 160°C; $^c$determined by DSC.

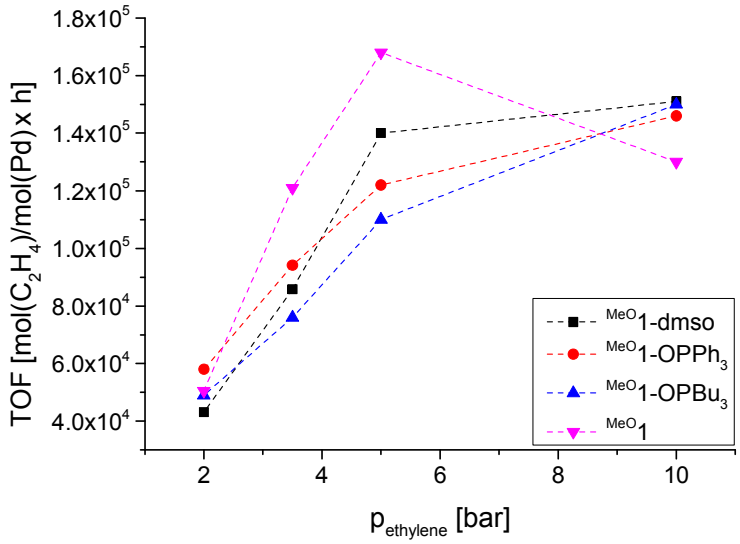


**Figure 3-16.** Dependence of average activity in ethylene homopolymerization on pressure for $^{MeO}$**1** and $^{MeO}$**1-L** (L = DMSO, $OPBu_3$, $OPPh_3$). Reaction conditions: t = 30 minutes; T = 90 °C; V(toluene) = 100 mL; [Pd] = 40 µmol $L^{-1}$. Dashed lines are merely a guide to the eye).

The polymerization results show that *in situ* generated $^{MeO}$**1** as well as $^{MeO}$**1-OPPh$_3$**, $^{MeO}$**1-OPBu$_3$**, and $^{MeO}$**1-dmso** exhibit essentially similar activities at a given ethylene pressure (2, 3.5, 5, and 10 bar, 90 °C, Figure 3-16). As far as slight differences beyond experimental error are observed, these tend to reflect the coordination strength of the ligand L, or absence of L ([{($^{MeO}$**1-Cl**)-μ-Na}$_2$] / $AgBF_4$). These findings qualitatively agree with previous studies of the effect of DMSO on ethylene polymerization activities with $^{MeO}$**1-dmso**, which showed that the equilibrium [(P^O)PdR(ethylene)] + DMSO ⇆ [(P^O)PdR(dmso)] + ethylene (R = growing chain) does render a portion of the metal centers inactive by coordination of the one equivalent of DMSO introduced with the catalyst precursor. However, the ethylene complex is strongly favored in this equilibrium already at low ethylene pressure, such that the inactive portion is rather small, and saturation kinetic conditions are met.[44]

As outlined, equilibria [(P^O)PdR(L)] + monomer ⇆ [(P^O)R(monomer)] + L are relevant in polymerization studies (activation of catalyst precursors, reversible deactivation of active species) as well as NMR investigations of insertion rate constants (pre-equilibria to insertion). It is worth noting that the effect of the coordination strength of L will be much more pronounced in NMR studies ([Pd] ~ $10^{-2}$ mol $L^{-1}$) vs. polymerizations studies ([Pd] ~ $10^{-4}$ to $10^{-6}$ mol $L^{-1}$), as here concentrations of metal species and consequently of free L, liberated from the metal precursor are typically much higher, while monomer concentrations are usually roughly similar. That might also explain why no influence of the ligand L on the degree of polymerization is observed in the polymerization study, in contrast to the previous observation that under NMR-conditions $^{MeO}$**1** showed pronounced β-H elimination compared to $^{MeO}$**1-OPPh$_3$** (*vide supra*).

While all the above experimental observations fit into this conclusive picture, they also suggest that the strong dependence of average polymerization rates in the regime of up to 5 bar ethylene pressure (Figure 3-16) is *not* simply related to competitive relative binding of monomer vs. L (or sulfonate). For the low pressure polymerizations at 2, 3.5, and 5 bar ethylene a pronounced drop in catalytic activity over time is observed by mass-flow monitoring. Thus at 2 bar the ethylene uptake into the reactor decreases to 65-40% of its initial value after 30 minutes polymerization time. At 5 bar the decrease of ethylene uptake is not as pronounced, but still drops to 80 – 70% of the initial values (Figure 3-17). This indicates that the catalyst stability depends on the ethylene pressure and might be explained with suppression of β-H elimination with increasing ethylene concentration.

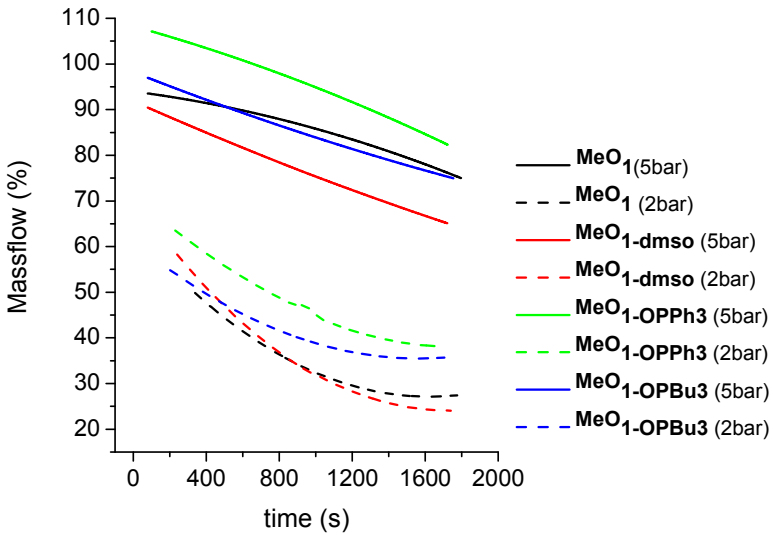


**Figure 3-17.** Ethylene mass flow versus time for polymerization at 2 bar and 5 bar ethylene pressure.

The choice of catalyst precursor, i.e. [{(**1-Cl**)-μ-Na}$_2$] plus $AgBF_4$, $^{MeO}$**1-OPBu$_3$**, $^{MeO}$**1-OPPh$_3$**, or $^{MeO}$**1-dmso**, has a measurable influence on the activity in ethylene-MA-copolymerizations at low ethylene concentrations which correlates to the presence and the nature of the coordinating ligand and its equilibrium constant $K_L$ vs. DMSO: At 3.5 bar ethylene, 0.5 mol $L^{-1}$ MA *in situ* generated $^{MeO}$**1** produces 50% more copolymer than $^{MeO}$**1-OPBu$_3$**, while the copolymer composition remains essentially identical (Table 3-5, entry 5-1 vs. 5-4). The increase in activity is steady in the order $^{MeO}$**1-OPBu$_3$** < $^{MeO}$**1-dmso** < $^{MeO}$**1-OPPh$_3$** < $^{MeO}$**1** which reflects the coordination strengths of the present $OPR_3$- and DMSO-ligands (*vide supra*, Table 3-1). Also note that with decreasing coordination strength a slight increase in molecular weight is evident (Table 3-5). This increase in molecular weight is tentatively explained by a ligand induced opening of six-membered chelates [(P^O)Pd*C*H(R)CH$_2$CH(C(*O*)COMe)CH$_2$R'] and concomitant β-H elimination, while opening by monomer leads to the following insertion.

While the increase in activity is limited, *in situ* generated $^{MeO}$**1**, i.e. [{($^{MeO}$**1-Cl**)-μ-Na}$_2$] plus $AgBF_4$ proves to be the most active catalyst for ethylene-MA copolymerizations. This is quite remarkable since from a synthetic point of view [{($^{MeO}$**1-Cl**)-μ-Na}$_2$] is easily available in a one step reaction from the sodium salt of the ligand $^{MeO}$**(P^O)Na** and [(cod)PdMeCl] without further time consuming transformations.

**Table 3-5.** Ethylene-methyl acrylate copolymerization.

| entry | catalyst precursor | yield [g] | $X_{MA}$ [%][a] | TOF($C_2H_4$)[b] × $10^2$ | TOF(MA)[c] × $10^2$ | $M_n$[d] | $M_w/M_n$[e] |
|---|---|---|---|---|---|---|---|
| 5-1 | $^{MeO}$**1-OPBu$_3$** | 0.8 | 14.2 | 19.2 | 3.2 | 2.0 | 1.7 |
| 5-2 | $^{MeO}$**1-dmso** | 0.9 | 14.8 | 20.4 | 3.6 | 2.3 | 1.7 |
| 5-3 | $^{MeO}$**1-OPPh$_3$** | 1.0 | 13.7 | 24.0 | 3.8 | 2.5 | 1.8 |
| 5-4 | $^{MeO}$**1** (*in situ*) | 1.2 | 13.2 | 28.9 | 4.4 | 2.6 | 1.8 |

Reaction conditions: total volume toluene + MA: 50 mL; [MA] = 0.5 mol $L^{-1}$, 3.5 bar ethylene pressure; 93 °C; 20 µmol Pd(II); 1 hour reaction time. [a]Determined by $^1$H NMR in $CDCl_3$; [b][mol($C_2H_4$) mol(Pd)$^{-1}$ $h^{-1}$]; [c][mol (MA) mol (Pd)$^{-1}$ $h^{-1}$]; [d][$10^3$ g $mol^{-1}$], determined by $^1$H NMR in $CDCl_3$ at 25 °C; [e]determined by GPC in THF at 50°C.

## 3.2.6 Role of Chelate Formation in Methyl Acrylate (Co)polymerization

While rate constants for the MA insertion from NMR studies vary by factors of 5-10 (Figure 3-14), the polymer yields only vary by a factor of 1.5 (Table 3-5). In addition to the aforementioned effect of different concentrations in NMR studies vs. polymerization experiments, the stability of 6-membered chelates **C** formed in copolymerization by coordination of a penultimate incorporated MA-derived repeat unit can contribute to reducing the effect of other ligands L on activity at a given amount of catalyst precursor added per reaction volume (Scheme 3-3). Equilibration of these chelates with incoming olefin is strongly shifted to **C** as compared to the olefin-coordinated species **D**. Even if olefin insertion from species **A** and **B** were sensitive to the coordination strength of L due to the equilibration according to $K_A$ and $K_B$, the following rate-determining insertion from **D** is mainly affected by $K_{C2}$ and so mostly insensitive to L as long as L is not significantly stronger coordinating than the *κ-O* carbonyl oxygen in **C**.

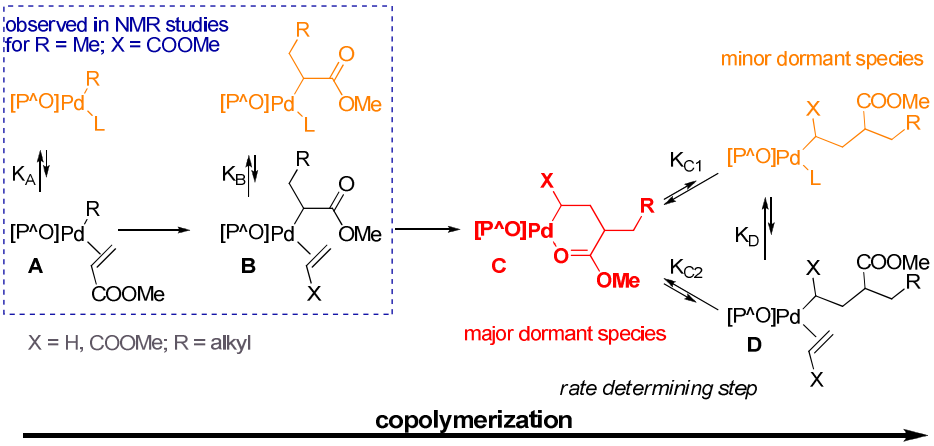


**Scheme 3-3.** Rate determining equilibria in the copolymerization of ethylene with MA.

For a quantitative investigation of the coordination strength of 6-membered chelates **C** the palladium complex $^{MeO}\mathbf{3}_{MA\text{-}rac/meso}$ was synthesized by two consecutive insertions of MA into the Pd-Me bond of $^{MeO}\mathbf{1}$. By contrast, to the synthetic route reported before, starting from the multinuclear complex $^{MeO}\mathbf{1}_{n}$,[44] an alternative approach affording pure $^{MeO}\mathbf{3}_{MA\text{-}rac/meso}$ in high yields was found. The reaction of [{($^{MeO}$**1-Cl**)-μ-Na}$_2$] with $AgBF_4$ in the presence of MA (20 equivalents) in dichloromethane at 60 °C in a sealed tube for 90 minutes, followed by evaporation of solvent and extraction with toluene afforded the two diastereomers $^{MeO}\mathbf{3}_{MA\text{-}meso}$ and $^{MeO}\mathbf{3}_{MA\text{-}rac}$ (2:1) in high purity and good yields (> 70%, Scheme 3-4).

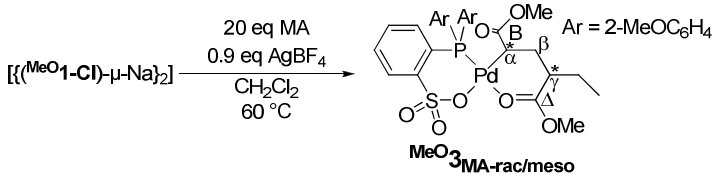


**Scheme 3-4.** Synthesis of $^{MeO}\mathbf{3}_{MA\text{-}rac/meso}$.

The stereochemistry of the two diastereomers $^{MeO}\mathbf{3}_{MA\text{-}meso}$, $^{MeO}\mathbf{3}_{MA\text{-}rac}$ could be assigned by single-crystal X-ray diffraction analysis (Figure 3-18). Suitable crystals were obtained from a saturated solution of $^{MeO}\mathbf{3}_{MA\text{-}rac/meso}$ in a benzene-pentane mixture at 4 °C. The solid state structure is disordered with both diastereomers $^{MeO}\mathbf{3}_{MA\text{-}rac/meso}$ occupying identical positions. The refinement converged to an occupancy of 64:36 for the both stereoisomers which is in agreement with the ratio determined by NMR spectroscopy.[44]

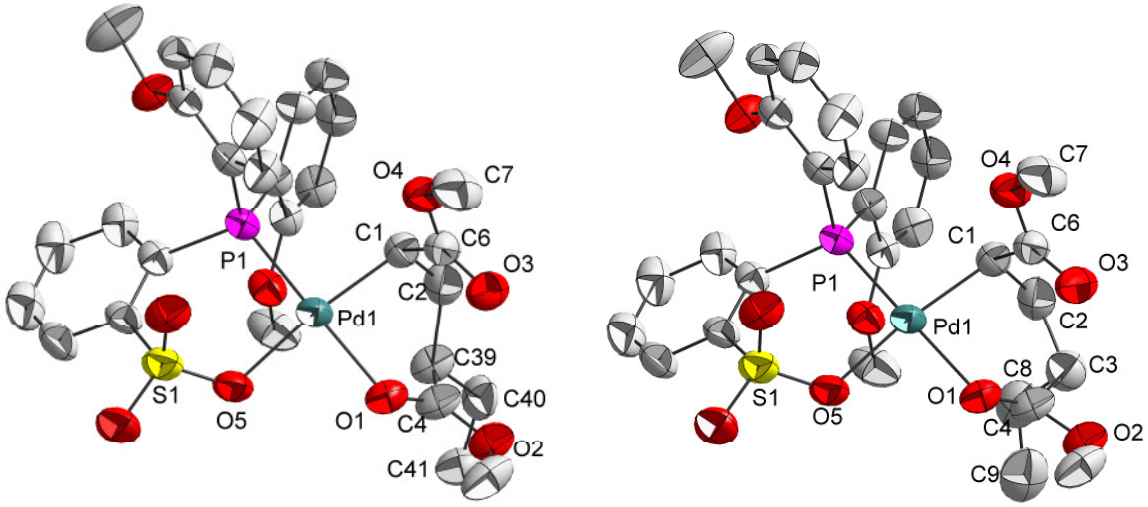


**Figure 3-18.** Molecular structures of $^{MeO}\mathbf{3}_{MA\text{-}rac}$ (left) and $^{MeO}\mathbf{3}_{MA\text{-}meso}$ at 50% probability ellipsoids. All hydrogen atoms and co-crystallized solvent molecules are omitted for clarity. Selected bond length [Å] and angles [°]: Pd(1)-P(1) = 2.217(1); Pd1-C1 2.062(4); Pd1-O1 = 2.129(3); Pd1-O5 = 2.113(3); C1-C2 = 1.509(7); C1-C6 = 1.502(6); C6-O3 = 1.208(6); C6-O4 = 1.337(7); C4-O1 = 1.217(6); C4-O2 = 1.295(6); P1-Pd1-O5 = 95.1(1); C1-Pd1-O1 = 86.4(2).

In the major stereoisomer $^{MeO}\mathbf{3}_{MA\text{-}rac}$, which results from two consecutive 2,1 acrylate insertions with the opposite stereochemistry the ethyl group (C40, C41) is positioned syn to the carbmethoxy group (O3-C6-O4-C7), while a anti-disposition is found in $^{MeO}\mathbf{3}_{MA\text{-}meso}$, which results from two insertions with the same stereochemistry (Figure 3-18). The bond lengths around the Pd-atom are comparable to those of the 5-membered chelate complex [(P^O)Pd((MeOOC)*C*HCH$_2$C(*O*)Me)][47] and other related CO-methyl acrylate insertion products differing from the latter in the nature of the (P^X) ligand.[111,112] The enlarged chelate size in $^{MeO}\mathbf{3}_{MA\text{-}rac/meso}$ accounts for an increase of the binding angle O1-Pd-C1 (86.4(2) vs. 82.6(2) in the aforementioned 5-membered chelate complex).

The coordination strength of the chelate was studied in relation to DMSO, since a directly observable equilibrium exists at room temperature, as has been reported before.[44] In contrast, a complete opening was observed for pyridine, whereas for the relevant olefins MA or ethylene no opening was observed at all.[44] The equilibrium constants $K_{C1\text{-}DMSO}(T) = [^{MeO}\mathbf{3}_{MA\text{-}rac/meso}\text{-}\mathbf{dmso}] / ([^{MeO}\mathbf{3}_{MA\text{-}rac/meso}] \times [DMSO])$ were determined by $^{13}$C NMR spectroscopy in the temperature range between 278 K to 308 K, based on the chemical shift of the Δ-carbonyl resonances (Figure 3-19, Table 3-6) according to the equations:

$$\delta_{measured} = \alpha\delta_{closed} + \beta\delta_{opened} \quad \text{and} \quad K_{C1-dmso} = \frac{\beta}{\alpha[\mathrm{DMSO}]_0 - \alpha\beta[^{MeO}\mathbf{3}_{MA\text{-}meso/rac}]_0}$$

The $^{13}$C NMR shift of the Δ-carbonyl resonances for the opened chelate ($\delta_{opened}$) is not directly accessible and it has been assumed that the Δ-carbonyl resonance has a similar shift as in $^{MeO}\mathbf{3}_{MA\text{-}rac/meso}\text{-}\mathbf{py}$, where the equilibrium is completely shifted to the open form (Figure **3-19**).

**Table 3-6.** Determination of $K_1(T)$ at variable temperatures for two different DMSO concentrations.

| **T** [K] | $\delta_{closed}$[a] [ppm] | $\delta_{opened}$[b] [ppm] | c($^{MeO}\mathbf{3}_{MA\text{-}rac/meso}$) [$10^{-2}$ mol/L] | **c(DMSO)** [mol/L] | $\delta_{measured}$ [ppm] | **chelate open** [%] | $K_{C1\text{-}DMSO}$ |
|---|---|---|---|---|---|---|---|
| 278 | 185.39 | 175.87 | 4.18 | 0.23 | 181.95 | 36.1 | 2.57 |
| 278 | 185.39 | 175.87 | 4.34 | 0.73 | 179.22 | 64.8 | 2.61 |
| 288 | 185.39 | 175.95 | 4.09 | 0.23 | 182.07 | 35.2 | 2.46 |
| 288 | 185.39 | 175.95 | 3.92 | 0.73 | 179.38 | 63.7 | 2.47 |
| 298 | 185.40 | 176.02 | 3.86 | 0.23 | 182.20 | 34.1 | 2.34 |
| 298 | 185.40 | 176.02 | 3.60 | 0.73 | 179.53 | 62.6 | 2.35 |
| 308 | 185.42 | 176.09 | 3.58 | 0.23 | 182.28 | 33.7 | 2.28 |
| 308 | 185.42 | 176.09 | 3.16 | 0.73 | 179.62 | 62.2 | 2.30 |

[a]Chemical shift of the carbonyl atom Δ, determined by $^{13}$C NMR of $^{MeO}\mathbf{3}_{MA\text{-}rac/meso}$ in $CD_2Cl_2$ (0.46 mol L$^{-1}$); [b]chemical shift of the carbonyl atom Δ, determined by $^{13}$C NMR of **3** $^{MeO}\mathbf{3}_{MA\text{-}rac/meso}\text{-}\mathbf{pyr}$ in $CD_2Cl_2$ (0.39 mol L$^{-1}$).

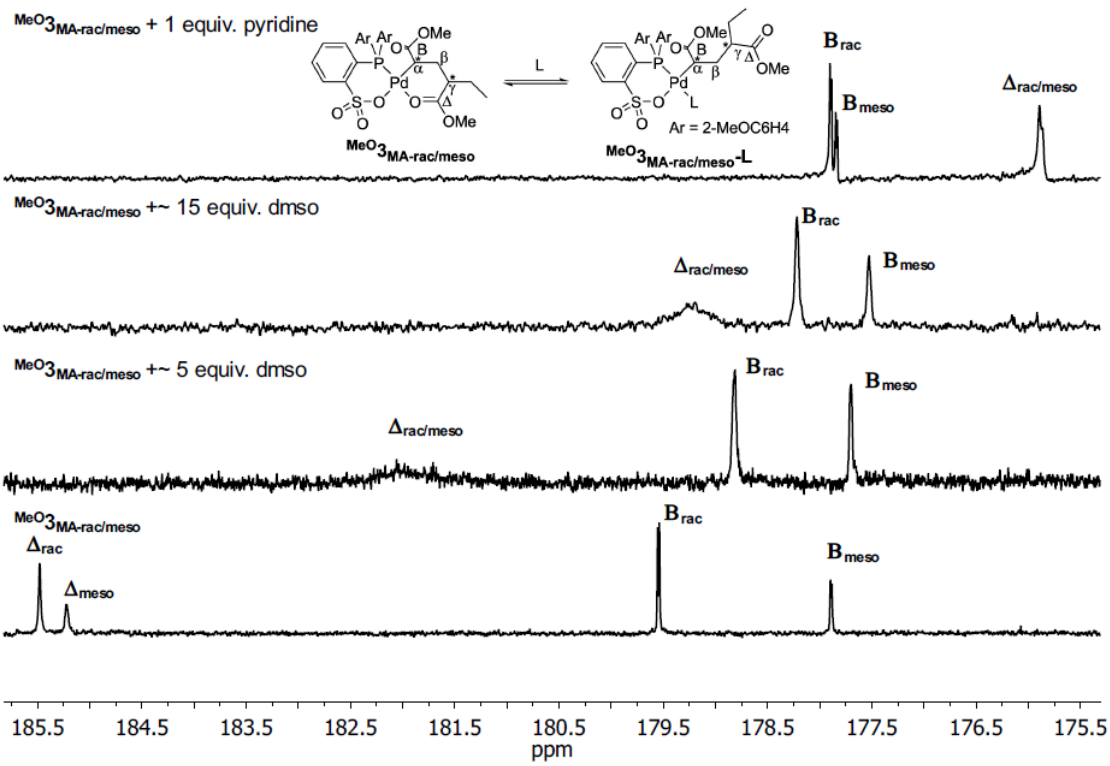


**Figure 3-19.** $^{13}C$ NMR spectra (carbonyl region, 150 MHz, $CD_2Cl_2$, 5 °C) of pure $^{MeO}\mathbf{3}_{MA\text{-}rac/meso}$, $^{MeO}\mathbf{3}_{MA\text{-}rac/meso}$ in the presence of 5 and 15 equiv. DMSO, and in the presence of 1 equiv. pyridine. Note that a fast site exchange between free and chelated carbonyl Δ resulted in the observation of one averaged resonance for $^{MeO}\mathbf{3}_{MA\text{-}meso}$ and $^{MeO}\mathbf{3}_{MA\text{-}rac}$.

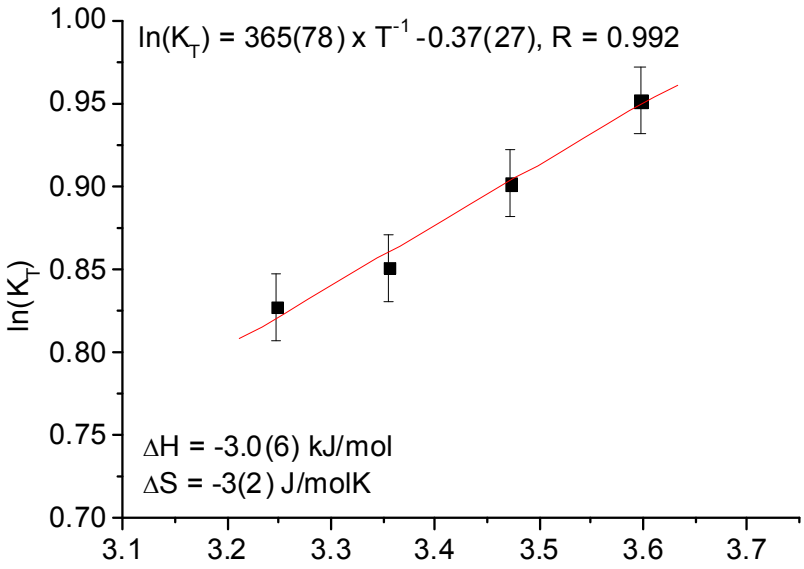


**Figure 3-20.** Van't Hoff plot of the equilibrium between $^{MeO}\mathbf{3}_{MA\text{-}rac/meso}$ and $^{MeO}\mathbf{3}_{MA\text{-}rac/meso}$**-dmso**, determined by variable temperature $^{13}C$ NMR spectroscopy at T = 278 to 308 K, $CD_2Cl_2$.

The values of the reaction enthalpy $\Delta H° = -3.0(6)$ kJ mol$^{-1}$ and entropy $\Delta S° = -3(2)$ J mol$^{-1}$ K$^{-1}$ were obtained by a Van't Hoff plot (Figure 3-20). The observed entropy loss is surprisingly low for a chelate opening process A + B ⇆ C. Indeed, for cationic

(N^N)Pd(II) complexes much more negative entropies have been observed.[18,113] However, it has also been noted that the nature of the incoming ligand (L) in chelate opening can have an unexpectedly strong impact on the reaction entropy. For the 5-membered chelate [(N^N)Pd(R*C*(H)OC(*O*)$CH_3$)] it was found that opening with acetonitrile resulted in a much lower entropy ($\Delta S$ = -38 J $mol^{-1}$ $K^{-1}$) in comparison to the opening with ethylene ($\Delta S$ = -96 J $mol^{-1}$ $K^{-1}$). This was tentatively related to acetonitrile losing fewer degrees of freedom by its linear coordination by comparison to $\eta^2$-coordination of ethylene, also a possible stronger organization of the solvent by free acetonitrile vs. ethylene; and motion of the OC(*O*)$CH_3$-moiety being more extensively restricted by ethylene coordination.[113]

As outlined the equilibrium constant for the opening of the double acrylate insertion product $^{MeO}$**3**$_{MA\text{-}rac/meso}$ with ethylene ($K_{C2\text{-}E}$, cf. Scheme 3-3) is of relevance in the context of copolymerizations affording linear ethylene-acrylate copolymers. An opening of the chelate by olefinic substrate could not be observed even at low temperatures, thus, a direct determination especially at the elevated temperatures typically employed for polymerization reactions (80 °C) is not possible.[43] $K_{C2\text{-}E}$(353 K) could be estimated by combining the equilibrium constant for chelate opening with DMSO ($K_{C1\text{-}DMSO}$, with R = Me) with the relative binding strength ($K_{A\text{-}E/DMSO}$) of DMSO vs. ethylene ([(P^O)PdR(dmso)] + $C_2H_4$ ⇆ [(P^O)PdR($C_2H_4$)] + DMSO). The relative binding strength was determined from the observed inhibition of polymerization rates by variable amounts of added DMSO in ethylene polymerization experiments at 80 °C and 10 bar ethylene pressure (Table 3-7, c.f. Chapter 7.1.11).

**Table 3-7.** Inhibition of catalyst activity by DMSO.

| entry | $c_{DMSO}$ [$10^{-3}$ mol $L^{-1}$] | TOF [$10^4$ mol($C_2H_4$) mol(Pd)$^{-1}$ $h^{-1}$] | polymer yield [g] | $M_n$ [a] [$10^3$ g $mol^{-1}$] | $M_w/M_n$ [a] |
|---|---|---|---|---|---|
| 7-1 | 0.04 | 9.4 (= $TOF_{max}$) | 4.6 | 16.2 | 1.9 |
| 7-2 | 1.27 | 3.5 | 1.7 | 7.8 | 2.2 |
| 7-3 | 2.06 | 2.2 | 1.1 | 5.6 | 1.7 |
| 7-4 | 4.11 | 1.4 | 0.7 | n.d. | n.d. |

Reaction conditions: 100 mL of toluene; 80 °C; 30 minutes polymerization time; 3.5 µmol Pd; 10 bar ethylene pressure. [a] determined by GPC.

A plot of $TOF_{max}$/TOF against the ratio of concentrations [DMSO]/[ethylene] gives $K_{A\text{-}E/DMSO}$(353 K) = 1.1(2) × $10^{-3}$ (Figure 3-21, c.f. Chapter 7.1.11). Recently, Claverie et al. estimated the relative binding strength of ethylene vs. pyridine for $^{MeO}$**1-pyr** to $K_{A\text{-}E/py} \sim 10^{-7}$.[70] The higher value for $K_{A\text{-}E/DMSO}$ compared to $K_{A\text{-}E/py}$ is consistent with DMSO being the more labile ligand.

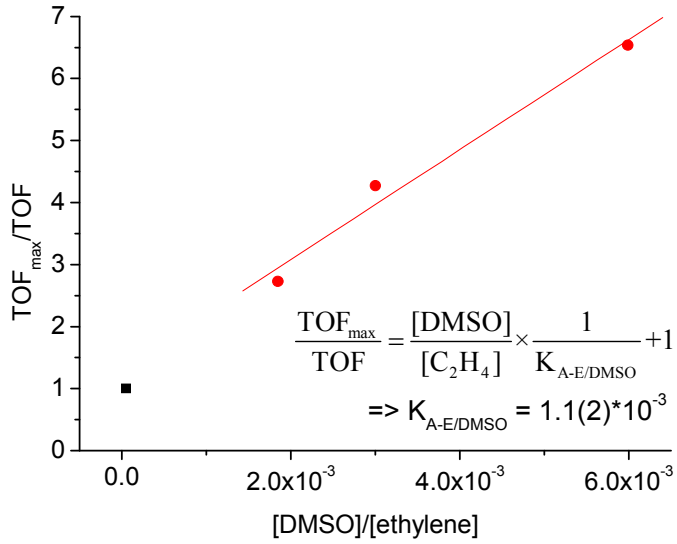


**Figure 3-21.** Plot of $TOF_{max}/TOF$ in ethylene polymerizations with variable amounts of added DMSO vs. the ratio of DMSO to ethylene concentration in the polymerization mixture (●). Note that DMSO liberated by dissociation of the catalyst precursor, $^{MeO}$**1-dmso**, is not considered, which results in a negligible error given that added DMSO is in excess (≥ 30 equiv.). The $TOF_{max}/TOF$ for a polymerization without added DMSO is also shown (■).

Combining $K_{A\text{-}E/DMSO}$ with $K_{C1\text{-}DMSO}(353\ K) \approx 1.9\ L\ mol^{-1}$ extrapolated from the thermodynamic data (*vide supra*), $K_{C2\text{-}E} = K_{C1\text{-}DMSO} \times K_{A\text{-}E/DMSO}$, yielded an estimated value of $K_{C2\text{-}E}(353\ K) \approx 2\times10^{-3}\ L\ mol^{-1}$ for the chelate opening with ethylene at 80 °C. The equilibrium constant for the chelate opening with ethylene corresponds to a $\Delta H$ of -32 kJ mol$^{-1}$ at 353 K. This is in good agreement with an energy gain of ca. 35 kJ mol$^{-1}$ for this process calculated previously by DFT methods.[44] Due to the weaker coordination strength of the electron poor methyl acrylate these calculations further predict that a chelate opening with MA is only associated with an energy gain of about 15 kJ mol$^{-1}$. In comparison to this 58 kJ mol$^{-1}$ are released by a coordination of MA to $^{MeO}$**1** with a free coordination site. This illustrates the stability of the six-membered chelate, which hinders polymerization. For L = $OPPh_3$ with the binding strength of $OPPh_3$ vs. DMSO at 80 °C being $3.5 \times 10^{-1}$ (*vide supra*, Figure 3-3) equilibrium constants are calculated to be $K_{A\text{-}E/OPPh3}$ ($\sim K_B \sim K_D$) = $3.1 \times 10^{-3}$ and $K_{C1\text{-}OPPh3} = 6.7 \times 10^{-1}$, which reflects the weaker binding of the $OPPh_3$ ligand compared to DMSO. Accordingly, olefin insertion from **D** represents a bottle-neck in the MA-ethylene copolymerization which is intrinsically linked to the coordination strength of the carbonyl oxygen in 6-membered chelates **C** (Scheme 3-3).

## 3.3 Summary and Conclusion

Phosphine oxides are easily available monodentate ligands with a defined coordination site and allow wide manipulation of coordination strength due to manifold possible steric and electronic modifications. Determination of the coordination strength $K_L$ towards the Pd center of (P^O)PdMe for several phosphine oxides $OPR_3$ in comparison to DMSO by $^1H$ NMR spectroscopy revealed that coordination strength decreases with increasing steric bulk and electron deficiency. The investigated $OPR_3$ ligands exhibit equilibrium constants from ~3 to 0.001 vs. DMSO decreasing in the order R: Bu ≈ Oct > Ph > *o*Tol ≈ *p*$CF_3$-$C_6H_4$ > 3,5-$(CF_3)_2C_6H_3$. Preparative synthesis afforded the new complexes $^{MeO}$**1-OPBu$_3$**, $^{MeO}$**1-OPOct$_3$** and $^{MeO}$**1-OPPh$_3$**, as shown by complete characterization by NMR- and IR-spectroscopy, mass spectrometry and elemental analysis. In addition, X-Ray diffraction analysis of $^{MeO}$**1-OPBu$_3$** and **1-OPPh$_3$** confirm the *κ-O* coordination of the phosphine oxides to palladium. So far $^{MeO}$**1-OPPh$_3$** with $K_{OPPh3}$ = 0.2 vs. DMSO is the weakest coordinated stable (P^O)PdMe complex synthesized. Studies with weaker coordinating ligands disclosed that for [(P^O)PdMe(L)] the minimum of coordination strength for L is limited due the ability of the (P^O)PdMe fragment to form ill-defined multinuclear palladium complexes $^{MeO}$**1$_n$** by bridging coordination of the sulfonate. Weaker coordinating ligands still can temporally stabilize the (P^O)PdMe fragment, but ultimately $^{MeO}$**1$_n$** forms as evidenced by NMR- and IR-spectroscopic studies.

Detailed insertion studies by NMR-techniques showed that *in situ* generated $^{MeO}$**1** exhibits the highest rate constants for ethylene-insertion and for the first and second MA-insertion.

Homo- and copolymerization studies revealed that the most active catalyst $^{MeO}$**1** is available by *in situ* chloride abstraction from [{($^{MeO}$**1-Cl**)-μ-Na}$_2$]. So far $^{MeO}$**1** generated by *in situ* chloride abstraction from [{($^{MeO}$**1-Cl**)-μ-Na}$_2$] represents the best model substances for a species free of significantly coordinating, monodentate ligand L with the highest possible activity in ethylene-MA-copolymerizations.

Comparison between the insertion and the copolymerization studies revealed that an influence of the ligand L on reactivity for catalyst precursors $^{MeO}$**1-L** exhibiting different weakly coordinating ligands –as obvious in the NMR experiments– is strongly diminished in the copolymerization studies. At the lower catalyst concentrations of preparative polymerization experiments by comparison to NMR studies, the monodentate ligand L formed by dissociation of the catalyst precursor has a lower impact. Here, activity is mainly

controlled by the opening of 6-membered $\kappa^2$-*C,O* chelates [(P^O)Pd*C*H(R)$CH_2$CH(C(*O*)COMe)$CH_2R^2$] formed in the copolymerization by coordination of a penultimate incorporated MA-derived repeat unit. The coordination strength of the related 6-membered chelate complex $^{\mathbf{MeO}}\mathbf{3}_{\mathbf{MA\text{-}rac/meso}}$ resulting from two consecutive insertion of MA into the Pd-Me bond has been studied as a model for these resting states. A fast equilibrium for the chelate opening is observed at room temperature with DMSO and the thermodynamic parameters $\Delta H_1° = -3.0(6)$ kJ $mol^{-1}$ and $\Delta S_1° = -3(2)$ J $mol^{-1}$ $K^{-1}$ could be obtained via a $^{13}C$ NMR study from a Van't Hoff plot. Combined with polymerization inhibition studies affording the relative binding strength of ethylene vs. DMSO, an approximation for the chelate opening with ethylene ($^{\mathbf{MeO}}\mathbf{3}_{\mathbf{MA\text{-}rac/meso}}$ + $C_2H_4$ ⇆ $^{\mathbf{MeO}}\mathbf{3}_{\mathbf{MA\text{-}rac/meso}}$-$C_2H_4$) under typical polymerization conditions (80 °C) yielded $K_{C2\text{-}E}$ (353 K) ≈ 2 x$10^{-3}$ L $mol^{-1}$. These results reveal that in the presence of weak coordinating ligands like DMSO or $OPPh_3$ the opening of such 6-memberd chelates represents a bottle-neck in the MA-ethylene copolymerization which is intrinsically linked to the coordination strength of the chelating carbonyl oxygen.

# 4. Exploring Electronic and Steric Effects on the Insertion and Polymerization Reactivity of Phosphinesulfonato Pd(II) catalysts

## 4.1 Introduction

The previous studies with catalyst precursors $^{MeO}$**1-L** revealed that weakly coordinating ligands L can enhance the catalyst activity at low ethylene concentrations and give access to copolymers with high methyl acrylate content. However, in copolymerization experiments with polar monomers it turned out that the activity is intrinsically limited by formation of six-membered κ-*O* coordinated chelates, which result from (co)monomer insertion after an incorporation of MA. Furthermore, an application of materials based on copolymers with a reasonable MA incorporation is still hampered by the low molecular weights. Such limitations cannot be overcome by variation of the monodentate ligand L in $^{MeO}$**1-L**, as this ligand is not coordinated in the active species and does not affect polymer microstructure. Accordingly, the catalyst design has to be adjusted by steric and electronic variations of the phosphinesulfonato ligand.

The influence of the non-chelating aryl substituents at phosphorus on the activity of (P^O)PdMe catalysts in polymerization reactions has been studied by Claverie[28,37] and Rieger et al.[31] The substitution of the anisyl moiety for bulky naphthyl, phenanthryl, anthracenyl or 1-methoxynaphtalene in general seems to reduce polymerization activity, molecular weight and polar monomer incorporation.[28,31] For catalysts with ligands bearing very bulky 2-(2',6'$(MeO)_2C_6H_3$)$C_6H_4$ moieties polar monomer incorporation is diminished, too, but molecular weights and catalyst activity are significantly enhanced in ethylene homopolymerization.[24,43] This might be explained by the adjustment of the steric bulk in the axial position in regard to the palladium atom in this case. For the related cationic Pd(II) diimine complexes the blocking of the axial positions has been found to be essential for the inhibition of chain transfer and the production of high molecular weight polymers.[3] The substitution of the ortho methoxy by a MeS-group drastically reduces activity but seems to lead to the formation of polymers with higher molecular weights ($M_w = 5 \times 10^5$ g/mol, $M_w/M_n = 6$). However, in this case the broad molecular weight distribution indicates the presence of various active sites.[31] Related to these findings, Jordan et al. reported the formation of high

molecular weight linear PE with a very broad molecular weight distribution ($M_w = 10^7$ g/mol, $M_w/M_n = 60$) with phosphinesulfonato complexes bearing ligands with two aryl sulfonate moieties leading to tetranuclear aggregates of the catalyst. This study revealed that PE with these characteristics is only formed if the aggregate stays intact during polymerization.[29] Substitution of the non-chelating aryl moieties by alkyl groups, especially *tert*-butyl groups, increases the activity in ethylene polymerization drastically, but simultaneously reduces catalyst temperature stability and decreases MA incorporation in copolymerization experiments. It could be shown that by substitution of one *tert*-butyl moiety by a phenyl group stability of the catalyst and MA incorporation in copolymerization is significantly increased, again.[37]

However, a conclusive comparison of theses studies is hampered for two reasons: The comparability is restricted due to varying polymerization conditions and the utilization of differing catalyst precursors. Furthermore, the separation of electronic and steric influences remains difficult in most of the cases.

In order to achieve a deeper understanding of the relations between the catalyst structure and the (co)polymer obtained a broad variety of (P^O)PdMe catalysts was synthesized and studied in detail. The reactivity towards (polar) olefins was screened under identical (polymerization) conditions, in order to obtain insights into steric and electronic influences and to identify catalysts suitable for certain aims e.g. production of copolymers with higher molecular weights. Furthermore, it should be evaluated if a more directed catalyst design becomes possible by combination of two different non-chelating (aryl) substituents at phosphorus, so that certain properties of two symmetric catalysts can be combined.

## 4.2 Results and Discussion

### 4.2.1 Nomenclature

For the sake of clarity the nomenclature of species discussed in this chapter is depicted in Scheme 4-1. Catalyst precursors (P^O)PdMe (**1**) react with MA to the mono-insertion products (**2**) and subsequently to the consecutive insertion products (**3**). β–H elimination of **2** and **3** leads to intermediate Pd-H species which can insert further MA to yield mono- (**4**) and consecutive insertion products (**5**). The insertion mode is noted by a subscripted, and the ligand of the corresponding complex by a superscripted acronym as depicted in Figure 4-1.

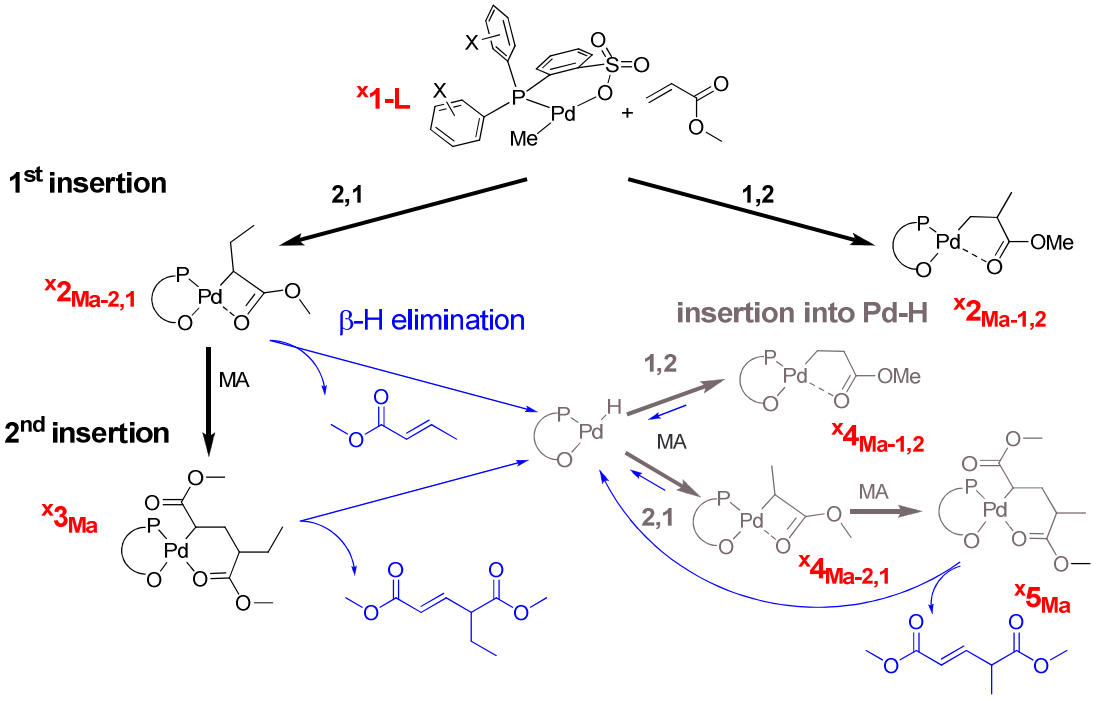


**Scheme 4-1.** Designation of complexes.

### 4.2.2 Synthesis and Characterization of Ligands and Metal Complexes

Several schemes for the synthesis of phosphinesulfonato ligands have been reported.[20,23,25,38] The symmetric and asymmetric (P^O)H ligands investigated in this study were synthesized by various approaches summarized in Scheme 4-2. Two main pathways can be distinguished. The ligand can be constructed stepwise starting from $Cl_2PNEt_2$ and introducing the non-chelating aryl moieties first by addition of Li-Ar. Suitable precursors for Li-Ar reagents exhibit either a bromine substituent, allowing for a bromine-lithium exchange

at low temperature or ortho directing groups like methoxy substituents, allowing for a lithiation with alkyl lithium reagents at room temperature. The intermediate $Ar_2PNEt_2$ has to be transformed to $Ar_2PCl$, which is reacted with *ortho*-lithium benzenesulfonate in the last step. This pathway results in various intermediate products which can be isolated and purified (black route). A disadvantage of this route can be the separation of $Ar_2PCl$ from the ammonium salt $H_2NEt_2Cl$, which is formed as a byproduct. The separation can be difficult depending on the aryl substituents. Alternatively, the ligand can be obtained in a one pot procedure starting from $PCl_3$ (blue route). Here, the *ortho*-lithium-benzenesulfonate has to be reacted first, mandatorily.[38] In this case the products are often contaminated with substoichiometric byproducts and purification is necessary. In most cases impurities can be removed by washing the protonated ligand (P^O)H with THF. Asymmetric substitution at phosphorus could be achieved by successive reaction of $Cl_2PNEt_2$ with two different lithiated aryl or alkyl compounds (red route). Here, it turned out that monitoring the particular substitution steps by *in situ* $^{31}$P NMR is helpful for the isolation of pure products.

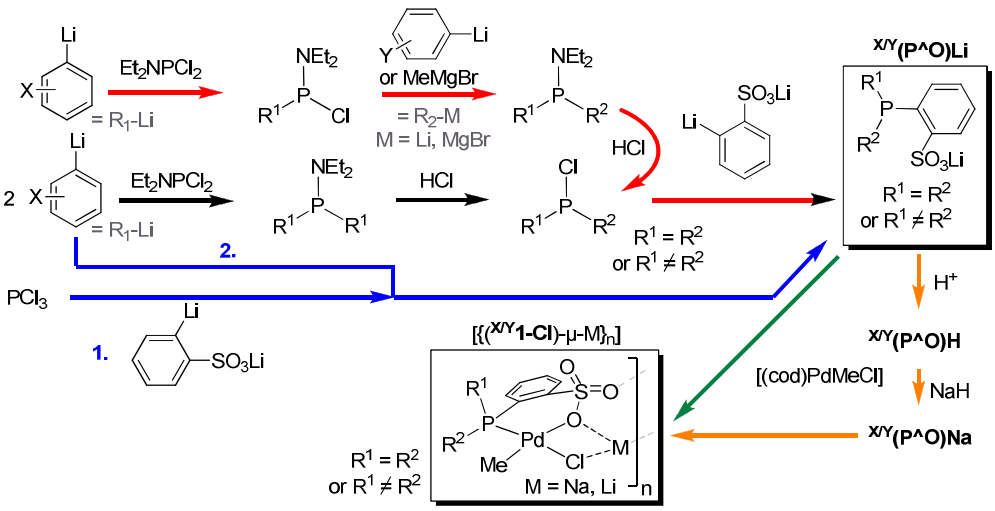


**Scheme 4-2.** Synthetic pathways to symmetric and asymmetric (P^O)PdMe catalyst precursors.

Complexes of the type [{(**$^X$1-Cl**)-μ-M}$_n$] can be synthesized by the reaction of [(cod)PdMe(Cl)] with the lithium salts (P^O)Li, which are obtained directly from the ligand synthesis (green route). Alternatively, the complexes can be synthesized by reacting [(cod)PdMe(Cl)] with the sodium salts (P^O)Na, which are obtained after acidic work-up to the protonated ligands and subsequent deprotonation with NaH (yellow route). Here, the latter route allows for additional purification steps, while (P^O)Li compounds often contain benzenesulfonate-derived impurities, which cannot always be removed satisfactorily. Still, the utilization of (P^O)Li can be advantageous, if the ligand framework contains acid-labile functionalities, since acidic conditions are avoided during work-up. The complexation

reactions always proceed within minutes, unless hampered by a limited solubility, and should be worked up immediately, since the complexes [{(**$^{X}$1-Cl**)-μ-M}$_n$] are not stable in solution and decomposition to palladium black is observed over time. The isolated compounds can obtain up to one equivalent of coordinating solvent e.g. acetone per counterion M (Na, Li) depending on the reaction conditions.

In order to comprehensively study the influence of the ligand on catalytic polymerization properties, fifteen complexes with symmetric and asymmetric substitution patterns at phosphorus differing in steric bulk and electronic properties were synthesized (Figure 4-1). The protonated ligands **$^{H}$(P^O)H**,[20] **$^{MeO}$(P^O)H**,[19] **$^{(MeO)2}$(P^O)H**[87] and **$^{Ar}$(P^O)H**[24] have been reported before, and the ligands **$^{Ph}$(P^O)H** and **$^{(MeO)3}$(P^O)H** have been described in the patent literature, previously.[38] Concerning the [{(**$^{X}$1-Cl**)-μ-M}$_n$]-type complexes, only the compound [{(**$^{MeO}$1-Cl**)-μ-Na}$_n$] has been reported previously.[61] Note that the related complexes **$^{MeO}$1-L** (L = DMSO, py, lut),[43,45,62] and **$^{Ar}$1-L** (L = TMEDA, py)[24] have been reported.

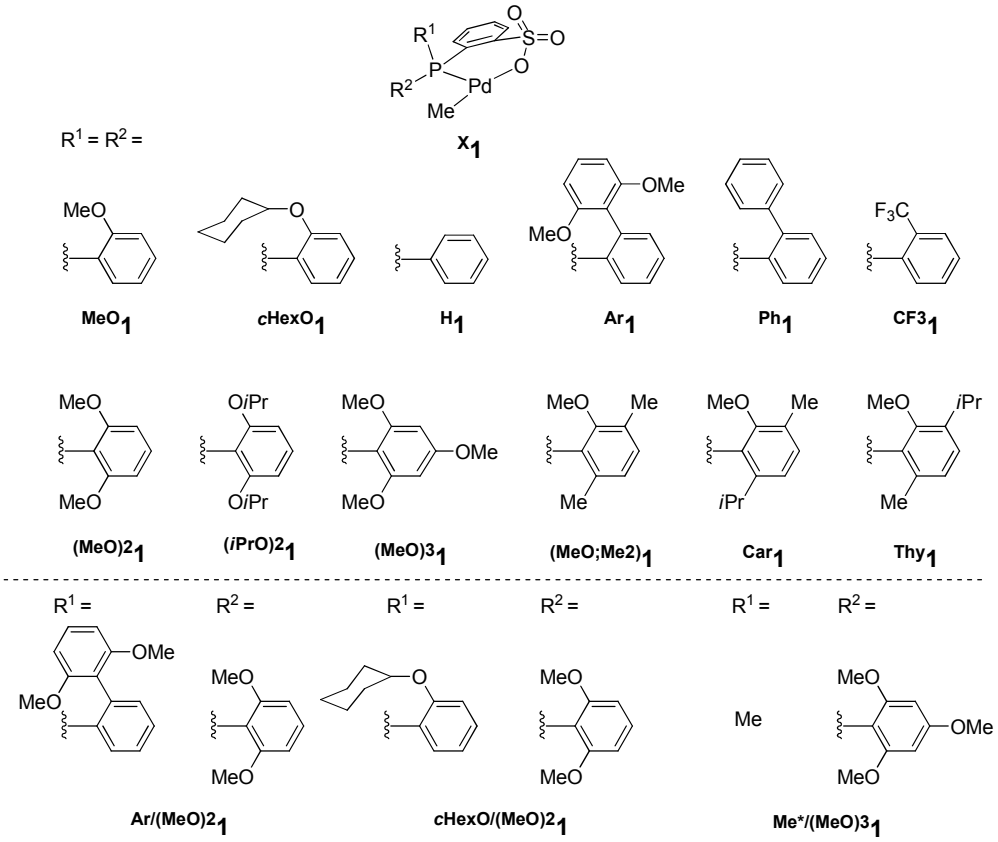


**Figure 4-1.** Phosphorus substitution patterns studied.

All protonated ligands studied exist in a zwitterionic form in $CD_2Cl_2$ with the proton being situated at phosphorus, leading to a P-H coupling of ca. 600 Hz in the $^{31}$P NMR. The $^{31}$P NMR shifts are situated in the range of 4 ppm to -31 ppm for the zwitterionic ligands

(P^O)H and between -12 ppm to -49 ppm for the ligand salts (P^O)M (Table 4-1). The $^{31}$P NMR shift is not an exact measure of the ligand basicity, since electronic influences are disturbed by steric interaction, but in principle $^{31}$P NMR resonances are low field shifted with increasing electron deficiency.[114] Accordingly, the ligands **$^{CF3}$(P^O)H** and **$^{Ar}$(P^O)H** can be considered to be relative electron deficient compared to electron richer ligands such as **$^{(MeO)2}$(P^O)H**, **$^{(iPrO)2}$(P^O)H**, and **$^{(MeO)3}$(P^O)H**.

**Table 4-1.** Comparison of $^{31}$P NMR shifts [ppm] in solution for the ligands **$^{X}$(P^O)H**, the corresponding salts **$^{X}$(P^O)M** and the corresponding complexes **$^{X}$(P^O)PdMe**[a].

| X = | $CF_3$ | H | Ar | Ph | *c*HexO/$(MeO)_2$ | *c*HexO | MeO | Ar/$(MeO)_2$ |
|---|---|---|---|---|---|---|---|---|
| **$^{X}$(P^O)H** | - | 4[20] | -2 | -5 | - | - | -10 | -18 |
| **$^{X}$(P^O)M** | -15 | -12 | -18 | -20 | -23 | -28 | -30 | -31 |
| **$^{X}$1**[a] | 43 | 30 | 30 | 28 | 30 | 30 | 25 | 15 |

| X = | Me*/$(MeO)_3$ | (MeO;$Me_2$) | Thy | Car | (*i*PrO)$_2$ | $(MeO)_2$ | $(MeO)_3$ |
|---|---|---|---|---|---|---|---|
| **$^{X}$(P^O)H** | -18 | -21 | -22 | -24 | -29 | -30 | -31 |
| **$^{X}$(P^O)M** | -41 | -32 | -32 | -39 | -46 | -45 | -49 |
| **$^{X}$1**[a] | 11 | 1 | 0 | -2 | -11 | -8 | -10 |

[a] **$^{X}$1** from [{(**$^{X}$1-Cl**)-μ-M}$_n$] after chloride abstraction with $AgBF_4$.

The complexes [{(**$^{X}$1-Cl**)-μ-M}$_n$] form multinuclear species which are bridged by intermolecular coordination of the chlorine atom and various oxygen atoms of the sulfonate group to the sodium or lithium counterion (M) in the solid state. For [{(**$^{MeO}$1-Cl**)-μ-Na}$_2$] X-ray structure analysis revealed that a dimeric structure is formed.[61] In contrast, the crystal structure of [{(**$^{(MeO)2}$1-Cl**)-μ-Na}$_n$] reveals that the Pd:MCl ratio can also be substoichiometric, as an aggregate of six palladium complexes is bridged by only four formula units NaCl in the solid state structure (Figure 4-2). Due to the limited stability of [{(**$^{X}$1-Cl**)-μ-M}$_n$] compounds in solution during crystallization and the various multinuclear arrangements that can be formed, crystals were grown from solutions of the very stable and mononuclear pyridine or 2,6-lutidine complexes for better comparability. These complexes are easily synthesized *in situ* by reaction of [{(**$^{X}$1-Cl**)-μ-M}$_n$] with the corresponding base and evaporation of the volatiles. The crystal structures of **$^{(MeO)3}$1-lut**, **$^{(MeO)2}$1-py**, **$^{(iPrO)2}$1-lut**, **$^{(MeO;Me2)}$1-lut**, **$^{CF3}$1-lut**, **$^{Ph}$1-lut**, **$^{c}$HexO/$^{(MeO)2}$1-py**, and **$^{Ar/(MeO)2}$1-lut** were determined. They all show a square-planar geometry around the palladium center, with the methyl group trans to the sulfonate group, as observed generally for (P^O)PdMe complexes (Figure 4-4, for the X-ray structures of **$^{c}$HexO/$^{(MeO)2}$1-py** and **$^{Ar/(MeO)2}$1-lut** see Chapter 5.2.1, Figure 5-5)

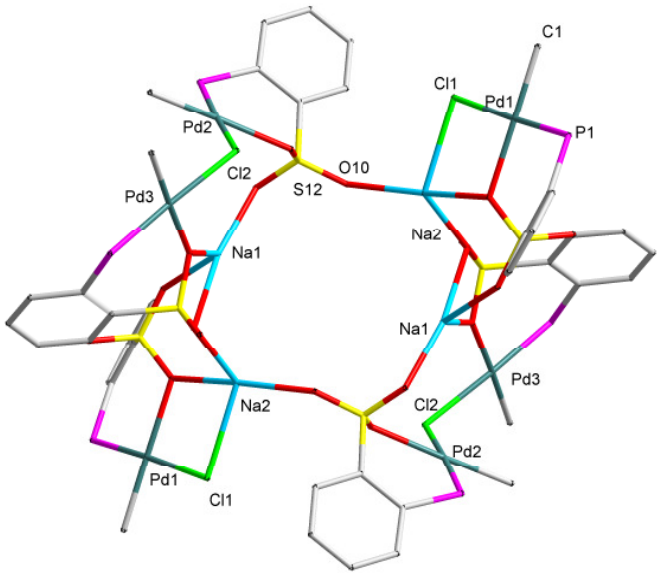


**Figure 4-2.** Molecular connectivity for the center of the multinuclear complex [{(**$^{X}$1-Cl-$^{X}$1**)-μ-Na-(**$^{X}$1-Cl**)-μ-Na}$_2$] as determined from X-ray analysis (2,6-(MeO)$_2$C$_6$H$_3$-aryl moieties attached to phosphorus and additional ligands coordinating to the sodium ion (acetone & MeO-group of the ligand) are not shown for clarity).

The aryl moieties of (P^O)PdMe complexes can either adopt an exo$_2$ or an exo$_3$ configuration. In the exo$_3$ configuration all equal ortho substituents are situated on the same side as the central phosphorus above a plane defined by the three aryl carbons bound to the phosphorus atom. In the various exo$_2$ configurations one of the ortho-substituents is situated below this plane (Figure 4-3).

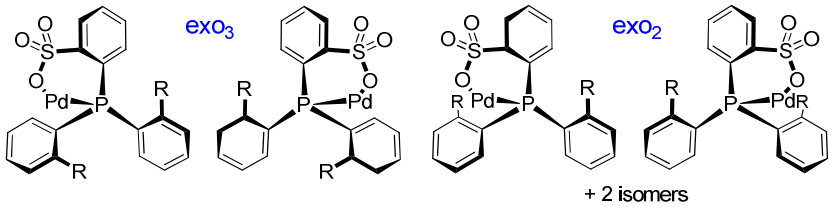


**Figure 4-3.** Exo$_2$ and exo$_3$ configuration for (P^O)PdMe complexes.

**$^{CF3}$1** and **$^{Ph}$1** show an exo$_2$ configuration, which is observed for most of the (P^O)PdMe structures determined (see Chapter 5.2.2). Interestingly, for **$^{Ar}$1-py** which is structurally closely related to **$^{Ph}$1-lut** an exo$_3$ configuration was observed, so that the additional methoxy substituents in **$^{Ar}$1** seem to have a distinct structural influence.[24] For **$^{(MeO;Me2)}$1-lut** an exo$_3$-like configuration with the ortho methyl group always situated on the same side as phosphorus is observed. Since the adoption of an exo$_3$ configuration is connected with a decrease of steric interaction between the corresponding ortho substituents this indicates an increased steric demand of the $^{(MeO;Me2)}$(P^O) fragment. For **$^{(MeO)2}$1-py** and **$^{(iPrO)2}$1-lut** a distinction of exo-configurations is not possible due to symmetry. Here, the

increased steric demand of $^{(i\text{PrO})2}$**1-lut** is reflected in the deformation of the boat configuration of the 6-membered (P^O)Pd chelate, which is observed in all other X-ray structures, to an envelope like ring conformation (see chapter 5.2.2).

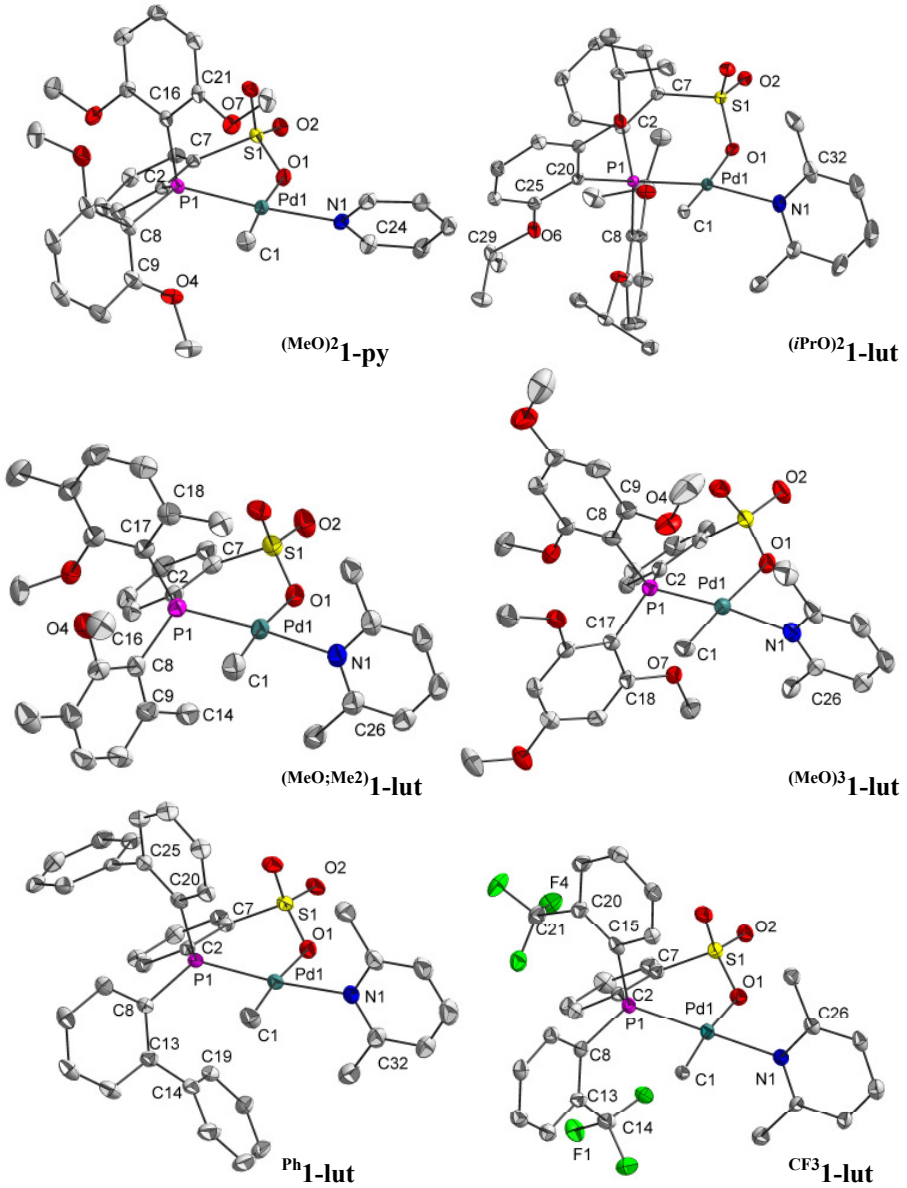


**Figure 4-4.** Solid state structures of $^{(MeO)2}$**1-py**, $^{(i\text{PrO})2}$**1-lut**, $^{(MeO;Me2)}$**1-lut**, $^{(MeO)3}$**1-lut**, $^{Ph}$**1-lut**, and $^{CF3}$**1-lut.** Ellipsoids represent 50% probability. Hydrogen atoms and solvent molecules are omitted for clarity.

**Table 4-2.** Selected bond length [Å] for $^{(MeO)2}$**1-py**, $^{(i\text{PrO})2}$**1-lut**, $^{(MeO;Me2)}$**1-lut**, $^{(MeO)3}$**1-lut**, $^{CF3}$**1-lut**, and $^{Ph}$**1-lut**.

| bond | $^{(MeO)2}$1-py | $^{(i\text{PrO})2}$1-lut | $^{(MeO;Me2)}$1-lut | $^{(MeO)3}$1-lut[a] | $^{CF3}$1-lut | $^{Ph}$1-lut |
|---|---|---|---|---|---|---|
| Pd1-P1 | 2.256(1) | 2.244(1) | 2.270(1) | 2.235(1) / 2.251(1) | 2.251(1) | 2.234(1) |
| Pd1-C1 | 2.031(2) | 2.052(2) | 2.022(3) | 2.060(5) / 2.036(6) | 2.068(4) | 2.042(5) |
| Pd1-O1 | 2.163(1) | 2.157(1) | 2.149(2) | 2.165(3) / 2.163(4) | 2.146(3) | 2.150(3) |
| Pd1-N1 | 2.113(1) | 2.146(2) | 2.138(2) | 2.140(4) / 2.152(4) | 2.118(3) | 2.128(3) |
| P1-C2 | 1.841(2) | 1.848(2) | 1.853(3) | 1.831(4) / 1.850(5) | 1.830(3) | 1.833(4) |
| P1-C8 | 1.832(2) | 1.838(2) | 1.841(4) | 1.832(5) / 1.830(6) | 1.831(4) | 1.837(4) |

[a]two molecules in the asymmetric unit.

A comparison of the NMR data of the various complexes (Table 4-1) reveals that easily accessible experimental parameters like $^{1}H$ or $^{31}P$ NMR shifts cannot satisfactorily reflect electronic properties. The exact $^{31}P$ NMR shifts depend also on steric parameters and on the exact measuring conditions. A comparison of the Pd-N bond lengths determined by X-ray structure analysis of pyridine and lutidine complexes revealed that the distance can partly be correlated to the electron density at the palladium (as anticipated from the electron donating or withdrawing nature of the substituents on the P-bond aryl of the phosphinesulfonato ligand, *vide supra*) if the same probe (lutidine/pyridine) is applied. Still steric effects can have a pronounced influence. The Pd-N bond length increases with increasing electron density at the palladium: $^{CF}$**1** (2.118(3) Å) < $^{Ph}$**1** (2.128(3) Å) < $^{MeO}$**1** (2.134(2) Å) < $^{(MeO;Me2)}$**1** (2.138(2) Å) < $^{(iPrO)2}$**1** (2.146(2) Å) ~ $^{(MeO)3}$**1** (2.146(2) Å). The correlation found is in line with the observed trend in $^{31}P$ NMR shifts of the ligand salts (P^O)M (Table 4-1). However, the cyclohexyloxy substituted compound $^{cHexO/(MeO)2}$**1-lut** exhibits an unusually short Pd-N bond (2.120(2) Å). For the pyridine complexes a pronounced elongation of the Pd-N bond is observed for the 2,6-MeO($C_6H_3$)-substituted compounds $^{Ar}$**1-py** and $^{Ar/(MeO)2}$**1-py** compared to $^{MeO}$**1-py** and $^{(MeO)2}$**1-py** (Table 4-3). This can be related to the high steric demand of the aryl substituents.

In conclusion, an exact determination of the electronic properties of the investigated complexes by experimental methods remains difficult and the data allows only for a rough classification.

**Table 4-3.** Comparison of Pd-N bond distances in the solid state for various (P^O)PdMe complexes.

| | $^{H}$**1** | $^{MeO}$**1** | $^{CF3}$**1** | $^{(MeO)2}$**1** | $^{(iPrO)2}$**1** | $^{(MeO;Me2)}$**1** |
|---|---|---|---|---|---|---|
| $^{X}$**1-lut**: Pd-N [Å] | - | 2.134(2)[45] | 2.118(3) | - | 2.146(2) | 2.138(2) |
| $^{X}$**1-py**: Pd-N [Å] | 2.110(9)[37] | 2.108(4)[62] | | 2.113(1) | - | - |
| | $^{(MeO)3}$**1** | $^{Ar}$**1** | $^{Ph}$**1** | $^{Ar/(MeO)2}$**1** | $^{cHexO/(MeO)2}$**1** | |
| $^{X}$**1-lut**: Pd-N [Å] | 2.146(4)[a] | - | 2.128(3) | - | 2.120(2)[a] | |
| $^{X}$**1-py**: Pd-N [Å] | - | 2.132(4)[24] | - | 2.135(3) | - | |

[a]average for the two independent molecules in the asymmetric unit.

### 4.2.3 Polar Monomer Insertion

In order to evaluate the reactivity of the complexes towards polar olefins, the insertion of MA into the Pd-Me bond of $^{X}$**1** to $^{X}$**2**$_{MA}$ and subsequently to $^{X}$**3**$_{MA}$ was monitored by $^{1}$H NMR spectroscopy at 25 °C over a period of 12-18 hours (Figure 4-5 - Figure 4-9). In addition, elimination and reinsertion reactions were analyzed. The active catalyst $^{X}$**1** was generated *in situ* by chloride abstraction from [{(**1-Cl**)-μ-M}$_n$] (see Chapter 3.2.4). The insertion products $^{X}$**2**, $^{X}$**3**, $^{X}$**4**, and $^{X}$**5** were identified by assignment of their spin systems by $^{1}$H $^{1}$H gCOSY and $^{1}$H $^{1}$H zTOCSY experiments, as well as by $^{1}$H $^{13}$C gHMBC experiments, if possible. All organic elimination products were identified by comparison with the $^{1}$H NMR shifts of the corresponding isolated substances (c.f. Chapter 7.2.6).

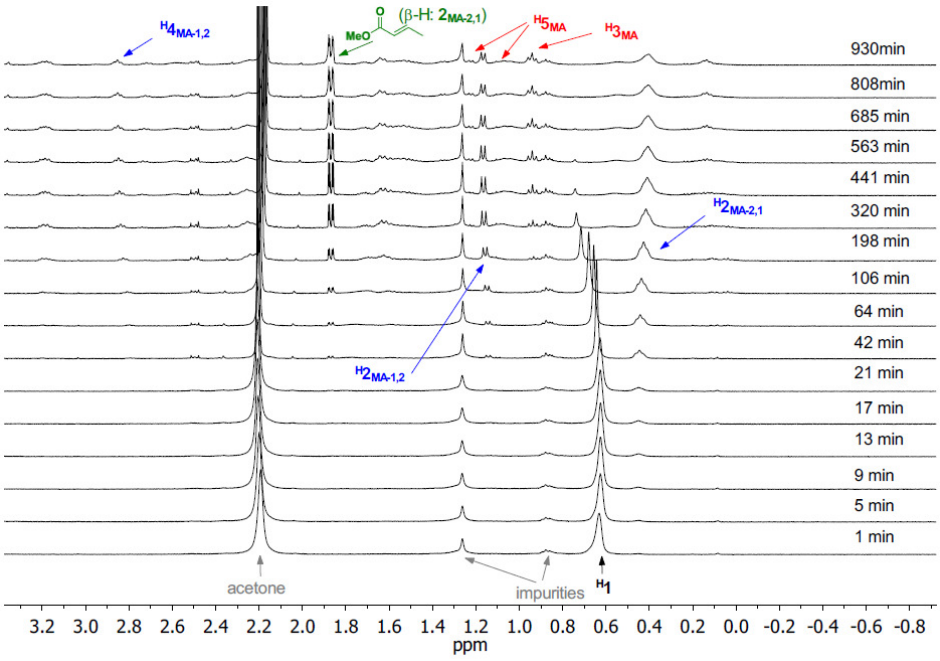


**Figure 4-5.** $^{1}$H NMR (400 MHz, $CD_2Cl_2$) monitoring of the reaction of $^{H}$**1** with MA, of subsequent elimination reactions of the formed insertion products, and of the reinsertion into Pd-H species at 25 °C.

For the compounds $^{MeO}$**1**, $^{(MeO)2}$**1**, $^{(MeO)3}$**1**, $^{c}$**1**, and $^{cHexO/(MeO)2}$**1** almost no β-H-elimination or other decomposition reactions of the insertion products formed were observable during the course of the experiment. In contrast, various decomposition and reinsertion reactions were observed for the insertion products formed from $^{H}$**1** (Figure 4-5), $^{Ph}$**1** (Figure 4-8), $^{Ar}$**1** (Figure 4-9), $^{Ar/(MeO)2}$**1**, $^{CF3}$**1** (Figure 4-6), $^{(MeO;Me2)}$**1**, $^{Car}$**1**, and $^{Thy}$**1** (Scheme 4-1). For the insertion products $^{X}$**2**$_{MA-2,1}$ and $^{X}$**3**$_{MA}$ ($^{X}$**5**$_{MA}$), β-H-elimination was found to be the predominant decomposition pathway. However, the intermediately formed palladium hydride species could not be detected. It is assumed that the palladium hydrides

either instantly reinsert methyl acrylate to form $^{X}\mathbf{4_{MA}}$, or decompose to Pd(0). It has been reported that strong donor ligands like phosphines are necessary to stabilize isolable (P^O)PdH species.[115] The addition of phosphines drastically reduces any reactivity, however.

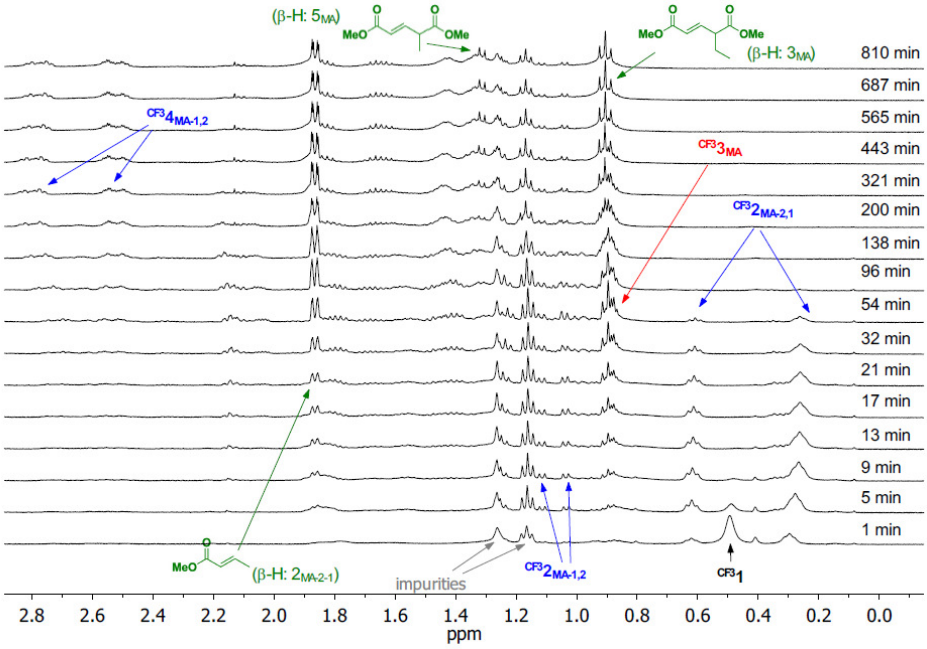


**Figure 4-6.** $^{1}$H NMR (400 MHz, $CD_2Cl_2$) monitoring of the reaction of $^{CF3}\mathbf{1}$ with MA, of subsequent elimination reactions of the formed insertion products, and of the reinsertion into Pd-H species at 25 °C.

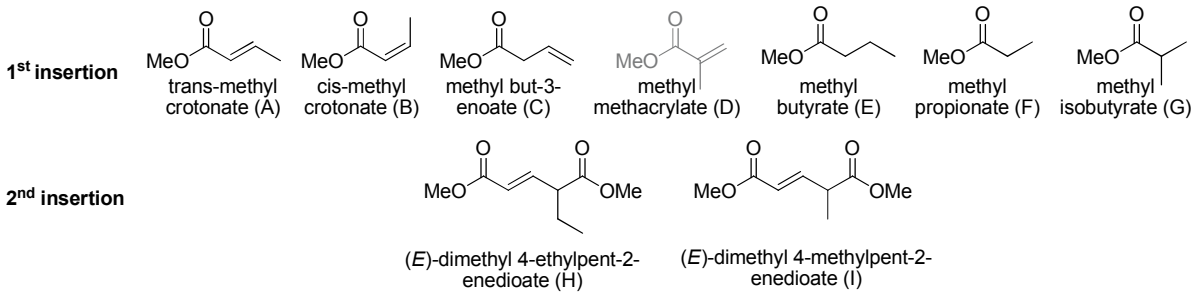


**Figure 4-7.** Observed decomposition products.

The main β-H-elimination product from $^{X}\mathbf{2_{MA-2,1}}$ is trans-methyl crotonate (**A**, Figure 4-7). However, in some cases also cis-methyl crotonate (**B**) can be observed in small amounts (**A**:**B** > 10:1, Figure 4-8). For $^{(iPrO)2}\mathbf{1}$, $^{(MeO;Me2)}\mathbf{1}$, $^{Ar}\mathbf{1}$, and $^{Ph}\mathbf{1}$ the formation of a significant amount of methyl but-3-eonate (**C**) was observed (up to **A**:**C** ~3:1 for $^{Ph}\mathbf{1}$, Figure 4-8), while for $^{CF3}\mathbf{1}$, $^{(MeO)2}\mathbf{1}$, $^{c HexO}\mathbf{1}$, and $^{Me*/(MeO)3}\mathbf{1}$ trace amounts of **C** were detected. The formation of **C** can be explained either by a 1,2-reinsertion of trans-methyl crotonate (**A**) into a palladium hydride and subsequent β-H-elimination, by a closely related series of β-H-eliminations and reinsertions at a given metal center starting from $^{X}\mathbf{2_{MA-2,1}}$ (chain walking), or by isomerization of **A** due to formed Pd-black (Scheme 4-3). Considering the huge excess of MA in

comparison to the sterically more demanding and thus less reactive trans-methyl crotonate (**A**), a reinsertion in significant amounts after separation of the substrate from the metal center is rather implausible. Furthermore, the exclusive formation of **C** by isomerization appears unlikely, since **C** forms simultaneously with **A**, and **C** is thermodynamically disfavored. The portion of **C** seems to increase for sterically demanding compounds like $^{Ph}$**1**. This might indicate a chain walking mechanism at a given metal center, as chain transfer is presumed to be hindered for sterically crowded metal centers.

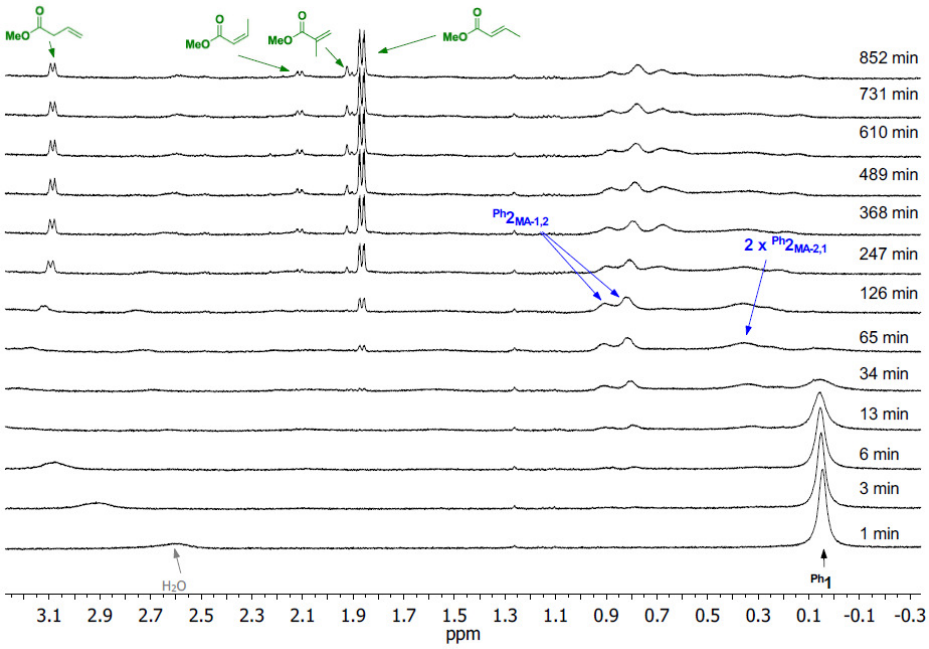


**Figure 4-8.** $^{1}$H NMR (400 MHz, $CD_2Cl_2$) monitoring of the reaction of $^{Ph}$**1** with MA, of subsequent elimination reactions of the insertion products formed, and of the reinsertion into Pd-H species at 25 °C.

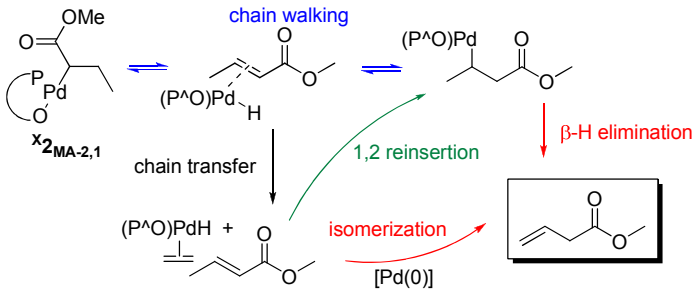


**Scheme 4-3.** Possible reaction pathways to methyl-3-buteonate.

The 1,2-insertion products $^{X}$**2**$_{MA-1,2}$ are stable towards β-H-elimination and only for $^{Ph}$**1** the formation of trace amounts of methyl methacrylate (**D**) as an elimination product was observed (Figure 4-8). The high stability can be explained by the formation of five-membered κ-*O* coordinated chelate complexes (Scheme 4-1). However, for $^{(iPrO)2}$**2**$_{MA-1,2}$, $^{(MeO;Me2)}$**2**$_{MA-1,2}$, and $^{Ar}$**2**$_{MA-1,2}$ (Figure 4-9) nonetheless significant decomposition and simultaneous formation

of the saturated ester methyl isobutyrate (**G**) was detected. This might be explained by some kind of proton transfer (Scheme 4-4): Recent investigations on the decomposition reactions for phosphinesulfonato compounds revealed that (P^O)Pd-H species can decompose to Pd(0) and the protonated ligand (P^O)H by reductive elimination. It has been shown that the protonated ligand (P^O)H can induce a protolytic cleavage of Pd-alkyl bonds. Alternatively, a direct H-transfer by palladium hydride species in a multinuclear arrangement was discussed.[115,116] For (N^N)Pd-alkyl complexes a homolytic cleavage of Pd-alkyl bonds has also been observed.[117,118] However, in the latter case a disproportionation reaction from the primarily formed free-radical should lead to a 1:1 mixture of MMA (**D**) and methyl isobutyrate (**G**), which was not observed for $^{(i\mathrm{PrO})2}\mathbf{1}$, $^{(\mathrm{MeO;Me2})}\mathbf{1}$, and $^{\mathrm{Ar}}\mathbf{1}$. As expected, no organic products indicating a recombination of free radical species, which is even less probable for steric reasons, were detected, either.

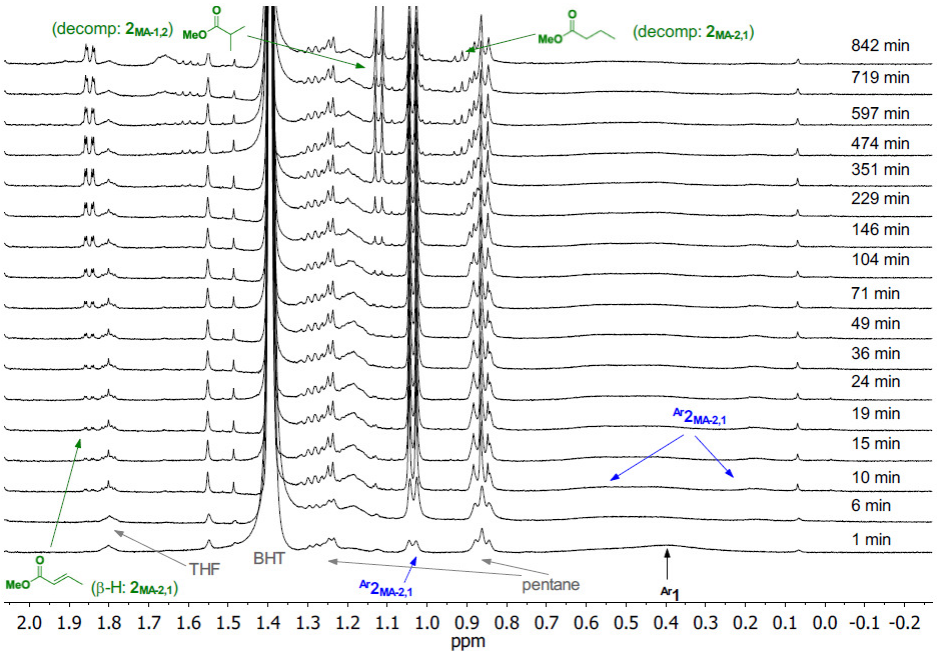


**Figure 4-9.** $^{1}$H NMR (400 MHz, $CD_2Cl_2$) monitoring of the reaction of $^{\mathrm{Ar}}\mathbf{1}$ with MA, of subsequent decomposition reactions of the formed insertion products, and of the reinsertion into Pd-H species at 25 °C.

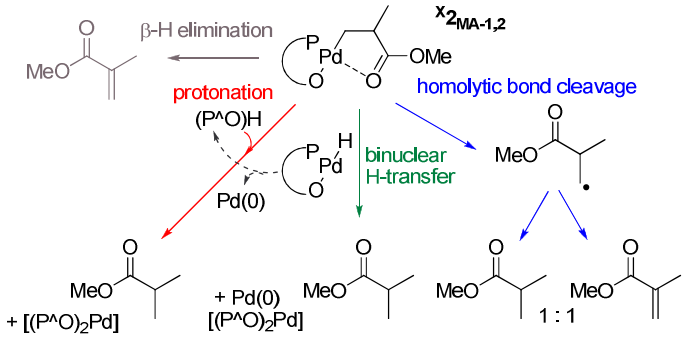


**Scheme 4-4.** Possible decomposition pathways for $^{\mathrm{X}}\mathbf{2}_{\mathrm{MA-1,2}}$.

Minor amounts of methyl butyrate (**E**) and methyl propionate (**F**) were observed in some cases (e.g. for $^{Ar}$**1**, Figure 4-9). This reveals that a similar decomposition pathway as assumed for $^{X}$**2**$_{MA-1,2}$ also exists for $^{X}$**2**$_{MA-2,1}$. However, as the methyl butyrate portion is small compared to the mainly formed trans-methyl crotonate, a homolytic bond cleavage cannot be excluded in this case.

In comparison to the products of the first 2,1-insertion into the Pd-Me bond $^{X}$**2**$_{MA-2,1}$, the products of the consecutive insertion $^{X}$**3**$_{MA}$ are generally very stable, due to the formation of six-membered κ-*O* coordinated chelates (Scheme 4-1). The only exception is $^{CF3}$**3**, which rather rapidly eliminates dimethyl 4-ethylpent-2-enedioate (**H**) (Figure 4-6).

Palladium hydride species resulting from the β-H-elimination reactions can reinsert MA to form $^{X}$**4** and subsequently $^{X}$**5** (Figure 4-5, Figure 4-6). An assignment of these species is difficult and requires several preconditions: A pronounced β-H elimination to form Pd-H species, a reasonable reactivity of the palladium hydrides towards insertion compared to decomposition, and a sufficient stability of the newly formed insertion products, or a distinct decomposition to specific products, respectively. For that reason only the 1,2-insertion product $^{X}$**4**$_{MA-1,2}$ could be assigned so far, just as for $^{H}$**4**$_{MA-1,2}$ and $^{CF3}$**4**$_{MA-1,2}$ (Figure 4-5, Figure 4-6). The corresponding 2,1-insertion products $^{X}$**4**$_{MA-2,1}$ probably β–H eliminate rapidly to form MA or in the case of $^{CF3}$**4**$_{MA-2,1}$ reacts to $^{CF3}$**5**$_{MA}$ which can be detected by the β-H-elimination product formed, dimethyl 4-methylpent-2-enedioate (**I**, Figure 4-6, Figure 4-7).

For a quantitative analysis of the influences of electronic and steric properties on the reactivity of the palladium methyl complexes towards polar olefins, the rate constants for the first and the consecutive MA insertion were determined by $^{1}$H NMR at 25 °C ([Pd] = 0.02 mol L$^{-1}$, Pd:MA = 1:15, Table 4-4). Note that the [{(**1-Cl**)-μ-M}$_n$] precursors can contain up to one equivalent of weak coordinating solvent e.g. acetone per formula unit. This might affect the determined rate constants. A comparison of the insertion rate constants for the first insertion does not reveal a clear trend. The rather electron poor $^{CF3}$**1** exhibits a larger rate constant compared to the more electron rich $^{MeO}$**1** ($k_{CF3\text{-}1st}$ = 5×10$^{-3}$ s$^{-1}$ vs. $k_{MeO\text{-}1st}$ = 3×10$^{-3}$ s$^{-1}$), while the steric demand of a $CF_3$ substituent exceeds the one of a MeO-group.[119] However, for the non-substituted $^{H}$**1** which should have an intermediate electron density the rate constant is strongly decreased to $k_{H\text{-}1st}$ = 0.1×10$^{-3}$ s$^{-1}$. Increase of the steric bulk by substitution of methyl by cyclohexyl in $^{cHexO}$**1** leads to a smaller rate constant ($k_{cHexO\text{-}1st}$ = 0.2×10$^{-3}$ s$^{-1}$ vs. $k_{MeO\text{-}1st}$ = 3×10$^{-3}$ s$^{-1}$).

**Table 4-4.** Rate constants for insertion and β-H elimination, as well as regioselectivities for the first MA insertion.

| entry | compound | $k_{1st}$ [$\times 10^{-3}$ $s^{-1}$] | $k_{2nd}$ [$\times 10^{-5}$ $s^{-1}$] | $k_{\beta H\text{-}1st}$ [$\times 10^{-6}$ $s^{-1}$] | regioselectivity $k_{2,1}$:$k_{1,2}$ |
|---|---|---|---|---|---|
| 4-1 | $^{CF3}$**1** | 4.8 | 43 | 100 | 4:1 |
| 4-2 | $^{H}$**1** | 0.1 | 0.3 | 5 | 5:1 |
| 4-3 | $^{MeO}$**1** | 3.2 | 9.2 | 10 | >15:1 |
| 4-4 | $^{cHexO}$**1** | 0.2 | n.o.[a] | ~10[b] | n.d. |
| 4-5 | $^{Ph}$**1** | 0.9 | n.o.[a] | 40 | 2:1 |
| 4-6 | $^{Ar}$**1** | ~1-5[b] | n.o.[a] | ~1-5[b] | 1:1 |
| 4-7 | $^{Ar/(MeO)2}$**1** | 4 | 6 | n.d.[c] | 1.6:1 |
| 4-8 | $^{cHexO/(MeO)2}$**1** | 3 | 5.3 | n.d.[c] | 6:1 |
| 4-9 | $^{(MeO)2}$**1** | 1.3 | 3.7 | <4 | >30:1 |
| 4-10 | $^{(iPrO)2}$**1** | 3.4 | ~1-5[b] | 5 | 7:1 |
| 4-11 | $^{(MeO)3}$**1** | 26 | 38 | n.o.[d] | >50:1 |
| 4-12 | $^{Me*/(MeO)3}$**1** | 0.09 | <0.1 | ~5 | >50:1 |
| 4-13 | $^{(MeO;Me2)}$**1** | n.d.[b] | traces | 3000 | 8:1 |

Conditions: [Pd] = 0.02 mol $L^{-1}$, 1.1 equiv. $AgBF_4$, Pd:MA = 1:15, solvent $CD_2Cl_2$, T = 25 °C; [a]no consecutive insertion observed; [b]exact determination not possible due to overlapping or broad resonances; [c]no β-H elimination rate determined, due to overlapping resonances; [d]no β-H elimination observed.

Considering the compounds having double ortho substituted aryl moieties, the highest rate constant was found for $^{(MeO)3}$**1** which can be considered as more electron rich vs. the sterically similar $^{(MeO)2}$**1** ($k_{(MeO)3}$= 26×$10^{-3}$ $s^{-1}$ vs. $k_{(MeO)2}$= 1×$10^{-3}$ $s^{-1}$). The substitution of one 2,4,6-$(MeO)_3C_6H_2$ substituent by a methyl group in $^{Me*/(MeO)3}$**1** leads to a strong reduction of the rate constant by a factor of more than 200 ($k_{Me*/(MeO)3\text{-}1st}$ = 0.1×$10^{-3}$ $s^{-1}$). In contrast to the decelerating effect of a cyclohexoxy-group, the substitution of the methoxy groups in $^{(MeO)2}$**1** by more sterically demanding isopropoxy groups in $^{(iPrO)2}$**1** has no negative effect, but the rate constant is even enhanced ($k_{(iPrO)2\text{-}1st}$ = 3×$10^{-3}$ $s^{-1}$ vs. $k_{(MeO)2\text{-}1st}$ = 1×$10^{-3}$ $s^{-1}$).

The rate constants for the consecutive insertion are one to two orders of magnitude smaller than for the first insertion. This can be explained by the increased steric bulk at the palladium and the insertion into an α-substituted carbyl instead of an alkyl species, as well as the opening of the 4-membered chelate formed after the first insertion. In general, the steric demand of the ligand has a much more pronounced influence on the second insertion, so that no consecutive insertion at all could be observed for the very bulky systems $^{Ar}$**1**, $^{Ph}$**1**, and $^{cHexO}$**1** (see also Chapter 5.2.4). The highest rate constants were found for $^{CF3}$**1** and $^{MeO3}$**1** and in general the relation of the insertion rate constants is similar as discussed for the first insertion.

The rate constants for the β-H-elimination of $^{X}$**2**$_{MA\text{-}2,1}$ are in the range of $10^{-5}$-$10^{-6}$ $s^{-1}$ for most of the compounds and significantly lower than the rate constants for the first insertion. Larger β-H-elimination rate constants are observed for $^{CF3}$**1** ($k_{CF3\text{-}\beta H}$ = $10^{-4}$ $s^{-1}$) and $^{(MeO;Me2)}$**1** ($k_{(MeO;Me2)\text{-}\beta H}$ = 3×$10^{-3}$ $s^{-1}$). Considering the formation of $^{X}$**3**, β-H-elimination

significantly competes with consecutive insertion for $^{CF3}$**1**, $^{H}$**1**, $^{cHexO}$**1**, $^{Ph}$**1**, $^{Ar}$**1**, $^{(iPrO)2}$**1**, $^{Me*/(MeO)3}$**1**, and $^{(MeO;Me2)}$**1**.

Steric influences clearly emerge in the regioselectivity as determined from the distribution of the 1,2- and 2,1-insertion products $^{X}$**2**$_{MA}$. An increase of steric constraints around the palladium center leads to a shift of the 2,1:1,2 ratio from >15:1 for $^{MeO}$**1**, $^{(MeO)2}$**1**, $^{(MeO)3}$**1**, $^{Me*/(MeO)3}$**1** over 6-7:1 for $^{(iPrO)2}$**1**, $^{cHexO/(MeO)2}$**1** to 1-2:1 for $^{Ar}$**1**, $^{Ar/(MeO)2}$**1**. This can be explained by steric interaction of the ligand with the MA monomer leading to increased barriers for the electronically favoured 2,1-insertion mode.[41] However, for the rather unconstrained $^{H}$**1** a rather low selectivity of 5:1 is observed (see also Chapter 5.2.4).

In summary each catalyst exhibits an individual reaction profile in the presence of MA, which is determined by the relation of insertion and elimination rate constants, the relation of the insertion modes and the relation of different decomposition reactions. The resulting reactivity can hardly be correlated to electronic properties. However, the influence of steric bulk is more explicit. An increase of steric bulk decreases insertion rate constants (with the only exception being $^{(iPrO)2}$**1**), disfavors a 2,1-insertion mode, and enhances chain walking. Single catalysts exhibit outstanding reactivities: For $^{CF3}$**1** and $^{(MeO)3}$**1** the largest insertion rate constants by far were found, especially for the second insertion. By contrast, the asymmetric substituted compound $^{Me*/(MeO)3}$**1** inserts MA slowest with a rate constant of ca. 200 times smaller than for $^{(MeO)3}$**1** for the first insertion. Concerning the stability of the insertion products, exceptionally high β-H elimination rate constants were observed for $^{CF3}$**2**$_{MA-2,1}$ and $^{(MeO;Me2)}$**2**$_{MA-2,1}$. Here the detected respective elimination products imply that the resulting palladium hydride species have opposite reactivities. Whereas $^{CF3}$(P^O)Pd-H inserts MA rapidly to species $^{CF3}$**5**$_{MA}$, no further insertions and hence only decomposition to Pd(0) was detected for $^{(MeO;Me2)}$(P^O)Pd-H.

### 4.2.4 Homopolymerization of Ethylene

All catalysts were tested in the homopolymerization of ethylene at 5 bar ethylene pressure in toluene at 80 °C. The active catalyst was generated *in situ* by chloride abstraction from [{(**1-Cl**)-μ-M}$_n$] with $AgBF_4$ in dichloromethane. The resulting insoluble salts were removed by filtration before adding the catalyst solution to the reactor. A comparison of the different precatalysts $^{MeO}$**1-dmso**, $^{MeO}$**1-Cl** ([{(**1-Cl**)-μ-M}$_n$] without chloride abstraction) and $^{MeO}$**1** revealed that $^{MeO}$**1-dmso** and $^{MeO}$**1** show comparable catalytic activity (entry 5-1 and 5-2, Table 4-5). This is in line with previous observations that at 5 bar ethylene pressure the

DMSO/ethylene pre-equilibrium is already shifted completely to ethylene coordination.[43] By contrast, $^{MeO}$**1-Cl** in the absence of $AgBF_4$ shows a significant reduced turn-over-frequency (TOF). This reveals that activation with $AgBF_4$ is necessary to reach full catalyst activity. However, complexes [{(**1-Cl**)-μ-M}$_n$] still lead to active catalysts and can be valuable precursors if application of silver salts has to be avoided (entry 5-1 vs. 5-3, Table 4-5, see Chapter 5.2.5).

A comparison of the activities for different catalysts is complicated by the different stabilities of the catalysts over time under polymerization conditions. Hence, the ethylene mass flow was monitored to evaluate catalyst stability. In Figure 4-10 the mass flow traces of catalysts that decompose significantly during 30 minutes polymerization time are compared to the one of the stable catalyst $^{MeO}$**1**. A pronounced decomposition was observed especially for all compounds exhibiting a ligand with an aryl substituent in ortho position of the non-chelating aryl moieties ($^{Ar}$**1**, $^{Ar/(MeO)2}$**1**, $^{Ph}$**1**) and for the ortho-$CF_3$ substituted compound $^{CF3}$**1** as well as for $^{(MeO;Me2)}$**1**, for which no significant mass flow activity was observed after 5 minutes. A fast decomposition in the ethylene polymerization correlates with high β-H elimination rate constants determined for the insertion products of $^{Ph}$**1**, $^{(MeO;Me2)}$**1**, and $^{CF3}$**1**, and the observed multifold decomposition reaction for $^{Ar}$**2** and $^{Ar/(MeO)2}$**2** to various saturated and unsaturated organic products.

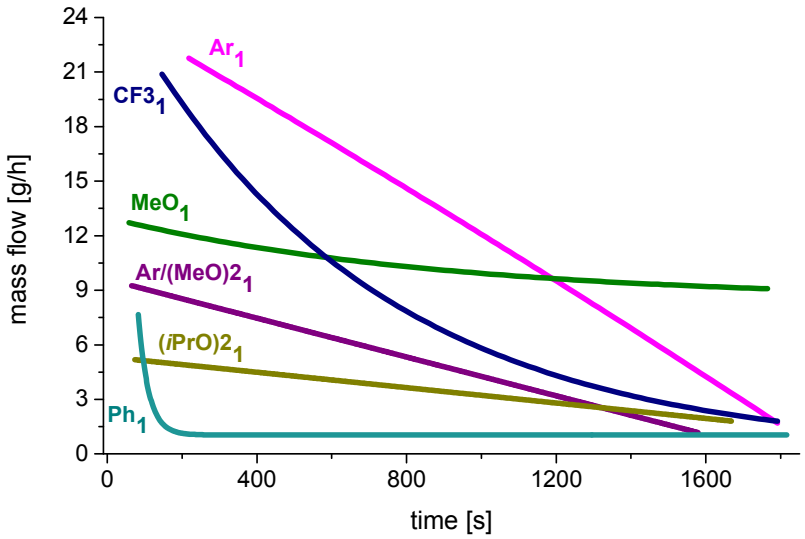


**Figure 4-10.** Mass flow traces (exponentially fitted) for ethylene homopolymerization (p = 5 bar) with $^{MeO}$**1**, $^{CF3}$**1**, $^{Ar}$**1**, $^{Ar/(MeO)2}$**1**, $^{Ph}$**1**, $^{(iPrO)2}$**1** showing catalyst decomposition over time (note that a mass flow below ca. 1-2 g h$^{-1}$ can not be monitored within the experimental set up).

For $^{(MeO;Me2)}$**1** and the related compounds $^{Thy}$**1** and $^{Cav}$**1** only very low amounts of PE could be isolated and only very low mass flow activity within the first five minutes was detected. This indicates low activity and rapid decomposition of the catalysts. Furthermore,

analysis of the formed polymers by GPC revealed a bimodal molecular weight distribution with the main fraction being low molecular PE (~1000 g/mol) and a small amount of a high molecular weight polymer (>20.000 g/mol). This points to the existence of several active sites during the short catalyst lifetime. A tentative explanation may be an alteration of the nature of the active site, e.g. by exchange of the aryl substituents of the ligand due to elimination/oxidative-addition as recently observed.[115] However, there is no obvious reason for the pronounced occurrence of such transformations for these particular catalysts. Notably, such short catalyst lifetime combined with the detection of a bimodal molecular weight distribution was exclusively observed for catalysts bearing ligands with a 3,6-alkyl-2-methoxy substitution pattern at the non-chelating aryl moieties within this study. Compared to the stable catalyst $^{(MeO)2}$**1** with a 2,6-methoxy substitution pattern the electronic properties should not differ exceptionally. This might point to steric influences due to the additional 3-alkyl substituent. In the crystal structure of $^{(MeO;Me2)}$**1-lut** it has been observed that the arrangement of the non-chelating aryl substituents differs from the usually observed $exo_2$ arrangement, which may also indicate a specific steric influence of the 3-alkyl substituent. Another difference in the complex conformation between $^{(MeO;Me2)}$**1** and $^{(MeO)2}$**1**, as observed in the solid state, is the alignment of the methyl- instead of methoxy-groups towards the palladium center in $^{(MeO;Me2)}$**1-lut**. Obviously, small changes in the substitution pattern can have a strong influence on catalyst activity and stability.

In order to evaluate catalyst activities and to reveal the actual influence of decomposition on the polymer yield, average activities for ethylene polymerization after 100 s, 200 s and 300 s polymerization time as determined from mass flow integration (after subtraction of a mass flow obtained under the same conditions in absence of catalyst, to account for saturation of the ligand phase with ethylene in the early stages of the experiment) and the TOF after 30 minutes polymerization time as determined from the isolated polymer yield are compared in Figure 4-11. For rather stable catalysts like $^{MeO}$**1** the activity is constant in all intervals determined, while for catalysts showing strong decomposition a pronounced decrease of activity is evident already within the first 300 second, like e.g. for $^{CF3}$**1**. However, for very low activities the accuracy of this method is limited as can be seen in the significantly higher activities determined from the polymer yield compared to the mass flow activities for the stable catalysts $^{(MeO)3}$**1** and $^{Me*/(MeO)3}$**1**. In these cases the activity determined from the polymer yield should be considered as the maximum activity.

**Table 4-5.** Ethylene homopolymerization with various catalysts.

| entry | catalyst | yield [g] | TOF [$10^3$ $mol_{PE}$/ $mol_{Cat}$*h] | $M_n$[a] [$10^3$ g $mol^{-1}$] | $DP_n$ | $M_w/M_n$[a] | branching[b] [Me per 1000 C] | $T_m$[c] [°C] | cryst[c] [%] |
|---|---|---|---|---|---|---|---|---|---|
| 5-1 | $^{MeO}$**1-dmso** | 5.1 | 87.6 | 9.3 | 330 | 2.2 | 3.5 | 131 | 81 |
| 5-2 | $^{MeO}$**1** | 5.0 | 91.0 | 11.5 | 411 | 2.1 | 3 | 132 | 86 |
| 5-3 | $^{MeO}$**1-Cl**[d] | 2.6 | 47.4 | 9.8 | 350 | 2.1 | n.d. | n.d. | n.d. |
| 5-4 | $^{cHexO}$**1** | 3.0 | 58.0 | 6.2 | 220 | 2.3 | 1.2 | 132 | 93 |
| 5-5 | $^{H}$**1** | 4.2 | 65.0 | 1.5 | 56 | 2.2 | 0.6 | 125/111[e] | - |
| 5-6 | $^{CF3}$**1** | 4.2 | 78.0 | 1.5 | 54 | 2.1 | 1.1 | n.d. | n.d. |
| 5-7 | $^{(MeO)2}$**1** | 1.2 | 23.0 | 1.6 | 59 | 1.9 | 4.7 | 122/108[e] | - |
| 5-8 | $^{(iPrO)2}$**1** | 1.6 | 27.0 | 11.9 | 425 | 2.2 | 3.8 | 130 | 78 |
| 5-9 | $^{(MeO)3}$**1** | 2.4 | 42.0 | 13.9 | 495 | 2.3 | 5.1 | 127 | 75 |
| 5-10 | $^{(MeO;Me2)}$**1** | 0.2 | 3.4 | 1.1/ 33.2[g] | 41[a] | 1.7/ 3.0[g] | 1.4 | 125[f] | - |
| 5-11 | $^{Thy}$**1** | 0.03 | 0.6 | 1.0/ 22.6 | - | 1.5/ 3.9 | - | 126[f] | - |
| 5-12 | $^{Car}$**1** | traces | - | - | - | - | - | - | - |
| 5-13 | $^{Ph}$**1** | 0.3 | 4.8 | 9.5 | 392 | 3.3 | 0.6 | 136 | 87 |
| 5-14 | $^{Ar}$**1** | 8.9 | 190.0 | 29.1 | 1037 | 2.8 | 0 | 136 | 81 |
| 5-15 | $^{Ar/(MeO)2}$**1** | 2.1 | 44.0 | 16.7 | 596 | 2.3 | 1.1 | 134 | 86 |
| 5-16 | $^{cHexO/(MeO)2}$**1** | 3.9 | 68.0 | 21.4 | 762 | 2.8 | 3.6 | 130 | 71 |
| 5-17 | $^{Me*/(MeO)3}$**1** | 0.9 | 16.0 | 6.7 | 238 | 2.1 | 0.8 | 133 | 96 |
| | T = 40 °C[h] | | | | | | | | |
| 5-18 | $^{MeO}$**1** | 0.1 | 1.7 | 3.7 | 132 | 2.0 | 0 | 128 | 93 |
| 5-19 | $^{Ar}$**1** | 0.2 | 3.4 | 12.6 | 448 | 3.0 | 0 | 134 | 90 |
| 5-20 | $^{CF3}$**1** | 0.5 | 9.0 | 0.9 | 32 | 2.4 | 0 | 120[f] | - |

Polymerization conditions: [Pd] = $4\times10^{-5}$ mol/L, t = 30 minutes, V(toluene) = 100 mL, T = 80 °C, U = 1000 rpm; [a]determined by GPC in 1,2,4-trichlorobenzene at 160°C; [b]determined by $^1$H NMR in $C_2D_2Cl_4$, 130 °C; [c]determined by DSC; [d]without activation with $AgBF_4$; [e]bimodal melting curve; [f]multimodal melting curve; [g]bimodal; [h]polymerization conditions: [Pd] = $4\times10^{-5}$ mol/L, t = 30 minutes, V(toluene) = 100 mL, T = 40 °C, U = 1000 rpm.

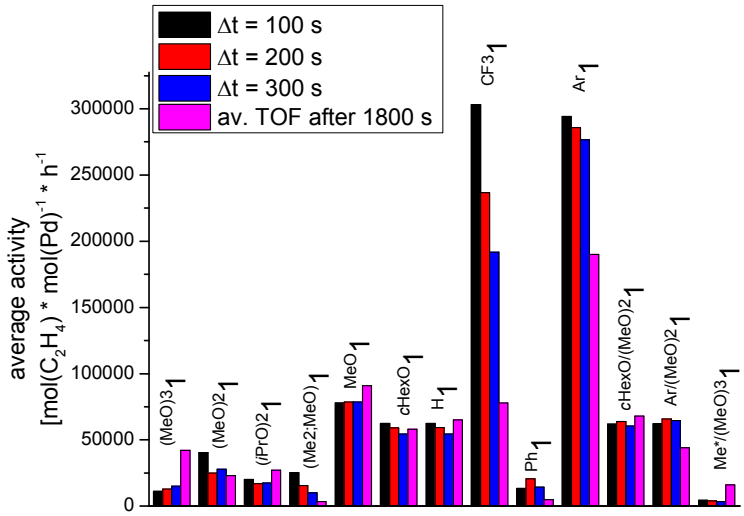


**Figure 4-11.** Average activity of various catalysts in ethylene homopolymerization for the first 100, 200, and 300 seconds of the polymerization as determined from mass flow and TOF after 30 minutes as determined from isolated PE yield.

By far the highest activities were found for $^{CF3}$**1** and $^{Ar}$**1** with an initial TOF of $3\times10^6$ mol($C_2H_4$) mol(Pd)$^{-1}$ h$^{-1}$. However, both catalysts decompose rapidly (*vide supra*). The high peak activity but also the highest tendency for decomposition found for the electron poor $^{CF3}$**1** are in line with the stoichiometric insertion studies. Similar as found for the MA insertion rate constants, $^{H}$**1** shows a lower activity than both the electron poor and the electron rich substituted $^{CF3}$**1** and $^{MeO}$**1**.

In contrast, the rather electron rich compound $^{(MeO)2}$**1** exhibits significantly reduced activities compared to $^{MeO}$**1**. Analysis of the solid state structures reveals that by introduction of a second ortho-substituent in the non-chelating aryl moieties the steric bulk around the metal center is slightly increased (Figure 4-4). In addition, weak interactions of the MeO-group with the palladium atom cannot be excluded. However, the substitution of the methoxy-group by sterically more demanding isopropoxy-groups in $^{(i\text{PrO})2}$**1** does not further affect activities (Table 4-5, entry 5-7 vs. 5-8). Introduction of a third MeO-group in the para position of the non-chelating aryl moiety in $^{(MeO)3}$**1** doubles activity to $4\times10^4$ mol($C_2H_4$) mol(Pd)$^{-1}$ h$^{-1}$ compared to $^{(MeO)2}$**1** (entry 5-7 vs. 5-9). By contrast, substitution of one 2,4,6-$(MeO)_3C_6H_2$ substituent by a methyl group in $^{Me*/(MeO)3}$**1** reduces activity to $2\times10^4$ mol($C_2H_4$) mol(Pd)$^{-1}$ h$^{-1}$ (entry 5-9 vs. 5-15). The asymmetric substituted compounds $^{Ar/(MeO)2}$**1** and $^{c\text{HexO}/(MeO)2}$**1** are significantly more active than the symmetric catalyst $^{(MeO)2}$**1**, and it appears that the activity of asymmetric compounds is roughly an average of the activities of the corresponding symmetric catalysts. Rather unexpectedly, a comparison of $^{Ar}$**1** and $^{Ph}$**1** reveals a strong difference between these closely related catalysts, as $^{Ar}$**1** processes a nearly 15 times increased peak activity. This points to a special role of the additional methoxy substituents in $^{Ar}$**1**.

In general, the relative activities observed in ethylene homopolymerization for different catalysts correspond to the ratio of the acrylate insertion rate constants determined from the NMR experiments with one important exception: $^{(MeO)3}$**1** and $^{CF3}$**1** exhibit the highest MA insertion rate constants of all catalysts, but in contrast to $^{CF3}$**1** only a moderate activity in the ethylene homopolymerization is found for $^{(MeO)3}$**1**. This might be due to a comparative lower reactivity of ethylene for binding and insertion for electronic reasons.

The systematic picture revealed by this study agrees with previous single observations. Claverie et al. reported a drop in activity from $^{Ar}$**1-lut** over $^{MeO}$**1-py** to $^{H}$**1-py**. However, in this case catalysts exhibiting electron deficient ligands bearing 3,5-$CF_3$ substituted or perfluorinated aryl moieties showed further decreased activities.[37] Rieger et al. observed a drastic decrease in catalytic activity upon replacement of the methoxy groups in $^{MeO}$**1** by more electron donating MeS-groups.[31] Jordan et al. showed that enhancing the electron deficiency

of the Pd center by binding of $B(C_6F_5)_3$ to the sulfonate group of (P^O)PdMe compounds increases activity, but simultaneously also the chain transfer rate. Regarding a P-alkyl substitution it was reported that a replacement of the 2-$MeOC_6H_4$ moieties by cyclohexyl groups decreases the activity.[51] By contrast, Claverie found that substitution by *tert*-butyl groups drastically increases polymerization activity, but at the same time the catalyst decomposes rapidly.[37]

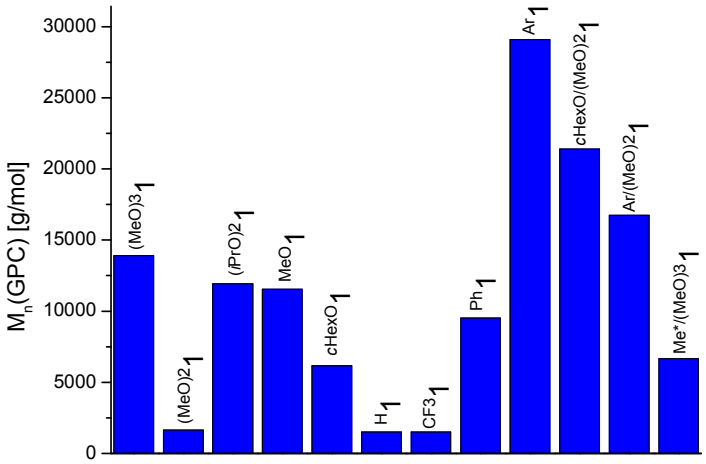


**Figure 4-12.** Molecular weights ($M_n$) of polyethylene obtained with different catalysts ($p_{C2H4}$ = 5bar, 80 °C).

The polyethylene molecular weight depends on electronic and steric factors (Table 4-5, Figure 4-12). The molecular weight decreases with increasing electron deficiency of the ligand from $^{MeO}$**1** to $^{H}$**1** and $^{CF3}$**1** ($M_n$: $1.2\times10^4$ vs. $1.5\times10^3$ vs. $1.5\times10^3$ g mol$^{-1}$). However, the introduction of bulky cyclohexyloxy substituents in $^{cHexO}$**1** ($M_n$: $6\times10^3$ g mol$^{-1}$) does not further increase the polymer chain length. With the introduction of a second ortho-methoxy group in $^{(MeO)2}$**1** molecular weight is decreased drastically compared to $^{MeO}$**1** ($M_n$: $1.6\times10^3$ vs. $1.2\times10^4$ g mol$^{-1}$), but can be significantly increased again by steric shielding, as in $^{(iPrO)2}$**1** ($M_n$: $1.2\times10^4$ g mol$^{-1}$), or by the introduction of another electron rich group in para-position, as in $^{(MeO)3}$**1** ($M_n$: $1.4\times10^4$ g mol$^{-1}$). The bulky aryl substituted $^{Ar}$**1** produces the highest molecular weight PE in this study (Figure 4-12, $M_n$: $2.9\times10^4$ g mol$^{-1}$). By comparing $^{Ar}$**1** to $^{Ph}$**1** ($M_n$: $9.5\times10^3$ g mol$^{-1}$) it becomes clear that steric shielding by the phenyl substituents does not automatically lead to an increase of chain length. This again might indicate a special role of the methoxy groups in $^{Ar}$**1**, which can arrange in the axial position of the Pd center.[24] In this context note that for catalysts with bulky naphthyl, phenanthryl, antracenyl or 1-methoxynaphtalene substituents no increase of molecular weights was observed compared to $^{MeO}$**1**.[28,31] A small positive effect of moderate steric shielding on the molecular weight is

found for the asymmetric catalysts $^{Ar/(MeO)2}$**1** ($M_n$: $1.7\times10^4$ g mol$^{-1}$) and $^{cHexO/(MeO)2}$**1** ($M_n$: $2.1\times10^4$ g mol$^{-1}$) compared to $^{(MeO)2}$**1** ($M_n$: $1.6\times10^3$ g mol$^{-1}$).

The polymers produced by the different catalysts show very similar microstructures. Highly linear polymers with no more than five methyl branches per 1000 carbon atoms and no longer branches are obtained. It seems to be an intrinsic property of these (P^O) chelated palladium catalysts either to show only a minimal amount of chain walking, or to strongly prefer insertions into primary carbons. As a result, catalysts that are prone to β-H-elimination such as $^{CF3}$**1** preferably chain transfer rather than create branches. Within the narrow range of 0-5 methylene branches it appears that more electron rich compounds produce slightly more branches (entry 5-1 vs. 5-4/5) and that steric shielding reduces the number of branches (entry 5-7 vs. 5-8 and 5-2 vs. 5-4/11/12).

The compounds $^{MeO}$**1**, $^{Ar}$**1** and $^{CF3}$**1** were also compared in polymerization at 40 °C to evaluate the influence of temperature on decomposition, chain length and branching (Table 4-5). At 40 °C $^{CF3}$**1** is the most active catalyst, which confirms the high peak activity of this compound in the mass flow at 80 °C. Interestingly, for all three catalysts it is observed that molecular weight and branching are both reduced at 40 °C, with the relation of the molecular weights observed with different catalysts unchanged. This is unexpected as usually an increase of molecular weights for polymerizations at lower temperatures is observed. Possibly chain growth is very slow and chain transfer due to impurities becomes relevant.

In comparison to the acrylate insertion rate constants determined by NMR it appears that electron deficient compounds ($^{CF3}$**1**, $^{Ar}$**1**) possess higher activities, than electron rich compounds ($^{(MeO)2}$**1**,$^{(MeO)3}$**1**), while catalyst stability is decreased with increasing electron deficiency. Concerning molecular weights, steric shielding can have a positive effect, if adjusted right ($^{Ar}$**1** vs. $^{MeO}$**1**). Electronic influences on the polymers´ molecular weights are ambiguous, but electron deficient compounds tend to produce lower molecular weights ($^{CF3}$**1** vs. $^{MeO}$**1**, $^{(MeO)2}$**1** vs. $^{(MeO)3}$**1**). Further, the combination of two distinct substituents at phosphorus in an asymmetric catalyst proved to be a fruitful concept for predictable modulation of catalyst properties to a desirable overall catalyst profile.

### 4.2.5 Copolymerization of Ethylene with Methyl Acrylate

The catalysts were studied in the copolymerization of ethylene with methyl acrylate at 5 bar ethylene pressure and various polar monomer concentrations at 95 °C. Catalysts $^{(MeO;Me2)}$**1**, $^{Car}$**1**, and $^{Thy}$**1** were not further investigated, since they exhibited very low activities in ethylene homopolymerization. The [{($^{X}$**1-Cl**)-μ-M}$_n$] precatalysts were activated *in situ* with $AgBF_4$ as described before. It could be shown that polymerizations with $^{MeO}$**1** and $^{MeO}$**1-dmso** result in the formation of similar polymers with comparable activities (Table 4-6, entry 6-4 vs. 6-18).

**Table 4-6.** Ethylene/methyl acrylate copolymerization.

| entry | catalyst | c(MA) [mol/L] | yield [g] | χ(MA) [mol%][a] | $DP_n$[a] | $M_n$[a,b] | TOF (MA)[b] | TOF (E)[d] | MA EG[e] [mol%] | $M_w/M_n$[f] |
|---|---|---|---|---|---|---|---|---|---|---|
| 6-1 | $^{MeO}$**1** | 0.16 | 4.9 | 2.8 | 112 | 3.3 | 2.3 | 81.5 | 19 | 2.0 |
| 6-2 | $^{MeO}$**1** | 0.3 | 2.3 | 5.9 | 132 | 4.2 | 2.2 | 34.7 | 43 | 1.8 |
| 6-3 | $^{MeO}$**1** | 0.6 | 2.3 | 9.6 | 111 | 3.7 | 3.4 | 31.9 | 63 | 1.7 |
| 6-4 | $^{MeO}$**1** | 1.2 | 0.9 | 21.7 | 47 | 1.9 | 2.5 | 9.0 | 85 | 1.9 |
| 6-5 | $^{MeO}$**1** | 2.5 | 0.5 | 34.3 | 33 | 1.6 | 1.6 | 3.0 | 93 | 2.0 |
| 6-6 | $^{MeO}$**1** | 4.9 | 0.3 | 46.4 | 26 | 1.4 | 1.3 | 1.6 | 97 | 1.8 |
| 6-7 | $^{(MeO)2}$**1** | 0.18 | 3.4 | 4.3 | 54 | 1.7 | 2.4 | 52.5 | 12 | 1.7 |
| 6-8 | $^{(MeO)2}$**1** | 0.3 | 4.1 | 10.0 | 72 | 2.4 | 5.9 | 54.0 | 44 | 1.8 |
| 6-9 | $^{(MeO)2}$**1** | 0.6 | 1.9 | 17.8 | 63 | 2.4 | 4.3 | 19.7 | 73 | 2.1 |
| 6-10 | $^{(MeO)2}$**1** | 1.2 | 1.5 | 29.7 | 47 | 2.1 | 4.9 | 11.6 | 90 | 2.0 |
| 6-11 | $^{(MeO)2}$**1** | 2.4 | 0.4 | 37.3 | 41 | 2.0 | 1.5 | 2.6 | 93 | 1.5 |
| 6-12 | $^{(MeO)2}$**1** | 5.0 | 0.4 | 50.2 | 33 | 1.9 | 2.0 | 1.9 | 96 | 1.5 |
| 6-13 | $^{(iPrO)2}$**1** | 0.6 | 0.6 | 3.2 | 125 | 3.7 | 0.3 | 9.9 | 17 | 2.0 |
| 6-14 | $^{(iPrO)2}$**1** | 1.2 | 0.8 | 5.2 | 145 | 4.5 | 0.6 | 11.5 | 29 | 1.9 |
| 6-15 | $^{(MeO)3}$**1** | 0.3 | 0.6 | 13.4 | 94 | 3.4 | 1.2 | 7.4 | 69 | 2.0 |
| 6-16 | $^{(MeO)3}$**1** | 0.6 | 0.7 | 21.8 | 76 | 3.1 | 1.2 | 4.3 | 78 | 2.0 |
| 6-17 | $^{(MeO)3}$**1** | 1.2 | 0.4 | 33.4 | 58 | 2.7 | 1.3 | 2.5 | 92 | 1.8 |
| 6-18 | $^{MeO}$**1-dmso** | 1.2 | 1.0 | 21.0 | 49 | 2.0 | 2.7 | 10.0 | 86 | 1.9 |
| 6-19 | $^{CF3}$**1** | 1.2 | 0.2 | 8.5 | 11 | 0.4 | 0.2 | 2.6 | 30 | - |
| 6-20 | $^{CF3}$**1**[g] (40 °C) | 1.2 | 0.3 | 3.7 | 11 | 0.3 | 1.3 | 2.2 | 9 | - |
| 6-21 | $^{Ar}$**1** | 1.2 | 1.8 | 1.6 | 515 | 14.9 | 0.5 | 31.7 | 3 | 2.3 |
| 6-22 | $^{Ar}$**1** | 4.9 | 2.6 | 8.2 | 365 | 12.0 | 3.3 | 36.9 | 61 | 1.9 |
| 6-23 | $^{c}$**HexO/(MeO)2 1** | 1.2 | 0.7 | 13.1 | 202 | 7.2 | 1.2 | 8.2 | 73 | 2.1 |
| 6-24 | $^{c}$**HexO/(MeO)2 1** | 0.6 | 0.5 | 5.4 | 382 | 11.9 | 0.5 | 8.2 | 43 | 2.1 |
| 6-25 | $^{H}$**1** | 1.2 | 0.2 | 19.1 | 44 | 1.7 | 0.5 | 2.0 | 67 | 1.7 |
| 6-26 | $^{cHexO}$**1** | 1.2 | 1.2 | 8.5 | 143 | 4.7 | 1.5 | 16.3 | 35 | 2.0 |
| 6-27 | $^{Ph}$**1** | 1.2 | 0.3 | 2.2 | 297 | 8.7 | 0.1 | 5.7 | 10 | 2.1 |
| 6-28 | $^{Ar/(MeO)2}$**1** | 1.2 | 0.4 | 5.0 | 190 | 5.9 | 0.3 | 14.9 | 27 | 2.0 |
| 6-29 | $^{Me*/(MeO)3}$**1** | 1.2 | 0.03 | 24.2 | 61 | 2.6 | 0.1 | 0.3 | 76 | 1.6 |

Polymerization conditions: total volume toluene + MA: 50 mL; 5 bar ethylene pressure; T = 95 °C; 20 μmol Pd(II); 1 hour reaction time. [a]Determined by $^1$H NMR in $CDCl_3$, 25 °C/ $C_2D_2Cl_4$, 130 °C; [b]$10^3$ g mol$^{-1}$; [c][$10^2$ mol (MA) mol (Pd)$^{-1}$ h$^{-1}$];.[d][$10^2$ mol($C_2H_4$) mol(Pd)$^{-1}$ h$^{-1}$]; [e]mol% of MA derived unsaturated endgroups, determined by $^1$H NMR; [f]determined by GPC; [g]polymerization conditions: total volume toluene + MA: 50 mL; 5 bar ethylene pressure; T = 40 °C; 20 μmol Pd(II); 1 hour reaction time.

For $^{MeO}$**1**, $^{(MeO)2}$**1**, and $^{(MeO)3}$**1** polymerizations were performed with methyl acrylate concentrations varying from 0.15 M to 5 M (Table 4-6, entries 6-1 – 6-17). With increasing methyl acrylate concentration MA incorporation increases, as expected. In addition, the average polymer chain length as well as the activity decrease with increasing MA concentration and incorporation as also observed for Pd diimine catalysts.[3] Copolymerization activities (TOF ethylene/MA) cannot be compared precisely between different catalysts since the determined TOFs depend not only on the nature of the active species. Only the activities for polymerizations yielding copolymers with similar degrees of polar monomer incorporation can be compared, as the formation of six-membered κ-*O* coordinated chelate resting states during the insertion hinders the following monomer insertion, and affects the activity significantly (*vide supra*). Even for copolymerizations with similar incorporation ratios the comparison of activities might be hampered, as the monomer can block the active site by κ-*X* coordination, so that monomer concentration has to be considered. However, the effect of κ-*O* coordination of acrylic acid esters on the activity has been found to be rather low for (P^O)Pd catalysts.[56]

At similar MA concentrations ([MA] = 1.2 M) the electron deficient $^{CF3}$**1** incorporates significantly less MA than $^{H}$**1** and $^{MeO}$**1** ($\chi_{MA,CF3}$ = 9 mol%, $\chi_{MA,H}$ = 19 mol% $\chi_{MA,MeO}$ = 22 mol%, Figure 4-13). Steric hindrance leads to a stronger discrimination of ethylene and the more bulky MA monomer as concluded from the lower incorporation ratio of $^{cHexO}$**1** ($\chi_{MA,cHexO}$ = 13 mol%). Steric effects limit incorporation strongly also for the very bulky $^{Ar}$**1** ($\chi_{MA,Ar}$ = 2 mol%) and $^{Ph}$**1** ($\chi_{MA,Ph}$ = 2 mol%). The introduction of a second methoxy group in ortho position of the non-chelating aryl moiety in $^{(MeO)2}$**1** increases MA incorporation significantly ($\chi_{MA,(MeO)2}$ = 30 mol%). The same applies for $^{(MeO)3}$**1** ($\chi_{MA,(MeO)3}$ = 33 mol%). The very high MA incorporation ratio of $^{(MeO)3}$**1** nicely reflects the relatively high MA insertion rate constants observed in the NMR experiment compared to an only intermediate activity in the ethylene homopolymerization with this catalyst. The observed increase of the incorporation ratio for electron rich systems can also be connected to the weaker π-donor capability of the C=C double bond of MA compared to ethylene. This leads to a shift of the MA/ethylene π-coordination pre-equilibrium for electron rich compounds towards MA coordination. That is, preferred binding of the stronger π-donor ethylene is less pronounced for the more electron rich metal center. Steric shielding in $^{(iPrO)2}$**1** again reduces the incorporation ratio dramatically ($\chi_{MA,(iPrO)2}$ = 5 mol%). Substitution of one of the 2,6-$(MeO)_2C_6H_3$ moieties in $^{(MeO)2}$**1** by bulky 2-*c*Hex$OC_6H_4$ or 2,6-$(MeO)_2C_6H_3(C_6H_4)$

substituents in $^{cHexO/(MeO)2}$**1** or $^{Ar/(MeO)2}$**1** also results in a reduced MA incorporation ($\chi_{MA,Ar/(MeO)2}$ = 5 mol%, $\chi_{MA,cHexO/(MeO)2}$ = 13 mol%).

In contrast, substitution of a 2,4,6-$(MeO)_2C_6H_2$ moiety of $^{(MeO)3}$**1** by a rather small methyl group in $^{Me*/(MeO)3}$**1** does not further increase the incorporation ratio ($\chi_{MA,Me*/(MeO)3}$ = 24 mol%) However, so far the exact influence of P-alkyl substituents remains generally ambiguous (*vide supra*).[37,51]

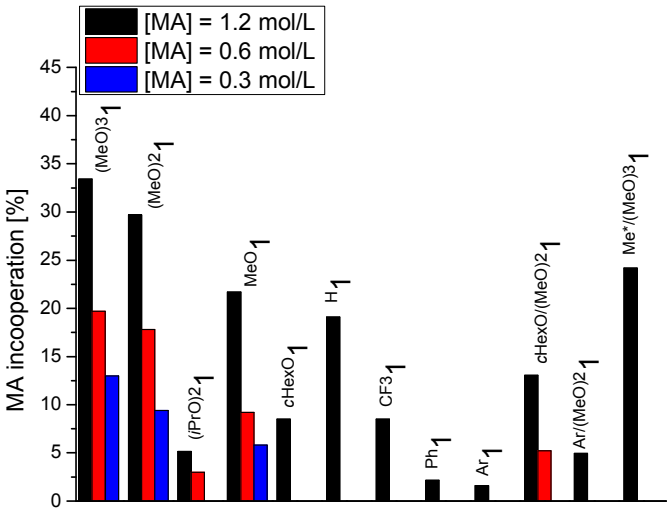


**Figure 4-13.** Relation between catalyst structure and MA incorporation in ethylene/MA copolymerization experiments with $p_{ethylene}$ = 5 bar, and various methyl acrylate concentrations (black: [MA] = 1.2 mol $L^{-1}$; red: [MA] = 0.6 mol $L^{-1}$; blue: [MA] = 0.3 mol $L^{-1}$).

For all catalysts, chain termination is strongly preferred after insertion of methyl acrylate, which becomes obvious by comparing the ratio of MA and ethylene derived unsaturated endgroups to the degree of MA incorporation (Table 4-5). For this reason a discussion of chain length is most meaningful for polymerization runs resulting in copolymers with similar degrees of MA incorporation. A comparison of chain lengths for degrees of incorporation of ~10% and ~5% revealed that steric shielding as in $^{cHexO}$**1**, $^{cHexO/(MeO)2}$**1**, $^{(iPrO)2}$**1**, or $^{Ar}$**1** leads to copolymers with higher average $DP_n$ compared to $^{MeO}$**1** and $^{(MeO)2}$**1** (Figure 4-14). This effect is presumably based on the blocking of the axial positions at the Pd center which hinders chain transfer. The compounds bearing a second methoxy group in ortho position of the non-chelating aryl moieties $^{(MeO)2}$**1** and $^{(MeO)3}$**1** produce significantly shorter polymer chains compared to $^{MeO}$**1**, as was also observed for the ethylene homopolymers. The same applies for the electron poor $^{CF3}$**1**.

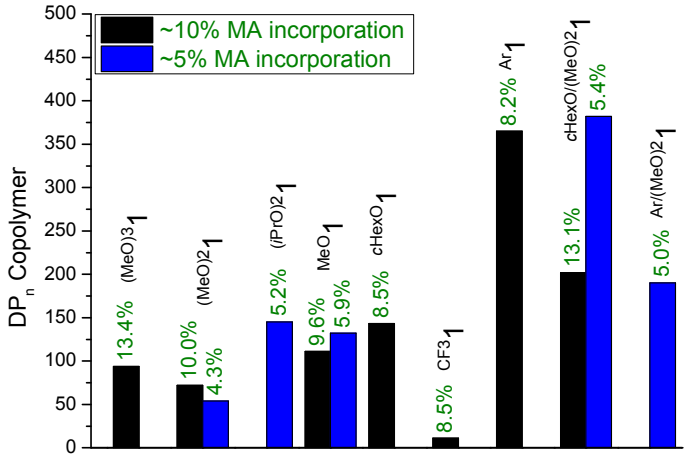


**Figure 4-14.** Relation between catalyst structure and copolymer average degree of polymerization ($DP_n$) for ~10 mol% (black) and ~5 mol% (blue) MA incorporation (determined by $^1H$ NMR).

In conclusion, chain length can be increased by steric shielding and is decreased by a second ortho methoxy or electron poor substituents at the non-chelating aryl moieties of the ligand. Most notably, copolymers with high MA incorporation ratios are accessible with sterically unconstrained systems and especially with double ortho MeO-substituted ligands.

The studies resulted in the identification of catalysts and conditions for the production of ethylene-MA copolymers with reasonable increased molecular weights compared to $^{MeO}$**1**. The asymmetric catalyst $^{cHexO/(MeO)2}$**1** combines good incorporation ratios with high molecular weights (0.6 M MA, $\chi$ = 5 mol%, $DP_n$ = 382, $M_n$ = 12000 g/mol, yield 0.5 g), whereas the chain length is tripled compared to a copolymer with a similar composition produced by $^{MeO}$**1**. Even copolymers with degrees of incorporation > 10 mol% with molecular weights of still ca. 7000 g/mol are accessible (1.2 M MA, $\chi$ = 13 mol%, $DP_n$ = 200, $M_n$ = 7000 g/mol, yield = 0.7 g). Compared to that, $^{MeO}$**1** only produces copolymers with molecular weight of ca 4000 g/mol for 6 mol% MA incorporation. However, the catalytic activity of $^{cHexO/(MeO)2}$**1** is rather low. Higher average degrees of polymerization are accessible with good activities with $^{Ar}$**1**, but in this case high MA concentrations are required for acceptable degrees of incorporation (5 M MA, $\chi$ = 8 mol%, $DP_n$ = 365, $M_n$ = 12000 g/mol, yield = 2.6 g).

## 4.3 Summary and Conclusion

Phosphinesulfonato palladium catalysts are unique in that they allow for the synthesis of linear copolymers of ethylene with polar olefins like alkyl acrylates. So far, the materials accessible are limited to low molecular weight copolymers. In addition, a directed catalyst development is hindered by the lack of insights into the catalyst structure-activity relationship. To this end twelve symmetric and three asymmetric precatalysts were synthesized and studied regarding their reactivity towards (polar) olefins and their performance in (co)polymerization.

The full characterization of the compounds and comparison of NMR and X-ray data led to a rough classification of the corresponding palladium centers in the complexes as rather electron rich ($^{(i\mathrm{PrO})2}$**1**, $^{(\mathrm{MeO})2}$**1**,$^{(\mathrm{MeO})3}$**1**) or rather electron deficient ($^{\mathrm{CF3}}$**1**, $^{\mathrm{Ar}}$**1**) compared to the prototypical $^{\mathrm{MeO}}$**1**. This agrees with the expected effect of the different types and numbers of substituents on the P-aryl moiety.

The results of stoichiometric MA insertion studies as well as ethylene homopolymerization and copolymerization studies are ambiguous regarding clear trends in the effect of electronic properties. However, certain relations can be extracted. Catalysts bearing electron deficient ligands such as $^{\mathrm{CF3}}$**1** and $^{\mathrm{Ar}}$**1** show high activities, but also decompose rapidly under polymerization conditions. The comparison of the polymers produced by $^{(\mathrm{MeO})2}$**1** and $^{(\mathrm{MeO})3}$**1** indicates that more electron donating ligands seem to lead to higher molecular weights. Additionally, it was found that the catalysts bearing ligands with a 2,6-$(MeO)_2$-substitution pattern at the non-chelating aryl moieties show very high incorporation ratios of methyl acrylate in the copolymerization.

From steric variations some clear relations could be identified. If steric bulk is adjusted correctly, molecular weights of homo- and copolymers are enhanced. This is illustrated by the doubling of the copolymer molecular weight by the introduction of isopropyl groups in $^{(i\mathrm{PrO})2}$**1** compared to $^{(\mathrm{MeO})2}$**1**. This trend is further exemplified by the high molecular weight produced by $^{\mathrm{Ar}}$**1** compared to $^{\mathrm{MeO}}$**1**, or to the also electronically deficient $^{\mathrm{CF3}}$**1**, which only produces very low molecular weight PE. That steric shielding by an ortho-aryl substituent alone is insufficient to enhance molecular weight and increase stability becomes obvious by comparing $^{\mathrm{Ar}}$**1** to the related ortho phenyl substituted catalyst $^{\mathrm{Ph}}$**1**, which produces PE of intermediate molecular weight with a low activity and decomposes immediately under polymerization conditions. Presumably, further influences, such as e.g. intramolecular coordination of methoxy groups also contribute. Regarding activity, no

negative effects of steric bulk were observed in the ethylene homopolymerization. In the copolymerization experiments an increase of steric bulk clearly led to an enhanced discrimination of the bulkier polar monomer vs. ethylene as impressively shown by the very low acrylate incorporation ratios of $^{Ar}$**1** and $^{Ph}$**1**.

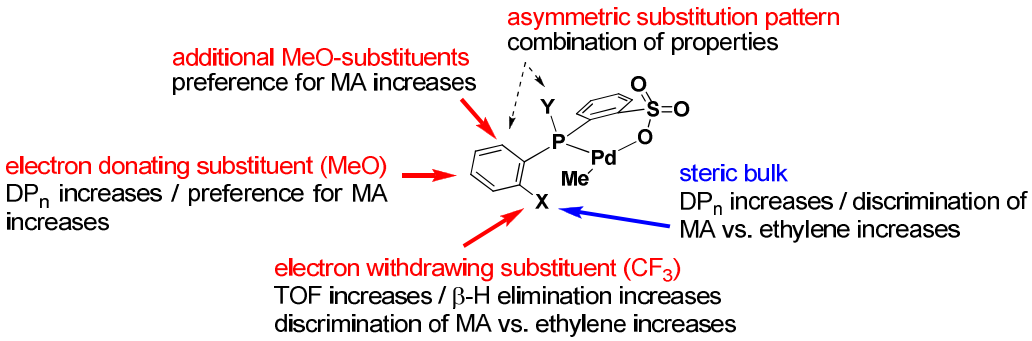


**Figure 4-15.** Influences on catalyst structure on reactivity.

The results of this study (Figure 4-15) can be compared to investigations on Pd(II) diimine catalysts.[3,18,120-122] Here, it is assumed that steric shielding of the active center is necessary to produce high molecular weight material by blocking associative chain transfer. Studies concerning electronic influences revealed that catalysts with more electron donating ligands produce PE with higher molecular weight.[121] For more electron deficient systems, a higher initial activity but a reduced stability at elevated temperatures was found.[18,122] In the copolymerization of ethylene with polar monomers it was observed that catalysts bearing more electron donating ligands incorporate higher amounts of the electron deficient monomer.[18,121] However, investigation on cyclic cyclophane-based Pd(II) diimine catalyst or salicylaldiminato Ni(II) catalyst partly revealed opposite trends.[123,124] This exemplifies the difficulties of general predictions regarding structure–activity relationships, even within the same catalyst class.

For phosphinesulfonato Pd(II) catalysts the precise prediction of influences of single substituents e.g. in ortho position and of their combination remains complicated, as underlined by the low activity and fast decomposition of compounds bearing a 2-MeO-3,6-(alkyl)$_2$ substitution pattern at the non-chelating aryl moieties, though they are closely related to the stable catalyst $^{(MeO)2}$**1**.

These insights highlight the demand for a more directed catalyst design. The results obtained (Figure 4-15) provide a guideline for an appropriate choice of the P-aryl (or P-alkyl) moieties. This concept is underlined by asymmetric catalysts with two different aryl (or aryl/alkyl) substituents, which effectively combine properties imparted by the individual substituents to a desirable overall catalyst profile. The virtues of this strategy are reflected by

the tripled molecular weights of copolymers produced by $^{c\text{HexO/(MeO)2}}$**1** compared to $^{\text{MeO}}$**1**. For 5 mol% MA incorporation copolymers with molecular weights >10000 g/mol were obtained with $^{c\text{HexO/(MeO)2}}$**1** at 0.6 M MA concentration and 5 bar ethylene pressure. In addition, conditions have been identified to produce similar polymers also with the symmetric catalyst $^{\text{Ar}}$**1**. However in this case, the incorporation ratio is limited: For a copolymer containing 8 mol% MA, an MA concentration of 5 mol/L is required at 5 bar ethylene pressure, already.

# 5. Concepts for Stereoselective Acrylate Insertion

## 5.1 Introduction

The regularity of stereocenters in a polymeric chain can profoundly affect the macroscopic materials properties. This is illustrated most impressively by tactic polypropylene, produced on a very large scale. These materials are prepared by catalytic insertion polymerization, in principle the most powerful and generic concept for stereoregular polymerization. However, stereoselective insertion polymerization is restricted to date to non-polar olefins, and excludes polar vinyl monomers. Isotactic and syndiotactic PMMA can be prepared by a coordination-addition mechanism akin to anionic polymerization with early transition metal catalysts. However, acrylates are not amenable to these polymerizations, due to the sterically less bulky and chemical more reactive proton in α-position.[125]

Isotactic polymers can be obtained from alkyl acrylates by anionic polymerization at low temperatures,[126,127] with chiral zirconocenes by a proposed site controlled addition mechanism,[128] or with chiral auxiliary controlled free-radical polymerization.[129] However, preparation of syndiotactic material proved to be even more difficult. Slightly syndioenriched (up to ~63% r-dyads) poly(*tert*-butyl acrylate) can be obtained if the polymerization is initiated by *t*BuLi in the presence of organoaluminium complexes,[130] or by free-radical polymerization at low temperatures.[131] Conclusively, so far not only a broad and universal way of influencing the stereocontrol of alkyl acrylate polymerization is missing, but there is also a conceptual gap to an effective tunable control mechanism.

Insertion polymerization is a very effective and versatile approach to control the tacticity in polypropylene homo- and copolymers as underlined by the successful industrial application of metallocene catalysts (Figure 5-1).[132,133] The clear advantage of insertion polymerization for a stereocontrol is that chain growth proceeds directly at the metal center to which the growing chiral polymer chain and an (un)symmetric ligand are attached in close proximity, enabling control of the insertion mode of the next prochiral monomer.

Chiral induction of insertion reactions can be derived from asymmetry of the ligand (enantiomorphic site stereocontrol), the asymmetry of the last inserted monomer (chain end stereocontrol), or a combination of the two.[134] Here, it is generally observed that in case of 1,2-propene insertion, chain end stereocontrol leads to lower stereoselectivities, because the difference in the insertion barriers for the two enantiofaces is typically lower than 8 kJ/mol.[135]

Before this general background, stereocontrolled alkyl acrylate polymerization by insertion in principle appears a promising approach. Copolymerization of polar vinyl monomers with ethylene was achieved first with cationic Pd(II) diimine complexes. In this case highly branched copolymers which consist of ethylene as major component (≥75 mol %) and contain acrylate units at the end of the branches preferentially are obtained.[3,16,18] The extensive chain walking appears problematic in advancing towards a stereoselective polymerization. Neutral arylphosphinesulfonato Pd(II) complexes are capable of copolymerizing methyl acrylate and ethylene to linear random copolymers.[19] Weakly coordinated catalyst precursors (e.g. $^{MeO}$**1-dmso**) enabled an insertion homopolymerization of MA to products with average degrees of oligomerization up to ca. $DP_n = 5$.[37,43] A mechanistic study of the underlying steps clearly revealed that this acrylate homopolymerization occurs by an insertion mechanism. For example, a six-membered chelate complex [(P^O)Pd{$\kappa^2$-*C*,*O*-*C*H(C(O)OMe)$CH_2$CH(C(*O*)OMe)$CH_2CH_3$}] results from two consecutive MA insertions into the Pd-Me bond (Scheme 5-2, c.f. Chapter 3.2.6, Figure 3-18).[44] The isolation of this six-membered chelate revealed another interesting detail, as it was obtained as a mixture of two diastereomers in a 2:1 ratio arising from the configuration of the two stereocenters at the methyl acrylate derived methine groups (see Chapter 3.2.6). The observation that a catalyst system with a rather sterically unconstrained and simple ligand regime ((P^O) = $\kappa^2$-*P,O*-$Ar_2PC_6H_4SO_2O$ with Ar = 2-$MeOC_6H_4$) is able to homooligomerize acrylate, and in addition enables for a small degree of stereocontrol for at least the first two insertion steps motivated a detailed investigation on the origins of stereocontrol.

For comparison and to briefly review proven concepts of stereocontrolled polymerization, the extremely stereoselective early transition metal metallocene and phenoxy-imine/amine post-metallocene catalysts are instructive. These early transition metal catalysts all show a tetrahedral or octahedral coordination sphere around the central atom, which allows for a space filling surrounding of the active center. Furthermore, the insertion polymerization of propene with early transition metals proceeds by migratory insertion, such that the growing chain and the monomer change places in every insertion step. For the rigid ansa-metallocene complexes and the rigid bridged phenoxy-amine catalysts this results in the production of isotactic polymers for $C_2$-symmetric catalysts. Syndiotactic polymer can be obtained with $C_S$-symmetric catalysts that propagate by 1,2 migratory insertions. Here, the alternating coordination sites are either homotopic or enantiotopic, respectively. The multidentate ligand and the growing chain arrange and determine the preferred monomer enantioface. The selectivity of the catalysts can be visualized by quadrant diagrams, where the more

constrained areas are accentuated. The chain arranges in the open quadrants, and the monomer enantioface is then directed by the chain (Figure 5-1). For the unbridged phenoxy-imine catalysts the mechanism differs from the aforementioned catalysts. The complex is $C_2$-symmetric, but in this case the ligand is assumed to be rather fluxional and the insertion proceeds with 2,1 regioselectivity leading to a syndiotactic polymer via a chain end stereocontrol mechanism.[125,132,136-139]

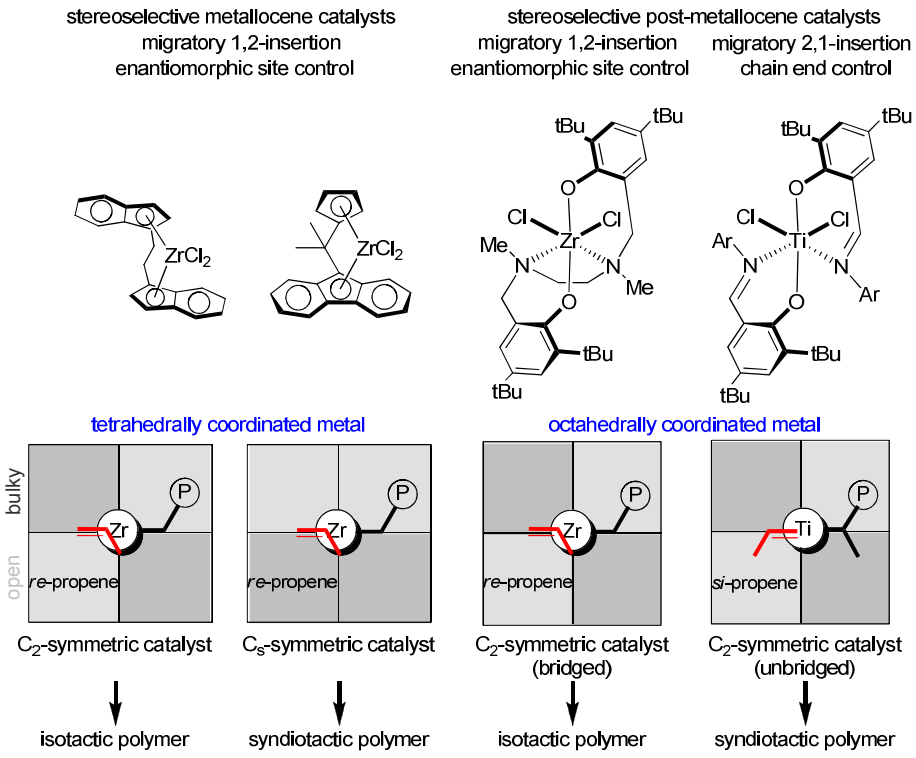


**Figure 5-1.** Metallocene and post-metallocene catalysts for stereoselective propene polymerization.[139]

Stereoselective insertion polymerization with late transition metal catalysts has been less studied. A prominent example is the Pd catalyzed copolymerization of CO with vinyl monomers like propene and styrene. In this case the coordination geometry is square planar, and accordingly less crowded than in tetrahedral or octahedral complexes. For styrene commonly a 2,1-insertion into a Pd-acyl is observed. Achiral, symmetric diimine or bipyridine (N^N)-ligands then lead to the formation of syndiotactic polymer via a chain end stereocontrol mechanism. The enantiomorphic site-controlled formation of isotactic polymer was described for $C_2$- and $C_1$-symmetric (N^N) and (P^N) ligands (complex **A** and **B**, Figure 5-2). For the (P^N) complex **B** the enantiomorphic site stereocontrol is explained by a site selective insertion of styrene trans to the phosphorus donor. Accordingly, stereocontrol is strongly decreased in complex **C**, where steric discrimination between the enantiofaces is reduced. Interestingly, for the asymmetric (N^N) complex **D** which resembles the (P^N)

complex **B** the formation of prevailingly syndiotactic polymer was observed and a chain end stereocontrol was assumed, which was explained by a reversed site selectivity.[125,140-142]

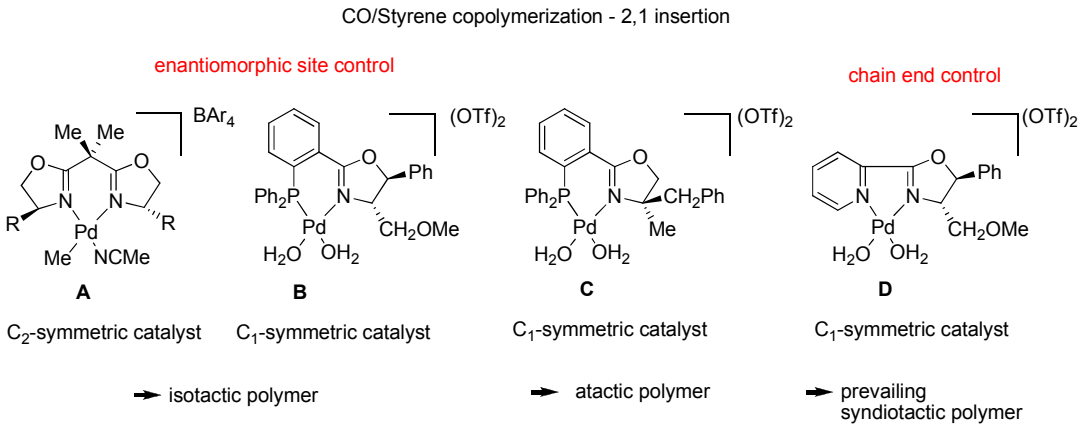


**Figure 5-2.** Pd complexes for CO/vinyl monomer copolymerization.

The formation of highly isotactic propylene/CO copolymers has been described with $C_1$-, $C_2$- and also with $C_s$- and $C_{2V}$-symmetric bisphosphine and phosphine/phosphite ligands, while the synthesis of a syndiotactic polymer was not reported so far. Here, propene is usually inserted in a 1,2 fashion, and the isolation of optically active isotactic polymers with e.g. $C_2$-symmetric ligands clearly reveals that an enantiomorphic site stereocontrol mechanisms is active. However, since related $C_2$-, $C_{2v}$- and $C_s$-symmetric catalysts resulted in the same chain configuration, it can be assumed that chain end and enantiomorphic site stereocontrol might work in the same direction and that the syndiotactic structure is generally not accessible. However, the exact transition state interactions have not been studied.[142,143-145]

In parallel to this work Nozaki et al. communicated that an *in situ* mixture of $C_1$-symmetric, enantiopure phosphinesulfonato ligands such as **$^{Ar/H}$(P^O)H** and [$Pd_2(dba)_3$] allows for the asymmetric copolymerization of CO with (polar) olefins to optically active copolymers (Scheme 5-1).[40]

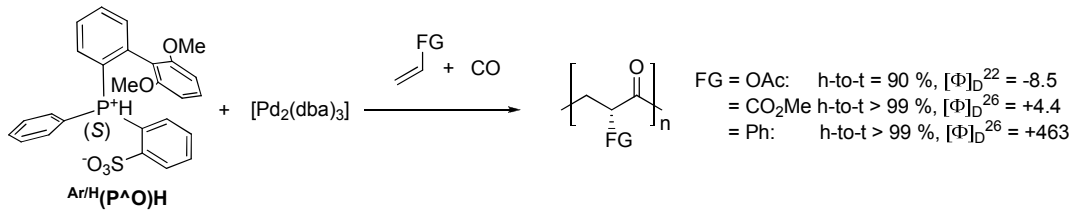


**Scheme 5-1.** Asymmetric copolymerization of polar monomers with CO by optically active phosphinesulfonato catalysts.

For propylene homopolymerization, it has been reported that $C_{2v}$- and $C_s$-symmetric Ni diimine complexes form prevailingly syndiotactic polymer through chain end stereocontrol

at -45 °C. By comparison, analogous $C_2$-symmetric complexes yielded iso enriched material, suggesting the simultaneous operation of chain end and enantiomorphic site stereocontrol.[15,146]

For (P^O)Pd systems the bidentate phosphinesulfonato ligand exhibits two completely different coordination sites at the metal, and the exact combination of the hard sulfonate with the soft phosphine donor seems to be a prerequisite for the unique properties of this catalytic system.[67,68] Whereas the steric bulk of the phosphine substituents can be adjusted and will have a distinct influence on the active center, the sulfonic acid moiety is rather small and does not offer a possibility for steric variation. This results in two completely open sides around the $SO_3$-group, and in general a relatively high flexibility of the ligand (Figure 5-3). In the solid state, as determined by single crystal X-ray diffraction, as well as in the transition states of olefin insertion as determined by DFT studies, one of the non-backbone aryl substituents at the phosphorus adopts a pseudo-axial position and is twisted towards the palladium center, while the other substituent adopts a pseudo-equatorial position with a larger distance to the central atom.[44] Overall, this leads to a quadrant scheme as depicted in Figure 5-3 where only one quadrant is distinctly sterically crowded.

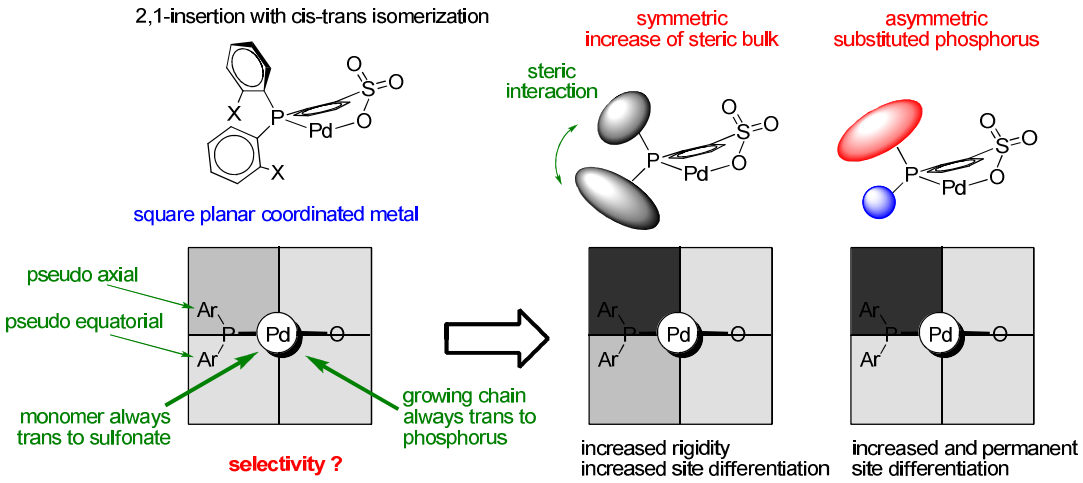


**Figure 5-3.** Analysis of square planar (P^O)Pd catalysts in regard of possible stereoselectivity.

In contrast to the migratory insertion mechanism for early transition metals, monomer insertion at (P^O)Pd systems only occurs after cis/trans isomerization of the growing chain and the coordinated monomer, so that insertion always occurs from the isomer in which the olefin is cis to the P-donor. The structural features enabling this acrylate insertion mechanism are a highly unsymmetric bidentate ligand not only in terms of soft/hard donor characteristics but also in terms of the steric demand of the two donors. In order to gain a deeper

understanding of stereocontrol mechanisms in such unsymmetrical environments, the stereoselective insertion with phosphinesulfonato Pd(II) catalysts has been studied in detail.

## 5.2 Results and Discussion

### 5.2.1 Synthesis and Characterization of Metal Complexes

Acrylate insertions into phosphinesulfonato palladium methyl complexes ($^{X}$**1**) to afford the single ($^{X}$**2**) and double ($^{X}$**3**) insertion products were investigated (Scheme 5-2).

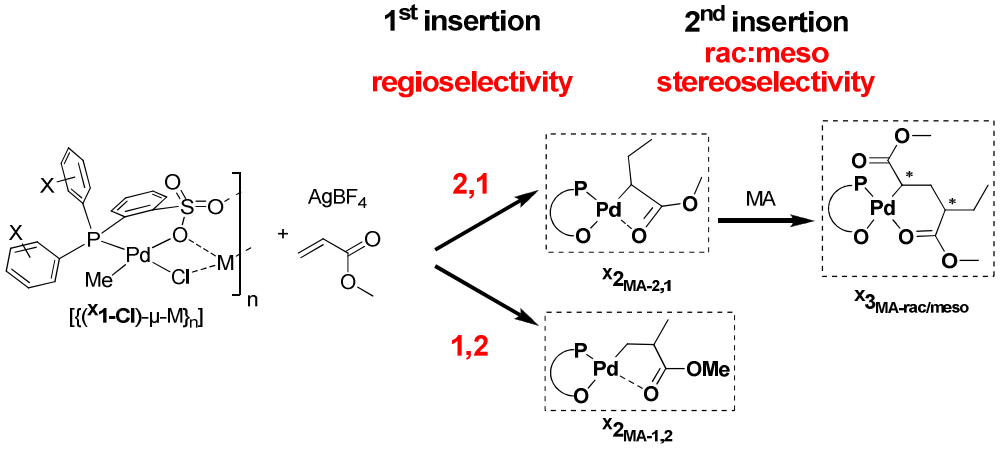


**Scheme 5-2.** Numbering of complexes.

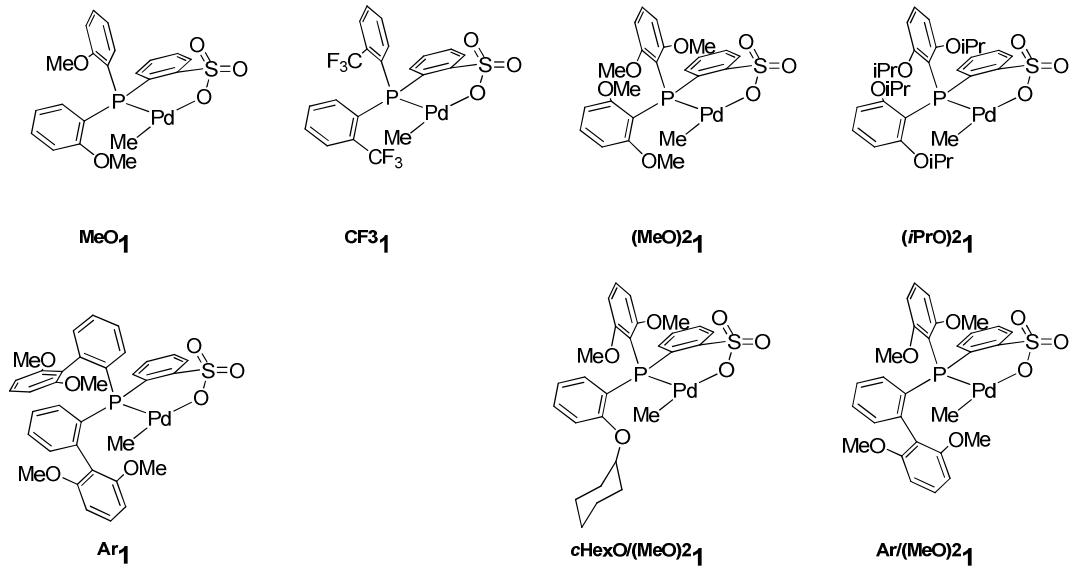


**Figure 5-4.** Phosphorus substitution patterns studied.

A range of substitution patterns at phosphorus differing in steric bulk, flexibility and symmetry were studied (Figure 5-4), including the previously reported compounds $^{MeO}$**1-L**, $^{(MeO)2}$**1-L**, and $^{Ar}$**1-L**.[19,24,87] Synthetic procedures and characterization of the symmetric compounds are extensively discussed in Chapter 4.2.2. Commonly, the [(P^O)PdMe] fragment was generated *in situ* by halide abstraction from the cation-bridged complexes [{($^{X}$**1-Cl**)-μ-M}$_n$] for the insertion and polymerization studies (c.f. Chapter 3.2.4).

In the crystal structures of $^{Ar/(MeO)2}$**1-lut** and $^{cHexO/(MeO)2}$**1-py** a racemic 1:1 mixture of the two configurations at the phosphorus (*R*/*S*) is found for the asymmetric complexes (Figure 5-5). In $^{cHexO/(MeO)2}$**1-lut** the double MeO-substituted aryl moiety is placed in the pseudo-equatorial and the cyclohexyloxy substituted aryl moiety in the pseudo-axial position, with the cyclohexyl-group aligned away from the Pd-center. In contrast, in $^{Ar/(MeO)2}$**1-py** the double MeO-substituted aryl moiety at phosphorus is arranged in the pseudo-axial position. The axial/equatorial alignment of the substituents does not depend on the configuration at the phosphorus atom (*R*/*S*). Hence, the substituents determine the configuration of the (P^O) chelates in the solid state. Here, the more constrained substituent is always located in the less crowded pseudo-equatorial ring-position. Consequently, the steric bulk of the substituents increase from 2-*c*HexO$C_6H_4$- to 2,6-$(MeO)_2C_6H_3$- to 2-(2',6'-$(MeO)_2C_6H_3$)$C_6H_4$- and the $^{Ar/(MeO)2}$**1** fragment is substantially more crowded than the $^{cHexO/(MeO)2}$**1** fragment. This is also indicated by shorter distances of the aryl substituents to the methyl carbon atom at the palladium center in $^{Ar/(MeO)2}$**1-py** ($^{Ar/(MeO)2}$**1-py**: C(1)-C(8) = 3.138(6) Å; C(1)-O(7) = 3.017(5) Å vs. $^{cHexO/(MeO)2}$**1-lut**: C(1)-C(20) = 3.242(5) Å; C(1)-C(9) = 3.527(5) Å). For a discussion of the crystal structures of $^{CF3}$**1-lut**, $^{(MeO2)}$**1-py**, and $^{(iPrO)2}$**1-lut** see Chapter 4.2.2 (Figure 4-4).

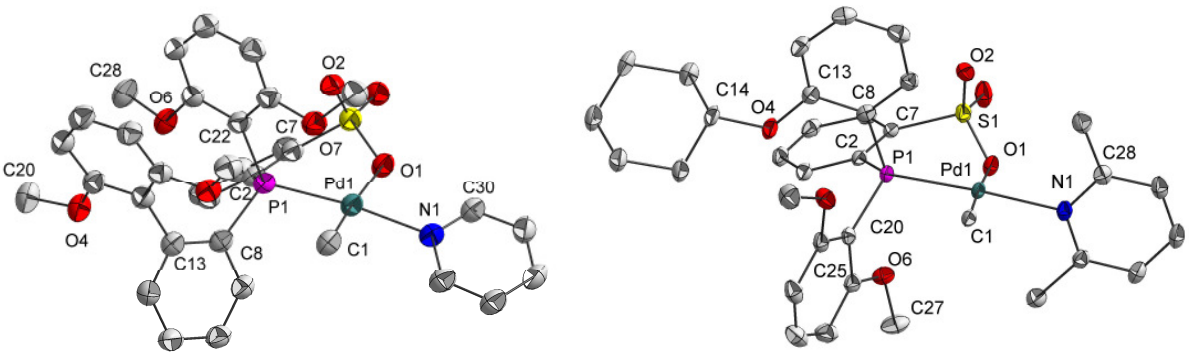


**Figure 5-5.** Solid state structure of $^{Ar/(MeO)2}$**1-py** (left) and $^{cHexO/(MeO)2}$**1-lut** (right). Ellipsoids represent 50% probability. Hydrogen atoms are omitted for clarity. Selected bond lengths [Å] and angles [°] for $^{Ar/(MeO)2}$**1-py**: Pd(1)-P(1) = 2.268(1); Pd(1)-C(1) = 2.025(5); Pd(1)-O(1) = 2.177(3); Pd(1)-N(1) = 2.135(3); C(1)-C(8) = 3.138(6); C(1)-O(7) = 3.017(5); P(1)-Pd(1)-O(1) = 96.3(1); O(1)-Pd(1)-N(1) = 86.0(1). Selected bond lengths [Å] and angles [°] for $^{cHexO/(MeO)2}$**1-lut**: Pd(1)-P(1) = 2.228(1); Pd(1)-C(1) = 2.048(3); Pd(1)-O(1) = 2.151(2); Pd(1)-N(1) = 2.120(3); C(1)-C(20) = 3.242(5); C(1)-C(9) = 3.527(5); P(1)-Pd(1)-O(1) = 95.3(1); O(1)-Pd(1)-N(1) = 89.4(1).

### 5.2.2 Analysis of Complex Flexibility

An essential starting point for this study is the analysis of the structure and possible motions of the (P^O)Pd system, as well as the timescale of such motions. In parts these have been addressed by Jordan,[25] Claverie[28], and Rieger et. al.[31] in a different context and these results will be included in the discussion. The (P^O)PdMe complex is capable of at least two independent motions which can have a significant influence on the surrounding of the active center: A ring flip of the six-membered chelate formed by coordination of the bidentate ligand to the palladium center, and a rotation of the two non-chelating P-bound aryl moieties around the P-C bond (Figure 5-6, left). The six-membered (P^O)Pd chelates adopt a boat-like ring configuration with the phosphorus and the sulfur at the ends, which can flip from above to below the plane created by the other ring atoms. The two conformers are enantiomers which are commonly found in the X-ray structures (A and B, Figure 5-6). Thus, the chelating coordination of the (P^O)-ligand leads to the formation of a stereocenter, which could in principle – if the conformation is stable on the timescale of an insertion – result in differentiation between the two enantiotopic sites of MA during an insertion step. A hindered ring flip would also render the two aryl moieties inequivalent, since they adopt either a pseudo-axial or a pseudo-equatorial position.

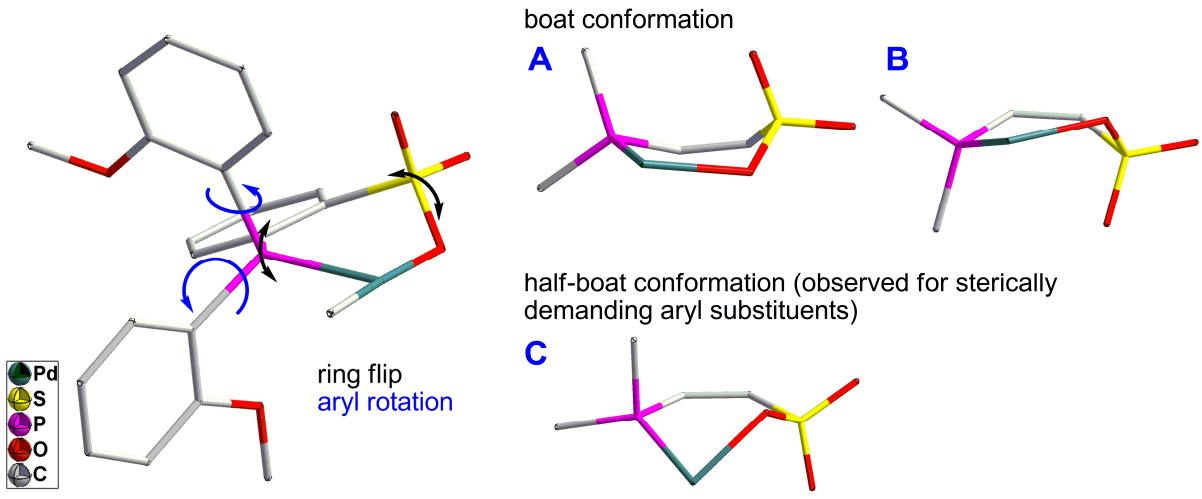


**Figure 5-6.** Observed molecular motions of (P^O)Pd complexes (left) and observed ring conformations for the 6-membered (P^O)Pd chelates.

Interestingly, the boat-like conformation is found in all published X-ray structures of (P^O)Pd chelates with P-bound phenyl moieties,[21,28,30,65] MeO substituents in the ortho position of the aryl-moieties (the only exception being [$^{MeO}$(P^O)Pd(py)$_2$]$^+$),[20,25,41,44,45,47,51,56,61,62,67,87,147] as well as for cyclohexyl substituents,[51] and

3,5-$(CF_3)_2C_6H_3$-moieties.[37] In case of more bulky ortho substituents, respectively more bulky aryl moieties, e.g. $C_6H_4Et$, $C_6H_4(2,6\text{-}(OMe)_2C_6H_3)$ and 1-methoxynaphatalene a distortion of the chelate ring towards a half-boat conformation with the palladium, or the oxygen bound to the palladium, placed at the top position is observed (Figure 5-6 C, a half-boat conformation is also observed for $[^{MeO}(P\text{^}O)Pd(py)_2]^+$, *vide supra*).[24,25,31,43,147] In the X-ray structures of $^{Ar/(MeO)2}$**1-py** and $^{cHexO/(MeO)2}$**1-lut** (Figure 5-5) a boat conformation of the chelate ring is observed, but the (P^O) ring is already slightly distorted towards a half boat configuration. Mechanisms and pathways for interconversion of the ring conformation are discussed below together with the results of theoretical calculations.

Considering the aryl rotation process, the configuration of the arylphosphinesulfonato ligands resemble an $Ar_3ZX$ structure (here: X = lone pair, or H in the free ligand phosphonium tautomer), where all four ligands are arranged approximately tetrahedrally around the central atom Z. Such molecules have been termed molecular propellers since the aryl rings are twisted in the same direction in the ground state, and consequently these molecules show a helical configuration implying axial chirality (*P* or *M*).[148] Consequently a rigid configuration of the P-bound aryl moieties results in a stereocenter and may allow for a stereocontrol. For the simplest case of $PPh_3$ two isomers exist which are enantiomers (Figure **5-7**).

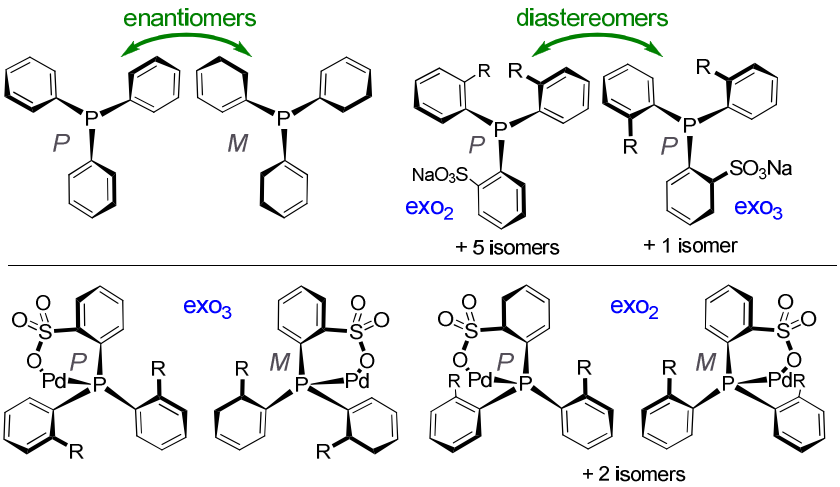


**Figure 5-7.** Helical chirality (*P*, *M*) as found for $Ar_3ZX$ motifs (top, left), and additional diastereomers for the case of ortho substitution of the aryl rings (shown for the free ligand sodium salt, $^{X}$**(P^O)Na**, top, right), and rotamers for $^{X}$(P^O)Pd fragments as observed in the solid state (bottom).

Due to ortho substitution of the aryl moieties, also a major number of possible stereoisomeric configurations can be adopted (16 isomers, 8 pairs of enantiomers), but experimentally only two different arrangements – namely $exo_3$ and $exo_2$ – have been observed for similar $Ar_3ZX$ structures: In the $exo_3$ configuration all ortho substituents are situated on

the same side as the central phosphorus above a plane defined by the three aryl carbons bound to phosphorus (2 isomers, 1 pair of enantiomers). In the various $exo_2$ configurations one of the ortho-substituents is situated underneath this plane (6 isomers, 3 pairs of enantiomers, Figure 5-7). X-ray structures for free (P^O)-ligands are rare, but the structure for **$^{MeO}$(P^O)HNEt$_3$** shows an $exo_3$ arrangement.[149] Interconversions of the different isomers are only possible by correlated rotations of the aryl substituents, e.g. as depicted in Scheme 5-3.

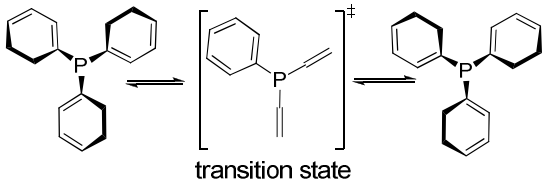


**Scheme 5-3.** Transformation of rotamers by correlated rotation of two aryl moieties.

For (P^O)PdMe complexes the aryl sulfonic acid moiety is fixed in the exo position by the chelating coordination of the ligand. Hence, the maximum number of isomers is reduced to six (three pairs of enantiomers). A comparison of the available X-ray structures further reveals that of the four possible $exo_2$ configurations only two (one pair of enantiomers) are observed (Figure 5-7).[24,25,41,44,45,62,67,147] The $exo_2$ configuration is observed for all [$^{MeO}$(P^O)PdMe(L)] structures (an exception being complexes with $\eta^3$-allyl derived ligands as well as the cationic [$^{MeO}$(P^O)Pd(py)$_2$]$^+$, which show an $exo_3$ arrangement).[93,147] Sterically more demanding aryl moieties like -$C_6H_4$Et, -$C_6H_4$(2,6-$(MeO)_2C_6H_3$) and 1-methoxynaphthalene generally favor the sterically less encumbered $exo_3$ configuration (the only exception being ($^{Ar}$**1**)$_2$(tmeda) which adopts an $exo_2$ configuration).[24,25,31,43] Apparently, steric bulk introduced by the aryl substituents or a crowded coordination sphere at the palladium center leads to a distortion of the boat configuration to a half-boat like chelate (*vide supra*) and favors an $exo_3$ arrangement at phosphorus. For the asymmetric complexes **$^{cHexO/(MeO)2}$1-lut** and **$^{Ar/(MeO)2}$1-py** configuration analysis is ambiguous, because of the $C_{2v}$-symmetry of the 2,6-$(MeO)_2C_6H_3$ substituent (Figure 5-5). However, since the second substituent is aligned in an endo fashion in each case, the configurations can be considered $exo_2$-like in analogy to the other compounds.

### 5.2.3 Dynamic NMR Studies

With regard to a stereoselection in catalysis, the dynamics in solution are relevant. To this end, the temperature dependent dynamics of $^{MeO}$**1-py**, $^{Et}$**1-py** and $^{Ar}$**1-py** have been reported previously. In all cases only one dynamic process – indicated by an inequivalence of the aryl substituents at low temperatures – has been observed and assigned to the ring-inversion without further evidence.[21,25,28] In order to shed light on the timescale of the relevant molecular motions various temperature dependent NMR studies (-90 °C to 130 °C) were conducted with the free ligands $^{X}$**(P^O)H**, the corresponding salts $^{X}$**(P^O)M** and the methyl complexes $^{X}$**1**.

For the protonated ligand $^{MeO}$**(P^O)H** no change in the spectrum is observed at temperatures down to -90 °C implying that still all molecular motions are fast. For the sodium salt $^{MeO}$**(P^O)Na** the anisyl moieties are inequivalent at -90 °C (Figure 5-8), but only one diastereomer is detected as the compound exhibits only one $^{31}$P NMR resonance. Here, it is assumed that the interconversion between two enantiomers is slow rendering the aryl moieties inequivalent and that either only a single $exo_3$/$exo_2$ conformation is populated or rather unlikely that the interconversion between these conformations is still fast. The similar shift of the anisyl ortho protons $H_{12a}$ and $H_{12b}$ (6.64/6.32 ppm, Figure 5-8, Table 5-1), which is a measure for the $exo_2$ content, indicates that probably only the $exo_3$ configuration is populated, as it was also observed for $PAr_2Ar'$ phosphines.[150,151] This can be confirmed by a $^1$H, $^1$H ROESY spectrum at -80 °C showing NOE-correlations between the sulfonic acid ortho proton $H_3$ to both the anisyl ortho protons $H_{12a}$ and $H_{12b}$ (Figure 5-9), and is also in line with the solid state structure of $^{MeO}$**(P^O)HNEt$_3$**.[149]

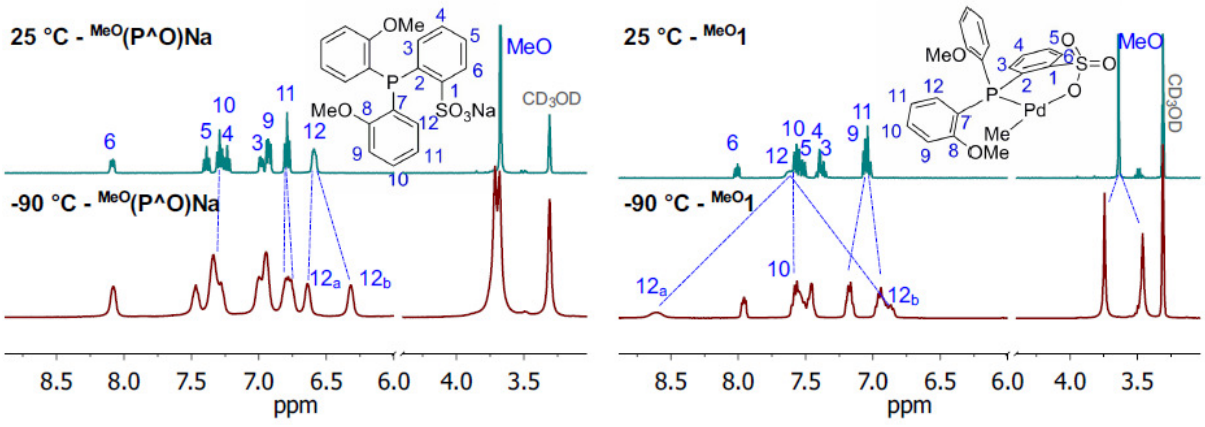


**Figure 5-8.** Variable temperature $^1$H NMR spectra (400 MHz, $CD_3OD$) of $^{MeO}$**(P^O)Na** and $^{MeO}$**1**.

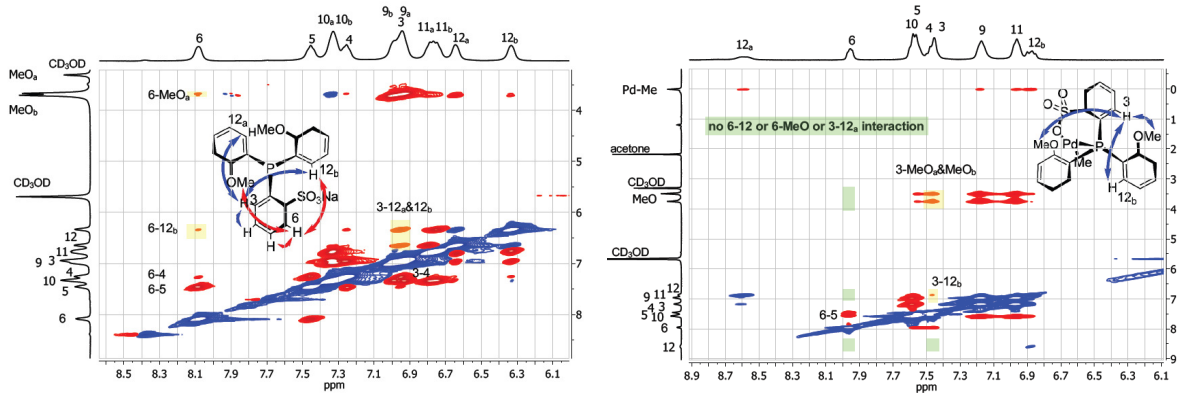


**Figure 5-9.** $^{1}$H,$^{1}$H ROESY spectra ($CD_3OD$, -80 °C) of $^{MeO}$**(P^O)Na** (left) and $^{MeO}$**1** (right) for conformational analysis, evidencing an $exo_3$ (left), respectively an $exo_2$ (right) configuration.

For the Pd complex $^{MeO}$**1** similarly only the aryl moieties are rendered inequivalent at -90 °C. In this case the anisyl ortho protons $H_{12}$ exhibit a strong shift difference at -90 °C (8.60/6.87, Figure 5-8, Table 5-1) indicating the population of a single $exo_2$ configuration, which is in line with the solid state structure for $^{MeO}$**1-lut**.[45] Accordingly, there is only a NOE-correlation between $H_3$ and $H_{12b}$ but not between $H_3$ and $H_{12a}$ visible in the $^{1}$H, $^{1}$H ROESY spectrum at -80 °C (Figure 5-9). The observed downfield shift to 8.60 ppm for the ortho $H_{12a}$ resonance assigned to the aryl moiety with the MeO-group in the endo position can be explained due to paramagnetic anisotropy. Because $H_{12a}$ is directed exo and thus forced into close proximity to the palladium $d_{z2}$ orbital.[152,153] Considering further aryl resonances, it can be observed that the protons in meta position of the anisyl ring ($H_{11}$, $H_9$), which resonate at 7.0 ppm, split up in separated signals with a moderate shift difference at -90 °C (7.17, 6.94 ppm). By contrast, the resonance of the para anisyl protons ($H_{10}$) remains rather unchanged (Figure 5-8).

**Table 5-1.** Configuration of the aryl moieties at phosphorus.

| entry | compound | **δ($^{1}$H NMR)** for $H_{12}$ at high T in $CD_3OD$ [ppm] | **δ($^{1}$H NMR)** for $H_{12}$ at low T in $CD_3OD$ [ppm] | **configuration in solution** | **configuration X Ray** |
|---|---|---|---|---|---|
| 1-1 | $^{MeO}$**(P^O)Na** | 5.59 (25 °C) | 6.64/6.32 (-90 °C) | $exo_3$[a] | $exo_3$[b,149] |
| 1-2 | $^{MeO}$**1** | 7.61 (25 °C) | 8.60/6.87 (-90 °C) | $exo_2$[a] | $exo_2$[45] |
| 1-3 | $^{CF3}$**(P^O)Li** | 6.91 (120 °C)[c] | 6.88/6.76 (25 °C) | $exo_3$[a] | n.d.[d] |
| 1-4 | $^{CF3}$**1** | n.o.[e] | 8.29/6.90 (25 °C) | $exo_2$ | $exo_2$ |
| 1-5 | $^{Ar}$**(P^O)H** | 7.41 (25 °C)[f] | 7.42/7.11(-20 °C) | $exo_3$[a] | n.d.[d] |
| 1-6 | $^{Ar}$**(P^O)Na** | 7.10 (60 °C) | 7.07/6.72 (25 °C) | $exo_3$ | n.d.[d] |
| 1-7 | $^{Ar}$**1** | 7.78 (25 °C) | n.d.[g] | n.d.[g] | $exo_2$/$exo_3$[24] |
| 1-8 | $^{cHexO/(MeO)2}$**1** | 7.45 (25 °C) | n.d.[g] | n.d.[g] | $exo_2$ |

[a]Confirmed by $^{1}$H $^{1}$H ROESY, [b]for $^{MeO}$(P^O)HNEt$_3$; [c]in DMSO-$d_6$. [d]X-ray structure not determined; [e]no coalescence for the $H_{12}$ $^{1}$H NMR resonances observed up to 130 °C; [f]in $CD_2Cl_2$; [g]not detected due to broad and overlapping resonances.

For the other symmetric substituted compounds, rather similar processes are observed by NMR spectroscopy (Table 5-1). **$^{CF3}$(P^O)Li** adopts an $exo_3$ arrangement, whereas the corresponding complex is arranged in an $exo_2$ fashion as evidenced by the variable temperature $^1$H NMR shifts. For the very bulky 2,6-$(OMe)_2C_6H_3$-moeity an $exo_3$ arrangement for **$^{Ar}$(P^O)H** is evidenced by a $^1$H $^1$H ROESY spectrum at -20 °C. Whereas for the corresponding complex **$^{Ar}$1** an NMR analysis of the configuration is not possible at -90 °C, due to broad resonances, solid state structures show that $exo_3$ as well as $exo_2$ are possible arrangements (Table 5-1).[24]

For symmetric substitution patterns at phosphorus (**$^{MeO}$1**, **$^{CF3}$1**, **$^{Ar}$1**) freezing of a molecular motions at low temperature results in the inequivalence of the aryl substituents only. This indicates that a single conformation (one pair of enantiomers) must be adopted (Figure 5-8, Table 5-1). Similarly to this, Rieger et al. reported that for a bulky (P^O)H ligand exhibiting 1-methoxynapthalene substituents a restriction of the molecular motion is evidenced by inequality of the two 1-methoxynapthalene substituents in the $^1$H NMR spectra at room temperature. For the corresponding palladium complexes also a single diastereomer exhibiting two inequivalent aryl moieties was observed.[31] In contrast, Claverie et al. observed that for very bulky naphthyl and phenanthryl substituted (P^O)-ligands two stable diastereomers exist in solution. Here, DFT calculations implied that the $exo_3$ and one of the $exo_2$ isomers coexist because of sterically hindered rotation. Consequences upon coordination to palladium could not be clarified completely due to complexity of the spectra.[28]

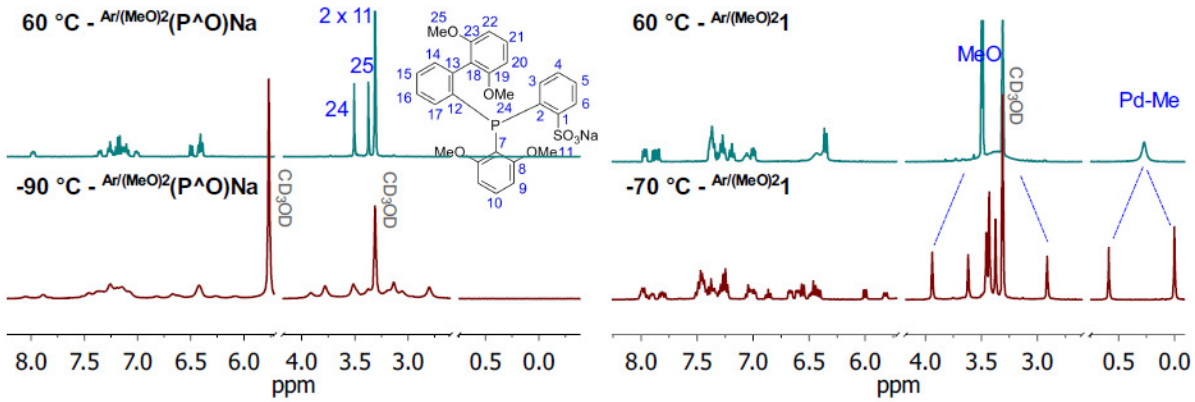


**Figure 5-10.** Variable temperature $^1$H NMR spectra (400 MHz, $CD_3OD$) of **$^{Ar/(MeO)2}$(P^O)Na** and **$^{Ar/(MeO)2}$1**.

The asymmetric compounds **$^{Ar/(MeO)2}$(P^O)Na** and **$^{Ar/(MeO)2}$1** form a pair of diastereomers at low temperature, which results not only in the inequivalence of the aryl substituents but in a complete second set of $^1$H NMR resonances (Figure 5-10). The formation of diastereomers can be related to the combination of the permanent asymmetric center at

phosphorus with the stereocenter derived at low temperature due to a fixed conformation. For the sodium salt as well as for the Pd complex, a 2:3 ratio of the diastereomers is observed.

A comparison of the dynamics for the free ligands and the complexes with coordinated ligands reveals that regularly rather similar processes for the corresponding ligand/complex couple are observed (Figure 5-8, Figure 5-9). The resonances of the non-chelating aryl substituents in the $^1$H NMR split upon freezing of the molecular motion. These new resonances provide further insights into the aforementioned process. In general, it is found here, that the pair of corresponding ortho-aryl protons experiences the largest shift difference, whereas the para proton resonances remain nearly unchanged (Figure 5-8). This is in line with an aryl rotation process, where the para-protons are within the axis of rotation. By contrast, a ring flip should have a more pronounced influence on these para-protons. Since the complexes and the corresponding free ligands show a similar, single motional process and the shift of the $^1$H NMR resonances of the aryl protons upon freezing of the motions is in line with an aryl rotation, it can be concluded that a ring flip process is not observed within the accessible temperature range.

In order to gain insights into the exact energetic barriers of the observed processes dynamic NMR studies of the ligands **$^{X}$(P^O)H**, the corresponding salts **$^{X}$(P^O)M**, and the corresponding complexes were performed. Rate constants at variable temperatures were determined by a full line shape analysis, and an Eyring plot yielded $\Delta H^{\neq}$ and $\Delta S^{\neq}$, respectively (Table 5-2). For comparison, $\Delta G^{\neq}_{Tc}$ (at the coalescence temperature $T_c$) was calculated from $\Delta H^{\neq}$ and $\Delta S^{\neq}$, and also derived independently from the distance of the resonances in the slow exchange region ($\Delta\nu$) according to the equations:[154]

$$\Delta G^{\neq}_{Tc} = 19.14 \cdot T_c \left( 10.32 + \log\left( \frac{T_c}{k_c} \right) \right) \frac{J}{mol}, \quad k_c = \pi \cdot \frac{\Delta\nu}{\sqrt{2}}$$

The latter relationship was also used for determination of $\Delta G^{\neq}_{Tc}$ when line shape analysis was not applicable, as was the case for most of the **$^{X}$(P^O)H** compounds. The $\Delta G^{\neq}_{Tc}$ values obtained by the two different approaches agree well and the comparison of $\Delta G^{\neq}_{Tc}$ for **$^{MeO}$1** ($\Delta G^{\neq}_{Tc}$ = 43 kJ/mol, $T_c$ = -50 °C, Table 5-2) determined for the MeO-groups nicely fits with the value determined by Jordan et al. for **$^{MeO}$1-py** ($\Delta G^{\neq}_{Tc}$ = 44 kJ/mol, $T_c$ = -50 °C).[25]

A comparison of the different ligands reveals that for the protonated ligands **$^{X}$(P^O)H** the rotational barrier increases with the steric bulk: MeO < $CF_3$ ~ Ar. Here, $CF_3$ appears much smaller than 2,6-$(MeO)_2C_6H_3$, but for steric interaction the steric bulk directly attached at the aryl moieties seems to be more important which leads to a similar influence on the rotational barrier for the tetrahedral $CF_3$-versus the flat aryl-substituent.

The barriers for the salts $^{X}$**(P^O)M** (M = Na, Li) are in general significantly higher than for the protonated species (e.g. $\Delta G^{\neq}_{Tc\text{-}CF3(P^O)H}$ = 59 kJ/mol vs. $\Delta G^{\neq}_{Tc\text{-}CF3(P^O)Li}$ = 68 kJ/mol) and in some cases even in the same order as for the complexes. It might be assumed that bulkiness of the sulfonate group is increased by coordination of M (note that in $^{X}$**(P^O)H** the proton is attached to the phosphorus atom) and that the rotational barriers consequently increase. Additionally, ionic interactions of e.g. the MeO-substituents with the counter ion might further contribute to the rotational barrier.

The rotational barriers for complexes $^{X}$**1** are always at least 10 kJ/mol higher than for the free ligands $^{X}$**(P^O)H**. The highest barriers were found for $^{CF3}$**1** for which even at 130 °C no fast interconversion was observed ($\Delta G^{\neq}_{Tc}$ > 76 kJ/mol). Since for $^{Et}$**1** in comparison to $^{MeO}$**1** also a higher barrier was observed ($\Delta G^{\neq}_{Tc}$ = 64 kJ/mol vs. $\Delta G^{\neq}_{Tc}$ = 44 kJ/mol for $^{MeO}$**1**)[25], it appears that small changes in the β-position of the ortho substituents (O*Me*, vs. C$H_2$*Me*, vs. C$F_3$) can have a significant impact on the rotational barriers, as also observed for the free ligands (*vide supra*). The increase of the rotational barriers of around 10-20 kJ/mol upon coordination of the free ligands to a Pd-center agrees with previous observations on arylphosphine complexes. Here, it was reported that for P(o-Tol)$_3$ $\Delta G^{\neq}$ increases steadily from the free phosphine ($\Delta G^{\neq}$<<30 kJ/mol, not observable),[151,155] to a single phosphine coordinated complexes ((CO)$_x$M-P(o-Tol)$_3$, $\Delta G^{\neq}$ = 36-45 kJ/mol),[156,157] to a bis-trans coordinated, quadratic planar complexes ((Cl)$_2$Pt(P(o-Tol)$_3$)$_2$, $\Delta G^{\neq}$ = 65 kJ/mol)[158] and complexes where two ortho-tolyl moieties are part of a five membered κ$^2$-P,C coordinated chelate (e.g. κ$^2$-*P*,*C*-[(o-tol)$_2$*P*(C$_6$H$_4$)*C*H$_2$Pt(*S*$_2$CR)], $\Delta G^{\neq}$ = 64 kJ/mol).[159]

For the asymmetric compounds the formation of diastereomers is observed for $^{Ar/(MeO)2}$**(P^O)Na** and $^{Ar/(MeO)2}$**1** with a higher barrier for the complex ($\Delta G^{\neq}_{Tc\text{-}Ar/(MeO)2(P^O)Na}$ = 39 kJ/mol vs. $\Delta G^{\neq}_{Tc\text{-}Ar/(MeO)21}$ = 59 kJ/mol). However, for the protonated ligand $^{Ar/(MeO)2}$**(P^O)H** no formation of diastereomers can be observed down to -90 °C ($\Delta G^{\neq}_{Tc\text{-}Ar/(MeO)2(P^O)H}$ < 35 kJ/mol), but a rather high barrier of 52 kJ/mol is found for an isolated process only affecting the rotation of the (MeO)$_2$C$_6$H$_3$ group.

In conclusion, of the two motional processes affecting stereoselectivity the aryl rotation possesses the significantly higher barriers in the range of 40-60 kJ/mol, whereas the ring flip process could not be observed in the accessible temperature range and must exhibit barriers always below ca. 35 kJ/mol. The observed barriers and corresponding coalescence temperatures are low in comparison to the temperatures required for an effective insertion, 60-90 °C. Only $^{CF3}$**1** is an exception. Thus, in general the ligand framework must be regarded as conformationally fluxional.

**Table 5-2.** Results of line shape analysis and derived energy barriers for $^{X}$**(P^O)H**, $^{X}$**(P^O)M**, and $^{X}$**1**.

| entry | compound | resonance | $T_c$ [°C] | $\Delta H^{\neq}$ [kJ/mol][a] | $\Delta S^{\neq}$ [kJ/mol][a] | $\Delta G^{\neq}_{Tc}$ [kJ/mol][b]/ [kJ/mol][c] |
|---|---|---|---|---|---|---|
| 2-1 | $^{MeO}$**(P^O)H** | -OMe | <<-90 | - | - | <35[d] |
| 2-2 | $^{MeO}$**(P^O)Na** | -OMe | -35 | 45(2) | -16(8) | 48(4)/50 |
| 2-3 | $^{MeO}$**1** | -OMe | -50 | 39(1) | -17(4) | 43(2)/44 |
| 2-4 | $^{CF3}$**(P^O)H** | -$CF_3$ | 25 | - | - | -/59 |
| 2-5 | $^{CF3}$**(P^O)Li** | -$CF_3$ | 70 | 59(1) | -20(3) | 66(2)/68 |
| 2-6 | $^{CF3}$**(P^O)Li** | Ar-H | 55 | 54(2) | -34(4) | 65(3)/67 |
| 2-7 | $^{CF3}$**1** | -$CF_3$ | >130 | - | - | >76[e] |
| 2-8 | $^{Ar}$**(P^O)H** | -OMe | 20 | - | - | -/59 |
| 2-9 | $^{Ar}$**(P^O)Na** | -OMe | 60 | 57(1) | -12(4) | 62(2)/63 |
| 2-10 | $^{Ar}$**(P^O)Na** | -OMe | 50 | 55(2) | -19(5) | 62(4)/65 |
| 2-11 | $^{Ar}$**1** | -OMe | -43 | 46(2) | 5(9) | 45(3)/46 |
| 2-12 | $^{Ar}$**1** | -OMe | -48 | 43(2) | -8(7) | 45(4)/46 |
| 2-13 | $^{Ar/(MeO)2}$**(P^O)H** | -OMe | -10 | - | - | -/52[f] |
| 2-14 | $^{Ar/(MeO)2}$**(P^O)H** | P | <<-90 | - | - | <35[d] |
| 2-15 | $^{Ar/(MeO)2}$**(P^O)Na** | P | -58 | 34(1) | -15(7) | 38(3)/39[g] |
| 2-16 | $^{Ar/(MeO)2}$**1** | P | 15 | 46(1) | -30(5) | 55(2)/56[g] |
| 2-17 | $^{Ar/(MeO)2}$**1** | PdMe | 25 | 48(1) | -27(1) | 56(1)/59[g] |

[a]determined from Eyring plot; [b]calculated from $\Delta G^{\neq} = \Delta H^{\neq} - T \times \Delta S^{\neq}$; [c]calculated from $k_c = \pi \cdot \Delta\nu/\sqrt{2}$ and $\Delta G^{\neq}_{Tc} = 19.14 \cdot T_c \left(10.32 + \log\left(T_c/k_c\right)\right) J \cdot mol^{-1}$; [d]no hindered rotation observed down to -90 °C, [e]no coalescence observed up to 130 °C; [f]no formation of diastereomers observed, only rotation of 2,6-$(OMe)_2C_6H_3$- is hindered, different process then for entry 2-9 to 2-10 occurs; [g]formation of diastereomers observed.

### 5.2.4 Stereochemistry of Methyl Acrylate Insertion

The reaction of the dimeric precursor [{(**$^{MeO}$1-Cl**)-μ-Na}$_2$] with $AgBF_4$ in the presence of MA in dichloromethane at 60 °C in a sealed tube affords the two diastereomeric products of the consecutive MA insertion into the Pd-Me bond **$^{MeO}$3$_{MA\text{-}rac/meso}$** in a 2:1 ratio (within the experimental error the ratio varies from 1.5:1 to 2.2:1, Figure 5-11, see also Chapter 3.2.6). The rac/meso designation is based on consideration of the stereocenters as part of a growing chain that is in this respect of identical (**$^{MeO}$3$_{MA\text{-}meso}$**) or opposite (**$^{MeO}$3$_{MA\text{-}rac}$**) stereoconfiguration.

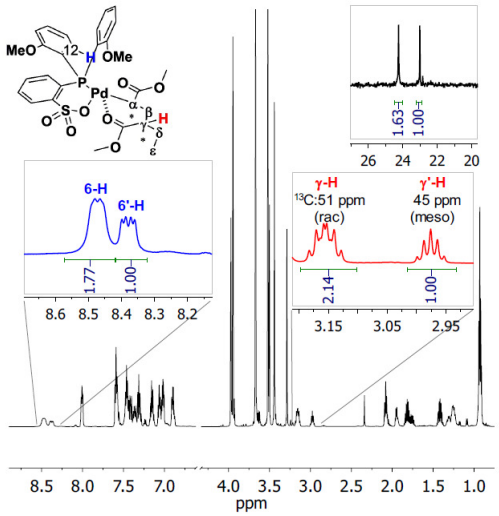


**Figure 5-11.** $^1$H NMR spectrum of **$^{MeO}$3$_{MA}$** (600 MHz, $CD_2Cl_2$, 25 °C; inset $^{31}$P NMR, 168 MHz). Amplifications: NMR resonances relevant for determination of stereoselectivity.[44]

An absolute assignment of the diastereomers is possible by comparison of the NMR-data[44] with the results of X-ray crystallography (see Chapter 3.2.6). X-ray diffraction analysis revealed that the structure is disordered with respect to the stereocenter at $C_\gamma$ (also $C_\delta$ and $C_\varepsilon$, Figure 5-11, Figure 3-18) and both diastereomers crystallize in the unit cell in identical positions. Refinement results in an occupancy of the disorder positions of 63:36 (1.75:1) with **$^{MeO}$3$_{MA\text{-}rac}$** being the major isomer. In addition, the conformation of **$^{MeO}$3$_{MA\text{-}rac/meso}$** in solution was analyzed by quantitative NOESY experiments and compared to the solid state structure (Figure 5-12, Figure 5-13). Proton-proton distances (d) were determined by integration of the corresponding NOESY crosspeak and referencing the integral intensity (I) to the one for the NOE of geminal protons such as H-β or H-δ ($I_{ref}$). For the proton-proton distances of geminal protons, a fixed distance $d_{ref}$ = 1.6 Å (corresponding to the standard H-H distance in an AFIX

constrained methylene group in X-ray structure analysis) was assumed. The distances d can then be obtained according to the equation:[31,160] $d = \sqrt[6]{I_{ref} / I} \cdot d_{ref}$

The comparison of the distances for the two isomers revealed that the only relevant difference between the meso and rac structure can be found in the distance between the two methine protons H-α and H-γ. This distance is found to be 3.5 Å in the major isomer and 4.1 Å in the minor isomer (Figure 5-13). Comparison of the distances obtained from the solid state structure are generally in good agreement with the values obtained from the NOESY experiment (Figure 5-13). In the X-ray structure a distance of 4.2 Å between H-α and H-γ is found for the meso isomer, whereas for the rac isomer a distance of 3.5 Å is measured. In conclusion, this study suggests that the spatial relation of $^{MeO}\mathbf{3}_{MA\text{-}rac/meso}$ in solution is similar to the structure found in the solid state and that a rac:meso ratio of ~2:1 (*vide supra*) is obtained in the insertion experiments (Figure 5-11, Figure 5-13).

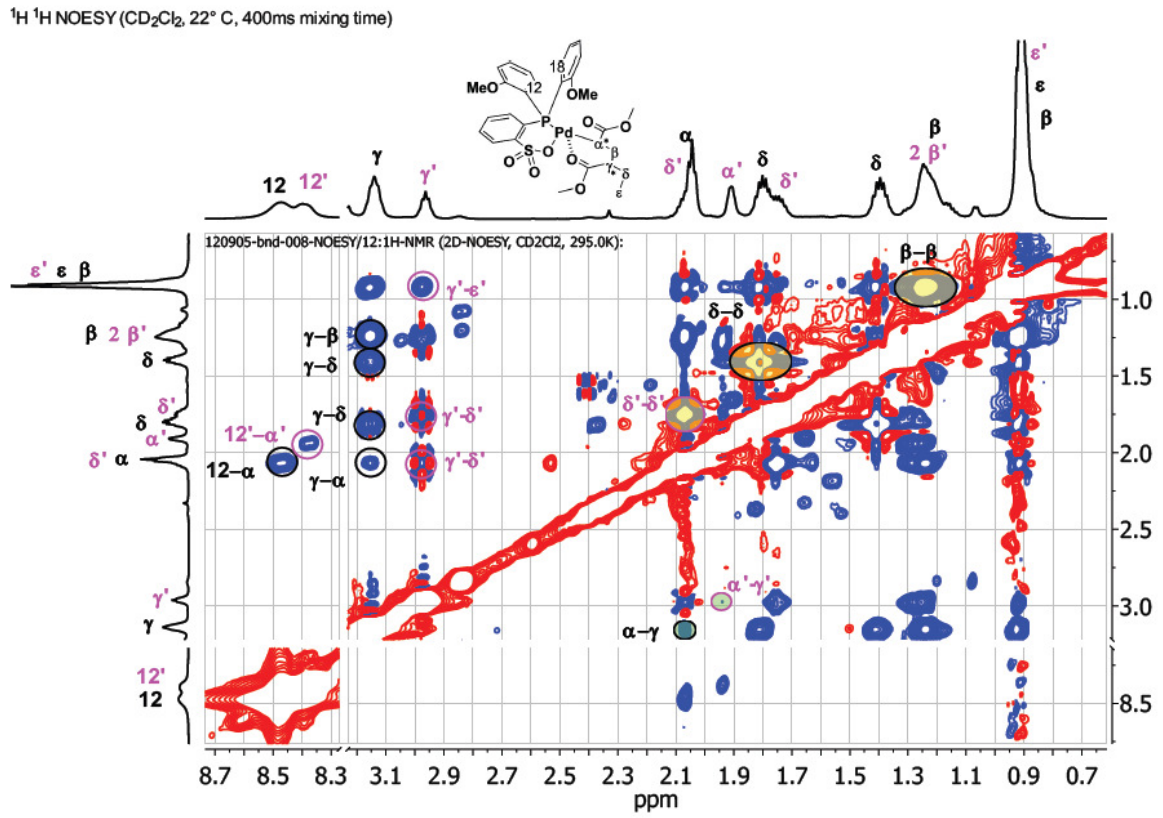


**Figure 5-12.** $^1$H $^1$H NOESY spectrum ($CD_2Cl_2$, 22 °C, 400 ms mixing time) of $^{MeO}\mathbf{3}_{MA\text{-}rac/meso}$. Crosspeaks used for integration are marked by circles. Yellow highlighted circles: possible reference signals; green highlighted circles: crosspeaks most important for structural assignment.

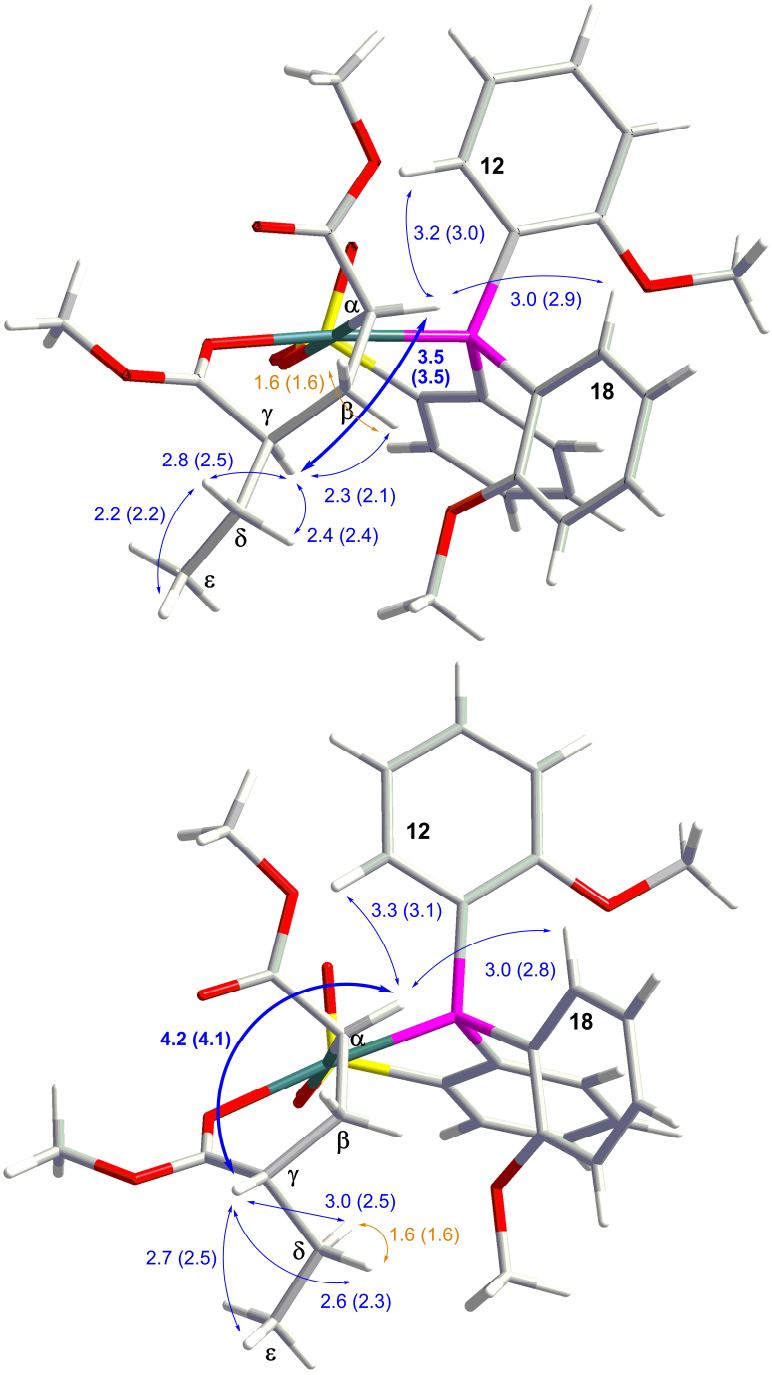


**Figure 5-13.** X-ray structure of $^{MeO}\mathbf{3}_{MA\text{-}rac}$ (top) and $^{MeO}\mathbf{3}_{MA\text{-}meso}$ (bottom) with H-H bond distances as determined from X-ray structure analysis and the corresponding values (major compound compared to $^{MeO}\mathbf{3}_{MA\text{-}rac}$, minor compound compared to $^{MeO}\mathbf{3}_{MA\text{-}meso}$) as determined from NOESY experiments (in brackets; reference values for NOESY bond length determination are marked in yellow).

In the solid state, the aryl moieties adopt an $exo_2$ conformation. Due to the chirality of the chelate formed by the inserted MA, the anisyl moieties of the ligand are diastereotopic in $^{MeO}\mathbf{3}$ and can be distinguished by NMR. An additional hindered rotation of these groups is unlikely, since it would lead to an additional stereocenter and hence the observance of four diastereomers for $^{MeO}\mathbf{3}$. A qualitative temperature dependent NMR study reveals that up to 120 °C no intramolecular interconversion is detectable, but that additional diastereomers are

observed at low temperature. The coalescence temperature for the MeO-resonances is in the same range as for $^{MeO}$**1**, indicating that rotational barriers are roughly similar and consequently that the steric flexibility of the ligand is probably unchanged during an oligomerization process upon chain growth.

For a systematic investigation of stereoselectivity with different catalysts, a rapid and broad analysis protocol is essential. The formation of the two diastereomeric complexes $^{X}$**3**$_{MA\text{-}rac}$ and $^{X}$**3**$_{MA\text{-}meso}$ allows for a screening of stereoselectivity for the first two insertions, as these compounds are rather stable ($t_{1/2}$ > 3 h) and the ratio of diastereomers can be analyzed by NMR spectroscopy (Figure 5-11). Analyzing the chelate formed by the MA insertion, the diastereomeric methine groups at Cγ and Cγ' in $^{MeO}$**3**$_{MA\text{-}rac/meso}$ [(P^O)Pd{*C*H(C(O)OMe)CH$_2$**C**H(C(*O*)OMe)CH$_2$CH$_3$}] give rise to well separated proton resonances around 3 ppm (Figure 5-11). In addition, also the $^{13}$Cγ resonances show a pronounced shift difference (Cγ(rac): 51 ppm, Cγ'(meso): 45 ppm), which allows for a transferable absolute assignment of the stereochemistry (*vide infra*). For a determination of stereoselectivity also the – in comparison to the starting material – low field shifted resonances of the anisyl ortho protons 12-H of the (P^O) ligand at around 8.7 ppm can be drawn upon (Figure 5-11). In addition, the $^{31}$P NMR spectrum and integrals can be utilized as well. Note that, due to underlying impurities the ratios determined by integration of the different resonance pairs can deviate from each other. For a rapid assignment of the crucial MA derived spin systems of new complexes, a combined $^{1}$H $^{1}$H TOCSY/COSY-NMR analysis starting from the unique low field shifted γ-H resonances proved to be most effective.

**Dependence of Stereoselectivity on Temperature**

For an effective homopolymerization of polar monomers temperatures between 60 °C and 90 °C are generally required.[44] Hence, the influence of temperature on the stereoselectivity of the consecutive MA insertion into $^{MeO}$**1** was studied at temperatures up to 95 °C. To a mixture of [{(**$^{MeO}$1-Cl**)-μ-Na}$_2$] and $AgBF_4$ in $C_2D_2Cl_4$ 20 equivalents of MA were added, and the reaction mixture was kept at the corresponding temperature in an NMR tube. Reaction times are strongly dependent on the reaction temperature. Whereas consecutive insertion was completed within 20 minutes at 95 °C, at 60 °C 90 minutes, and at 25 °C 24 hours were required. Insertion at 4 °C was still not completed after a week. Here, solvents and monomer were removed at 0 °C and the remaining mixture of $^{MeO}$**2**$_{MA}$ and $^{MeO}$**3**$_{MA}$ was analyzed. The slow progress of reaction at 4 °C indicates that a further temperature decrease

is not reasonable for the catalyst system $^{MeO}$**1**. The insertion experiments clearly reveal that an influence of temperature on stereocontrol is negligible, and that the ratio of the stereoisomers is constantly ~1:2 and identical within experimental error (Figure 5-14).

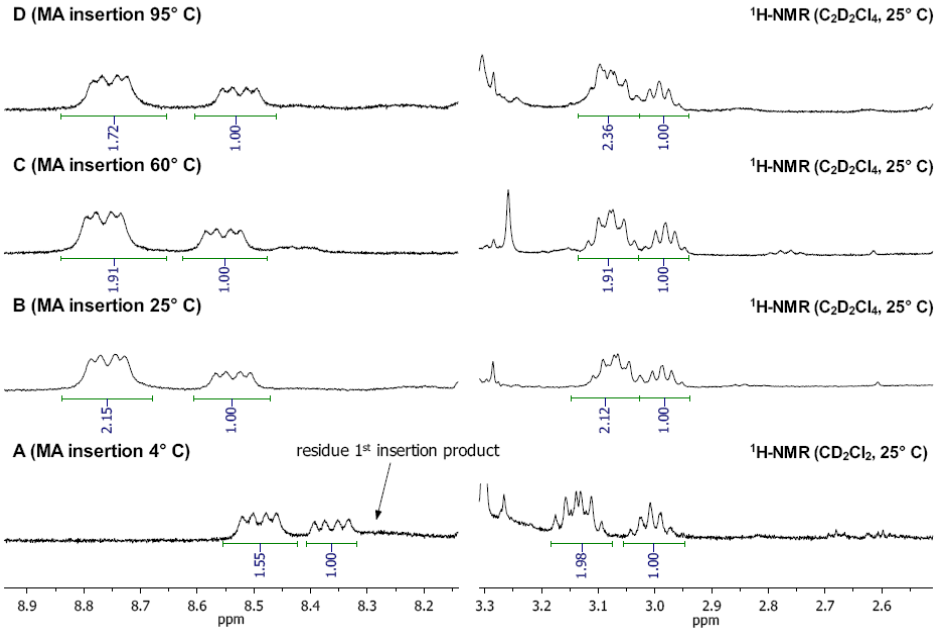


**Figure 5-14**. $^{1}$H NMR spectra (400 MHz, 25 °C): Stereoselectivity for consecutive MA insertion into the Pd-Me bond of $^{MeO}$**1** to form $^{MeO}$**3**, at different temperatures. The stereoselectivity is determined by integration of the aryl proton 12-H (left) and the methine proton γ-H resonances. Note that the spectra B-C were recorded directly from the crude reaction mixture in $C_2D_2Cl_2$, whereas spectrum A was recorded from isolated material in $CD_2Cl_2$.

## Dependence of Stereoselectivity on Steric Bulk of the Monomer

Since $^{MeO}$**1** exhibits no permanent chiral center, and the above studies revealed a fast interconversion of the conformers, methyl acrylate insertion is likely dominated by a chain-end stereocontrol mechanism as proposed previously.[44] In order to further analyze this issue, the influence of the monomers bulk on the stereoselectivity was studied. For this purpose, the insertion of MA, isopropyl acrylate (*i*PrA) and *tert*-butyl acrylate (*t*BuA) at 25 °C was compared under the same experimental conditions as described above. The comparison of the crude insertion products revealed that the steric bulk of the monomer primarily influences the regioselectivity. For MA only trace amount of the 1,2-insertion product $^{MeO}$**2**$_{MA\text{-}1,2}$ are observed, whereas for *t*BuA a ratio $^{MeO}$**2**$_{tBuA\text{-}1,2}$: $^{MeO}$**2**$_{tBuA\text{-}2,1}$ of ~1:5 is found. For *i*PrA the portion of 1,2-insertion product cannot be determined due to overlapping resonances, but it appears to be similar as for *t*BuA. Concerning the stereoselectivity of the consecutive insertion, an unexpected trend was found (Figure 5-15): With increasing steric bulk of the

monomer stereoselection is reduced, as concluded from the integration of the ortho aryl protons. The rac:meso ratio decreases from ca. 2:1 for $^{MeO}\mathbf{3}_{MA}$ over ca. 1.5:1 for $^{MeO}\mathbf{3}_{iPrA}$ to ca. 1:1 for $^{MeO}\mathbf{3}_{tBuA}$. Hence, it appears here that chain-end stereocontrol and any enantiomorphic site stereocontrol work uncooperatively in different directions.

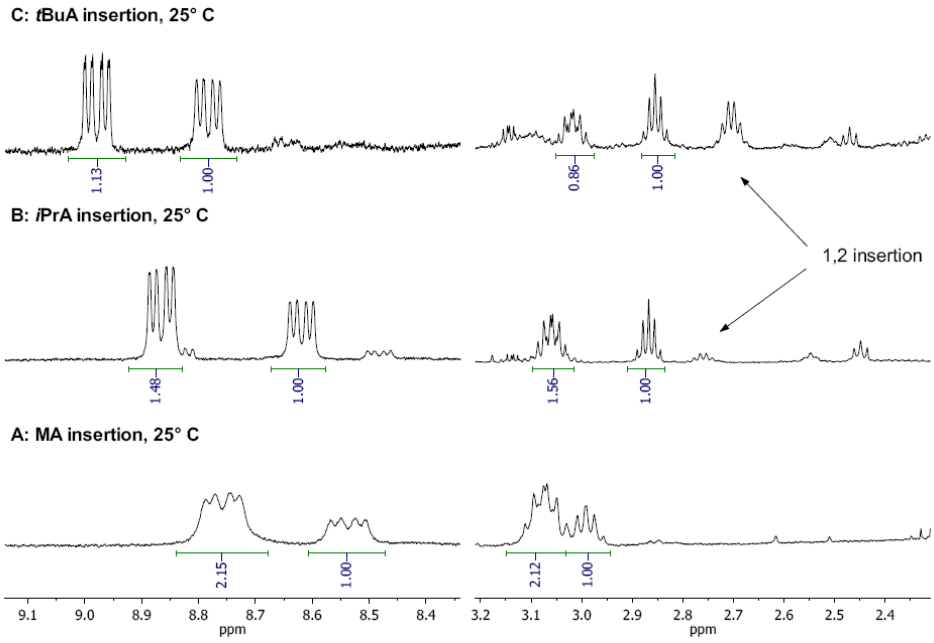


**Figure 5-15.** Stereoselectivity acrylate insertion in the Pd-Me bond of $^{MeO}\mathbf{1}$ at 25 °C for monomers with variable steric bulk. A: methyl acrylate ( $^1$H NMR , 400 MHz, $C_2D_2Cl_4$, 25 °C); B: isopropyl acrylate ($^1$H NMR 600 MHz, $CD_2Cl_2$, 25 °C); C: *tert*-butyl acrylate ($^1$H NMR, 600 MHz, $CD_2Cl_2$, 25 °C).

## Influence of Ligand Structure and Complex Conformation on Stereoselectivity

In order to shed light on the influence of the complex structure on the insertion behavior, the reaction of $^{MeO}\mathbf{1}$, $^{CF3}\mathbf{1}$, $^{(MeO)2}\mathbf{1}$, $^{(iPrO)2}\mathbf{1}$, $^{Ar}\mathbf{1}$, $^{Ar/(MeO)2}\mathbf{1}$, and $^{cHexO/(MeO)2}\mathbf{1}$ (generated *in situ* from [{($^{X}$**1-Cl**)-μ-M}$_n$]) with MA to the mono insertion products $^{X}\mathbf{2}_{MA}$ and the products of consecutive insertion $^{X}\mathbf{3}_{MA}$ were monitored by NMR spectroscopy over time (Scheme 5-2, see also Chapter 4.2.3).

The regioselectivity in the first insertion is determined from the distribution of the 1,2- to the 2,1-insertion products $^{X}\mathbf{2}_{MA}$. Note that concerning polymerization the formation of the 1,2-insertion product is generally disadvantageous since the resulting five membered chelates inhibit further insertions.[44] Regarding the first insertion, the influence of the phosphinesulfonato substitution pattern on the rate constant $k_{1st}$ is rather low for the complexes investigated, and cannot always be distinguished from electronic effects (for a detailed discussion see Chapter 4.2.3). By contrast, the steric bulk has a significant influence

on the regioselectivity. Here, an increase of the constraints around the active center leads to a shift towards the 1,2-insertion product as illustrated e.g. by the shift of the $^{X}\mathbf{2}_{MA\text{-}2,1}$:$^{X}\mathbf{2}_{MA\text{-}1,2}$ ratio from >15:1 for $^{MeO}\mathbf{1}$, over 4:1 for $^{CF3}\mathbf{1}$, to ~1:1 for $^{Ar}\mathbf{1}$ (Table 5-3). A complete inversion of regiochemisty to 1,2-insertion vs. the 2,1-insertion, which is due to a destabilization of the 2,1-insertion transition states, has been observed previously for catalysts bearing very bulky ($\kappa^2$-*P*,*O*)-diazaphospholidine-sulfonato ligands.[41]

**Table 5-3.** Rate constants of insertion and β-H elimination, as well as regio- and stereoselectivity for various catalysts $^{X}\mathbf{1}$.

| entry | compound | $k_{1st}$ [$10^{-3}$ $s^{-1}$] | Regioselectivity 1st Insertion ($^{X}2_{2,1}$ : $^{X}2_{1,2}$) | Stereoselectivity 1st Insertion | $k_{2nd}$ [$10^{-5}$ $s^{-1}$] | Stereoselectivity 2nd Insertion (rac:meso) |
|---|---|---|---|---|---|---|
| 4-1 | $^{MeO}\mathbf{1}$ | 3.2 | >15:1 | - | 9.2 | 2:1 |
| 4-2 | $^{CF3}\mathbf{1}$ | 4.8 | 4:1 | - | 43 | 2:1 |
| 4-3 | $^{(MeO)2}\mathbf{1}$ | 1.3 | >30:1 | - | 3.7 | 1:1 |
| 4-4 | $^{(iPrO)2}\mathbf{1}$ | 3.4 | 7:1 | - | ~1[a] | 1:1 |
| 4-5 | $^{Ar}\mathbf{1}$ | ~1[a] | 1:1 | [b] | [c] | [c] |
| 4-6 | $^{Ar/(MeO)2}\mathbf{1}$ | 3 | 1.6:1 | 6:1 | 6 | 3:1 |
| 4-7 | $^{c\text{HexO}/(MeO)2}\mathbf{1}$ | 3 | 6:1 | ~1:1[d] | 5.3 | 1:1 |

Conditions: [Pd] = 0.02 mol $L^{-1}$, 1.1 equiv. $AgBF_4$, Pd:MA = 1:15, solvent $CD_2Cl_2$, T = 25 °C; [a]estimate, exact determination not possible; [b]a 2:1 ratio of two $^{Ar}\mathbf{2}_{MA\text{-}2,1}$ products is found. However, diastereomer formation is probably due to hindered aryl rotation in $^{Ar}\mathbf{2}$ and interconversion of the isomers is possible; [c]no consecutive insertion observed; [d]additional 2,1-insertion products observed, clear assignment not possible.

For the asymmetric substituted compounds $^{Ar/(MeO)2}\mathbf{1}$ and $^{c\text{HexO}/(MeO)2}\mathbf{1}$, several 2,1-insertion products are formed due to the permanent stereocenter at phosphorus. A selectivity of 6:1 was found for $^{Ar/(MeO)2}\mathbf{1}$ indicating an effective enantiomorphic site stereocontrol. For $^{c\text{HexO}/(MeO)2}\mathbf{2}$ analysis is complicated due to formation of additional species, probably due to hindered rotation, but stereoselectivity for the first insertion is roughly 1:1. Consequently, the exchange of a *c*HexO$C_6H_4$ substituent by a 2-{2',6'-$(MeO)_2C_6H_3$}$C_6H_4$ moiety significantly increases selectivity. This corresponds with the increased steric bulk at the palladium center for $^{Ar/(MeO)2}\mathbf{1}$ in the solid state and is reflected in the different alignment (pseudo-axial/equatorial) of the second 2,6-$(MeO)_2C_6H_3$ substituent in the X-ray structures for theses two complexes (Figure 5-5).

The insertion rate constants for the consecutive MA insertion are one to two orders of magnitude lower than for the first insertion. This is due to a slower insertion into an α-substituted carbyl vs. insertion into a methyl group, and due to chelating coordination of the carbonyl group of the incorporated acrylate unit, which competes with the incoming monomer (see Chapter 4.2.3).[44] Other than for the first insertion, a more pronounced influence of the

steric bulk of the ligand on the rate constant $k_{2nd}$ is found. As expected, $k_{2nd}$ decreases with increased steric bulk as illustrated by comparison of $^{MeO}$**1** ($k_{2nd} = 9\times10^{-5}$ $s^{-1}$) and $^{Ar/(MeO)2}$**1** ($k_{2nd} = 6\times10^{-5}$ $s^{-1}$). Introduction of a second 2,6-$(MeO)_2C_6H_3$ substituent in $^{Ar}$**1** even leads to a complete inhibition of the consecutive insertion (entry 4-1 vs. 4-7 vs. 4-6).

The stereoselectivity for the symmetric complexes was determined from the product distribution after consecutive MA insertion to form $^{X}$**3**$_{MA}$ (*vide supra*). A comparison of the MA insertion into $^{MeO}$**1** with $^{CF3}$**1** at room temperature reveals that the enhanced rotational barrier of the $CF_3$-substituted complex does not lead to a significant increase of selectivity (~1:2, Figure 5-16). In the complexes with $C_{2v}$-symmetric aryl moieties $^{(MeO)2}$**3**$_{MA}$ and $^{(iPrO)2}$**3**$_{MA}$ the selectivity is even diminished in comparison to the compounds with $C_s$-symmetric aryl moieties, again a substitution of the MeO-groups by the sterically more demanding *i*PrO-groups does not influence the selectivity significantly. From the carbon shifts of the $C_\gamma$ methine groups an absolute assignment of stereochemistry is possible (*vide supra*). An increase of steric bulk leads to an equilibration of the rac:meso product ratio, which was also observed for an increase of monomer steric bulk (vide supra).

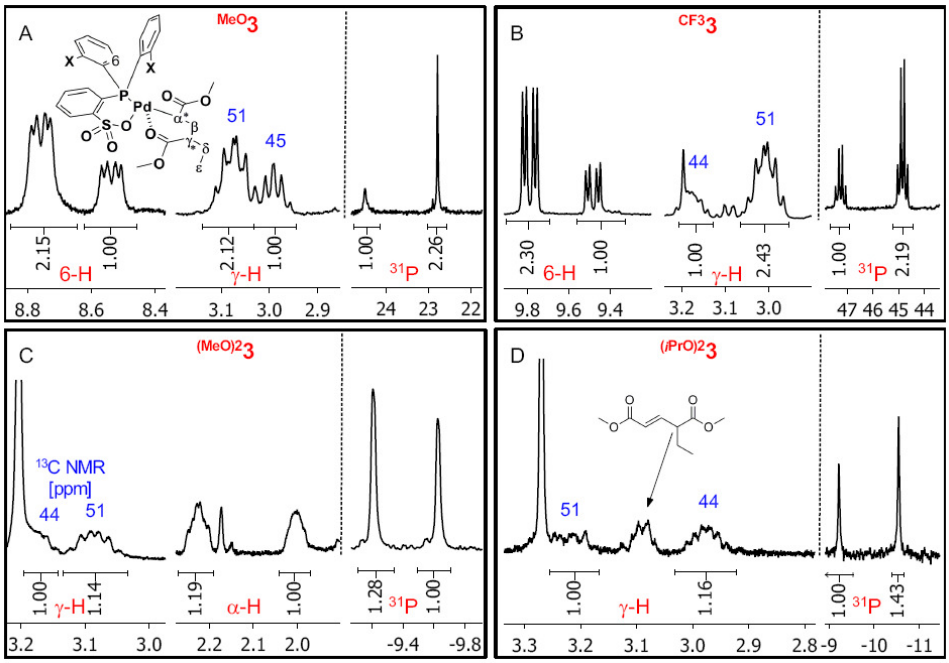


**Figure 5-16.** Stereoselectivity for complexes with symmetric substitution at phosphorus: A) $^1$H NMR spectrum (400 MHz, $C_2D_2Cl_4$) of $^{MeO}$**3**$_{MA}$ formed by MA insertion at 25 °C; B) $^1$H NMR spectrum (400 MHz, $C_2D_2Cl_4$) of $^{CF3}$**3**$_{MA}$ formed by MA insertion at 25 °C; c) $^1$H NMR spectrum (400 MHz, $CD_2Cl_2$) of $^{(MeO)2}$**3**$_{MA}$ formed by MA insertion at 60 °C; B) $^1$H NMR spectrum (400 MHz, $CD_2Cl_2$) of $^{(iPrO)2}$**3**$_{MA}$ formed by MA insertion at 60 °C; all scales in ppm.

For the compounds $^{c\text{HexO/(MeO)2}}\mathbf{3}_{\mathbf{MA}}$ and $^{\text{Ar/(MeO)2}}\mathbf{3}_{\mathbf{MA}}$ analysis of the insertion products is more complex, since the presence of the permanent stereocenter at phosphorus leads to the formation of at least four diastereomers $^{\text{X}}\mathbf{3}_{\mathbf{MA}}$. For $^{c\text{HexO/(MeO)2}}\mathbf{3}_{\mathbf{MA}}$ all four diastereomers can be detected by $^{1}$H $^{1}$H TOCSY-NMR analysis (Figure 5-17). Integration of the γ-H methine proton yields a distribution of roughly 1:4:5:8. Assignment of the diastereomers to rac and meso species is possible by analysis of the $^{13}$C NMR spectra, assuming that a similar chain configuration reflects in similar carbon shifts. Consequently the $C_\gamma$-methine $^{1}$H resonances of $^{c\text{HexO/(MeO)2}}\mathbf{3}_{\mathbf{MA}}$ at 3.27 ($^{13}$C: 44 ppm) and 2.82 ($^{13}$C: 45 ppm) can be assigned to the meso isomers and the resonances at 3.21 ($^{13}$C: 51 ppm) and 3.00 ppm ($^{13}$C: 52 ppm) to the rac isomers, corresponding to a rac:meso selectivity of ~1:1.

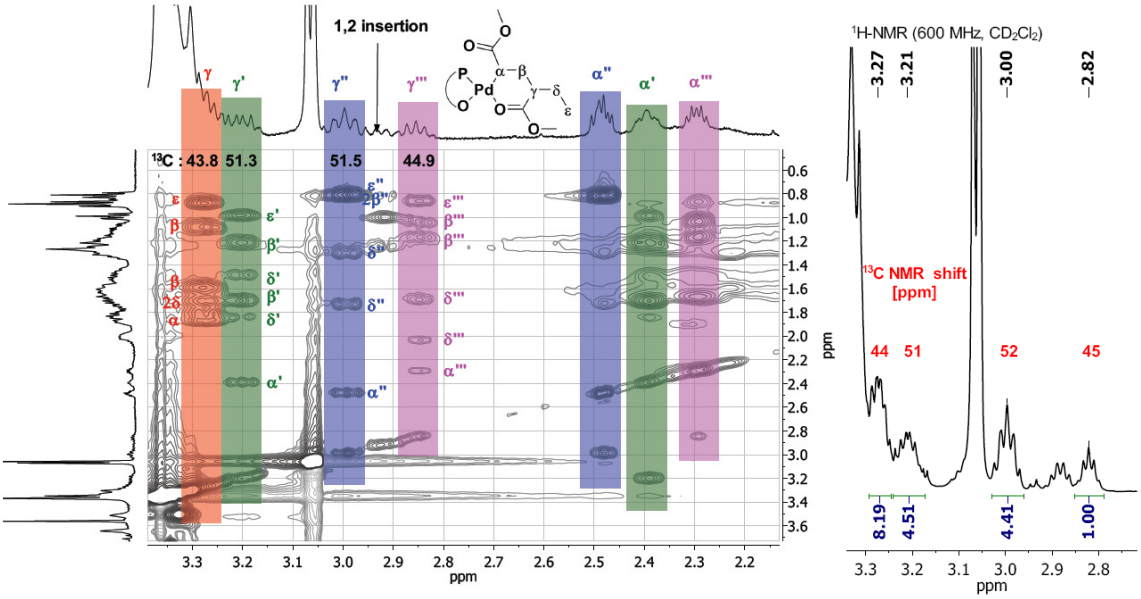


**Figure 5-17.** Assignment (left, $^{1}$H $^{1}$H TOCSY, 400 MHz, $CD_2Cl_2$) and distribution (right, $^{1}$H NMR, 600 MHz, $CD_2Cl_2$) of the four diastereomers of $^{c\text{HexO/(MeO)2}}\mathbf{3}_{\mathbf{MA}}$ (For the resonances at 3.27 ppm only the right half of the resonance was integrated, and doubled).

For $^{\text{Ar/(MeO)2}}\mathbf{3}_{\mathbf{MA}}$ analysis is complicated by overlapping resonances, but the insertion products evidently are formed in rather similar proportions. In this case the α-H methine resonances integrals were employed. Assignment of the spin systems by $^{1}$H $^{1}$H TOCSY and $^{1}$H $^{13}$C gHSQC experiments is in line with the formation of only three main diastereomers and yields a rac:meso distribution of 3:1 (Figure 5-18). Thus, the high selectivity for the first insertion (6:1) is diminished for the consecutive insertion, indicating that the possible chain-end control which becomes active from the second insertion on is opposite to the enantiomorphic site stereocontrol, which controls the first insertion alone.

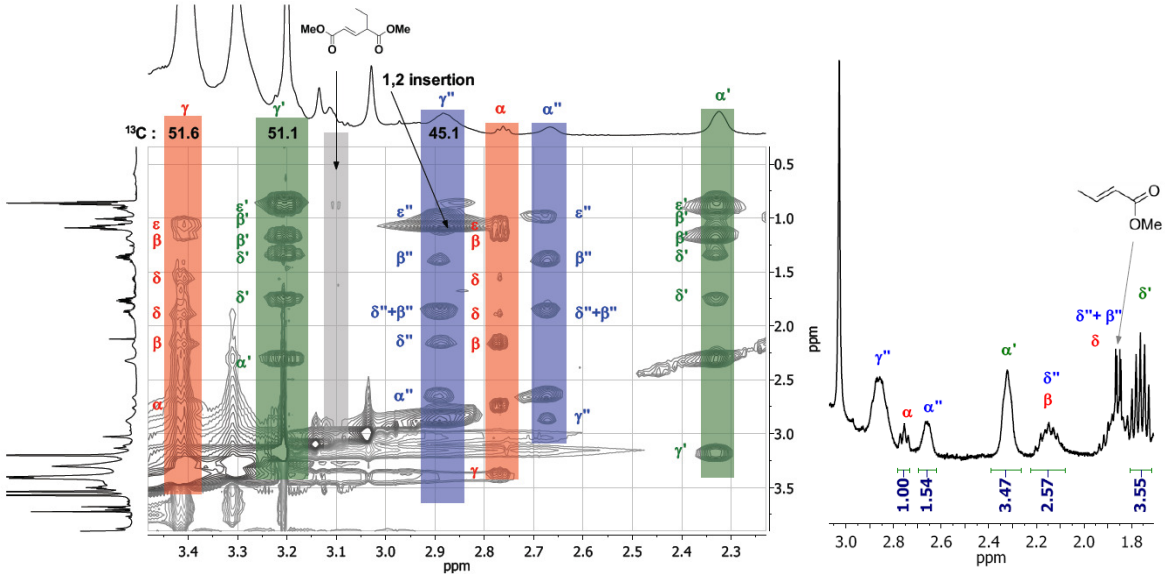


**Figure 5-18.** Assignment (left, $^{1}$H $^{1}$H TOCSY, 400 MHz, $CD_2Cl_2$) and distribution (right, $^{1}$H NMR, 400 MHz, $CD_2Cl_2$) of the three diastereomers of $^{\mathbf{Ar/(MeO)2}}\mathbf{3}_{\mathbf{MA}}$.

### 5.2.5 Oligomerization Studies

Previous studies revealed that $^{MeO}$**1-dmso** is a suitable precursor for MA oligomerization producing oligomers with an average $DP_n$ of ca. 5 with around 100 turnovers in 12 hours.[43] DFT calculations have shown that the overall barrier for consecutive MA insertion amounts to 100 kJ $mol^{-1}$ and are generally in line with an insertion mechanism.[44] Further experimental proof for a chain growth mechanism is desirable. In order to further verify the insertion mechanism the chain growth at the metal center was investigated starting from the fully characterized insertion product of two consecutive MA insertions into the Pd-Me bond $^{MeO}$**3**$_{MA\text{-}rac/meso}$. NMR-studies and characterization of higher insertion products are hampered by the extreme complexity of the spectra resulting from the growing number of stereocenters in the metal-bound growing chain, and simultaneous β-hydride elimination reactions. However, mass spectrometry enabled the direct observation of the organometallic products of further insertion of acrylates into $^{MeO}$**3**$_{MA\text{-}rac/meso}$ (Scheme 5-4, Figure 5-19, Figure **5-20**).

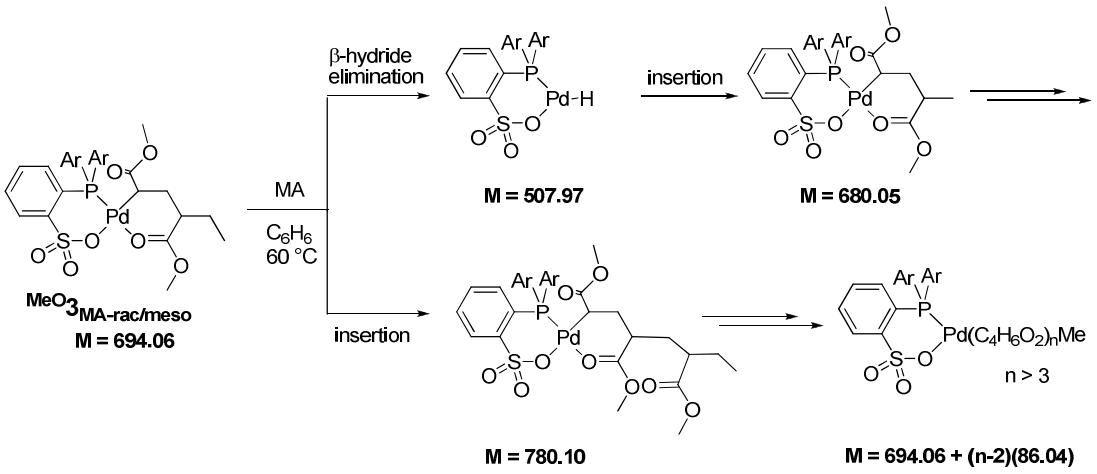


**Scheme 5-4.** Insertion of methyl acrylate into complexes $^{MeO}$**3**$_{MA\text{-}rac/meso}$ (M represents major mass of the isotope pattern, detected by ESI-MS as the $HNEt_3$-adducts (M+102.13)).

A solution of $^{MeO}$**3**$_{MA\text{-}rac/meso}$ and 30 equivalents methyl acrylate in benzene was kept for 4 hours at 60 °C. Evaporation of solvent and extraction with $Et_2O$ yielded a white precipitate upon addition of pentane to the ether extract. Electrospray ionization (ESI) as a particularly mild technique allowed for the recording of mass spectra from MeOH solutions. Triethylammonium salts were found to be suited as a cationizing agent. $HNEt_3^+$ adducts of the [(P^O)PdR] complexes (M + 102) represent the major species observed by ESI-MS (Figure 5-19). The observed very specific isotope pattern is in agreement with the expected peak structure (Figure 5-19, insert). Apart from the starting material (*m/z* = 796), the products of

two further consecutive methyl acrylate insertion into $^{MeO}\mathbf{3}_{MA\text{-}rac/meso}$ are clearly detected (*m/z* = 882; 968). Note that an observed tailing of the isotope patterns for the $HNEt_3^+$ adducts (*m/z* = 796, 882, 968) can be explained by appearance of minor peaks from the Na adducts of the complexes (M+23), which becomes evident from the isolated peak for the starting material $[^{MeO}\mathbf{3}_{MA\text{-}rac/meso} + Na]^+$ (*m/z* = 717). Further minor signals (*m/z* = 782; 868) result from the consecutive insertion of methyl acrylate into the Pd-H bond of the hydride [(P^O)PdH], which is formed by β-hydride elimination.

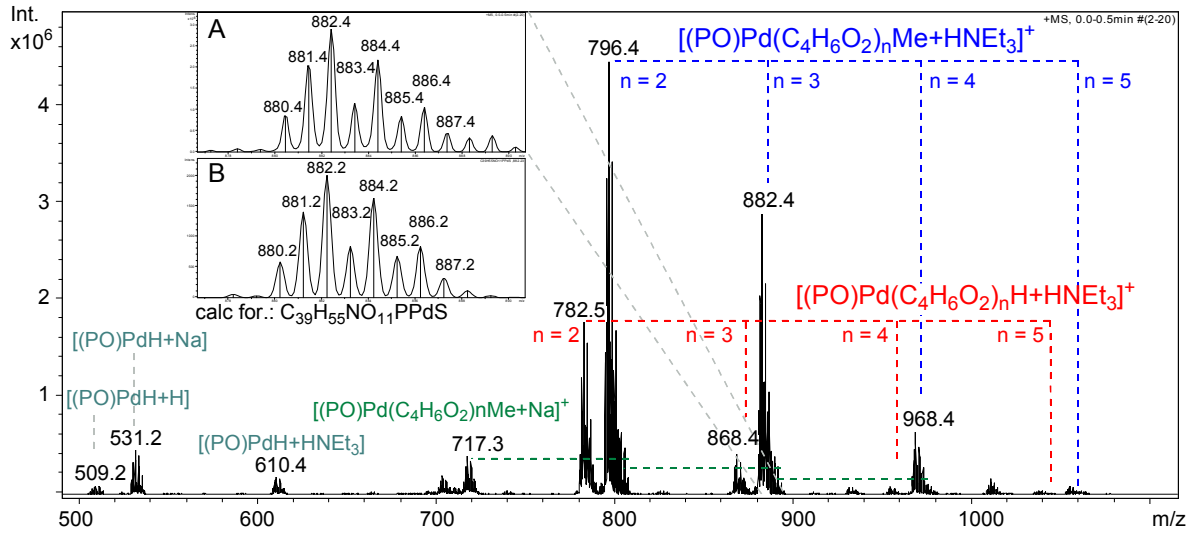


**Figure 5-19.** Positive-ion ESI-mass spectrum of multiple MA insertion products (methanol solution with added $[HNEt_3][B(C_6F_5)_4]$). Inset A: found isotope pattern, inset B: calculated isotope pattern for $C_{39}H_{55}NO_{11}PPdS$.

In a similar manner, products from multiple insertion of butyl acrylate into $^{MeO}\mathbf{3}_{MA\text{-}rac/meso}$ and [(P^O)PdH] were generated and characterized (Figure 5-20). In this case a solution of $^{MeO}\mathbf{3}_{MA\text{-}rac/meso}$ and 30 equivalents butyl acrylate in benzene was kept for 24 hours at 60 °C. The prolonged reaction time lead to a significant shift in the product mixture, due to the propensity of the catalyst for β-hydride elimination, so that here consecutive insertion of butyl acrylate into [(P^O)PdH] dominates (*m/z* = 866, 944, 1122, 1250, 1378). The signals for products of multiple insertion of butyl acrylate into $^{MeO}\mathbf{3}_{MA\text{-}rac/meso}$ (*m/z* = 924, 1052, 1180, 1308, 1436) are rather weak, but can clearly be assigned. Overall, the direct observation of these higher insertion products further confirms that (P^O)Pd catalysts are capable of polymerizing acrylates by an insertion pathway. In this context note that for other types of organometallic Pd(II) complexes free-radical polymerization of acrylates to high-molecular-weight polymer triggered by acrylate insertion and homolytic cleavage of the Pd-C bond has been found.[117,161]

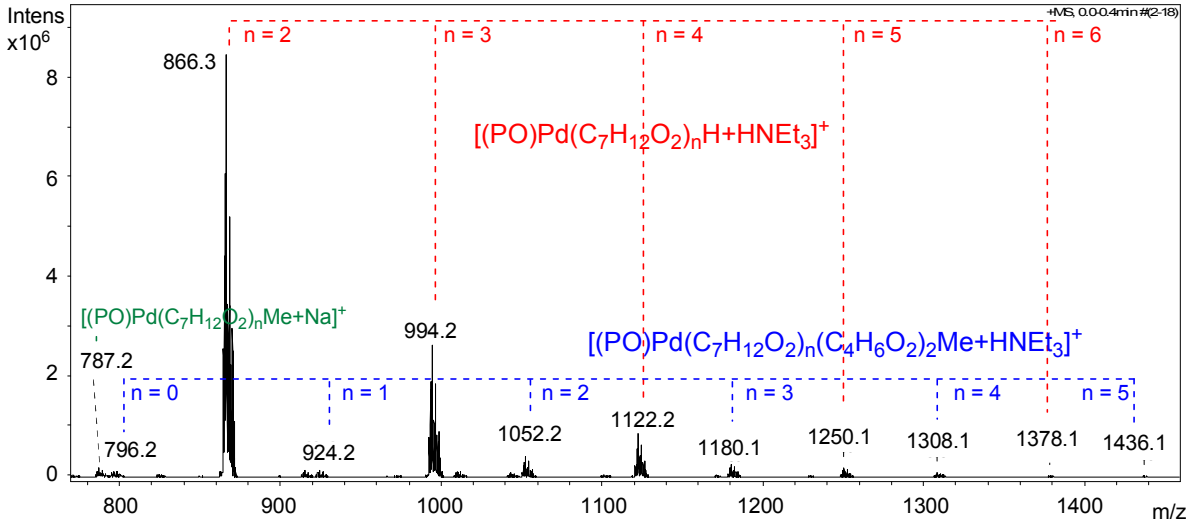


**Figure 5-20.** Positive-ion ESI-mass spectrum of multiple BA insertion products (methanol solution with added $[HNEt_3][B(C_6F_5)_4]$.

Since a chain growth mechanism could be verified, the tacticity of the produced oligomers should depend on the catalyst. While the insertion studies revealed a rather low degree of stereocontrol under NMR-conditions, the influence of the monomer steric bulk and of the ligand structure should be evaluated under polymerization conditions. Oligomerization studies were performed with $^{MeO}$**1**, $^{CF3}$**1**, $^{(MeO)2}$**1**, $^{(iPrO)2}$**1**, $^{Ar}$**1**, $^{Ar/(MeO)2}$**1** and $^{cHexO/(MeO)2}$**1** for MA and in addition with $^{MeO}$**1** for *t*BA and *i*PrA. For acrylate oligomerizations a 2.5 mol $L^{-1}$ solution of the corresponding acrylate in 4 mL toluene and 25 µmol $[\{(^{X}$**1-Cl**$)$-µ-M$\}_n]$ as the sole catalyst precursor with added BHT (Pd:BHT = 1:15) was kept at 95 °C for 3 hours. Here, the utilization of $[\{(^{X}$**1-Cl**$)$-µ-M$\}_n]$ without further activation can be advantageous, since the addition of silver salts or chlorinated solvents, which might lead to free-radical side reactions or decomposition under this conditions, can be avoided. Polymerization studies have revealed the catalytic activity of these compounds before (see Chapter 4.2.4). However, reasonable amounts of oligomers (> 5 mg) could only be isolated for $^{MeO}$**1** and $^{(MeO)2}$**1** under these conditions (Table 5-4). For the other catalysts studied either the homooligomerization activity is too low, or the catalyst decomposition proceeds fast under these conditions. $^{(MeO)2}$**1** produces reasonably more oligomer than $^{MeO}$**1**, but in this case also the formation of high molecular weight PMA via a free-radical pathway was observed. Since a formation of free-radical formed PMA was not observed in comparative experiments under the same conditions without a catalyst, $^{(MeO)2}$**1** or decomposition products thereof obviously contribute to the formation of free-radicals. This is in line with the frequently observed formation of PMA during MA insertion into $^{(MeO)2}$**1** under NMR-conditions.

**Table 5-4.** Oligomerization of acrylates with catalysts $^{X}$**1**.

| entry | catalyst | monomer | yield[a] [mg] | TON | $DP_n$[c] |
|---|---|---|---|---|---|
| 5-1 | $^{MeO}$**1** | MA | 74 | 33 | 5 |
| 5-2 | $^{MeO}$**1** | iPrA | 90 | 29 | 4 |
| 5-3 | $^{MeO}$**1** | tBA | 26 | 8 | 3 |
| 5-4 | $^{(MeO)2}$**1** | MA | 150[b] | 70[b] | 10 |

Reaction conditions: Solvent = toluene, V = 4 mL, [acrylate] = 2.5 mol $L^{-1}$, [Pd] = 6.3 x$10^{-3}$ mol $L^{-1}$, Pd:BHT = 1: 15, T = 95 °C, t = 3h. [a]Yield after removal of volatiles under vacuum less m(BHT) and m((P^O)PdMe). [b]Formation of free-radical polymer observed. [c]$Et_2O$ soluble fraction.

The stereoregularity of polyacrylates can be determined by $^1$H NMR spectroscopy. The protons of the methylene group are diastereotopic and split into three resonances in the $^1$H NMR spectrum which reveal the diad-tacticity.[126] For PMA the resonances at around 2.05 and 1.60 ppm are assigned to $CH_2$-groups in an isotactic environment, or more specific to the protons syn (threo-meso) and anti (erythro-meso) to the isotactic methine proton, respectively (Figure 5-21, Figure 5-22).

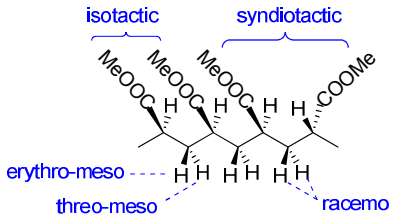


**Figure 5-21.** Nomenclature for methylene protons of an isotactic and a syndiotactic diad of a PMA chain.

By contrast, methylene protons arranged in a syndiotactic environment resonate at around 1.80 ppm. Consequently, the isotacticity of the chain can be calculated according to:[126]

$$\text{isotacticity (\%)} = \frac{I_{threo-meso} + I_{erythro-meso}}{I_{threo-meso} + I_{erythro-meso} + I_{racemo}} \cdot 100 = \frac{2I_{threo-meso}}{2I_{threo-meso} + I_{racemo}} \cdot 100$$

Since the integrals $I_{threo\text{-}meso}$ and $I_{erythro\text{-}meso}$ should be identical, they can be substituted by each other if necessary. The analysis of stereoregularity of PMA derived from free-radical polymerization is depicted in Figure 5-22 revealing the expected atactic character of the polymer with around 50% isotacticity (Figure 5-22).

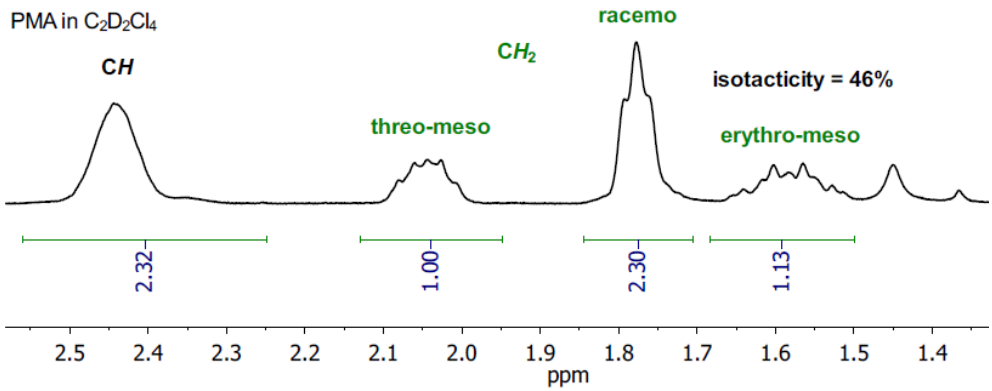


**Figure 5-22.** $^{1}$H NMR (400 MHz, $C_2D_2Cl_4$, 120 °C): Tacticity of PMA from free-radical polymerization (commercial sample, $M_n$ = 100000 g mol$^{-1}$).

The determination of stereoregularity for the acrylate oligomers derived by an insertion mechanism is hampered by the low average chain length ($DP_n$: 3-5, Table 5-4). Investigations by $^{1}$H NMR revealed that for such oligomer mixtures end groups have a significant influence on the relevant integrals as expected. For MA-oligomers derived from oligomerization with $^{MeO}$**1** higher molecular weight fractions could be isolated by column chromatography. The comparison of oligomer fractions with an average $DP_n$ from 6 to around 30 revealed that for an analysis of stereoregularity at least a $DP_n$ of 15 is needed, because overlapping resonances of the chain ends falsify analysis otherwise (Figure 5-23). Whereas for *t*BuA and *i*PrA no oligomer fraction with a chain length sufficient for analysis of stereoregularity could be isolated, an isotacticity of ca. 30% was determined for an MA oligomer fraction with a $DP_n$ of ca. 30, which indicates that these oligomers are syndio-enriched. The isolation of slightly syndiotactic material is in line with the insertion studies, in which $^{MeO}$**3**$_{MA\text{-}rac}$ – a precursor for a syndiotactic chain – is formed in small excess compared to the meso isomer. The observed 2:1 ratio in the insertion experiments would lead to a prediction of 66% syndiotacticity for a polymer, which agrees well qualitatively with the found 69 %.

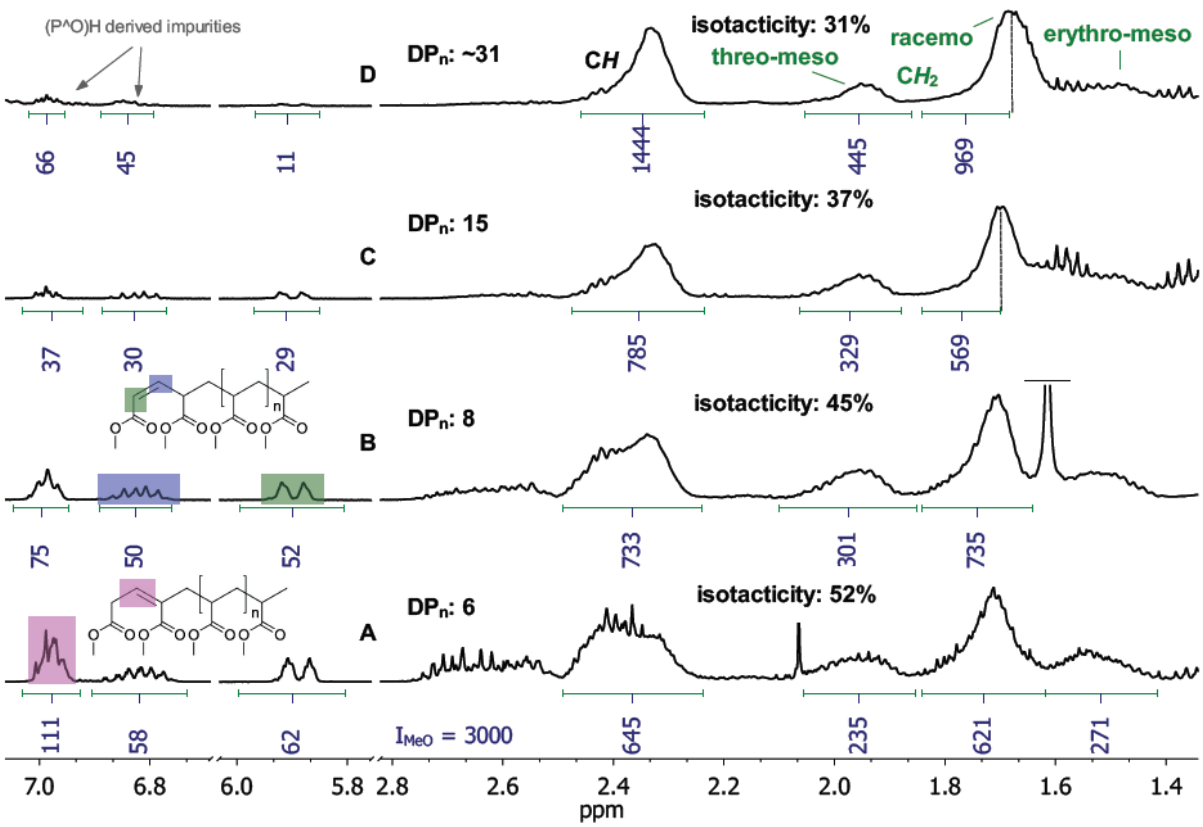


**Figure 5-23.** $^{1}$H NMR (400 MHz, $CD_2Cl_2$, 25 °C) spectra showing the tacticity and $DP_n$ of MA oligomers formed by migratory insertion with $^{MeO}$**1** after flash chromatography ($CH_2Cl_2$/MeOH, Fraction A-C and D: residual material on column).

### 5.2.6 Computational Studies (performed by Prof. Lucia Caporaso)

In order to gain a deeper understanding of the dynamics and regio- and stereocontrol mechanisms in (P^O)PdMe complexes, the alkyl acrylate insertions into $^{MeO}$**1**, $^{(MeO)2}$**1**, $^{Ar}$**1**, and $^{Ar/(MeO)2}$**1** were studied theoretically by density functional theory calculations. Considering the limited selectivity achieved experimentally, the energy differences are expected to be rather low, almost within the error expected for such calculations.[162]

Since the steric interactions between the monomer, the ligand and the growing chain, which determine the selection of the monomer enantioface, are expected to largely depend on the fluxionality of the complexes, the transition state (TS) for the main intramolecular motions of the (P^O) ligand frame were located. The energy of the transition state for the ring flip (RF-TS) and aryl rotation (AR-TS) of the complexes $^{X}$**1** are reported in Table 5-5. Energies are reported relative to the energy of the corresponding most stable Pd-Me complex (Scheme 5-5, cf. SI). Aryl rotation proceeds via concerted rotation of the non-chelating aryl groups. In agreement with published data the two aryl moieties are almost in plane in the transition state.[148]

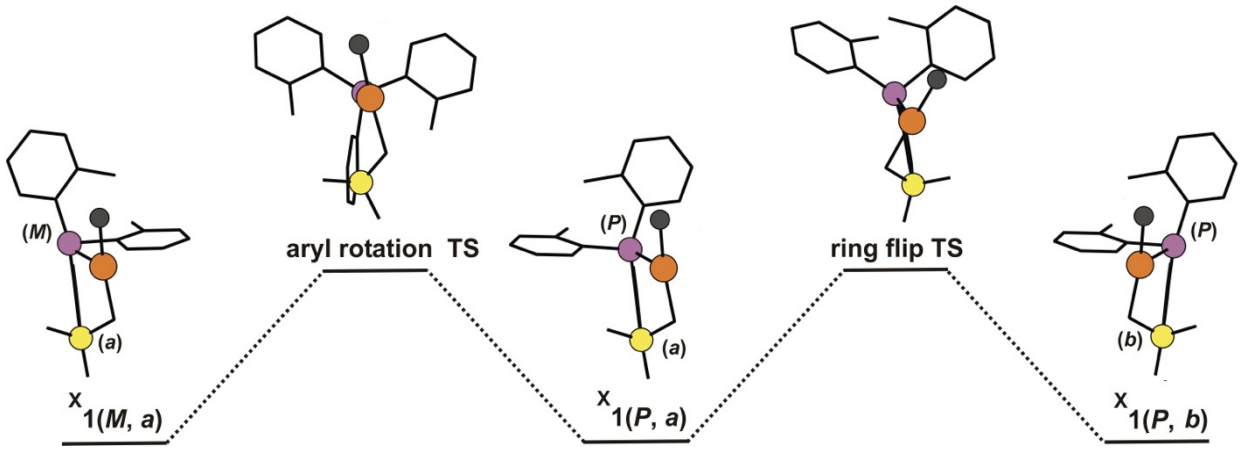


**Scheme 5-5.** Transition states for aryl rotation and ring flip for $^{X}$**1**.

The calculated energy barriers for the aryl rotation increase with the steric bulk of the non-chelating aryl moieties in the range of 36 to 63 kJ/mol (Table 5-5). Interestingly, the double ortho substitution at the aryl moieties in $^{(MeO)2}$**1** completely inhibits a rotation as the two methoxy groups of the ligand inevitably collide in the corresponding transition state. By contrast, the barrier for the ring flip is not increased. Consequently, $^{(MeO)2}$**1** exhibits a conformational chirality at the P-atom (*P* or *M*), whereas the ring conformation is fluxional and does not contribute to chirality. This agrees with the NMR studies with $^{(MeO)2}$**1** and $^{(i\text{PrO})2}$**1**, where in the temperature range between -90 °C to 130 °C no rotational process could

be detected. However, due to the high symmetry of these compounds also no inequivalence of the aryl moieties was observed by NMR (Figure 5-24).

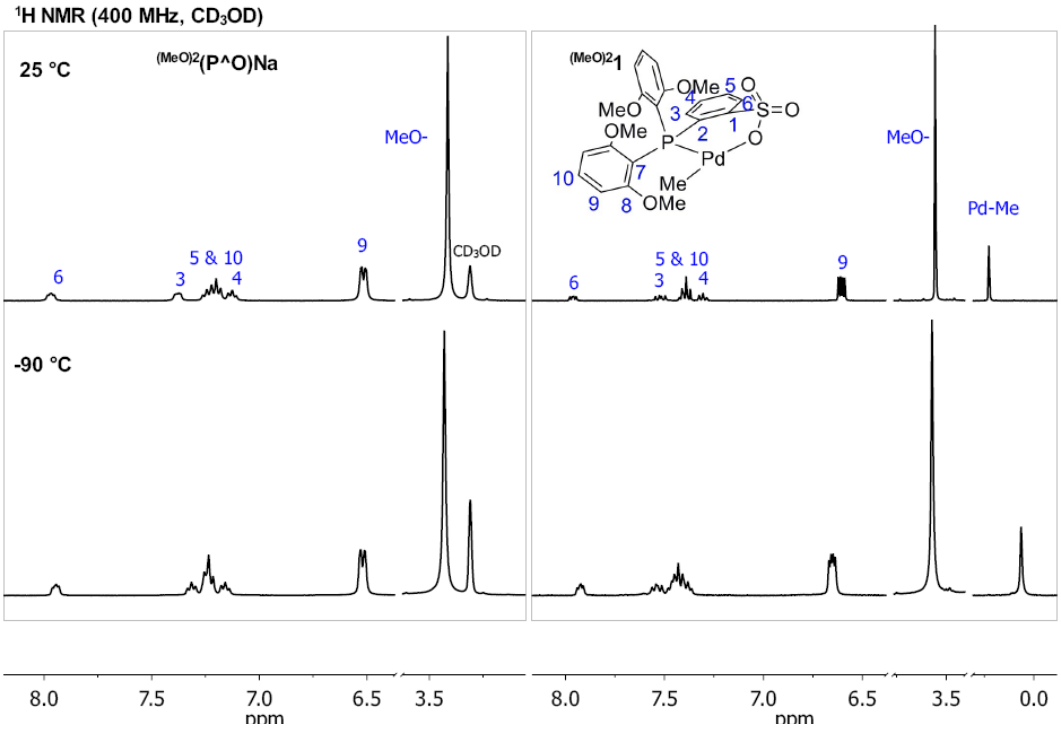


**Figure 5-24.** Variable temperature $^{1}$H NMR spectra (400 MHz, $CD_3OD$) of **$^{(MeO)2}$(P^O)Na** and $^{(MeO)2}$**1**.

The calculated barriers are in an acceptable agreement with the experimental data. The highest calculated energy barrier, found for $^{Ar/(MeO)2}$**1** (63 kJ/mol, Table 5-5) compares to an experimentally determined $\Delta G^{\neq}_{Tc}$ of 59 kJ/mol and a $\Delta H^{\neq}$ of 48 kJ/mol respectively. In contrast, the energy barrier for the ring flip is independent of the steric bulk of the non-chelating aryl moieties, but is always more than 10 kJ/mol lower than the aryl rotation barrier. These results nicely support the reasoning that the aryl rotation is the higher energy process observed in the NMR experiments. The ring flip exhibits barriers below 25 kJ/mol and therefore can be assumed to always be fast in the accessible temperature range of the NMR experiments (down to -90 °C).

**Table 5-5.** Calculated energies ΔE (kJ/mol) for ring flip (RF) and aryl rotation (AR) transition states of $^{X}$**1** in relation to the most stable Pd complexes.

| entry | compound | RF-TS | AR-TS |
|---|---|---|---|
| 6-1 | $^{MeO}$**1** | 25 | 36 |
| 6-2 | $^{(MeO)2}$**1** | 16 | -[b] |
| 6-3 | $^{Ar}$**1** | 22 | 53 |
| 6-4 | $^{Ar/(MeO)2}$**1**[a] | 27 | 63 |

[a]configuration at the phosphorus: (*R*); [b]aryl rotation is not possible, since the MeO-groups inevitably collide in the corresponding TS.

In order to explain the processes that influence the selectivity, the insertion mechanism for (P^O)Pd catalysts as theoretically described by Ziegler, Morokuma and Caporaso et al. is shortly summarized for the example of the first insertion of MA into the Pd-Me bond of $^{MeO}$**1** (Scheme 5-6).[44,45,67,69] The growing chain is always oriented trans to the sulfonate group in the ground state and coordination of the monomer occurs cis to phosphorus as in $^{X}$**1-MA$_{cis}$**. The preferred pathway for insertion into the Pd-C bond proceeds through isomerization via $TS_{cis/trans}$ including a Berry-pseudo rotation of the $SO_3$-group at the Pd to the less stable $^{X}$**1-MA$_{trans}$** species. A 2,1-insertion of the monomer in the Pd-C bond of $^{X}$**1-MA$_{trans}$** via $TS_{ins}$ then affords the kinetic product $^{X}$**2$_{MA-KP}$** stabilized by a γ-agostic interaction and finally the insertion product $^{X}$**2$_{MA-Ch}$**, in which the carbonyl group of the inserted acrylate is coordinated to the metal center. The mechanism of further insertions is similar, the major difference being the nature of the starting and final complexes and their respective energies, due to the formation of 4- or 6-membered chelates after the first and the second insertion, respectively.[44,67-69]

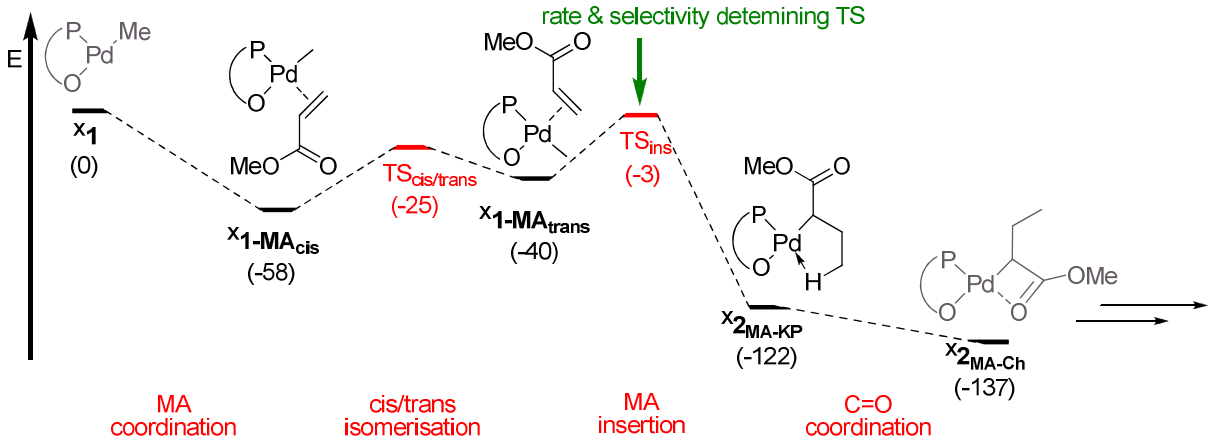


**Scheme 5-6.** Methyl acrylate coordination and insertion in $^{MeO}$**1**. Relative energies of the species are given in parentheses (kJ/mol; black: intermediates: red: transition states).[44]

Site stereocontrol requires a permanent rigid chiral configuration on the time scale of insertion. Hence, for a symmetrically substituted phosphorus atom as in $^{MeO}$**1**, $^{(MeO)2}$**1**, and $^{Ar}$**1** at least a stable helical configuration at the phosphorus atom or a stable ring configuration is necessary. If the ring flip and aryl rotation exhibit significantly lower barriers in comparison to the insertion the first MA insertion cannot be enantioselective.

The corresponding transition states for the ring flip and the aryl rotation motions in the MA complexes $^{X}$**1-MA** are compared to the transition state for the first 2,1-insertion in Table 5-6. The transition state energy values are reported relative to the most stable MA insertion transition state ($TS_{Ins}$, Table 5-6). In agreement with the results reported in Table 5-5, the

energy barrier for aryl rotations is always higher than the barrier for ring flip and the difference between the ring flip and aryl rotation barriers for each complex is nearly unchanged in comparison to the corresponding monomer-free complexes $^{X}$**1**. Again, an increase of the rotational barrier with steric bulk is observed. In the case of $^{MeO}$**1-MA** and $^{Ar}$**1-MA** the energy of AR-TS is roughly 14-34 kJ/mol lower than the energy of the corresponding $TS_{Ins}$, which indicates that the first MA insertion is not stereoselective. Considering that the ring flip is again calculated to be a low energy process, which in addition can also proceed during the cis/trans isomerization in connection with the Berry-pseudo rotation step with a low energy barrier, the ring flip motion is assumed to be generally rapid compared to aryl rotation and acrylate insertion and is not further discussed in the following.

**Table 5-6.** Comparison of the transition state energies (kJ/mol) for the stereoselective insertion of MA into $^{X}$**1** with TS energies for ring flip and aryl rotation for $^{X}$**1-MA**.

| entry | compound | $TS_{Ins}$ | ring flip-TS | aryl rotation-TS |
|---|---|---|---|---|
| 7-1 | $^{MeO}$**1** | 0 | -49 | -34 |
| 7-2 | $^{(MeO)2}$**1** | 0 | -51 | -[b] |
| 7-3 | $^{Ar}$**1** | 0 | -49 | -14 |
| 7-4 | $^{Ar/(MeO)2}$**1**[a] | 0 | -18 | -5 |

[a]configuration at phosphorus: (*R*); [b]aryl rotation is not possible, since the MeO-groups inevitably collide in the corresponding TS.

For the bulky $^{(MeO)2}$**1-MA** system, rotation of the aryl moieties is hampered (*vide supra*) and the fixed chiral conformation (*P* or *M*) of the complex should in principle select between the *re* or *si*-MA transition state. However, analysis of the transition state geometry for a *P* configuration at the active site reveals no significant differences in the interaction between the two enantiofaces of the monomer and the ligand, due to the high symmetry of the system (Figure 5-25). Consequently the energy difference between the *re*- and *si*-MA $TS_{Ins}$ is negligible (less than 1 kJ/mol).

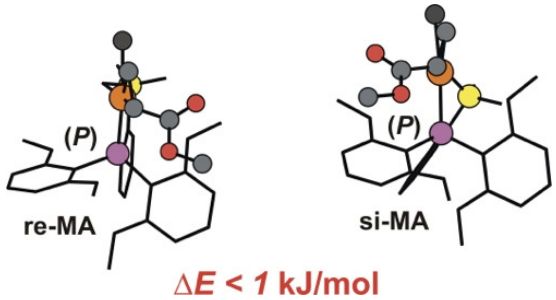


**Figure 5-25.** Transition states for *si* and *re* insertion of MA in $^{(MeO)2}$**1** with a (*P*) helical configuration of the aromatic rings.

The asymmetric system $^{Ar/(MeO)2}$**1** exhibits a permanent stereocenter at the phosphorus and can in principle distinguish between the different MA enantiofaces even if molecular motions are fast. In fact, a significant energy difference $\Delta E_{stereo}$ = 11 kJ/mol between the two respective lowest energy transition states for acrylate insertion into the Pd-Me bond was found. In case of an *R* configuration at the phosphorus atom (which favors a *P* helical chirality) insertion of a *re*-coordinated MA is favored (Figure 5-26). The calculated difference of 11 kJ/mol is in reasonable agreement with the experimental stereoselectivity ratio of 6:1. As depicted in Figure 5-26 the interaction between the 2,6-$(MeO)_2(C_6H_3)$-moiety and the monomer is responsible for the higher energy of the *si*-MA insertion into the Pd-Me bond of the $^{Ar/(MeO)2}$**1** complex with a *R* configuration at the phosphorus (shortest distances of 3.7 Å for *si*-MA compared to 3.9 and 3.8 Å in the favored *re*-TS).

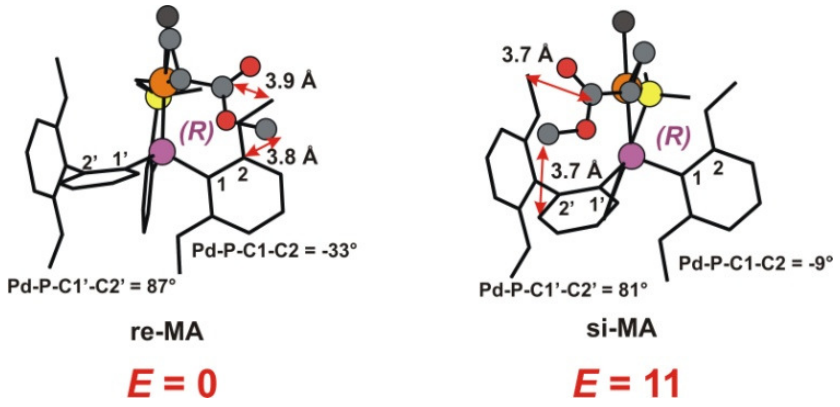


**Figure 5-26.** Analysis of the transition states for *si* and *re* insertion of MA into $^{Ar/(MeO)2}$**1** with a *P* helical configuration of the aromatic rings.

The first MA insertion generates a chiral carbon atom directly bound to the metal center, with *re*- and *si*-MA insertion resulting in an *R* and *S* configuration of the chiral carbon atom, respectively. Considering this, the consecutive MA insertion differs from the first insertion in that either an interaction of the chiral chain end with the ligand may force the catalytic site to assume a specific chiral conformation, or the chiral chain itself may direct the approaching monomer enantiofaces directly. Table 5-7 reports transition state energies for the selection between the two MA enantiofaces in the first two MA insertion steps. Regarding stereoselectivity, the results reported in Table 5-7 indicate no meaningful differentiation between the monomer enantiofaces for the second MA insertion, which is in agreement with the experimental results. The combined experimental and computational studies indicate that the chiral chain end is unable to force a chiral conformation of the active site able to discriminate between the two MA enantiofaces, even in case of bulky ligands. Furthermore, these results indicate that stereoselectivity due to direct interaction between the chiral growing

chain and the monomer is negligible, which is reasonable considering that 2,1-insertion places the functional group of the monomer away from the growing chain (Figure 5-27).

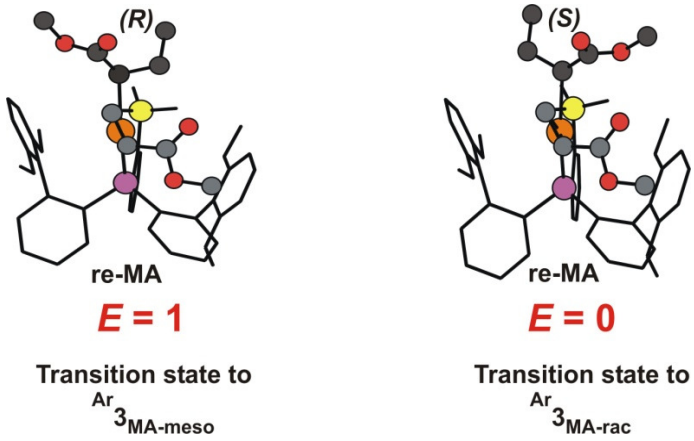


**Figure 5-27.** Transition states for the MA insertion into $^{Ar}\mathbf{2}_{MA}$ to $^{Ar}\mathbf{3}_{MA\text{-}meso}$ and $^{Ar}\mathbf{3}_{MA\text{-}rac}$; *P* helical configuration of the aromatic rings.

**Table 5-7.** Stereo- and regioselectivity for the first and the second MA insertion into $^{X}\mathbf{1}$ (energies in kJ/mol).

| entry | compound | monomer | $\Delta E_{stereo}$ (1st ins.) | $\Delta E_{stereo}$ (2nd ins.)[a] | $\Delta E_{regio}$ (1st ins.)[b] | $\Delta E_{regio}$ (2nd ins.)[d] |
|---|---|---|---|---|---|---|
| 8-1 | $^{MeO}\mathbf{1}$ | MA | - | -1(1)[c] | 9(10)[c] | 27 |
| 8-2 | $^{(MeO)2}\mathbf{1}$ | MA | 0 | 0 | 11 | 29 |
| 8-3 | $^{Ar}\mathbf{1}$ | MA | - | -1 | 0 | 14 |
| 8-4 | $^{Ar/(MeO)2}\mathbf{1}$ | MA | 11 | 3 | 7 | 12 |
| 8-5 | $^{MeO}\mathbf{1}$ | tBuA | - | 2 | -2 | 11 |

[a] positive numbers correspond to preference of the meso product $^{X}\mathbf{3}_{MA\text{-}meso}$; [b]positive numbers correspond to preference of the 2,1 MA insertion product; [c] the values in parenthesis are obtained with ADF programs and were reported previously;[44] [d]$\Delta E_{regio} = E_{2,1\text{-}1,2}\text{-}E_{2,1\text{-}2,1}$: positive numbers correspond to preference of $^{X}\mathbf{3}_{MA}$; Helical chirality for all compounds: (*P*).

For the asymmetric system $^{Ar/(MeO)2}\mathbf{1}$ four different consecutive insertion products $^{Ar/(MeO)2}\mathbf{3}$ can be formed, due to the chirality at phosphorus. The energy differences $\Delta E_{stereo}$ between the four transition states are reported in Table 5-8. In the first insertion an *R* chain is preferentially generated from the most stable *re*-MA $TS_{Ins}$ (Figure 5-26). For the second MA insertion stereoselectivity is again diminished. However, in contrast to the NMR studies the calculations indicate a slight preference for the meso isomer. The loss of enantiomorphic site control in favor of the *re*-MA enantioface in the second insertion step has to be explained by steric interaction between the ethyl group of the chain and the ligand. The 2,6-$(MeO)_2(C_6H_3)$ moiety at the phosphorus is rotated in comparison to the *re*-TS of the first insertion and one of the methoxy groups is now arranged in a critical distance of 3.5 Å from the monomer (dihedral angle <(Pd-P-C1-C2): -33°(*re*-$MA_{1st}$) vs. -9°(*re*-$MA_{2nd}$); compare -9°(*si*-$MA_{1st}$) vs. -14°(*si*-$MA_{1st}$); Figure 5-28 vs. Figure 5-26). As a consequence enantiomorphic site

stereocontrol and chain end stereocontrol act in different directions for $^{Ar/(MeO)2}$**2** so that the stereoselectivity on the second MA insertion is definitively lost. The calculation indicates that due to the flexibility of the system the ligand evades the growing chain and any kind of MA stereoselectivity in the polymerization is prevented.

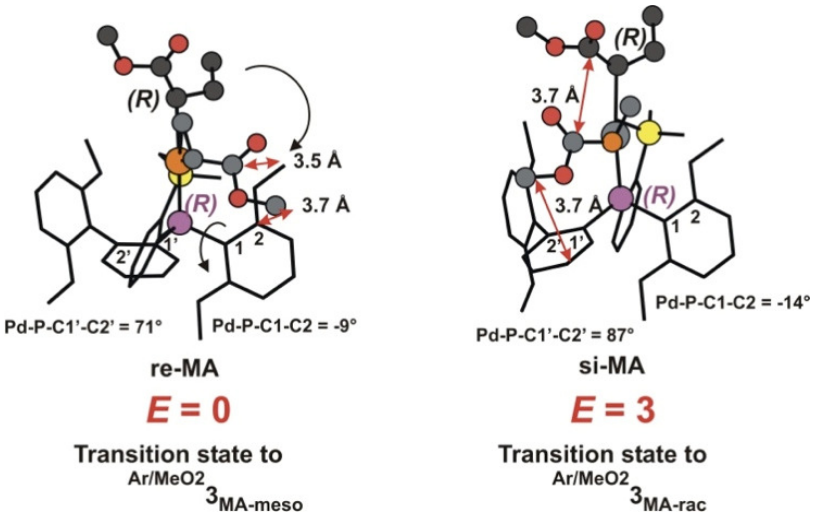


**Figure 5-28.** Transition states for the MA insertion into $^{Ar/(MeO)2}$**2**$_{MA}$ to $^{Ar/(MeO)2}$**3**$_{MA\text{-}meso}$ and $^{Ar/(MeO)2}$**3**$_{MA\text{-}rac}$; *R* configuration at the phosphorus atom and *P* helical configuration of the aromatic rings.

**Table 5-8.** $\Delta E_{stereo}$ (kJ/mol) for all transition states to the insertion products of the first and second MA insertion into $^{Ar/(MeO)2}$**1** with a (*R*) configuration at the phosphorus and a *P* helical configuration of the aromatic rings.

| $^{Ar/(MeO)2}$**1** | MA 1st insertion (2,1) | | MA 2nd insertion (2,1; 2,1) | | | |
|---|---|---|---|---|---|---|
| | *re* | *si* | *re/R* | *si/R* | *re/S* | *si/S* |
| $\Delta E_{stereo}$ | 0 | 11 | 0 | 3 | 10 | 4 |
| product | $^{Ar/(MeO)2}$**2**$_{MA\text{-}2,1}$ | $^{Ar/(MeO)2}$**2**$_{MA\text{-}2,1}$', | $^{Ar/(MeO)2}$**3**$_{MA\text{-}meso}$ | $^{Ar/(MeO)2}$**3**$_{MA\text{-}rac}$ | $^{Ar/(MeO)2}$**3**$_{MA\text{-}rac}$', | $^{Ar/(MeO)2}$**3**$_{MA\text{-}meso}$', |

In order to investigate the influence of the monomer steric bulk the transition states for *t*BuA insertion with $^{MeO}$**1** were calculated (Table 5-7). As for MA insertion, both first and second *t*BuA insertions are not stereoselective. In agreement with the experimental results the calculations show that the complex flexibility prevents any enantioface selection in the transition state even for the bulky *t*BuA monomer. In the competitive transition states leading to $^{MeO}$**3**$_{tBuA\text{-}meso}$ and $^{MeO}$**3**$_{tBuA\text{-}rac}$ (Figure 5-29) the system arranges the steric bulk of the monomer and of the chain, such that no difference in terms of steric pressure and energy emerges.

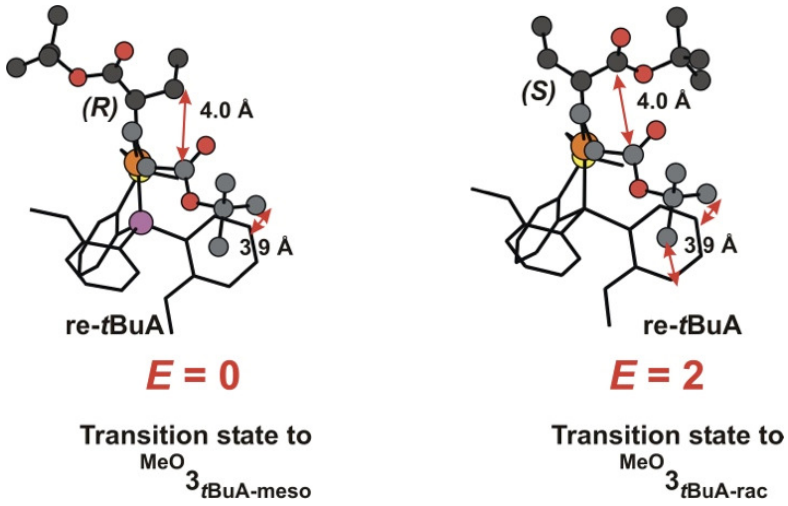


**Figure 5-29.** Analysis of the transition states for the *t*BA insertion into $^{MeO}\mathbf{2}_{tBA}$ to $^{MeO}\mathbf{3}_{tBA\text{-}meso}$ and $^{MeO}\mathbf{3}_{tBA\text{-}rac}$.

Since the production of defined tactic polymers does not only depend on stereoselectivity but also on regioregularity, and the experimental work showed that both insertion modes (1,2; 2,1) are observable at least for the first insertion, the influence of the ligand structure on regioselectivity was investigated. Here, the energy differences between the 2,1 and 1,2 monomer insertions into Pd-Me bond were calculated for the first insertion ($\Delta E_{regio,1st}$, Table 5-7). In addition, also the consecutive 1,2 MA insertion into $^{X}\mathbf{2}_{\mathbf{2,1\text{-}MA}}$ was considered in comparison to the consecutive 2,1-insertion ($\Delta E_{regio,2nd}$, Table 5-7). By contrast, a consecutive 1,2-insertion into $^{X}\mathbf{2}_{\mathbf{1,2\text{-}MA}}$ is energetically not favorable because of steric interaction between the monomer and the 1,2 chain end, and was also not observed experimentally so far. For all systems the TS for the consecutive 1,2-1,2 MA insertion is at least 25 k/J mol higher than for the corresponding consecutive 2,1-2,1-MA insertion TS.

As expected and in agreement with previous studies, the calculations show that the shift from the electronically favored 2,1-transition state to the less sterically constrained 1,2-transition state depends on the structure of the ligand and the size of the monomer.[41] The 1,2-transition state becomes more favoured by increasing either the size of the P-aryl substituents of the chelating ligands $^{MeO}\mathbf{1}$ ($\Delta E_{regio,1st}$ = 9 kJ/mol) to $^{Ar/(MeO)2}\mathbf{1}$ ($\Delta E_{regio,1st}$ = 7 kJ/mol) to $^{Ar}\mathbf{1}$ ($\Delta E_{regio,1st}$ = 0 kJ/mol) or the size of the monomer (Table 5-7). The 2,1-and 1,2-transition states for the first insertion of MA into $^{Ar}\mathbf{1}$ and of *t*BuA into $^{MeO}\mathbf{1}$ are compared in Figure 5-30. In both cases regioselectivity is completely lost ($\Delta E_{regio,1st}$ = 0-2 kJ/mol). In the 2,1-transition state the incoming monomer interacts with the ligand to a higher extent than in the less sterically encumbered 1,2-insertion transition state. For this reason, the 2,1-insertion becomes disfavored with increasing bulkiness of either the ligand or the monomer. These results are in qualitative agreement with the experiments, that indicated a clear preference for 2,1 MA insertion for the sterically less demanding systems $^{MeO}\mathbf{1}$ and $^{(MeO)2}\mathbf{1}$, whereas from

$^{Ar/(MeO)2}$**1** to $^{Ar}$**1** regioselectivity is diminished or even lost. For the second MA insertion the calculations show the same trend, but $\Delta E_{regio,2nd}$ still amounts to 8-29 kJ/mol in favor of a consecutive 2,1-insertion, which explains the absence of a 2,1-1,2-insertion product in the NMR experiments.

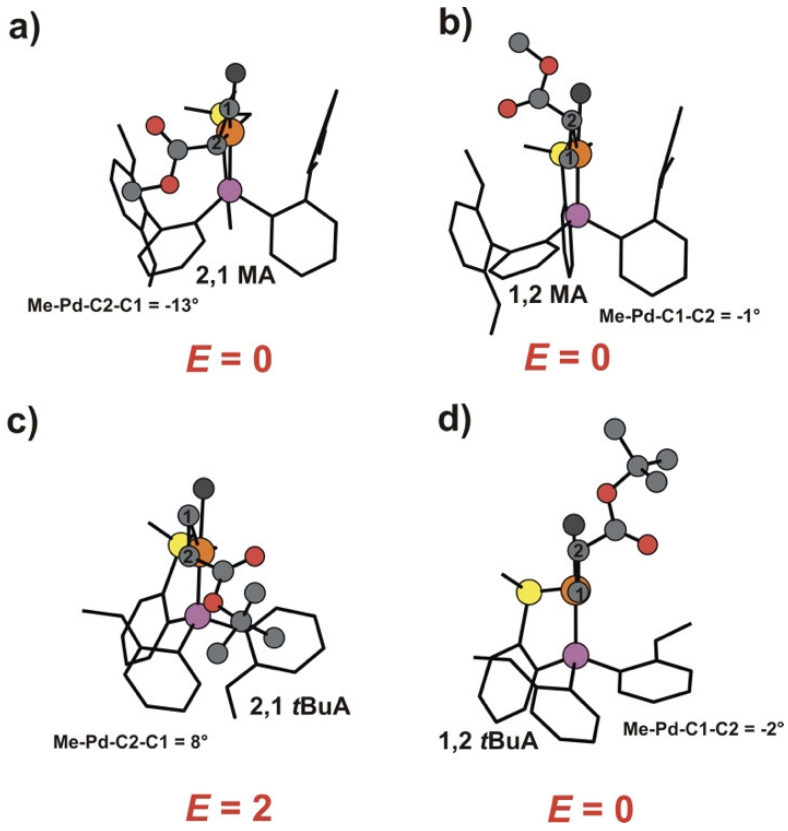


**Figure 5-30.** Regioselectivity of MA insertion into $^{Ar}$**1** (a, b) and of *t*BuA insertion into $^{MeO}$**1** (c, d).

Moving from MA to the more bulky *t*BuA monomer, regioselectivity for insertion with $^{MeO}$**1** is sharply reduced, which is in line with the experimental results. As reported previously the decrease of regioselectivity can be rationalized by an analysis of the deviation from planarity of the four center Cossée-Arlman-like transition state that increases by increasing the sterical pressure of the system.[41] The extent of this deviation can be estimated by comparing Me-Pd-C1-C2 dihedral angles for the 2,1-transition states in Figure 5-30 with the value for the 2,1-transition state for $^{MeO}$**1** reported previously.[41] The deviation from 0° for insertion into $^{MeO}$**1** increases from MA insertion (-4°) to *t*BuA insertion (8°) (Figure 5-30 and Table 5-7). Conclusively, in agreement with the experimental observations an increase of steric constrains via the phosphinesulfonato ligand or the monomer decreases the regioselectivity of the insertion.

### 5.2.7 Towards Asymmetric, Cyclic Phosphinitesulfonato and Phosphinesulfonato Pd(II) Complexes

The previous studies with classical arylphosphinesulfonato Pd(II) complexes revealed two key requirements for stereoselective acrylate insertion: An asymmetric substitution pattern at phosphorus and a restricted flexibility of the ligand regime. The studies indicate that these requirements are complicated to integrate within the recent ligand framework, as restriction of flexibility so far has to be induced by steric bulk, which hinders chain growth and diminishes regiocontrol. An alternative approach is the design of asymmetric, bridged ligands, as bridging might reduce flexibility without excessive increase of steric bulk.

An interesting building block for such compounds is 6-chloro-6*H*-dibenz[c,e][1,2]oxaphosphorine, which is easily available from the cyclisation of 2-phenylphenol with $PCl_3$ (Scheme 5-7).[163] Recently, 6-chloro-6*H*-dibenz[c,e][1,2]oxaphosphorine has been used for the synthesis of phosphonite-oxazoline ligands and the corresponding Pd(II) complexes were active for insertion of CO and ethylene.[164] Related phosphonite-pyridine complexes of Ni(II) have also been studied in the catalytic oligomerization of ethylene.[165] The reaction of chloro-dibenzo-oxaphosporine with lithiated benzenesulfonic acid and protonation with trifluoroacetic acid (TFA) yielded the phosphonitesulfonato ligand **$^{oxa}$($^{O}$P^O)H** (Scheme 5-7). The molecular structure exhibiting an asymmetric substitution at phosphorus could be established by NMR and X-ray analysis (Figure 5-31). In the solid state structure the ligand is zwitterionic and the proton is located at phosphorus as also found regularly for the phosphinesulfonato ligands. However, in solution the proton can tautomerize depending on the solvent and e.g. is located at the sulfonate in DMSO-$d_6$ as evidenced by $^1$H NMR spectroscopy.

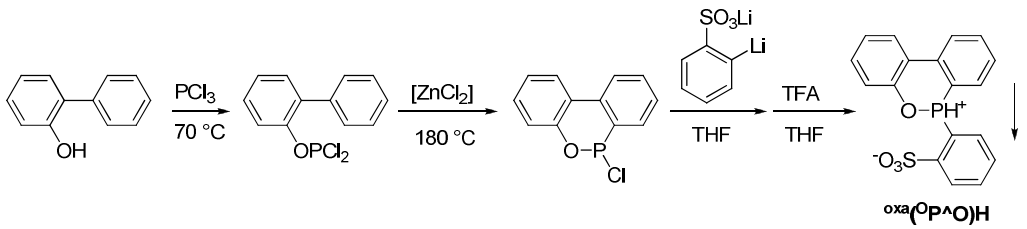


**Scheme 5-7.** Synthesis of **$^{oxa}$($^{O}$P^O)H**.

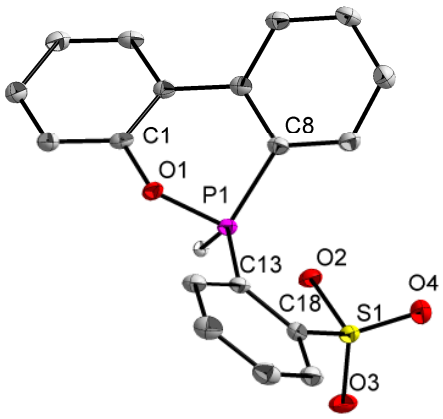


**Figure 5-31.** Solid state structure $^{oxa}(^{O}P\text{^}O)H$ Ellipsoids represent 50% probability. Hydrogen atoms are omitted for clarity. Selected bond lengths [Å]: P(1)-O(1) = 1.653(1); P(1)-C(8) = 1.798(1); P(1)-C(13) = 1.809(2); S(1)-O(1) = 1.509(1); S(1)-O(2) = 1.509(1); S(1)-O(3) = 1.435(1); O(1)-C(1) = 1.391(2).

Reacting $^{oxa}(^{O}P\text{^}O)H$ with [(tmeda)PdMe$_2$] in THF resulted in the formation of a mononuclear complex **[$^{oxa}(^{O}P\text{^}O)$PdMe(tmeda)]**, which precipitated from solution (Scheme **5-8**). Since only one diastereomer can be observed by NMR spectroscopy a mononuclear structure is assumed (Figure 5-32). For a multinuclear arrangement two (or more) diastereomers should be observable, as each $^{oxa}(^{O}P\text{^}O)$ unit exhibits a permanent, (racemic) stereocenter at the phosphorus atom (Figure 5-31).

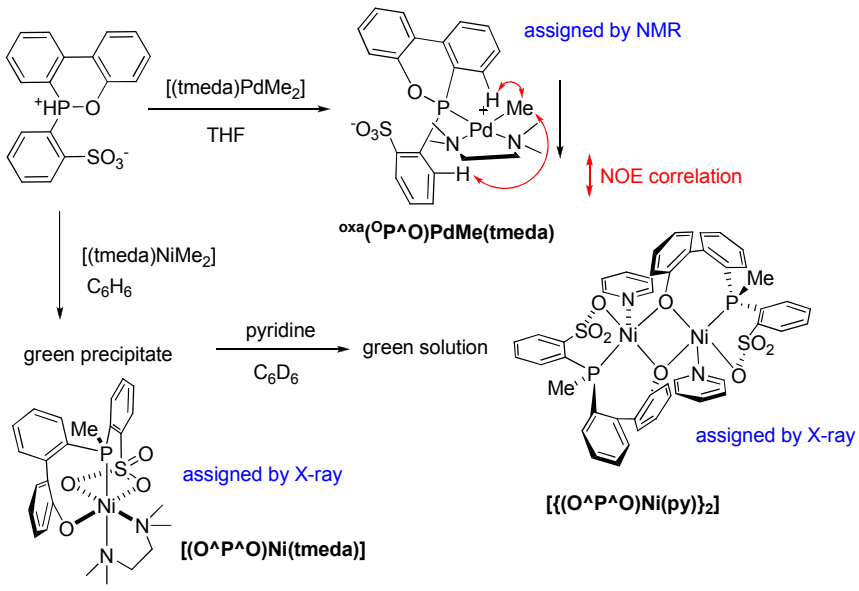


**Scheme 5-8.** Synthesis of palladium and nickel complexes of $^{oxa}(^{O}P\text{^}O)H$.

The mononuclear arrangement of **[$^{oxa}(^{O}P\text{^}O)$PdMe(tmeda)]** is in contrast to TMEDA complexes of phosphinesulfonato Pd(II) complexes, for which the formation of dimeric structures [{(P^O)PdMe}$_2$(tmeda)] was observed.[24,31] Analysis of the molecular geometry by NOESY experiments revealed that the TMEDA ligand probably is coordinated in a chelating

fashion at the Pd-center, whereas the $^{oxa}(^{O}P\text{^}O)$-ligand only coordinates by the phosphorus atom (Scheme 5-8). This presumption arises from observed NOE correlations between the Pd-Me group and the ortho-aryl protons of the benzenesulfonate, as well as between the Pd-Me group and the ortho-aryl protons of the oxaphosphorine moiety (Figure 5-32). For a coordination of the sulfonate group to the palladium center, the ortho-aryl proton of the benzenesulfonate moiety would be aligned away from the palladium center and no NOE-correlation to the Pd-Me groups should be observed. In contrast, a single phosphine oxide coordination was observed for the much weaker coordinated compound [**$^{oxa}(^{O}P\text{^}O)PdMe(OPBu_3)$**], synthesized *in situ* by reaction of **$^{oxa}(^{O}P\text{^}O)Na$** with [(cod)PdMeCl] in presence of $AgBF_4$ and $OPBu_3$. Here, NOESY experiments showed only a single NOE correlation between the Pd-Me and the ortho-aryl-proton of the oxaphosphorine moiety and a chelating coordination of the $^{oxa}(^{O}P\text{^}O)$-ligand can be assumed. Overall this implies a much weaker coordination of **$^{oxa}(^{O}P\text{^}O)H$** to a Pd(II) center compared to phosphinesulfonato ligands.

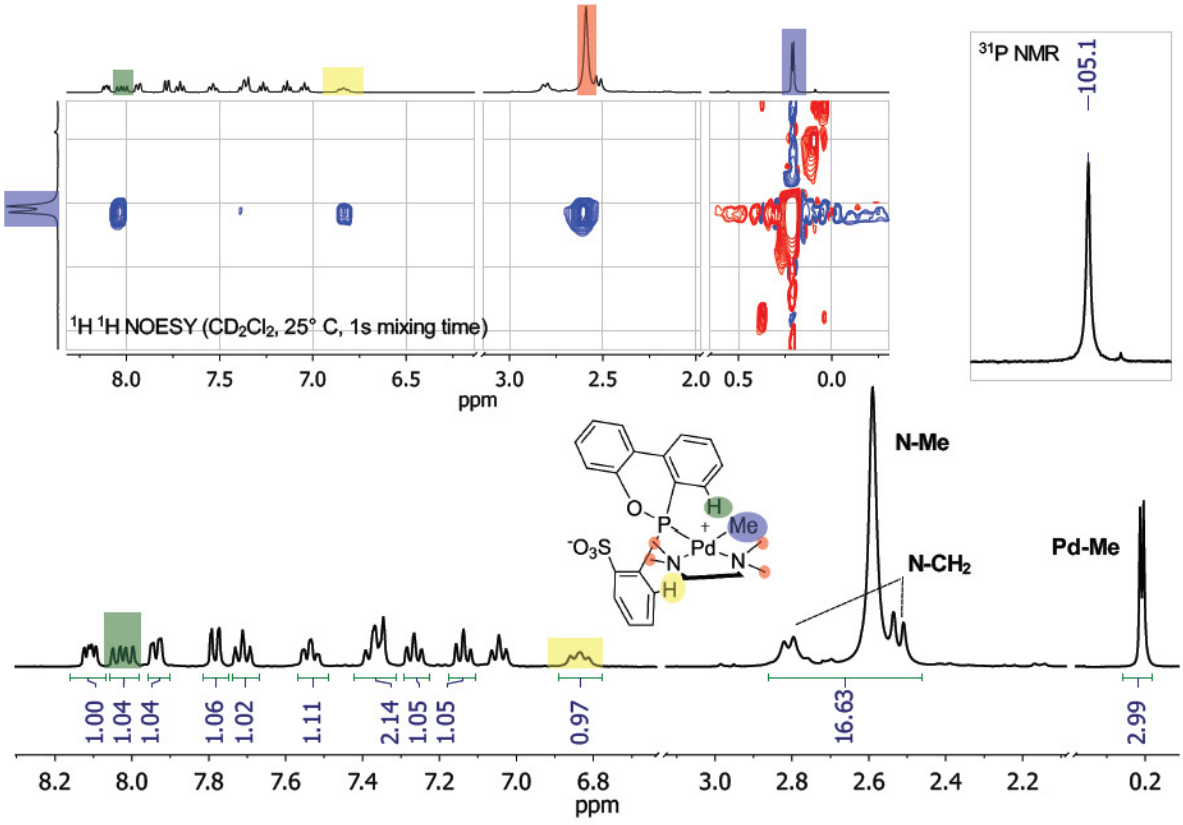


**Figure 5-32.** $^{1}$H NMR spectrum (400 MHz, $CD_2Cl_2$, 25 °C) of **$^{oxa}(^{O}P\text{^}O)PdMe(tmeda)$**. Inset (left): $^{1}$H $^{1}$H NOESY spectrum (1 s mixing time) showing the correlations of the Pd-Me group; Inset (right) $^{31}$ P NMR (162 MHz, $CD_2Cl_2$).

In order to evaluate the reactivity of [**$^{oxa}$($^{O}$P^O)PdMe(L)**] (L = $OPBu_3$ and TMEDA) towards polar olefins solutions of the complexes were reacted with 10 equivalents of MA in $CD_2Cl_2$ or $C_6D_6$ in a NMR tube. For both compounds no insertion reaction could be observed for temperatures up to 95 °C. The reactivity towards ethylene was evaluated under typical polymerization conditions (toluene, 80 °C, 30 minutes, 20 bar ethylene pressure). During polymerization no mass flow was observed and only trace amounts of PE could be isolated. The results of the insertion and polymerization studies indicate that an insertion reaction for $^{oxa}$($^{O}$P^O)PdMe complexes is hampered compared to phosphinesulfonato systems. Here, it should be noted, that the phosphonitesulfonato ligands exhibits a phosphorus atoms which is a weaker σ-donor compared to the one of arylphosphinesulfonates.

In order to gain further insights, Ni(II) complexes were synthesized by the reaction of **$^{oxa}$($^{O}$P^O)H** with [(tmeda)$NiMe_2$] (Scheme 5-8). The reaction in benzene yielded a greenish precipitate, which can be dissolved by addition of pyridine. NMR analysis of the species formed is not possible, since the products exhibit paramagnetism. X-ray structure analysis of a pyridine and a TMEDA complex indicate an interesting decomposition process (Figure 5-33). A methyl group is transferred from the Ni-center to the phosphorus atom and the P-O bond of the oxaphosphorine moiety is cleaved resulting in a new dianionic, formally three-dentate $(O^P^O)^{2-}$ ligand. In the case of the TMEDA ligand an octahedral Ni complex **[(O^P^O)Ni(tmeda)]** is formed if twofold coordination of the sulfonate group is considered (Ni-O(2) = 2.554(1) Å, Ni-O(4) = 2.139 Å). For the pyridine complex **[{(O^P^O)Ni(py)}$_2$]** a binuclear structure bridged by the phenoxy group is obtained. The Ni-Ni distance is close to the sum of the van-der-Waals-radii (Ni-Ni = 3.136 Å vs. 3.260 Å (v.d.W)) indicating a weak Ni-Ni interaction. In this case the coordination sphere at the nickel appears square pyramidal, since the second sulfonate oxygen is not situated exactly beneath the nickel. However, $O_2SO$-Ni bond distance are quite similar compared to the TMEDA compound (Ni-O(2) = 2.568(2) Å, Ni-O(3) = 2.084(2) Å). The observed transfer of a methyl group to the ligand under cleavage of the O-P bond may represent a general decomposition pathway for $^{oxa}$($^{O}$P^O)M-Me compounds (M = Pd, Ni), which could also explain the low activity under polymerization conditions of the palladium complexes, due to irreversible deactivation. However, a similar reaction could not be observed by NMR spectroscopy for the Pd compounds, which can be concluded from the absence of a Me-P resonance in the $^1$H NMR spectra, which would give rise to a defined doublet (compare $^{Me*/(MeO)3}$**1**, Chapter 7.2.5.2).

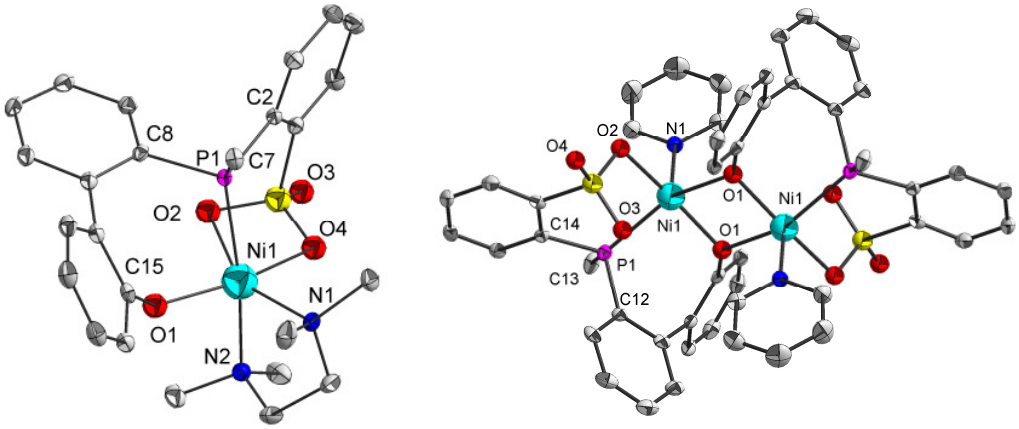


Figure 5-33. Solid state structure of the decomposition product **[(O^P^O)Ni(tmeda)]** (left) and **[{(O^P^O)Ni(py)}$_2$]** (right). Ellipsoids represent 50% probability. Hydrogen atoms are omitted for clarity. Selected bond lengths [Å] and angles for **[(O^P^O)Ni(tmeda)]** [°]:Ni(1)-O(1) = 2.011(2); Ni(1)-O(2) = 2.544(1); Ni(1)-O(4) = 2.139(1); Ni(1)-P(1) = 2.374(0); Ni(1)-N(1) = 2.095(1); Ni(1)-N(2) = 2.150(1); P(1)-C(2) = 1.827(2); P(1)-C(7) = 1.826(2); P(1)-C(8) = 1.823(2); S(1)-O(2) = 1.459(1); S(1)-O(3) = 1.440(1); S(1)-O(4) = 1.480(1); O(1)-C(15) = 1.329(2); N(1)-Ni(1)-O(4) = 89.9(1); O(4)-Ni(1)-O(2) = 60.5(0); O(2)-Ni(1)-O(1) = 103.6(0); O(1)-Ni(1)-N(1) = 106.4(1); O(1)-Ni(1)-P(1) = 87.5(0); O(1)-Ni(1)-N(2) = 89.9(1). Selected bond lengths [Å] and angles [°] for **[{(O^P^O)Ni(py)}$_2$]**: Ni(1)-Ni(1) = 3.136(1); Ni(1)-O(1) = 2.011(2); Ni(1)-O(2) = 2.084(2); Ni(1)-O(3) = 2.568(2); Ni(1)-P(1) = 2.410(1); Ni(1)-N(1) = 2.015(2); S(1)-O(2) = 1.484(2); S(1)-O(3) = 1.460(2); S(1)-O(4) = 1.439(2); P(1)-C(12) = 1.829(3); P(1)-C(13) = 1.833(3); P(1)-C(14) = 1.831(3); O(1)-C(1) = 1.359(3); O(1)-Ni(1)-O(2) = 94.4(1); O(2)-Ni(1)-P(1) = 93.5(1); P(1)-Ni(1)-O(1) = 88.7(1); O(1)-Ni(1)-O(1) = 77.9(1); O(2)-Ni(1)-N(1) = 89.0(1); O(1)-Ni(1)-O(3) = 107.3(1).

The synthesis of the phosphonitesulfonato ligand $^{oxa}$(**$^{O}$P^O)H** and the corresponding Pd complexes revealed that pronounced variations at the arylphosphinesulfonato ligand framework can easily lead to compounds which loose the ability to polymerize or even insert olefins. For this reason, a bridging within the classic phosphinesulfonato scaffold appears attractive. Preliminary computational studies indicate that the (P^O)PdMe complex **C** (Scheme 5-9) bridged by a chiral BINOL backbone might be capable of stereoselective MA insertion. Based on this prediction a retrosynthesis was developed as depicted in Scheme 5-9. The synthetic route contains two key steps: The synthesis of a BINOL phenoxy ether **A** and the subsequent macrocyclization to **B**. The synthesis of **A** could be achieved by a copper(I) catalyzed *O*-arylation.[166] However, the ring closure to an 11-membered ring failed so far. Ring closure reactions of macrocycles are usually achieved under high dilution conditions. This proved to be problematic since a double ortho-lithiated and therefore highly reactive intermediate has to be used in the cyclisation. This species is easily quenched by minor impurities in the solvent. So far either only mono- or unfunctionalized or polymeric material could be isolated.

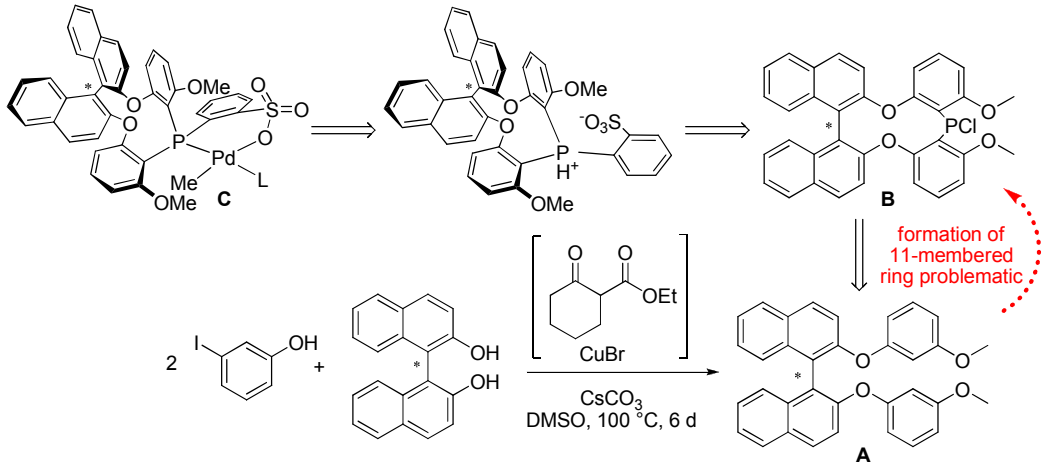


**Scheme 5-9.** Retrosynthesis of complex **B** and synthetical problems.

As a model reaction the ring closure of 1,4-bis(3-methoxyphenoxy)butan to a 9-membered ring was attempted (Scheme 5-10). However, also in this case the same problems hampered a product formation.

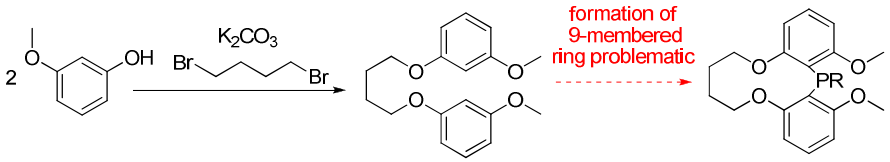


**Scheme 5-10.** Attempted cyclization to a 9-membered macrocyclic phosphine.

Conclusively, the synthesis of cyclic, asymmetric compounds could be achieved but the palladium complexes of the new phosphonite ligand $^{oxa}$(**$^{O}$P^O)H** were not reactive for olefin insertion as shown by polymerization and NMR studies, which can be explained by the pronounced electronic differences to classical arylphosphinesulfonato compounds. For the synthesis of cyclic asymmetric compounds, which electronically more resemble the classical phosphinesulfonato ligand scaffold, a cyclization to macrocyclic phosphines proved to be a critical step in synthesis. Future syntheses should avoid a ring closure at phosphorus, which also might allow for additional synthetic tools.

## 5.3 Summary and Conclusion

As has been understood in the past few years, palladium complexes with unsymmetrical, hard/soft chelating phosphinesulfonato ligands are unique in allowing for ethylene copolymerization with a large range of polar vinyl monomers and even enable insertion homooligomerization of acrylates.

An analysis of intramolecular interconversion processes showed that the ligand framework is rather flexible and undergoes several transformations including an aryl rotation in a propeller-like conformation environment and a ring flip process of the six-membered (P^O)Pd chelate. The highest barriers $\Delta G^{\neq}$ of these processes – namely of the aryl rotation – were found to add up to 40-60 kJ/mol for the methyl complexes ($^{X}$**1**). Theoretical calculations revealed that also for the monomer-coordinated complexes $^{X}$**1-MA** the transition states for the intramolecular motions are significantly lower then the insertion transition states. An exception was found for systems that bear double ortho substituted aryl moieties at phosphorus. Here, an aryl rotation is inhibited, but still the transition states for both enantiofaces of the monomer are rather similar due to the symmetry of the ligand.

Conclusively, a permanent chiral center at phosphorus by asymmetric substitution is a prerequisite for a stereocontrol of insertion. This concept is underlined by the experimental observation of a 6:1 stereoselectivity in the first insertion with the asymmetric complex $^{Ar/(MeO)2}$**1**. For the consecutive insertions stereocontrol is reduced to 3:1. The theoretical calculations indicate that the high flexibility of the ligand is responsible for loss of stereocontrol. The ligand evades the growing chain and transition states are equilibrated for the consecutive insertion, since site stereocontrol and chain end stereocontrol work uncooperatively. NMR-insertion studies with $^{MeO}$**1** showed that within the accessible temperature range stereoselectivity cannot be influenced by temperature. Furthermore, insertion studies of monomers with variable steric bulk (MA, *i*PrA, *t*BuA) revealed that stereocontrol decreases with increasing steric bulk, which indicates that also in this case chain end stereocontrol and enantiomorphic site stereocontrol work together uncooperatively.

A low level of stereocontrol is also found in oligomerization experiments. Under polymerization conditions only $^{MeO}$**1** proved to be a suitable catalyst for acrylate oligomerization, able to form a significant amount of acrylate oligomer without byproducts from free-radical polymerization. Analysis of the tacticity of a methyl acrylate oligomer fraction with a $DP_n$ ~30 revealed that $^{MeO}$**1** produces oligomers with a syndio-enriched

structure (syndiotacticity ~69%), which is in line with the low selectivities determined in the insertion studies.

Beyond the effects on stereocontrol a clear relation between steric bulk and the regioselectivity of insertion was found, such that increased steric bulk in the ligand or in the monomer leads to a shift from the desired 2,1- to the 1,2-insertion mode. The resulting 1,2-insertion products are not amenable to further insertions due to the stability of the five-membered chelate formed by coordination of the carbonyl group of the incorporated acrylate. Theoretical considerations clearly show that deviation from the planarity of the four center Cossée-Arlman-like transition state increases the sterical pressure of the system and results in energetically similar 1,2- and 2,1-insertion transition states. That is, site differentiation by extreme steric bulk is not a feasible approach to tactic polymers since the regioregularity is lost. In addition, the insertion studies also disclosed an intrinsic problem of these catalysts: Increase of steric bulk always leads to a reduction of the acrylate insertion rates, and thus hinders chain growth. This culminates in a complete suppression of consecutive acrylate insertions for $^{Ar}\mathbf{1}$.

In this context note that in the asymmetric copolymerization of CO with asymmetric phosphinesulfonato complexes like $^{Ar/H}\mathbf{1}$ – communicated very recently – CO insertion introduces a non-chiral spacer between the chiral side chains. This apparently advantageously reduces a chain end stereocontrol, which in this work counteracts the enantiomorphic site stereocontrol of the homoinsertions.[40]

The limitations understood it is also evident that there is a 'window' of intermediate steric bulk which allows stereoselection without compromising regioregularity. In more general terms, it is remarkable that any stereoselection at all is possible in the open environment of the hard/soft unsymmetric phosphinesulfonato ligand (Figure 5-4). One decisive feature appears to be the insertion from the alkyl-olefin complex with the π-bound acrylate in cis-position to the P-donor. This allows for influencing the stereoselectivity of the insertion step via the P-substituents. With the concept of an unsymmetric substitution, stereocontrol was realized. A reduction of flexibility in such asymmetric complexes appears a possible approach towards stereoselective polymerization. Reduction of flexibility has been shown to be possible by a double ortho substitution of the aryl moieties at phosphorus. However, a more effective concept may be the introduction of a rigid spacer between the two different aryl moieties (Figure 5-34). This could further allow placing the chiral information in the spacer, which might reduce steric bulk at the active center.

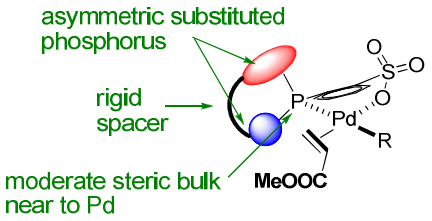


**Figure 5-34.** Concept towards stereoselective catalysts.

For this reason, asymmetric, cyclic ligands based on an arylphosphonitesulfonato scaffold where developed. However, the resulting phosphonitesulfonato palladium(II) complexes showed no activity for olefin insertion or polymerization. This might be explained by the pronounced electronic difference of the phosphorus donor as compared to the arylphosphinesulfonato compounds. Alternatively, specific decomposition pathways have been observed for the corresponding nickel complexes, which might be responsible for a fast irreversible deactivation of the palladium compounds under polymerization conditions. The synthesis of chiral, cyclic ligands based on the classical arylphosphinesulfonato ligand framework has not been successful so far. Here, a synthetic key problem was found to be the formation of the macrocyclic phosphines, for which so far no synthetic protocols have been reported.

# 6. Summary

The insertion (co)polymerization of polar substituted olefins represents an important new tool within synthetic polymer chemistry and offers access to new materials. If certain requirements concerning molecular weight and microstructure are met, these polymers are very attractive for numerous applications. In contrast to early transition metal catalysts employed for the industrial production of PE and PP on a multimillion ton scale, catalysts that can handle polar environments are based on late transition metals. Today only two catalytic systems capable of insertion copolymerization of ethylene with polar monomers are established. α-Diimine Pd(II) catalysts produce highly branched copolymers, with the polar units located at the ends of branches preferentially.[3] By contrast, neutral phosphinesulfonato Pd(II) catalysts produce linear copolymers with incorporation of the polar monomer unit in the polymer backbone.[22] Whereas the reactivity of phosphinesulfonato Pd(II) catalysts towards a broad scope of different polar substituted olefins has been investigated, profound considerations on directed catalyst precursor design to overcome limitations of these catalysts are rare. Furthermore, stereocontrolled insertion polymerization with these catalysts has never been achieved, even though this could enable a broad control over materials properties.

Regarding catalyst development, it has been reported previously that the DMSO coordinated catalyst precursor **$^{MeO}$1-dmso** leads to a highly active catalyst giving access to copolymers with high polar monomer ratio in contrast to the pyridine or 2,6-lutidine coordinated precursors (Scheme 6-1).[43] Within this thesis the role of the Lewis donor ligand L in [(P^O)PdMe(L)] catalyst precursors was studied in detail to achieve an understanding for future catalyst precursor design. Phosphine oxides, the coordination strength of which can be easily tuned by their steric and electronic nature, were explored as defined weakly coordinating monodentate ligands L. The coordination strength of several phosphine oxides was evaluated in comparison to DMSO, and $OPPh_3$ was found to coordinated ca. five times weaker than DMSO to the (P^O)PdMe fragment. The synthesis of the very weakly coordinated complex **$^{MeO}$1-OPPh$_3$** was achieved (Scheme 6-1). Studies with weaker coordinating ligands revealed that for [(P^O)PdMe(L)] the minimum of coordination strength for L is limited, due to the ability of the (P^O)PdMe fragment to form ill-defined multinuclear palladium complexes **1$_n$** (Scheme 6-1). In these aggregates the sulfonate group is coordinated in an intermolecular fashion to various palladium centers, leading to insoluble material.

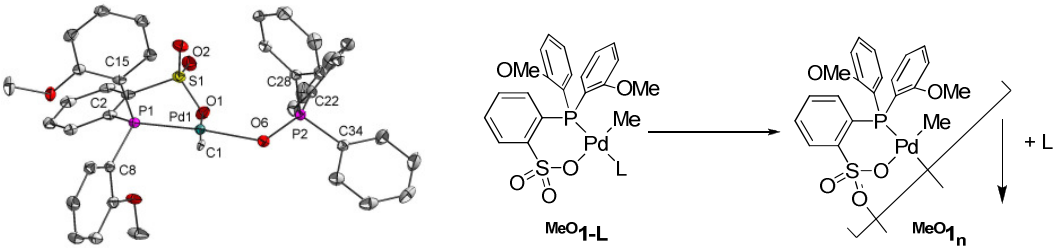


**Scheme 6-1.** X-ray structure of the weakest coordinated stable mononuclear complex of the $^{MeO}$**1** fragment, $^{MeO}$**1-OPPh$_3$** (left) and intrinsic limitation for more weakly coordinating monodentate ligands L.

An alternative route towards very active catalysts was found to be *in situ* chloride abstraction from [{($^{X}$**1-Cl**)-μ-Na}$_n$] precursors (Figure 6-1) with $AgBF_4$. The resulting catalysts $^{X}$**1** represent the best model for a species free of significantly coordinating monodentate ligand L with e.g. the highest possible activity in ethylene−MA copolymerizations. Generally, it was observed that the activity in copolymerization experiments does not depend significantly on the coordination strength for weakly coordinating ligands anymore. Mechanistic considerations revealed that six-membered κ-*O*-coordinated chelates are key intermediates and stable resting states of the copolymerization,[44] which essentially control polymerization activity in the absence of stronger coordinating ligands (Scheme 6-2). These chelates are inevitably formed by (co)monomer insertion after an MA insertion. The coordination strength of such chelates could be quantified for the model compound $^{MeO}$**3$_{rac/meso}$** (Figure 6-4) resulting from two consecutive MA insertions into the Pd-Me bond. An equilibrium constant of $K_{C2\text{-}E} = 2\times10^{-3}$ was estimated for the opening of the chelate with ethylene ($^{MeO}$**3$_{MA\text{-}rac/meso}$** + $C_2H_4$ ⇆ $^{MeO}$**3$_{MA\text{-}rac/meso}$**-$C_2H_4$). This reveals that chelate formation retards chain growth significantly, but not prohibitively.

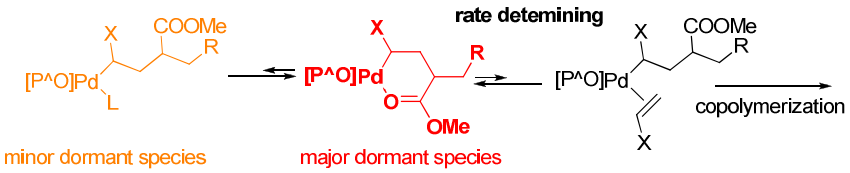


**Scheme 6-2.** Six-membered chelate resting state in the ethylene/acrylate copolymerization (X = H, COOMe).

In order to overcome intrinsic limitations of this type of catalysts as identified by the aforementioned investigations, electronic and steric modification of the phosphinesulfonato ligand is of interest. In order to gain insights on the influences of the phosphinesulfonato Pd(II) catalyst structure on the (co)polymers produced, different substitution patterns for the non-chelating aryl moieties at the phosphorus atom were studied. Fourteen new complexes of the type [{($^{X}$**1-Cl**)-μ-M}$_n$] were synthesized (Figure 6-1). This type of precursors were chosen based on the aforementioned finding that *in situ* chloride abstraction from such precursors is a

facile and reliable route to highly active catalysts. Furthermore, the utilization of these precursors eliminates coordination equilibria of additional ligands (L) which would otherwise blur an analysis of the structure-activity relationship of the bidentate (P^O) ligand.

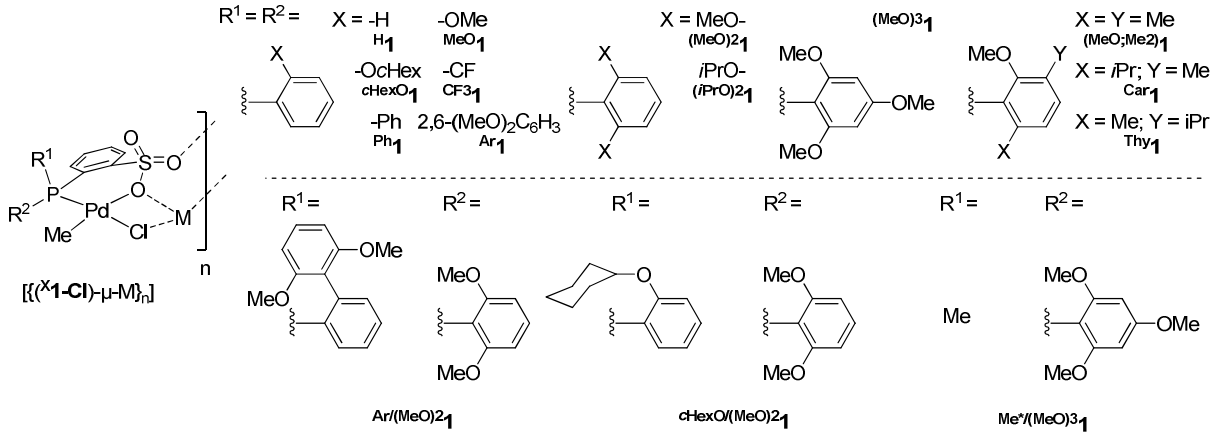


**Figure 6-1.** Complexes synthesized and studied in this thesis.

The reactivity towards methyl acrylate was studied for all compounds by NMR methods and rate constants for the insertion of MA into the Pd-Me bond were determined. In addition, β-H elimination and decomposition of the insertion species to unsaturated and saturated products were analyzed in detail to highlight different reaction pathways. The activity of the *in situ* activated catalyst precursor [{(**X1-Cl**)-μ-M}$_n$] in ethylene homopolymerization as well as in copolymerization with methyl acrylate was evaluated and the composition and microstructure of the resulting polymers was analyzed by NMR. The results are ambiguous regarding clear trends of electronic effects. However, some relations can be extracted. Electron deficient ligands rather enhance the intrinsic activity of the catalysts, but also reduce catalyst stability over time during polymerization (**CF3 1**, **Ar 1**). Within the ligand set bearing double ortho substituted aryl moieties, more electron donating ligands lead to catalysts that produce higher molecular weight polymers (**(MeO)3 1** vs. **(MeO)2 1**). In addition, **(MeO)3 1** and **(MeO)2 1** show a significantly increased preference for incorporation of methyl acrylate in the copolymerization compared to the other catalysts. A clear influence of the sterics of the ligands on the (co)polymers produced could be identified. Steric bulk enhances the molecular weight of copolymers as revealed by a comparison of **(*i*PrO)2 1**, ***c*HexO 1** and **Ar 1** with the corresponding unconstraint analogs. However, the comparison of the related catalysts **Ar 1** and **Ph 1** reveals that small differences can have a huge impact on the outcome of the polymerization reaction, since **Ph 1** produces polymers with significantly lower molecular weights and suffers from very low activity and stability. In the copolymerization experiments

it was also found that steric bulk always leads to a stronger discrimination of the bulkier polar monomer compared to ethylene, resulting in reduced comonomer incorporation.

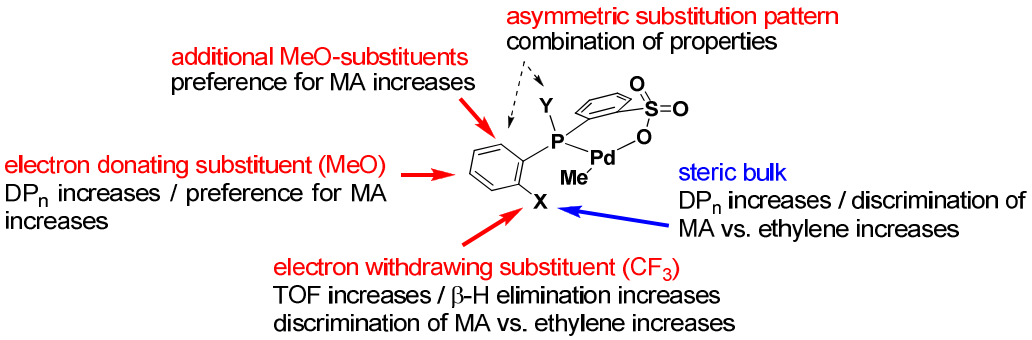


**Figure 6-2.** Influences of ligand substitutions on catalytic performance in polymerization.

Although the exact *a priori* prediction of structure-activity relationships remains challenging, these insights (Figure 6-2) provide a guideline for an appropriate choice of the P-aryl (alkyl) moiety. This concept is underlined by unsymmetric catalysts with two different aryl (alkyl) substituents, which effectively combine the properties imparted by the individual substituents to a desirable overall catalyst profile. The practicability of this approach was shown by the synthesis of the asymmetric catalyst $^{c\text{HexO/(MeO)2}}$**1** and $^{\text{Ar/(MeO)2}}$**1** (Figure 6-4). With $^{c\text{HexO/(MeO)2}}$**1** copolymers with significantly increased molecular weights are accessible. As an example, copolymers with a tripled molecular weight ($\chi_{MA}$ ~5 mol% MA, $M_n$ ~12000 g/mol), compared to material with similar MA incorporation produced by the prototypical $^{\text{MeO}}$**1**, could be obtained with $^{c\text{HexO/(MeO)2}}$**1**. Regarding the desirable synthesis of copolymers with enhanced molecular weights, conditions could be found to produce such copolymers also with the symmetric catalyst $^{\text{Ar}}$**1** (8 mol% MA, $M_n$ ~ 12000 g/mol). However, in this case very high MA concentrations are required, which limits a further increase of the MA incorporation ratio, while with $^{c\text{HexO/(MeO)2}}$**1** also copolymers with increased incorporation ratios of the polar monomer and still high molecular weights are accessible ($\chi_{MA}$ ~13 mol% MA $M_n$ ~7000 g/mol).

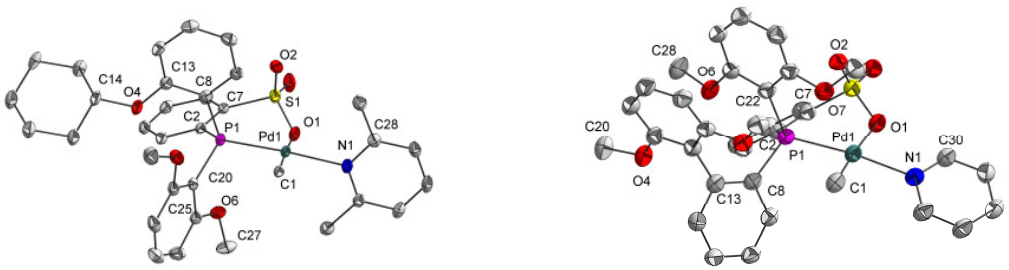


**Figure 6-3.** Solid state structures of the asymmetric substituted complexes $^{c\text{HexO/(MeO)2}}$**1** (left) and $^{\text{Ar/(MeO)2}}$**1**.

In principle, an insertion mechanism allows for a stereocontrolled polymerization if the incoming monomer enantioface can be controlled, as has been very successfully demonstrated for propylene polymerization with metallocenes.[132] It was shown previously that the consecutive insertion of MA into the Pd-Me bond of $^{MeO}$**1** affords the diastereomeric insertion product $^{MeO}$**3**$_{rac/meso}$ in a ca. 2:1 ratio and hence that a certain very low degree of stereocontrol for the consecutive MA insertion exists. Within this work the configuration of the stereoisomers $^{MeO}$**3**$_{rac}$ and $^{MeO}$**3**$_{meso}$ was determined by X-ray structure analysis and confirmed by NOESY experiments in solution (Figure 6-4).

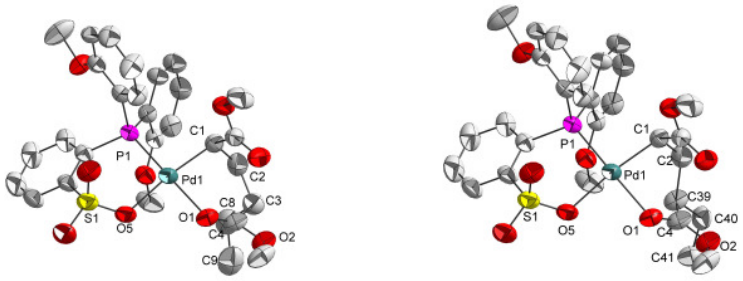


**Figure 6-4.** Solid state structures of the diastereomeric complexes $^{MeO}$**3**$_{MA\text{-}meso}$ (left) and $^{MeO}$**3**$_{MA\text{-}rac}$ resulting from consecutive MA insertion into the Pd-Me bond.

This revealed that the rac-isomer $^{MeO}$**3**$_{rac}$, which emerges from two MA insertions with the opposite stereoselectivity leading to a syndiotactic polymeric chain, is preferably formed in the consecutive MA insertion with $^{MeO}$**1**. This agrees with the isolation of syndio-enriched MA oligomers from the reaction of MA with $^{MeO}$**1** at elevated temperatures. Consequently, the stereoselectivity determined after the consecutive MA insertion allows for a prediction of the chain configuration of the polymer produced. In order to shed light on the mechanisms of stereocontrol with square planar phosphinesulfonato Pd(II) complexes, the influence of the ligand structure on stereoselectivity was studied in detail. An analysis of the possible constitutions and conformations revealed that phosphinesulfonato complexes exhibit two intrinsic asymmetric centers given by the ring configuration of the six membered (P^O)Pd chelate and by the helical configuration at the triaryl substituted phosphorus atom. Dynamic NMR studies showed that for most of the catalysts both stereocenters are inverted rapidly under polymerization conditions by a ring flip or an aryl rotation process, respectively. Here, significantly higher barriers were determined for the aryl rotation process inverting helical chirality. Consequently, only a low degree of stereocontrol, presumably due to a chain end control mechanism, could be detected in the insertion studies with symmetrically substituted compounds. Catalysts with a 2,6-$(RO)_2$-substitution at the non-chelating aryl moieties are helically stable, but no stereoselectivity for the consecutive MA

insertion could be detected. Here, the high symmetry of the ligand equilibrates the competing transition states as shown by DFT calculations. Due to the generally high fluxionality of the ligand framework, a permanent asymmetric center is a prerequisite for a stereoselective insertion. An asymmetric substitution pattern at phosphorus leads to complexes exhibiting a permanent chiral center. Indeed a high stereoselectivity of ~6:1 was found for the first MA insertion with $^{c\mathrm{HexO/(MeO)2}}\mathbf{1}$ (Figure 6-1, Figure 6-3). However, for the consecutive insertion regioselectivity is diminished to ~3:1, which indicates that chain end control and enantiomorphic site control work uncooperatively. DFT calculations were performed by Prof. Lucia Caporaso to unravel further mechanistic details. The results reveal that in the corresponding transition states the ligand evades the growing chain and arranges the steric bulk. For the phosphinesulfonato-systems investigated the high flexibility of the ligand turns out to be the key problem preventing an effective stereocontrol. Furthermore, the experimental insertion studies revealed that an increase of steric bulk, which could enhance the complexes rigidity and stereocontrol, decreases insertion rates and diminishes 2,1-regioselectivity. Theoretical considerations clearly show that deviation from the planarity of the four center Cossée-Arlman-like transition state increases the sterical pressure of the system and results in energetically similar 1,2- and 2,1-insertion transition states. For sterically demanding systems like $^{\mathrm{Ar}}\mathbf{1}$, no consecutive MA insertion was observed and the regioselectivity of the insertion is completely lost. Consequently, the ligand design has to be adjusted. Asymmetric cyclic ligands with a rigid spacer between the aryl moieties seem to be promising to reduce flexibility without increasing the steric bulk disadvantageously (Figure 6-5). For this reason, cyclic phosphonitesulfonato ligands were synthesized, but the corresponding complexes were not able to insert olefins. This might be due to the pronounced electronic deviation from phosphinesulfonato ligands. Additional deactivation pathways, which were identified for the corresponding nickel complexes, may also contribute to fast catalyst decomposition. Preliminary attempts to synthesize asymmetric cyclic systems within the classical phosphinesulfonato scaffold, revealed that the formation of corresponding macrocyclic phosphines is a key synthetic step.

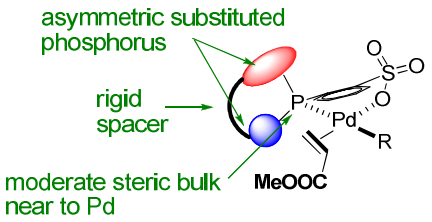


**Figure 6-5.** Possible design for phosphinesulfonato catalysts capable of effective stereoselective polymerization.

In conclusion, a comprehensive study of catalyst precursor and ligand design was performed. These studies resulted in the identification of a suitable precursor class, representing the maximum in weak coordination and high reactivity of well-defined phosphinesulfonato catalyst precursors. Insights on the influence of the substitution pattern of the bidentate phosphinesulfonato ligand on catalytic properties – namely catalyst stability, polymerization rate, and polar monomer incorporation – provide guidelines for a more directed catalyst design. The principles of stereoselective insertion polymerization were studied for the first time for phosphinesulfonato palladium(II) catalysts. A viable protocol for rapid analysis of stereoselectivity was developed, and decisive conditions and constraints for the design of stereoselective catalysts could be identified.

# 7. Experimental Section

## 7.1 Materials and General Considerations

### 7.1.1 General Synthetic Procedures

Unless noted otherwise, all manipulations of air sensitive compounds were carried out under an argon atmosphere using standard Schlenk or glovebox techniques. A BRAUN *MB200B* glovebox was used to store compounds and to prepare samples for analytics or NMR-experiments under a nitrogen atmosphere.

### 7.1.2 Solvents and Reagents

THF and benzene were dried over sodium/benzophenone. $CH_2Cl_2$, DMF, and TMEDA were dried over $CaH_2$.[167] These solvents were distilled before use. Pentane, toluene and $Et_2O$ were dried by passing through columns equipped with aluminum oxide/molecular sieve 3Å. All other solvents (p. A. grade) were used as received. Ethylene (3.5 grade) supplied by PRAXAIR and methyl acrylate (99%) supplied by ALDRICH were used as received.

[(tmeda)$NiMe_2$] was purchased from MCAT. All other reagents and starting materials were supplied by ALDRICH, ACROS, ABCR or TCI.

Hexaethylene gycol monomethyl ether,[168] [(tmeda)$PdMe_2$],[169] [(cod)PdMeCl],[170] **$^{H}$(PO)H**[20] and **$^{MeO}$1-dmso**[43] were prepared by known procedures.

### 7.1.3 Single Crystal X-Ray Diffraction

X-Ray diffraction analyses were performed at 100 K on a STOE *IPDS-II* diffractometer equipped with a graphite monochromated radiation source (Mo-$K_\alpha$, $\lambda$ = 0.71073 Å) and an image plate detection system. Crystals were mounted on a fine glass fiber with silicon grease. The selection, integration, and averaging procedure of the measured reflex intensities, the determination of the unit cell dimensions and a least-squares fit of the 2θ values as well as data reduction, LP-correction and space group determination were performed using the X-Area software package provided with the diffractometer.[171] A numerical absorption correction was performed. The structures were solved by the Patterson and direct methods (*SHELXS-*

*97*),[172] completed with difference Fourier syntheses, and refined with full-matrix least-square using *SHELXL-97*[173] minimizing $\omega(F_0^2-F_c^2)^2$ . Weighted *R* factor ($wR_2$) and the goodness of fit (GooF) are based on $F^2$. All non-hydrogen atoms were refined with anisotropic displacement parameters. All hydrogen atoms were treated in a riding model. Structures were plotted using *Diamond 3.1*.[174] The drawn ellipsoids represent 50% probability.

### 7.1.4 NMR Spectroscopy

NMR spectra were recorded on: VARIAN *Unity INOVA 400* spectrometer ($^1$H: 400 MHz; $^{13}$C: 101 MHz, $^{31}$P: 162 MHz; $^{19}$F: 376 MHz); BRUKER *Avance III 400* spectrometer ($^1$H: 400 MHz; $^{13}$C: 101 MHz, $^{31}$P: 162 MHz; $^{19}$F: 376 MHz); BRUKER *Avance III 600* spectrometer ($^1$H: 600 MHz; $^{13}$C: 151 MHz); BRUKER *Avance III 600* spectrometer, equipped with a cryoprobe head ($^1$H: 600 MHz; $^{13}$C: 151 MHz). $^1$H and $^{13}$C NMR chemical shifts were referenced to the solvent signal ($^1$H NMR: $CD_2Cl_2$: 5.32 ppm, $CDCl_3$: 7.26 ppm, $C_2D_2Cl_4$: 6.00 ppm, THF-$d_8$: 3.58 ppm, $C_6D_6$: 7.15 ppm, $CD_3OD$: 3.31 ppm, acetone-$d_6$: 2.05 ppm; $^{13}$C-NMR: $CD_2Cl_2$: 53.5 ppm, $CDCl_3$: 77.0 ppm, $C_2D_2Cl_4$: 74.45 ppm, THF-$d_8$: 67.4 ppm, $C_6D_6$: 128.1 ppm, $CD_3OD$: 49.00 ppm, acetone-$d_6$: 29.84 ppm).$^{19}$F and $^{31}$P NMR chemical shifts were referenced to external $CFCl_3$ and 85% $H_3PO_4$, respectively. All chemical shifts δ are given in ppm. All coupling constants *J* are given in Hz. Multiplicities are given as follows (or combinations thereof): s: singlet, d: doublet, t: triplet, h: heptet, m: multiplet, v: virtual. Broad resonances are designated as: br: broad, vbr: very broad. Diastereomeric atoms/groups/molecules are distinguished by apostrophes; e.g. X vs.X‘.

### 7.1.5 IR Spectroscopy

IR-Spectra were recorded on a PERKIN ELMER *Spectrum 100* FT-IR spectrometer equipped with a PERKIN ELMER *Universal ATR-unit*. The absorption bands are reported as wave numbers $\tilde{\nu}$ in cm$^{-1}$. The intensity of the absorption bands is characterized by *w* = weak, *m* = middle, *s* = strong, *ss* = very strong, *br* = broad.

### 7.1.6 Mass Spectrometry

Fast atom bombardement (**FAB**) mass spectra were measured by the Analytical Services at the Department of Chemistry, University of Konstanz. FAB mass spectra were obtained with a double-focusing FINNIGAN *MAT 8200* mass spectrometer equipped with an ION TECH (Teddington, U.K) FAB Ion Source. Electron spray ionisation (**ESI**) mass spectra were recorded on a BRUKER *Esquire 3000+* instrument. High resolution-ESI MS spectra were recorded on a BRUKER *Daltonics microTOF II* by Anna-Lena Steck at the University of Konstanz.

The detected ion masses are reported as mass-to-charge ratio (*m/z*) and refer to the isotope with the highest natural abundance. The isotope patterns of the reported signals are in agreement with the expected isotope distribution. The complete, neutral molecule is designated as M.

**Mass Spectrometry of Insertion Products**

For the MA insertion $^{MeO}\mathbf{3}_{\mathbf{MA\text{-}rac/meso}}$ (23 mg, 33 µmol, 1 equiv.), *p*-methoxyphenol (12 mg, 96 µmol, 3 equiv.) and methyl acrylate (82 mg, 953 µmol, 29 equiv.) were dissolved in 2 mL benzene and heated for 6 hours at 60 °C in the dark. The solvent was evaporated and the residue suspended in $Et_2O$ and filtrated. The yellow filtrate was layered with pentane yielding a white precipitate which was isolated and dried under vacuum. For mass spectrometry a few drops of a solution of $[HNEt_3][B(C_6F_5)_4]$ in MeOH (~ 0.006 mol $L^{-1}$) were added to a solution of the aforementioned precipitate in MeOH. This solution was injected into the ESI-mass spectrometer. In a similar experiment, a solution of $^{MeO}\mathbf{3}_{\mathbf{MA\text{-}rac/meso}}$, *p*-methoxyphenol and butyl acrylate in benzene was heated for 24 hours at 60 °C. After workup ESI-mass spectra of the yellow solid were recorded.

Note that experiments under the same conditions with known substances led to the expected results: **1-dmso** (*m/z* = 624 $[M\text{-}DMSO+HNEt_3]^+$, $\mathbf{1_n}$ (*m/z* = 624 $[M+HNEt_3]^+$, $^{MeO}\mathbf{3}_{\mathbf{MA\text{-}rac/meso}}$ (*m/z* = 796 $[M+HNEt_3]^+$).

### 7.1.7 Elemental Analysis

Elemental analyses were obtained by the Analytical Services at the Department of Chemistry, University of Konstanz. Elemental analyses were performed on an ELEMENTAR VARIO *MICRO cube* instrument.

### 7.1.8 Differential Scanning Calorimetry

Differential Scanning Calorimetry (DSC) was carried out on a NETZSCH *DSC 204 F1* in closed 40 µL PAN alumina crucible under a nitrogen atmosphere. The samples were heated with a bicyclic temperature program from -50 to 160 °C with heating and cooling rates of 10 K/min. For determination of melting temperatures and degrees of crystallization the second heating curve was used. For determination of the degree of crystallization the enthalpy of fusion of the measured polymer was compared to 100% crystalline PE (290 J/g).[175]

### 7.1.9 Gel Permeation Chromatography

High temperature gel permeation chromatography (GPC) for determination of PE molecular weights) was carried out by Lars Bolk at the University of Konstanz in 1,2,4-trichlorobenzene at 160°C at a flow rate of 1 mL $min^{-1}$ on a POLYMER LABORATORIES *GPC 220* instrument equipped with PLGEL *Olexis* columns with differential refractive index-, viscosity- and light scattering- (15° and 90°) detectors. Data reported were determined via the RI-detector against linear polyethylene standards.

For copolymers molecular weights were determined by $^1$H NMR and the molecular weight distribution ($M_w/M_n$) was determined by GPC on a POLYMER LABORATORIES *PL-GPC 50* instrument with two PLGEL 5 µm *MIXED-C* columns and an RI-detector in THF against polystyrene standard for THF soluble copolymers. For copolymers not soluble in THF at 50 °C high temperature GPC was applied (*vide supra*).

### 7.1.10 Coordination Equilibria

**Equilibrium constants for [(P^O)PdMe(dmso)] + L ⇆ [(P^O)PdMe(L)] + DMSO**

$^1$H NMR experiments were performed to study the coordination strength of DMSO in comparison to various ligands L.

Standard procedure: $^{MeO}$**1-dmso** (5.2 mg, 8.6 µmol) was weighted in an NMR tube and dissolved in $CD_2Cl_2$ (0.55 mL, c = 1.6 x $10^{-2}$ mol $L^{-1}$). A $^1$H NMR spectrum was recorded to determine the shift of the O=S*Me*$_2$ resonance for Pd-coordinated DMSO ($\delta_{Pd\text{-}dmso}$~2.95 ppm). To this solution an additional ligand L was added and a $^1$H NMR spectra was recorded for determination of the new upfield shifted O=S*Me*$_2$ resonance ($\delta_{eq}$). The ratio of added ligand was determined by integration. For comparison, the shift of uncoordinated

DMSO was determined from a 1.6 x $10^{-2}$ M solution of DMSO in $CD_2Cl_2$ ($\delta_{DMSO}$ ~ 2.54 ppm). The portion of the ligand L coordinated complex ($\chi_{Pd\text{-}L}$) was then calculated from the chemical shifts δ according to:

$$\chi_{Pd-L} = \frac{\delta_{eq} - \delta_{dmso-Pd}}{\delta_{dmso} - \delta_{dmso-Pd}}$$

The equilibrium constant $K_L$ could then be calculated according to:

$$K_L = \frac{[\text{Pd-L}][\text{dmso}]}{[\text{Pd-dmso}][\text{L}]}$$

$$\Rightarrow K_L = \frac{\{\chi_{Pd-L}[\text{Pd-dmso}]_0\}^2}{\{(1-\chi_{Pd-L})[\text{Pd-dmso}]_0\}\{[L]_0 - \chi_{Pd-L}\cdot[\text{Pd-dmso}]_0\}}$$

Note that the main error of this method arises from NMR shift determination, since resonances are broad. Most accurate results are obtained if the new DMSO shift is situated rather in the middle of the range between coordinated and free DMSO. Hence, for different $K_L$ different amounts of the ligand L have to be added for comparable accuracies.

**Equilibrium constants for $^{MeO}$3$_{MA\text{-}rac/meso}$+ DMSO ⇆ $^{MeO}$3$_{MA\text{-}rac/meso}$-dmso**

The equilibrium constant $K_{C1\text{-}DMSO}$ was determined via the $^{13}$C NMR shift of the Δ-carbonyl resonance of the chelate [(P^O)Pd*C*H(COOMe)$CH_2$CHEt(**C***O*OMe)] for two different DMSO concentrations. In the investigated temperature range from 5 °C to 35 °C the equilibrium is fast on the NMR timescale and only one resonance (δ, average of $^{MeO}$**3**$_{MA\text{-}rac/meso}$ and $^{MeO}$**3**$_{MA\text{-}rac/meso}$**-dmso**) is observed. The resonances for the DMSO-opened chelate, $^{MeO}$**3**$_{MA\text{-}rac/meso}$**-dmso** ($\delta_{opened\text{-}DMSO}$) are not directly accessible. Hence, it was assumed that the Δ-carbonyl resonance has a similar shift as in $^{MeO}$**3**$_{MA\text{-}rac/meso}$**-py** ($\delta_{opened}$), which only exists in its open form. The mole fractions (α + β) were calculated from the NMR shifts according to the equation $\delta = \alpha\delta_{closed} + \beta\delta_{opened}$ and $K_{C1\text{-}dmso}$ was determined from the known starting concentrations of $^{MeO}$**3**$_{MA\text{-}rac/meso}$ and DMSO according to:

$$K_{C1-dmso} = \frac{\beta}{\alpha[dmso]_0 - \alpha\beta[^{MeO}\mathbf{3}_{MA\text{-}meso/rac}]_0}$$

In order to avoid errors by temperature dependence of the shifts, the spectra for $^{MeO}$**3**$_{MA\text{-}rac/meso}$ ($\delta_{closed}$) and $^{MeO}$**3**$_{MA\text{-}rac/meso}$**-pyr** ($\delta_{opened}$) were recorded at every investigated temperature. With increasing temperature the Δ-carbonyl resonances of $^{MeO}$**3**$_{MA\text{-}rac}$ and $^{MeO}$**3**$_{MA\text{-}meso}$ are independently shifted. In some spectra two different carbonyl resonances for the two diastereomers were detected (25 °C, 35 °C). In these cases a weighted average of the two chemical shifts was used.

### 7.1.11 Binding Strength of Ethylene versus DMSO

The ratio of the measured activity (TOF) to the maximum activity ($TOF_{max}$) is identical to the ratio of Pd atoms coordinated with ethylene (Pd-$C_2H_4$) to all Pd atoms in the polymerization mixture.

$$\frac{TOF}{TOF_{max}} = \frac{[Pd\text{-}C_2H_4]}{[Pd]_0} \quad \Leftrightarrow \quad [Pd\text{-}C_2H_4] = \frac{TOF}{TOF_{max}} \cdot [Pd]_0 \quad \text{(Eq.1)}$$

The equilibrium binding constant $K_{A\text{-}E/DMSO}$ (**$^{MeO}$1-dmso** ⇆ **$^{MeO}$1-$C_2H_4$** + DMSO) is defined according to:

$$K_{A\text{-}E/DMSO} = \frac{[Pd\text{-}C_2H_4][DMSO]}{[Pd\text{-}dmso][C_2H_4]} \quad \text{(Eq.2)}$$

Substitution of Eq.1 and the mass conservation Eq.3 into equation Eq.2 results in Eq.4a.

$$[Pd]_0 = [Pd\text{-}dmso]_0 = [Pd\text{-}dmso] + [Pd\text{-}C_2H_4] \quad \text{(Eq.3)}$$

$$\Rightarrow K_{A\text{-}E/DMSO} = \frac{[Pd]_0 \cdot \frac{TOF}{TOF_{max}}}{[Pd]_0 \cdot \left(1 - \frac{TOF}{TOF_{max}}\right)} \cdot \frac{[DMSO]}{[C_2H_4]} \quad \text{(Eq.4a)}$$

$$\Leftrightarrow K_{A\text{-}E/DMSO} = \frac{TOF}{TOF_{max} - TOF} \cdot \frac{[DMSO]}{[C_2H_4]}$$

$$\Leftrightarrow \frac{TOF_{max}}{TOF} = \frac{[DMSO]}{[C_2H_4]} \cdot \frac{1}{K_{A\text{-}E/DMSO}} + 1 \quad \text{(Eq.4b)}$$

Consequently $K_{A\text{-}E/DMSO}$ can be determined by a plot of the $TOF_{max}$/TOF ratio versus the [DMSO]/[$C_2H_4$] ratio according to Eq. 4b. This includes the assumption that the relative binding of ethylene vs. DMSO is similar in **$^{MeO}$3$_{MA\text{-}rac/meso}$** and the non-substituted alkyls [(P^O)PdR] occurring in ethylene homopolymerization. The rate of ethylene homopolymerization in the absence of essential inhibition by coordination of DMSO ($TOF_{max}$) was derived from ethylene polymerizations with **$^{MeO}$1-dmso** as a catalyst precursor without additional DMSO at ethylene pressures higher then 5 bar. The observed independence of polymerization rate from ethylene concentration in this pressure regime shows that indeed no significant inhibition by the DMSO introduced with the catalyst precursor occurred. With increasing amount of added DMSO (36 to 117 equivalents with respect to **$^{MeO}$1-dmso**), the TOF values decrease.

The solubility of ethylene was determined experimentally: A 70 mL steel autoclave was filled with 40 mL of toluene, heated to 80 °C, and pressurized with ethylene under

stirring until equilibration was reached. The amount of ethylene up-take was determined by the weight gain of the reactor. The solubility was calculated by correcting this value for the amount of ethylene in the gas phase. For this purpose, the amount of ethylene in the gas phase was determined in a similar experiment with the reactor filled with 40 mL of solid glass beads. The solubilities determined agree with values determined by Lee at al. for the solubility of ethylene in toluene at 50 °C and 100 °C.[176]

### 7.1.12 Determination of H-H Distance by quantitative NOESY Experiments

In order to evaluate the structure of $^{MeO}\mathbf{3}_{MA\text{-}rac/meso}$ in solution the proton distances were determined from quantitative NOESY experiments. The NOE intensity correlates with the proton distance by $I \sim 1/d^6$ if a mixing time is chosen that lies within the linear growth regime for the crosspeak build-up intensities. The crosspeak integrals ($I_{xy}$) are compared to a reference integral ($I_{ref}$) of a known distance $d_{ref}$ for determination of $d_{xy}$ according to:[160]

$$d_{xy} = \sqrt[6]{\frac{I_{ref}}{I_{xy}}} \cdot d_{ref}$$

NOESY spectra were recorded at 3 °C and 23 °C and for mixing times of 200 ms, 400 ms and 600 ms, respectively. Evaluation of the spectra revealed that the NOE crosspeak intensity is higher at 22 °C and that as expected the intensity increases with mixing time. For 22 °C a mixing time of 400 ms was found to be optimally suited since it allows for sufficient NOE intensity and lies within the linear growth regime. The integrals were referenced to the crosspeak integrals for geminal proton couplings in comparison to the corresponding standard H-H distance in an AFIX constrained methylene group in X-ray structure analysis, which is found to be 1.6 Å.

It should be noted that for $^{MeO}\mathbf{3}_{MA\text{-}rac/meso}$ results have to be interpreted with care, since a 2:1 mixture of two diastereomers is investigated and many crosspeaks cannot be analyzed due to overlapping resonances. The values determined compare well with distances determined from the solid state structure. However, molecules in solution are dynamic and for a profound comparison all possible configurations in solution have to be evaluated and weighted by theoretical methods.

### 7.1.13 DNMR – Line Shape Analysis

Line shape analysis was carried out with the WINDNMR software.[177] The spectra were processed unreferenced. Some of the analyzed resonances exhibit a strong temperature dependent shift and especially show a temperature dependence of the line distance independent from the exchange of the nuclei. For an exact determination of the rate constants this temperature dependence was determined in the slow exchange regime, extrapolated to the fast exchange regime, and the corrected shifts were used for the simulations of spectra.

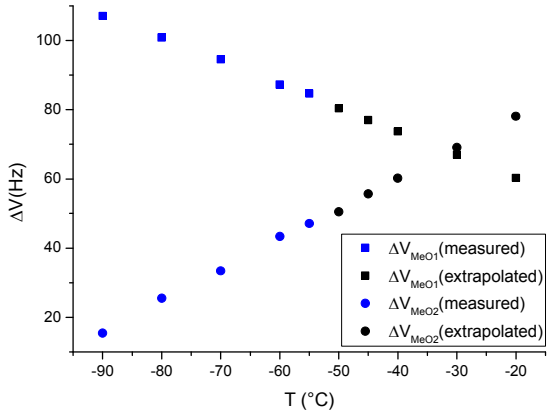


**Figure 7-1.** Measured and extrapolated temperature dependence of the line distance ΔV between the split *Me*O-resonances of $^{Ar}$**1** at low temperature.

For a determination of the rate constants, reasonable values for the intrinsic linewidth (in the absence of exchange processes) are important. Commonly, these values are adopted from linewidths in the slow exchange regime. This is not possible here, since additional dynamic process influence the linewidth at low temperature. For an educated guess, the linewidth was measured for a mixture of anisole and MeCN in $CD_3OD$ for various temperatures and a strong increase of the linewidth at low temperatures was observed. For $^{31}$P- and $^{19}$F NMR spectra the temperature dependence of the intrinsic linewidth was observed to be within the experimental error and was not further considered for this purpose.

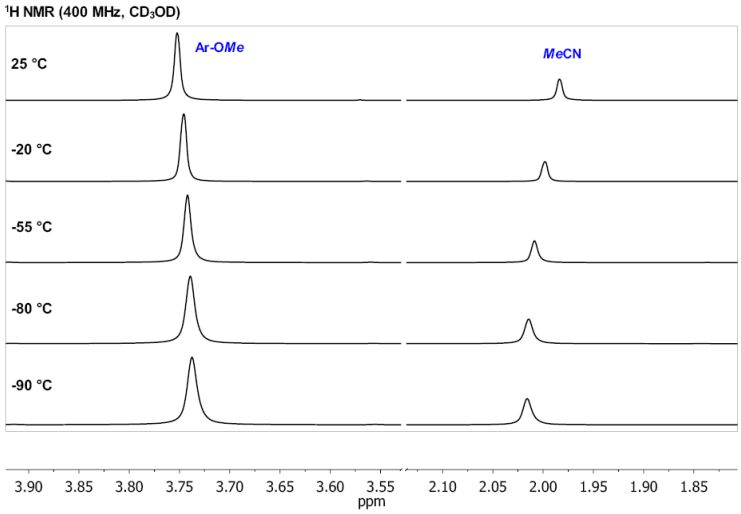


**Figure 7-2.** Variable temperature $^{1}$H NMR spectra (400 MHz, $CD_3OD$) of the methyl/methoxy-regions for anisole and MeCN.

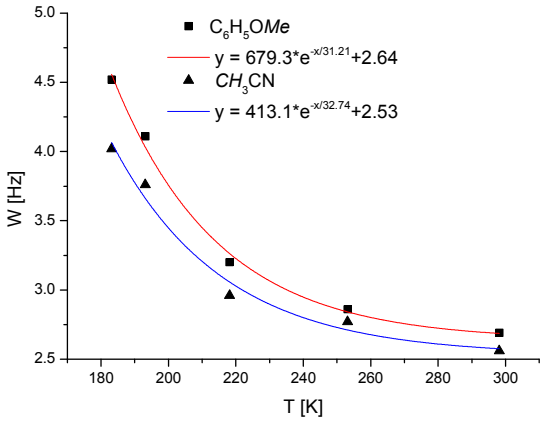


**Figure 7-3.** Temperature dependence of the linewidth for the methyl/methoxy-resonances of anisole and MeCN.

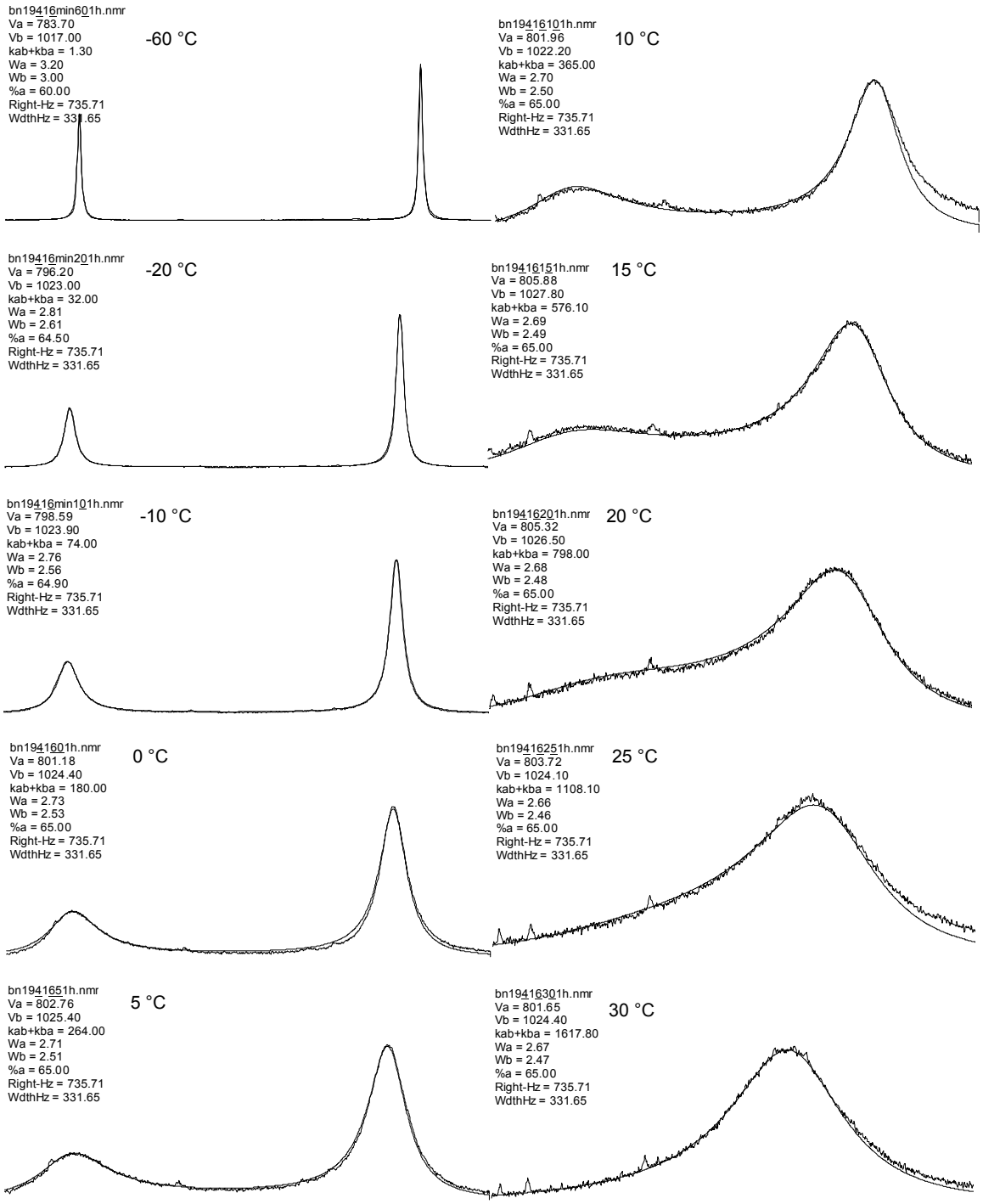


**Figure 7-4.** Temperature dependent line shape analysis for $^{Ar/(MeO)2}$**1** in the temperature range from -80 °C to 30 °C.

## 7.1.14 Insertion Kinetics

**Ethylene**

The insertion of ethylene into the Pd-Me bond was monitored by $^1$H NMR spectroscopy at the given temperature for $^{MeO}$**1-L** and *in situ* generated $^{MeO}$**1** ([{($^{MeO}$**1-Cl**)-μ-M}$_n$] + $AgBF_4$ → $^{MeO}$**1** + AgCl ↓ + $NaBF_4$↓) under pseudo first order conditions.

General procedure: A *J. Young* tube containing a solution of 7.2 μmol of $^{MeO}$**1-L** in $CD_2Cl_2$ (1.3 mM) was pressurized with 0.6 bar ethylene at -80 °C (Pd:$C_2H_4$ = 1:22). At -15 °C the disappearance of the Pd-*Me* resonance was monitored by $^1$H NMR spectroscopy. While higher palladium-alkyl complexes also insert ethylene, a huge excess of ethylene vs. ∑Pd-alkyl (> 10:1) was present during the entire duration of the experiment. For kinetic analysis of a 'base-free' species $^{MeO}$**1** a solution of 7.2 μmol of [{($^{MeO}$**1-Cl**)-μ-M}$_n$] in $CD_2Cl_2$ (13 mM) was treated with 1.1 equiv. $AgBF_4$ in a J. *Young* tube and shaken for 1 minute, then 0.6 bar ethylene overpressure were applied (Pd:$C_2H_4$ = 1:22).

**Methyl Acrylate**

The insertion of MA into the Pd-Me bond of $^X$**1**(**-L**) and the subsequent insertion of a second equivalent of MA was monitored by $^1$H NMR spectroscopy under pseudo first order conditions.

General Procedure: To a mixture of the catalyst precursor ($^X$**1-L** or [{($^X$**1-Cl**)-μ-M}$_n$] and 1.1 equiv. $AgBF_4$) and $H_2CClCCl_3$ (as an internal standard) was added $CD_2Cl_2$ ([Pd] ~ 0.02 mol $L^{-1}$). The suspension was shaken for one minute. The NMR tube was sealed with a septum, cooled in liquid nitrogen and MA (~15 equiv.) was added by a micro syringe. The sample was heated in the NMR probe to 25 °C and the insertion was monitored by NMR spectroscopy. For determination of the rate constants for the first insertion the disappearance of the Pd-*Me* resonance was analyzed. The rate constants of the 1,2- vs. 2,1-insertion product were either derived from the appearance of the Pd-CH(C(O)OMe)$CH_2$*Me* (2,1-insertion) or the Pd-CH*Me*$CH_2$COOMe (1,2-insertion) resonance, respectively, or estimated from the product ratio after completed first insertion. The rate constants for the β-H elimination from the 2,1-insertion products were determined from the appearance of the trans-*Me*CH=CHCOOMe resonance or estimated from the product ratio trans-*Me*CH=CHCOOMe:Pd[CH(COOMe)$CH_2$]$_2$*Me*. The rate constants of the second insertion product were derived from the disappearance of the Pd-CH(C(O)OMe)$CH_2$*Me* ($^X$**2$_{2,1}$**)

resonance of the primary 2,1-insertion products. The stereoselectivity was analyzed by the ratio of meso:rac insertion products of the $^{X}\mathbf{3}_{\mathbf{MA}}$ species after completed consecutive MA insertion

### 7.1.15 Homopolymerization of Ethylene

Polymerizations were carried out in a 250 mL stainless steel mechanically stirred (1000 rpm) pressure reactor (BÜCHI) equipped with a heating/cooling jacket supplied by a thermostat controlled by a thermocouple dipping into the polymerization mixture. A valve controlled by a pressure transducer allowed for applying and maintaining a constant ethylene pressure. The required flow of ethylene, corresponding to ethylene consumed by polymerization, was monitored by a mass flow meter (BRONKHORST) and recorded digitally. Prior to a polymerization experiment, the reactor was heated under vacuum to the desired reaction temperature for 30 minutes and then back-filled with argon.

Standard procedure: A stock solution of the catalyst precursor (8 μmol $mL^{-1}$) in methylene chloride was prepared in the glovebox. Solutions of $^{X}\mathbf{1}$ were prepared by reaction of [{($^{X}$**1-Cl**)-μ-M}$_n$] with one equiv. $AgBF_4$ in $CD_2Cl_2$ and filtration. Theses solutions were kept in the refrigerator of the glovebox (-30°C) and were never stored longer than 12 hours. The reactor was vented, in a slight argon stream the solvent was transferred via cannula (100 mL toluene), and 0.5 mL of the precursor solution was inserted by a syringe to the reactor ([Pd] = 40 μmol $L^{-1}$). The reactor was closed and a constant ethylene pressure was applied. After the desired reaction time the reactor was vented rapidly. The polymerization mixture was poured into 200 mL of MeOH. The polymer was isolated by filtration, washed several times with methanol, and dried in vacuo at 50 °C.

**Catalyst stability**

Mass flow traces were recorded to monitor catalyst stability. For comparison, the mass flow traces were fitted by exponential decay curves or by the algorithm of Savitzky-Golay.[178] For integration of the mass flow curve, the unprocessed data was used, and the mass flow trace of an experiment under identical conditions without catalyst was subtracted from the data before integration, to account for saturation of the ligand phase with ethylene in the early stages of the experiment.

### 7.1.16 Copolymerization of Ethylene and Methyl Acrylate

The copolymerization of ethylene and methyl acrylate was conducted in analogy to ethylene homopolymerizations: A solution of toluene and MA (with a total volume of 50 mL) was cannula transferred into the reactor under an argon counter stream. The catalyst precursor was dissolved in dichloromethane (2 mL) and inserted by a syringe to the reactor. Solutions of $^{X}$**1** were prepared by reaction of [{($^{X}$**1-Cl**)-μ-M}$_n$] with one equiv. $AgBF_4$ in 2 mL $CD_2Cl_2$ and filtration. In order to prevent any free-radical homopolymerization of methyl acrylate, the radical inhibitor 3,5-di-t-butyl-4-hydroxy-toluene (BHT) was added to the reaction mixture. After one hour reaction time the reactor was rapidly vented. The polymerization mixture was poured into 100 mL of MeOH. For copolymers with degrees of MA incorporation exceeding 10 mol% toluene and comonomer were removed under vacuum and the residue was dried in vacuo at 50 °C for several days in order to prevent loss of any oligomeric material.

### 7.1.17 Oligomerization of Alkyl Acrylates

An 8 mL screw-cap vial was charged with 10 mmol of the corresponding acrylate, BHT (75 mg, 344 mmol), 25 μmol of [{($^{X}$**1-Cl**)-μ-M}$_2$] precatalyst, and toluene to afford 4 mL of a suspension. The mixture was stirred at 95 °C for 3 hours. After the desired reaction time, unreacted monomers and solvent were removed under vacuum. The resulting liquid was dissolved in diethyl ether and filtrated. If necessary the oligomer mixture obtained was purified by column chromatography (PE:EE 20:1 – $CH_2Cl_2$ – $CH_2Cl_2$/MeOH) to separate BHT and to isolate fractions of higher $DP_n$.

In parallel, a control experiment in the absence of catalyst was carried out. An 8 mL screw-cap vial was charged with 10 mmol of the corresponding acrylate, BHT (75 mg, 344 mmol), and toluene to afford 4 mL of a clear solution. The mixture was stirred at 95°C for 3 hours. All volatiles were removed under vacuum yielding a white powder (75 mg). This powder was characterized by NMR and assigned to be pure BHT.

### 7.1.18 Computations

Theoretical Calculations in Chapter 5.2.6 were carried out by Prof. Lucia Caporaso at the University of Salerno, Italy.

DFT calculations were performed with *Gaussian09*[179] using the BP86[180-182] functional and the LANL2DZ ECP[183] with the associated valence basis set on the Pd atom and the 6-31G (d) basis set on all the other atoms. All geometries were localized in the gas phase at the BP86 level. Minima were localized by full optimization of the starting structures, while transition states for monomer insertion were approached through a linear transit procedure starting from the monomer-coordinated intermediate and then located by a full transition state search. All structures were confirmed as minimum or transition state through frequency calculations.

# 7.2 Synthetic Procedures

Compounds mentioned, synthesized or characterized previously are marked by the corresponding literature reference.

## 7.2.1 Syntheses of Phosphine Oxides

*General procedure for the synthesis of phosphine oxides:*

To a solution of the corresponding phosphine in THF an excess of aqueous $H_2O_2$ (30%) was added. The reaction mixture was stirred for 2 hours at 25 °C. To the solution $MnO_2$ was added and the reaction mixture was heated for 15 minutes. After cooling to 25 °C the reaction mixture was filtered over celite® and the filtrate was evaporated under vacuum. The resulting solid was purified as denoted.

***OP(3,5-(CF$_3$)$_2$C$_6$H$_3$)$_3$***; *O=P(C$_7$H$_3$F$_6$)$_3$*[184]

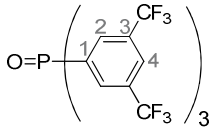


Further purification was not necessary. $OP(3,5\text{-}(CF_3)_2C_6H_3)_3$ was obtained as a white solid (306 mg, 0.5 mmol, 66 %)

**$^1$H NMR** (400 MHz, $CD_2Cl_2$): δ = 8.22 (3H, 4-H), 8.16 (d, $^3J_{PH}$ = 12.1, 6H, 2-H).

**$^{13}$C{$^1$H} NMR** (101 MHz, $CDCl_3$): δ = 133.8 (d, $^1J_{CP}$ = 105.6, C1), 133.6 (qd, $^2J_{CF}$ = 34.3, $^3J_{CP}$ = 12.7, C3), 132.7-132.4 (m, C2), 128.0 (dq, $^4J_{CP}$ = 7.0, $^3J_{CF}$ = 3.4, C4), 123.2 (q, $^1J_{CF}$ = 273.0, *C*F$_3$).

**$^{31}$P{$^1$H} NMR** (162 MHz, $CDCl_3$): δ = 21.4.

**$^{19}$F{$^1$H} NMR** (377 MHz, $CDCl_3$): δ = -63.5.

**Anal. Calcd.** (%) for ($C_{24}H_9F_{18}OP$): C, 42.00; H, 1.32; Found: C, 41.95; H, 1.42.

**ATR-IR:** 1/$\lambda$ [cm$^{-1}$] = 1622 (w), 1607 (w), 1361 (m), 1278 (s), 1216 (m, *v*(P=O)), 1173 (m), 1136 (s), 1121 (ss), 1097 (s), 903 (m), 837 (m), 701 (s), 681 (s).

**MS(FAB):** *m/z* = 687 [M+H]$^+$.

***OP(p-CF$_3$C$_6$H$_4$)$_3$;*** *O=P(C$_7$H$_4$F$_3$)$_3$*[185]

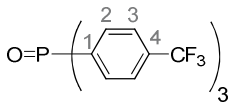


The crude product was washed with pentane and dried under vacuum to yield OP(*p*-$CF_3C_6H_4$)$_3$ as a white solid (532 mg, 1.1 mmol, 91%).

**$^1$H NMR** (400 MHz, $CD_2Cl_2$): δ = 7.86-7.77 (m, 12H, 2-H & 3-H).

**$^{13}$C{$^1$H} NMR** (101 MHz, $CD_2Cl_2$): δ = 136.4 (d, $^1J_{CP}$ = 103.3, C1), 134.7 (q, $^2J_{CF}$ = 35.7, C4), 133.1 (d, $^2J_{CP}$ = 10.3, C2), 126.3 (dq, $^3J_{CP}$ = 11.8, $^3J_{CF}$ = 3.7, C3), 124.2 (q, $^1J_{CF}$ = 272.3, *C*F$_3$).

**$^{31}$P{$^1$H} NMR** (162 MHz, $CDCl_3$): δ = 24.5.

**$^{19}$F{$^1$H} NMR** (377 MHz, $CDCl_3$): δ = -63.7.

**Anal. Calcd.** (%) for ($C_{21}H_{12}F_9OP$): C, 52.30; H, 2.51; Found: C, 52.28; H, 2.66.

**ATR-IR:** 1/$\lambda$ [cm$^{-1}$] = 1611 (w), 1505 (w), 1402 (m), 1322 (ss), 1198 (m, *v*(P=O)), 1165 (s), 1123 (s), 1110 (s), 1061 (ss), 1018 (s), 834 (s), 710 (ss).

**MS(FAB):** *m/z* = 483 [M+H]$^+$.

***OP(o-Tol)$_3$;*** *O=P(C$_7$H$_7$)$_3$*[186]

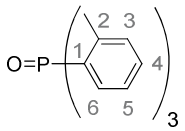


The crude product was washed with pentane and dried under vacuum to yield OP(*o*-Tol)$_3$ as a white solid (196 mg, 0.6 mmol, 34%).

**$^1$H NMR** (400 MHz, $CDCl_3$): δ = 7.43 (vt, *J* = 7.4, 3H, 4-H), 7.31 (dd, $^3J_{HH}$ = 7.3, $^4J_{PH}$ = 4.0, 3H, 3-H), 7.17–7.06 (m, 6H, 5-H & 6-H), 2.50 (s, 9H, Me).

**$^{13}$C{$^1$H} NMR** (101 MHz, $CDCl_3$): δ = 143.7 (d, $^2J_{CP}$ = 7.7, C2), 133.0 (d, $^2J_{CP}$ = 12.7, C6), 132.1 (d, $^3J_{CP}$ = 10.4, C3), 131.9 (d, $^4J_{CP}$ = 2.6, C4), 130.9 (d, $^1J_{CP}$ = 101.2, C1), 125.6 (d, $^3J_{CP}$ = 12.8, C5), 22.1 (d, $^3J_{CP}$ = 4.0, Me).

**$^{31}$P{$^1$H} NMR** (162 MHz, $CDCl_3$): δ = 37.0.

**Anal. Calcd.** (%) for ($C_{21}H_{21}OP$): C, 78.73; H, 6.61; Found: C, 78.90; H, 6.79.

**ATR-IR:** 1/$\lambda$ [cm$^{-1}$] = 3062 (w), 2958 (w), 2922 (w), 1591 (w) 1566 (w), 1450 (m), 1279 (m), 1185 (s, *v*(P=O)), 1162 (m), 1136 (s), 1083 (m), 807 (s), 770 (s), 754 (ss), 719 (ss), 686 (ss).

**MS(FAB):** *m/z* = 321 [M+H]$^+$.

***OPNaph$_3$,*** *O=P(C$_{10}$H$_7$)$_3$*[187]

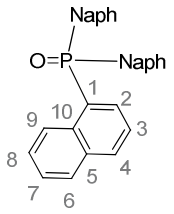


$OPNaph_3$ precipitated as the THF adduct from solution during the oxidation. The reaction mixture was heated for a prolonged period of time (ca. 2h) and filtrated to yield the product as a white solid (1.0 mmol, 87 %)

**$^1$H NMR** (400 MHz, $CD_2Cl_2$): δ = 8.90 (d, $^3J_{HH}$ = 8.4, 3H, 9-H), 8.07 (d, $^3J_{HH}$ = 7.9, 3H, 4-H), 7.98 (d, $^3J_{HH}$ = 8.0, 3H, 6-H), 7.56 (vt, *J* = 7.4, 3H, 7-H), 7.47 (vt, *J* = 7.5, 3H, 8-H), 7.34–7.27 (m, 3H, 3-H), 7.23 (dd, $^3J_{PH}$ = 15.9, $^3J_{HH}$ = 6.8, 3H, 2-H), 3.68 (m, 4H, THF), 1.82 (m, 4H, THF).

**$^{31}$P{$^1$H} NMR** (162 MHz, $CD_2Cl_2$): δ = 49.6.

**$^{13}$C{$^1$H} NMR** (101 MHz, $CD_2Cl_2$): δ = 134.9 (d, $^2J_{PH}$ = 13.8, 10-C), 134.8 (d, $^3J_{PH}$ = 14.9, 5-C), 134.2 (d, $^2J_{PH}$ = 12.1, 2-C), 133.8 (d, $^4J_{PH}$ = 2.8, 4-C), 129.6 (d, $^1J_{PH}$ = 102.0, 1-C), 129.4 (6-C), 128.6 (d, $^3J_{PH}$ = 5.0, 9-C), 127.8 (8-C), 127.1 (7-C), 125.0 (d, $^3J_{PH}$ = 14.5, 3-C), 68.3 (THF), 26.2 (THF).

**Anal. Calcd.** (%) for ($C_{30}H_{21}OP$*$C_4H_8O$): C, 81.57; H, 5.84; Found: C, 81.62; H, 5.64.

**ATR-IR:** υ [cm$^{-1}$] = 2969 (br, w), 2847 (br, w), 1620 (w), 1592 (w), 1570 (w) 1503 (s), 1336 (m), 1217 (m), 1175 (s), 1156 (s), 1066 (m), 1021 (m), 987 (m), 832 (s), 799 (s), 774 (ss).

**MS(ESI):** *m/z* = 1370.3 $[M_3+Na]^+$, 879.3 $[M_2+Na]^+$, 451.2 $[M+Na]^+$.

***O=P{2-(CH$_2$O(C$_2$H$_4$)$_6$OMe)C$_6$H$_4$}$_3$***

***2-[2-(2-{2-[2-(2-Methoxy-ethoxy)-ethoxy]-ethoxy}-ethoxy)-ethoxy]-ethyl-(4-bromophenyl)-methylether***

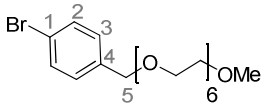


A solution of hexaethylene gycol monomethyl ether (2.15 g, 7.2 mmol, 1.0 equiv.) in THF (10 mL) was added slowly to a suspension of NaH (208 mg, 8.6 mmol, 1.2 equiv.) in THF (20 mL) at 0 °C. The reaction mixture was stirred for 2 hours at 25 °C and 4-bromobenzyl bromide (1.80 g, 7.2 mmol, 1.0 equiv.) was added. The reaction mixture was stirred over night. Volatiles were removed under vacuum and the residue was dissolved in water. The aqueous solution was extracted with $CH_2Cl_2$ (3 x 20 mL) and the combined organic phase was dried over $MgSO_4$. Solvents were removed under vacuum to yield a colorless oil (2.8 g, 6.0 mmol, 84%). The product could be purified further by flash chromatography (ethyl acetate, silica).

**$^1$H NMR** (400 MHz, $CDCl_3$): δ = 7.47–7.39 (m, 2H, 2-H), 7.21–7.14 (m, 2H, 3-H), 4.48 (s, 2H, 5-H), 3.68–3.56 (m, 22H, $(OC_2H_4)_n$), 3.53–3.49 (m, 2H, $(OC_2H_4)_5OCH_2CH_2$-OMe), 3.34 (s, 3H, OMe).
**$^{13}$C{$^1$H} NMR** (101 MHz, $CDCl_3$): δ = 137.5 (C4), 131.6 (C2), 129.5 (C3), 121.5 (C1), 72.6 (C5), 72.1 ($(OC_2H_4)_5OCH_2CH_2$-OMe), 71.0–70.6 (m, $(OC_2H_4)_n$), 69.7 ($ArCH_2OCH_2CH_2(OC_2H_4)_5OMe$), 59.2 (OMe).

***O=P{2-(CH$_2$O(C$_2$H$_4$)$_6$OMe)C$_6$H$_4$}$_3$***

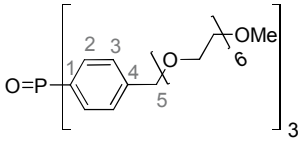


2-[2-(2-{2-[2-(2-Methoxy-ethoxy)-ethoxy]-ethoxy}-ethoxy)-ethoxy]-ethyl-(4-bromophenyl)-methylether (1.25 g, 2.7 mmol, 3.0 equiv.) was dissolved in THF (20 mL) and *n*-BuLi (1.2 mL, 2.5 M in hexane, 3.0 mmol, 3.3 equiv.) was added dropwise at -78 °C. The reaction mixture was stirred at -78 °C for 2 hours and $PCl_3$ (78 µL, 0.9 mmol, 1.0 equiv.) was added. The reaction mixture was allowed to warm to 25 °C and the reaction was quenched by addition of MeOH (5 mL). Volatiles were removed under vacuum to yield a yellow oil. The oil was dissolved in THF (10 mL) and an excess aqueous $H_2O_2$ (30%) was added. The reaction mixture was stirred for 10 minutes at 25 °C. To the solution was added $MnO_2$ and the reaction mixture was heated for 15 minutes. After cooling to 25 °C the reaction mixture was filtered over celite® and the filtrate was evaporated under vacuum. The crude product was purified by flash chromatography (ethyl acetate/MeOH; 15:4, silica) to yield a colorless oil (383 mg, 0.32 mmol, 35 %).

**$^1$H NMR** (400 MHz, $CDCl_3$): δ = 7.60 (dd, $^3J_{PH}$ = 11.8, $^3J_{HH}$ = 8.1, 2H, 2-H), 7.41 (dd, $^3J_{HH}$ = 8.2, $^4J_{PH}$ = 2.6, 2H, 3-H), 4.59 (s, 2H, 5-H), 3.69–3.57 (m, 2H, $(OC_2H_4)_5OCH_2CH_2$-OMe), 3.54–3.49 (m, 2H, $(OC_2H_4)_5OCH_2CH_2$-OMe), 3.34 (s, 3H, MeO).
**$^{31}$P{$^1$H} NMR** (162 MHz, $CDCl_3$): δ = 29.6.
**$^{13}$C{$^1$H} NMR** (101 MHz, $CDCl_3$): δ = 142.7 (d, $^4J_{CP}$ = 2.8, C4), 132.2 (d, $^2J_{CP}$ = 10.2, C2), 131.7 (d, $^1J_{CP}$ = 103.6, C1), 127.4 (d, $^3J_{CP}$ = 12.4, C3), 72.6 (C5), 71.9 ($(OC_2H_4)_5OCH_2CH_2$-OMe), 70.8–70.3 (m, $(OC_2H_4)_n$), 69.9 ($ArCH_2OCH_2CH_2(OC_2H_4)_5OMe$), 59.0 (MeO).

## 7.2.2 Syntheses of Building Blocks for Phosphinesulfonates

***Thymol methyl ether***[188]

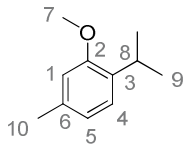


A 100 mL round bottom flask was charged with thymol (15 g, 100 mmol, 1.0 equiv.) and aqueous NaOH solution (10%, 50 mL) and MeI (6.2 mL, 100 mmol, 1.0 equiv.) were added dropwise. The biphasic solution was stirred for 20 minutes at 25 °C and then heated to 90 °C for 10 hours. The aqueous phase was extracted with $Et_2O$ (3 x 50 mL) and the combined organic phases were washed with aqueous NaOH solution (1.5 M) and water, and dried over $MgSO_4$. Volatiles were removed under vacuum to yield a yellow oil which was purified further by flash chromatography (petrol ether, silica gel). The product was obtained as a colorless oil (8.0 g, 49 mmol, 49%).

**$^1$H NMR** (400 MHz, $CDCl_3$): δ = 7.12 (d, $^3J_{HH}$ = 7.7, 1H, 4-H), 6.88 (d, $^3J_{HH}$ = 7.7, 1H, 5-H), 6.81 (s, 1H, 1-H), 3.49 (s, 3H, 7-H), 3.44 (h, $^3J_{HH}$ = 6.9, 1H, 8-H), 2.47 (s, 3H, 10-H), 1.35 (d, $^3J_{HH}$ = 6.9, 6H, 9-H)
**$^{13}$C{$^1$H} NMR** (101 MHz, $CDCl_3$): δ = 156.8 (C2), 136.4 (C6), 134.1 (C3), 125.9 (C4), 121.2 (C5), 111.5 (C1), 55.3 (C7), 26.6 (C8), 22.9 (C9), 21.5 (C10).

***Carvacrol methyl ether***[188]

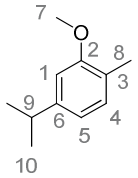


A 100 mL round bottom flask was charged with carvacrol (8.9 g, 60 mmol, 1.0 equiv.) and aqueous NaOH solution (10 w%, 50 mL, 75 mmol, 1.25 equiv.) and $Me_2SO_4$ (5.8 mL, 60 mmol, 1.0 equiv.) was added dropwise. The reaction mixture was refluxed for 2 hours. The aqueous phase was extracted with $Et_2O$ (3 x 100 mL) and the combined organic phases were washed with aqueous ammonia solution (10%, 3 x 75 mL) and water (50 mL), and dried over $MgSO_4$. Volatiles were removed under vacuum to yield a yellow oil which was purified further by flash chromatography (petrol ether/ethyl acetate 9:1, silica gel). The product was obtained as a colorless oil (6.4 g, 39 mmol, 65%).

**$^1$H NMR** (400 MHz, $CDCl_3$): δ = 7.07 (d, $^3J_{HH}$ = 7.5, 1H, 4-H), 6.76 (d, $^3J_{HH}$ = 7.7, $^4J_{HH}$ = 1.5, 1H, 5-H), 6.72 (s, 1H, 1-H), 3.85 (s, 3H, 7-H), 2.89 (h, $^3J_{HH}$ = 6.9, 1H, 9-H), 2.20 (s, 3H, 8-H), 1.27 (d, $^3J_{HH}$ = 6.9, 6H, 10-H)
**$^{13}$C{$^1$H} NMR** (101 MHz, $CDCl_3$): δ = 157.8 (C2), 148.1 (C6), 130.5 (C4), 124.0 (C3), 118.1 (C5), 108.6 (C1), 55.4 (C7), 34.3 (C9), 24.3 (C10), 15.9 (C8).

***2,2'-Bis(3-methoxyphenoxy)-1,1'-binaphtalene***

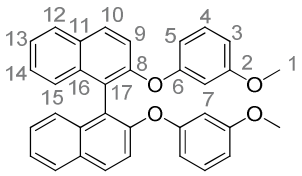


A flask was charged with 1,1'-bi-2-naphthol (3.3 g, 11.4 mmol, 1.0 equiv.), 3-iodo-methoxybenzene (10.7 g, 45.7 mmol, 4.0 equiv.), and dry DMSO (10 mL) and stirred for 30 minutes. A second flask was charged with 2-carbethoxycyclohexanone (1.6 g, 9.7 mmol, 0.8 equiv.), CuBr (0.7 g, 4.8 mmol, 0.4 equiv.), dry $CsCO_3$ (11.8 g, 45.7 mmol, 4.0 equiv.), and dry DMSO (10 mL) and stirred for 30 minutes. The content of the first flask was transferred slowly to the second flask. The reaction mixture was heated to 100 °C for 6 days. Aqueous NaOH solution (1 M, 100 mL,) was added and the mixture was extracted with $Et_2O$ (3 x 300 mL). The combined organic phases were extracted with aqueous NaOH solution (1 M, 2 x 50 mL) and brine (20 mL) and dried over $MgSO_4$. The volatiles were removed under vacuum to yield a red oil. After addition of a small portion of $Et_2O$ the product precipitated as a white solid. The white precipitate was separated by filtration, washed with $Et_2O$ and dried under vacuum (4.3 g, 8.6 mmol, 76%).

**$^1$H NMR** (400 MHz, $CDCl_3$): δ = 7.90-7.88 (m, 4H, 10-H, 12-H), 7.45-7.37 (m, 2H, 13-H), 7.35- 7.29 (m, 4H, 14-H, 15-H), 7.26 (d, $^3J_{HH}$ = 9.0, 2H, 9-H), 7.04 (dd, $^3J_{HH}$ = 8.2, $^3J_{HH}$ = 8.2, 2H, 4H), 6.52 (dd, $^3J_{HH}$ = 8.2, $^4J_{HH}$ = 2.3, 2H, 3-H), 6.44 (dd, $^3J_{HH}$ = 8.2, $^4J_{HH}$ = 2.1, 2H, 5-H), 6.39 (dd, $^4J_{HH}$ = 2.3, $^4J_{HH}$ = 2.3, 2H, 7-H), 3.59 (s, 6H, 1-H).
**$^{13}$C{$^1$H} NMR** (101 MHz, $CDCl_3$): δ = 160.7 (C2), 158.8 (C6), 152.6 (C8), 134.4 (C16), 130.64 (C11), 129.8 (C4, C10), 128.2 (C12), 126.7 (C14), 126.0 (C15), 124.8 (C13), 122.3 (C7), 119.6 (C9), 111.3 (C5), 109.0 (C3), 104.8(C7), 55.3 (C1).
**Anal. Calcd.** (%) for ($C_{34}H_{36}O_4$): C, 81.91; H, 5.26; Found: C, 81.28; H, 5.44.

***1,4-Bis(3-methoxyphenoxy)butane***

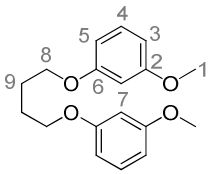


A flask was charged with 3-methoxyphenol (20.0 g, 160 mmol, 3.0 equiv.), $K_2CO_3$ (44.5 g, 320 mmol, 6.0 equiv.), and dry DMF (100 mL) and the suspension was stirred for 1 h at 100 °C. 1,4-Dibromobutane (6.3 mL, 50 mmol, 1.0 equiv.) was added and the reaction mixture was heated to 100 °C for 4 hours. Water was added (200 mL) and the mixture was extracted with $CH_2Cl_2$ (6 x 100 mL). The combined organic phase was washed with water (3 x 50 mL) and dried over $MgSO_4$. Volatiles were removed under vacuum to yield a red oil. Addition of a small portion of $Et_2O$ yielded a white precipitate, which was separated by filtration, washed with $Et_2O$ and dried under vacuum to yield a white solid (11.2 g, 37.0 mmol, 67%).

**$^1$H NMR** (400 MHz, $CDCl_3$): δ = 7.19 (dd, $^3J_{HH}$ = 8.2, $^3J_{HH}$ = 8.2, 2H, 4-H), 6.53 (d, $^3J_{HH}$ = 2.4, 2H, 3-H or 5-H), 6.51 (d, $^3J_{HH}$ = 2.3, 2H, 3-H or 5-H), 6.49 (dd, $^3J_{HH}$ = 2.3, $^3J_{HH}$ = 2.3, 2H, 7-H), 4.05-4.01 (m, 4H, 8-H), 3.80 (s, 6H, 1-H), 2.00-1.96 (m, 4H, 9H).

**$^{13}$C{$^1$H} NMR** (101 MHz, $CDCl_3$): δ = 161.0 (C2), 160.4 (C6), 130.0 (C4), 106.8 (C3), 106.4 (C5), 101.1 (C7), 67.6 (C8), 55.4 (C1), 26.1 (C9).

**Anal. Calcd.** (%) for ($C_{34}H_{36}O_4$): C, 71.50; H, 7.33; Found: C, 71.14; H, 7.33.

## 7.2.3 Syntheses of Lithiated Precursors for Phosphinesulfonates

***2-Lithium-1,3-dimethoxybenzene***[189]

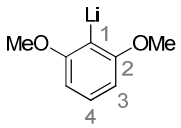


At room temperature *n*-BuLi (11 mL, 2.5 M in hexane, 28 mmol, 1.1 equiv.) was added dropwise to a solution of 2-bromo-1,3-dimethoxybenzene (5.4 g, 25 mmol, 1.0 equiv.) in pentane (125 mL). The reaction mixture was stirred over night, concentrated to 40 mL, and the resulting precipitate was isolated by filtration. The yield could be improved if the volatiles of the filtrate were removed and the resulting solid was suspended in pentane and isolated by filtration. After drying of the precipitates under vacuum the product was obtained as a white solid (3.5 g, 24 mmol, 96%).

**$^1$H NMR** (400 MHz, THF-d8): δ = 6.86 (t, $^3J_{HH}$ = 7.8, 1H, 4-H), 6.32 (d, $^3J_{HH}$ = 7.8, 2H, 3-H), 3.73 (s, 6H, OMe).

***2-Lithium-3,6-dimethylanisole***

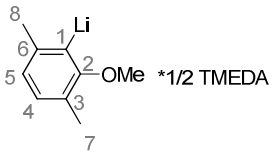


At room temperature *n*-BuLi (29 mL, 2.5 M in hexane, 73 mmol, 1.0 equiv.) was added dropwise to a solution of 3,6-dimethylanisole (9.6 g, 72 mmol, 1.0 equiv.) and TMEDA (12 mL, 81 mmol, 1.1 equiv.) in pentane (100 mL). The reaction mixture was stirred over night and the resulting precipitate was separated and washed with pentane to yield a white solid (10.9 g, 54 mmol, 75%).

**$^1$H NMR** (400 MHz, THF-d8): δ = 6.70–6.62 (m, 2H, 4- & 5-H), 3.73 (s, 3H, OMe), 2.42 (s, 3H, 8-H), 2.31 (s, 2H, $CH_2$-TMEDA), 2.18 (s, 3H, 7-H), 2.15 (s, 6H, Me-TMEDA).

***2-Lithium-cyclohexyloxybenzene***

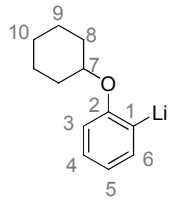


At room temperature *n*-BuLi (11.5 mL, 2.5 M in hexane, 29 mmol, 1.0 equiv.) was added dropwise to a solution of cyclohexyloxybenzene (5.1 g, 29 mmol, 1.0 equiv.) and TMEDA (2.6 mL, 17 mmol 0.6 equiv.) in $Et_2O$ (125 mL). The reaction mixture was stirred for 6 hours. The resulting precipitate was isolated by filtration, washed with $Et_2O$ and dried under vacuum. The product was obtained as a white solid (4.0 g, 22 mmol, 78%).

**$^1$H NMR** (400 MHz, THF-d8): δ = 7.70 (d, $^3J_{HH}$ = 6.2, 1H, 6-H), 6.83 (vt, $^3J_{HH}$ = 8.0, 1H, 4-H), 6.66 (vt, $^3J_{HH}$ = 6.7, 1H, 5-H), 6.56 (d, $^3J_{HH}$ = 8.0, 1H, 3-H), 4.21–4.15 (m, 1H, 7-H), 2.07–2.02 (m, 2H, 8-H), 1.81–1.75 (m, 2H, 8-H), 1.61–1.17 (m, 6H, 9- & 10-H).

***2-Lithium-2',6'-dimethoxybiphenyl***

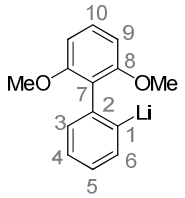


At room temperature *n*-BuLi (12 mL, 2.5 M in hexane, 30 mmol, 1.1 equiv.) was added dropwise to a slurry of 2-bromo-2',6'-dimethoxybiphenyl (7.9 g, 27 mmol, 1.0 equiv.) in $Et_2O$ (200 mL). The reaction mixture was stirred over night. The precipitate was isolated by filtration, rinsed with $Et_2O$ and dried under vacuum (4.9 g, 22 mmol, 82%).

***ortho-Lithium-thymol methyl ether***

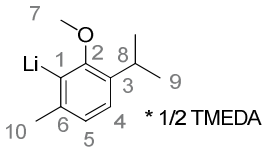


At 0 °C *n*-BuLi (18.4 mL, 2.5 M in hexane, 46 mmol, 1.1 equiv.) was added dropwise to a solution of thymol methyl ether (7.6 g, 46 mmol, 1.0 equiv.) and TMEDA (6.2 g, 53 mmol, 1.15 equiv.) in pentane (100 mL). The reaction mixture was stirred at reflux for 10 hours. The resulting precipitate was isolated by filtration, rinsed with pentane and dried under vacuum (7.5 g, 33 mmol, 72%).

**$^1$H NMR** (400 MHz, THF-d8): δ = 7.01 (d, $^3J_{HH}$ = 7.7, 1H, 4-H), 6.66 (d, $^3J_{HH}$ = 7.6, 1H, 5-H), 3.77 (s, 3H, 7-H), 3.25 (m, 1H, 8-H), 2.31 (s, 2H, C$H_{2\text{-TMEDA}}$), 2.27 (s, 3H, 10-H), 2.15 (s, 6H, C$H_{3\text{-TMEDA}}$), 1.16 (d, $^3J_{HH}$ = 6.9, 6H, 9-H).

***ortho-Lithium-cavacrol methyl ether***

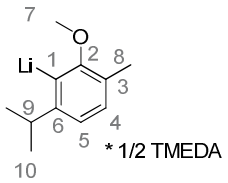


At 0 °C *n*-BuLi (15.6 mL, 2.5 M in hexane, 39 mmol, 1.1 equiv.) was added dropwise to a solution of carvacrol methyl ether (6.4 g, 39 mmol, 1.0 equiv.) and TMEDA (5.2 g, 45 mmol, 1.15 equiv.) in pentane (60 mL). The reaction mixture was stirred at reflux for 10 hours. The resulting precipitate was isolated by filtration, rinsed with pentane (2 x 15 mL), and dried under vacuum to yield a white solid (6.0 g, 26 mmol, 67%).

## 7.2.4 Syntheses of Phosphine- and Phosphonitesulfonates

***$^{(MeO)}$(P^O)H***; *$^{(MeO)}$(P^O) = (2-MeOC$_6$H$_4$)$_2$P(2-SO$_3$C$_6$H$_4$)*[23]

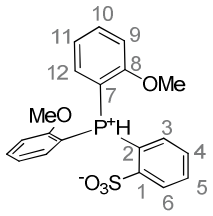


To a suspension of (2-methoxyphenyl)lithium (13.0 g, 114 mmol, 2.2 equiv.) in $Et_2O$ (250 mL) a solution of $Cl_2PNEt_2$ (9.2 g, 53 mmol, 1.0 equiv.) in $Et_2O$ (20 mL) was added dropwise at 0 °C. The reaction was stirred for two hours at 25 °C and a white precipitate formed. The suspension was filtered over celite® and washed with $Et_2O$ (100 mL). The filtrate was extracted with $H_2O$ (3 x 10 mL). The organic phase was dried over $Na_2SO_4$ and volatiles were removed under vacuum to yield N,N-diethyl-1,1-bis(2-methoxy-phenyl)phosphinamine as a colorless solid (14.8 g, 47 mmol, 88%).

**$^{31}$P{$^1$H} NMR** (162 MHz, $CDCl_3$): δ = 41.6

N,N-diethyl-1,1-bis(2-methoxy-phenyl)phosphinamine (14.8 g, 47 mmol, 1.0 equiv.) was dissolved in 200 mL $Et_2O$ and HCl in $Et_2O$ (1 M, 94 mL, 94 mmol, 2.0 equiv.) was added slowly at 0 °C the reaction mixture was stirred for one hour at 25 °C to form a massive precipitate. The suspension was filtered over celite® and washed with $Et_2O$ (200 mL). Volatiles were removed under vacuum to yield chlorobis(2-methoxyphenyl)phosphine as a white solid (9 g, 32 mmol, 69 %).

**$^{31}$P{$^1$H} NMR** (162 MHz, $CDCl_3$): δ = 72.4

At 0 °C *n*-BuLi (12 mL, 1.6 M in hexane, 19 mmol, 2.1 equiv.) was added to a solution of benzene sulfonic acid (1.5 g, 9.7 mmol, 1.1 equiv.) in THF (40 mL) and the reaction mixture was allowed to warm to room temperature and stirred for 30 minutes. The suspension formed was cooled to 0 °C and a solution of chlorobis(2-methoxyphenyl)phosphine (2.6 g, 9.2 mmol, 1.0 equiv.) in THF was added. The reaction mixture became clear within minutes and was stirred at 25 °C for 2 hours. Volatiles were removed under vacuum to afford a yellowish residue. Degassed water (50 mL) was added and the resulting white suspension was acidified to pH 2 using aqueous HCl (3 M). The mixture was extracted with $CH_2Cl_2$ (3 x

20 mL) and the combined organic phase was dried over $MgSO_4$. Volatiles were removed under vacuum to yield a white solid (3.0 g, 7.5 mmol, 82%). The product could be purified further by washing with THF or by crystallization from $CH_2Cl_2$.

**$^1$H NMR** (400 MHz, $CDCl_3$): δ = 8.24 (d, $^1J_{PH}$ = 514.7, 1H, PH), 8.36 (dd, $^3J_{HH}$ = 7.6, $^4J_{PH}$ = 5.3, 1H, 6-H), 7.73 (vt, $^3J_{HH}$ = 7.6, 1H, 5-H), 7.70-7.63 (m, 2H, 11-H), 7.41 (vdt, *J* = 7.8, *J* = 2.1, 1H, 4-H), 7.14-6.98 (m, 7H, 3- & 9 & 10 & 11-H), 3.77 (s, 3H, OMe).
**$^{31}$P{$^1$H} NMR** (162 MHz, $CDCl_3$): δ = -10.0

***$^{MeO}$(P^O)Na***; *$^{(MeO)}$(P^O) = $(2\text{-}MeOC_6H_4)_2P(2\text{-}SO_3C_6H_4)$*[61]

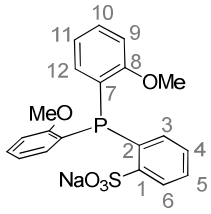


A vial was charged with **$^{MeO}$(P^O)H** (1.6 g, 4.1 mmol, 1.0 equiv.), NaH (117 mg, 4.9 mmol, 1.2 equiv.), and THF (8 mL). The suspension was stirred over night. To the suspension phenol (70 mg, 0.7 mmol, 0.2 equiv.) was added and the reaction mixture was stirred for one hour. The precipitate was isolated by centrifugation, washed with THF and $Et_2O$, and dried under vacuum to yield a white solid (1.5 g, 3.5 mmol, 85%).

**$^1$H NMR** (400 MHz, $CD_3OD$): δ = 8.09 (ddd, $^3J_{HH}$ = 7.9, $^4J_{PH}$ = 4.0, $^4J_{HH}$ = 1.4, 1H, 6-H), 7.39 (vtd, *J* = 7.6, 1.4, 1H, 5-H), 7.29 (dddd, *J* = 8.2, 7.4, 1.8, 0.9, 2H, 10-H), 7.24 (vtd, *J* = 7.5, 1.4, 1H, 4-H), 6.99 (ddd, $^3J_{HH}$ = 7.7, $^3J_{PH}$ = 3.4, $^4J_{HH}$ = 1.3, 1H, 3-H), 6.93 (ddd, $^3J_{HH}$ = 8.3, 4.7, 1.0, 2H, 9-H), 6.79 (vtt, *J* = 7.4, 0.8, 2H, 11-H), 6.60 (ddd, $^3J_{HH}$ = 7.5, $^3J_{PH}$ = 4.0, $^4J_{HH}$ = 1.7, 2H, 12-H), 3.67 (s, 6H, MeO).
**$^{31}$P{$^1$H} NMR** (162 MHz, $CD_3OD$): δ = -30.3.
**$^{13}$C{$^1$H} NMR** (101 MHz, $CD_3OD$): δ = 162.5 (d, $^3J_{CP}$ = 16.2, C8), 151.1 (d, $^2J_{CP}$ = 27.6, C1), 136.8 (d, $^2J_{CP}$ = 1.9, C3), 136.5 (d, $^1J_{CP}$ = 22.3, C2), 134.9 (C12), 130.9 (C10), 130.8 (C5), 129.5 (C4), 128.6 (d, $^3J_{CP}$ = 4.9, C6), 127.5 (d, $^1J_{CP}$ = 14.3, C7), 121.9 (C11) , 111.5 (d, $^3J_{CP}$ = 1.4, C9), 56.0 (MeO).

***$^{Ar}$(P^O)H***; *$^{Ar}$(P^O) = (2-(2',6'-(OMe)$_2$C$_6$H$_3$)C$_6$H$_4$)$_2$P(2-SO$_3$C$_6$H$_4$))*[24]

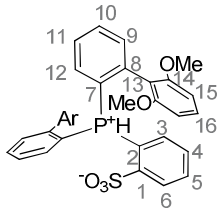


At 0 °C *n*-BuLi (2.9 mL, 2.5 M in hexane, 7.1 mmol, 2.1 equiv.) was added to a solution of benzene sulfonic acid (562 mg, 3.6 mmol, 1.1 equiv.) in THF (15 mL) and the reaction mixture was stirred at 25 °C for 30 minutes. The suspension formed was cooled to -78 °C and added at -78 °C under vigorous stirring to a solution of $PCl_3$ (470 mg, 3.4 mmol, 1.0 equiv.) in THF (15 mL). In a second flask at -78 °C *n*-BuLi (2.7 mL, 2.5 M in hexane, 6.9 mmol, 2.0 equiv.) was added to a solution of 2'-bromo-2,6-dimethoxybiphenyl (2.0 g, 6.9 mmol, 2.0 equiv.) in THF (30 mL). The mixture was stirred at -78 °C for 30 minutes and then added to the first flask at 0 °C by cannula. The reaction mixture was allowed to warm slowly to room temperature and stirred over night. Volatiles were removed under vacuum to yield a sticky, brown solid. Degassed water (120 mL) and $CH_2Cl_2$ (100 mL) were added and the mixture was acidified using aqueous HCl (37%, 1.5 mL). The mixture was extracted with $CH_2Cl_2$ (2 x 100 mL) and the combined organic phase was dried over $MgSO_4$. Volatiles were removed under vacuum and the remaining residue was purified further by washing with THF (3 x 6 mL) and $Et_2O$ (2 x 6 mL). After drying under vacuum the product was obtained as a white solid (690 mg, 1.1 mmol, 33%).

**$^1$H NMR** (600 MHz, $CD_2Cl_2$): δ = 8.88 (d, $^1J_{PH}$ = 593.2, 1H, PH), 8.03 (dd, $^3J_{HH}$ = 7.4, $^4J_{PH}$ = 5.2, 1H, 6-H), 7.70–7.64 (m, 2H, 10-H), 7.62 (vt, $^3J_{HH}$ = 7.7, 1H, 5-H), 7.44–7.18 (m, 9H, 4- & 9- & 11- & 12- & 16-H), 7.15 (dd, $^3J_{PH}$ = 14.2, $^3J_{HH}$ = 7.7, 1H, 3-H), 6.60–6.37 (m, 3H, 15-H), 6.37–6.12 (m, 1H, 15-H), 3.71–3.38 (m, 9H, OMe), 3.03 (s, 3H, OMe).

**$^{31}$P NMR** (162 MHz, $CDCl_3$): δ = -2.38 (d, $^1J_{PH}$ = 534.6).

**$^{13}$C{$^1$H} NMR** (101 MHz, $CD_2Cl_2$): δ = 158.2–156.8 (m, C14), 152.9 (d, $^2J_{CP}$ = 9.2, C1), 141.2 (d, $^2J_{CP}$ = 8.4, C8), 135.6 (br s, C12), 134.6-134.3 (m, C3 & C9), 133.9 (d, $^4J_{CP}$ = 3.0, C5), 133.7 (s, C10), 131.4 (s, C16), 129.0 (d, $^3J_{CP}$ = 12.7, C4), 128.6 (d, $^3J_{CP}$ = 9.3, C6), 128.1–127.2 (m, C11), 120.1 (d, $^1J_{CP}$ = 91.1, C7), 115.2 (d, $^1J_{CP}$ = 95.4, C2), 115.3–113.5 (m, C13), 105.7–103.0 (m, C15), 57.25–54.55 (m, OMe).

**MS(FAB)**: *m/z* = 615 $[M+H]^+$.

**HRMS(ESI)**: *m/z* calcd. for = $C_{34}H_{30}O_7PS$: 613.1444 $[M-H]^-$; found: 613.1422.

***$^{Ar}$(P^O)Na**; $^{Ar}$(P^O) = (2-(2',6'-(OMe)$_2$C$_6$H$_3$)C$_6$H$_4$)$_2$P(2-SO$_3$C$_6$H$_4$)*

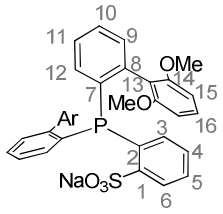


A flask was charged with **$^{Ar}$(P^O)H** (258 mg, 0.4 mmol, 1.0 equiv.) and NaH (20 mg, 0.8 mmol, 1.0 equiv.), and THF (10 mL) was added. The suspension was stirred over night. Phenol (40 mg, 0.4 mmol, 1.0 equiv.) was added and the reaction mixture was stirred for 1 hour. The white precipitate was isolated by filtration, washed with pentane, and dried under vacuum (225 mg, 0.3 mmol, 82%).

**$^1$H NMR** (600 MHz, $CD_3OD$): δ = 7.99 (ddd, $^3J_{HH}$ = 7.6, $^4J_{PH}$ = 3.9, $^4J_{HH}$ = 1.5, 1H, 6-H), 7.35 (vtd, $^3J_{HH}$ = 7.5, 1.4, 1H, 5-H), 7.31 (vtd, $^3J_{HH}$ = 7.5, 1.6, 1H, 4-H), 7.25 (vt, *J* = 7.6, 2H, 10- & 10'-H), 7.22–7.16 (m, 5H, 11- & 11'- & 12- & 16- & 16'-H), 7.17 (ddd, $^3J_{HH}$ = 7.7, $^3J_{PH}$ = 3.4, $^4J_{HH}$ = 1.2, 1H, 3-H), 7.06–6.94 (m, 2H, 9- & 9'-H), 6.71 (br s, 1H, 12'-H), 6.58 (br s, 1H, 15-H), 6.50–6.38 (m, 2H, 15- & 15'-H), 6.22 (br s, 1H, 15'-H), 3.58 (s, 3H, *Me*O), 3.50 (s, 3H, MeO), 3.22 (s, 3H, MeO), 2.71 (s, 3H, MeO).

**$^{31}$P{$^1$H} NMR** (162 MHz, $CD_3OD$): -17.5.

**$^{13}$C{$^1$H} NMR** (151 MHz, $CD_3OD$): δ = 158.9, 158.7, 158.0, 157.8 (4C, C14 & C14'), 149.8 (d, $^2J_{CP}$ = 26.4, C1), 141.4 (d, $^1J_{CP}$ = 34.3, C7/7'), 140.6 (C8/8'), 140.1 (d, $^1J_{CP}$ = 23.4, C7/7'), 138.2 (C8/8'), 137.6 (C3), 136.9 (C12), 136.8 (d, $^1J_{CP}$ = 26.4, C2) , 134.7 (C12') , 132.6 (C9/9'), 132.4 (C9/9'), 130.2 (C4) , 129.7 (C16/16'), 129.6 (C16/16'), 128.5 (C5), 128.3 (C10/10'), 128.1 (d, $^3J_{CP}$ = 4.6, C6), 128.1 (C10/10'), 127.6 (C11/11'), 126.7 (C11/11'), 121.5 (C13/13'), 119.3 (C13/13'), 108.5 (C15), 105.6 (C15), 104.7 (C15'), 103.8 (C15'), 59.2 (*Me*O), 56.8 (*Me*O), 55.2 (*Me*O), 54.2 (*Me*O).

**Anal. Calcd.** (%) for ($C_{34}H_{30}NaO_7PS \times 0.5\ H_2O$): C, 63.25; H, 4.84; Found: C, 63.29; H, 4.84.

**MS(FAB)**: *m/z* = 637 $[M+H]^+$, 615 $[^{Ar}(PO)H+H]^+$.

***$^{Ph}$(P^O)H***; *$^{Ph}$(P^O) = (2-PhC$_6$H$_4$)$_2$P(2-SO$_3$C$_6$H$_4$)*[38]

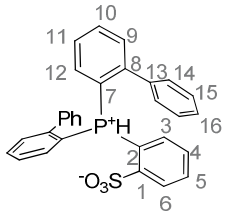


At 0 °C *n*-BuLi (12.5 mL, 1.6 M in hexane, 20 mmol, 2.2 equiv.) was added to a solution of benzene sulfonic acid (1.5 g, 9 mmol, 1.0 equiv.) in THF (45 mL) and the reaction mixture was stirred at 25 °C for 30 minutes. The suspension formed was cooled to -78 °C and added at -78 °C under vigorous stirring to a solution of $PCl_3$ (1.3 g, 9 mmol, 1.0 equiv.) in THF (45 mL). In a second flask at -78 °C *n*-BuLi (13.0 mL, 1.6 M in hexane, 22 mmol, 2.3 equiv.) was added to a solution of 2-bromobiphenyl (4.6 g, 19 9 mmol, 2.2 equiv.) in THF (45 mL), the mixture was stirred at -78 °C for 30 minutes and then added to the first flask at -78 °C by cannula. The reaction mixture was allowed to warm slowly to room temperature and stirred over night to yield a clear solution. Volatiles were removed under vacuum to yield a reddish solid. Degassed water (60 mL) was added and the resulting suspension was acidified to pH 2 using aqueous HCl (3 M). The mixture was extracted with $CH_2Cl_2$ (6 x 20 mL) and the combined organic phase was dried over $MgSO_4$. Volatiles were removed under vacuum and the remaining residue was purified further by washing with THF and $Et_2O$. After drying under vacuum the product was obtained as a white solid (1.9 g, 3.8 mmol, 42%).

**$^1$H NMR** (400 MHz, $CD_2Cl_2$): δ = 8.71 (d, $^1J_{PH}$ = 596.3, 1H, PH), 8.25 (ddd, $^3J_{HH}$ = 7.8, $^4J_{PH}$ = 4.8, $^4J_{HH}$ = 1.2, 1H, 6-H), 7.87 (vtt, $^3J_{HH}$ = 7.7, *J* = 1.7, 1H, 5-H), 7.72 (vtt, $^3J_{HH}$ = 7.7, *J* = 1.5, 2H, 10-H), 7.55 (vtdd, $^3J_{HH}$ = 7.6, $^4J_{PH}$ = 2.9, $^4J_{HH}$ = 1.3, 1H, 4-H,), 7.49 (vtdd, $^3J_{HH}$ = 7.7, $^4J_{PH}$ = 2.6, $^4J_{HH}$ = 1.2, 2H, 11-H), 7.42–7.27 (m, 5H, 3- & 9- & 16-H), 7.24 (vt, $^3J_{HH}$ = 7.6, 4H, 15-H), 7.15 (dd, $^3J_{PH}$ = 14.1, $^3J_{HH}$ = 7.7, 3H, 12-H), 6.78 (br, 4H, 14-H).

**$^{31}$P NMR** (162 MHz, $CD_2Cl_2$): δ = -4.6 (d, $^1J_{PH}$ = 597.7).

**$^{13}$C{$^1$H} NMR** (101 MHz, $CD_2Cl_2$): δ = 153.4 (d, $^2J_{CP}$ = 8.7, C1), 147.8 (br, C8), 138.0 (br, C13), 136.0 (C5), 135.9 (d, $^2J_{CP}$ = 8.2, C3), 134.7 (br d, $^2J_{CP}$ = 8.5, C12), 134.4 (d, $^4J_{CP}$ = 2.7, C10), 131.9 (d, $^3J_{CP}$ = 9.5, C9), 130.6 (d, $^3J_{CP}$ = 12.9, C4), 129.9 (d, $^3J_{CP}$ = 9.2, C6), 129.5 (C15), 129.4 (C16), 129.4 (C14), 128.7 (d, $^3J_{CP}$ = 12.5, C11), 119.8 (d, $^1J_{CP}$ = 91.6, C7), 113.3 (d, $^1J_{CP}$ = 97.4, C2).

**MS(FAB)**: m/z = 495 [ M+H]$^+$, 517 [ M+Na]$^+$.

**HRMS(ESI)**: *m/z* calcd for = $C_{30}H_{24}O_3PS$: 495.11783 [M+H]$^+$; found: 495.11654.

***$^{Ph}$(P^O)Na***; *$^{Ph}$(P^O) = (2-PhC$_6$H$_4$)$_2$P(2-SO$_3$C$_6$H$_4$)*

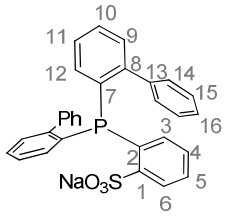


A flask was charged with **$^{Ph}$(P^O)H** (591 mg, 1.2 mmol, 1.0 equiv.) and NaH (34 mg, 1.4 mmol, 1.2 equiv.), and THF (10 mL) was added. The mixture was stirred over night and the resulting turbid solution was filtered. Volatiles were removed under vacuum and the resulting residue was washed with $Et_2O$ (2 x 7 mL). After drying under vacuum the product was obtained as a white solid (440 mg, 0.85 mmol, 71%).

**$^1$H NMR** (400 MHz, acetone-d6): δ = 8.06 (ddd, $^3J_{HH}$ = 7.6, $^4J_{PH}$ = 3.9, $^4J_{HH}$ = 1.6, 1H, 6-H), 7.33–7.27 (m, 3H, 5- & 11-H), 7.24 (vtd, $^3J_{HH}$ = 7.5, $^4J_{HH}$ = 1.6, 1H, 4-H), 7.21–7.05 (m, 14H, 10- & 12- & 14-16-H), 7.01 (vdt, $^3J_{HH}$ = 7.5, *J* = 1.9, 1H, 3-H), 6.91 (ddd, $^3J_{HH}$ = 7.6, $^4J_{PH}$ = 2.9, $^4J_{HH}$ = 1.5, 2H, 11-H).

**$^{31}$P{$^1$H} NMR** (162 MHz, acetone-d6): δ = -19.8.

**$^{13}$C{$^1$H} NMR** (101 MHz, acetone-d6): δ = 151.4 (d, $^2J_{CP}$ = 24.9, C1), 147.5 (vbr, C7), 142.8 (br, C8), 138.9 (vbr, C13), 136.1 (d, $^1J_{CP}$ = 31.4, C2), 135.8 (C3), 130.5 (d, $^3J_{CP}$ = 4.8, C12), 130.4 (br, C9), 129.8 (C4), 129.2 (d, $^3J_{CP}$ = 3.2, C6), 128.6 (C5- & C11), 128.1 (C14 & C15), 127.4 (C10), 127.2 (C16).

**Anal. Calcd.** (%) for ($C_{30}H_{22}NaO_3PS$*1/2$H_2O$): C, 68.56; H, 4.41; Found: C, 68.80; H, 5.04.

**MS(FAB)**: m/z = 539 $[M+Na]^+$, 517 $[M+H]^+$.

***(MeO)3(P^O)H***; *(MeO)3(P^O) = (2,4,6-(OMe)3C6H2)2P(2-SO3C6H4)*[38]

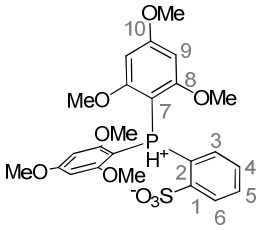


In flask (A) *n*-BuLi (16.0 mL, 2.5 M in hexane, 40.0 mmol) was added to a solution of 1,3,5-trimethoxybenzene (6.4 g, 37 9 mmol) in THF (50 mL) at 0 °C. The mixture was stirred at room temperature for 3 h to give a 0.76 M solution of 1-lithium-2,4,6-trimethoxybenzene. In Flask (B) *n*-BuLi (6.7 mL, 2.5 M in hexane, 16.8 mmol, 2.1 equiv.) was added to a solution of benzene sulfonic acid (1.29 g, 8.2 mmol, 1.0 equiv.) in THF (35 mL) at 0 °C. The reaction mixture was stirred at 25 °C for 30 minutes. The suspension formed was cooled to -78 °C and added at -78 °C and under vigorous stirring to flask (C) containing a solution of $PCl_3$ (1.10 g, 8.0 mmol, 1.0 equiv.) in THF (35 mL). Then the contents of flask (A) -the 1-lithium-2,4,6-trimethoxybenzene solution (22 mL, 0.76 M in THF, 16.7 mmol, 2.1 equiv.)- was added at 0 °C to flask (C) by cannula. The reaction mixture was allowed to warm slowly to room temperature and stirred over night. Volatiles were removed under vacuum. Degassed water (50 mL) was added and the mixture was acidified to pH 2. The mixture was extracted with $CH_2Cl_2$ (3 x 100 mL) and the combined organic phase was dried over $MgSO_4$. Volatiles were removed under vacuum and the remaining residue was purified further by washing with THF and acetone. After drying under vacuum the product was obtained as a white solid (0.89 g, 1.8 mmol, 22.5 %).

**$^1$H NMR** (400 MHz, $CDCl_3$,): δ = 9.27 (d, $^1J_{PH}$ = 595.2, 1H, PH), 8.26 (dd, $^3J_{HH}$ = 7.3, $^4J_{PH}$ = 5.5, 1H, 6-H), 7.64–7.52 (m, 2H, 5-H), 7.45–7.30 (m, 2H, 4- & 3-H), 6.09 (d, $^4J_{PH}$ = 4.6, 4H, 9-H), 3.82 (s, 6H, *p*-OMe), 3.60 (s, 12H, *o*-OMe).

**$^{31}$P NMR** (162 MHz, $CDCl_3$): δ = -30.8 (d, $^1J_{PH}$ = 596.2).

**$^{13}$C{$^1$H} NMR** (101 MHz, $CDCl_3$,): δ = 166.9 (C10), 164.1 (C8), 151.4 (d, $^2J_{CP}$ = 10.2, C1), 134.0 (d, $^2J_{CP}$ = 12.0, C3), 133.1 (d, $^4J_{CP}$ = 3.3, C5), 129.2 (d, $^3J_{CP}$ = 9.9, C6), 128.8 (d, $^3J_{CP}$ = 13.5, C4), 117.0 (d, $^1J_{CP}$ = 103.2, C2), 91.8 (d, $^3J_{CP}$ = 6.5, C9), 89.4 (d, $^1J_{CP}$ = 108.7, C7), 56.5 (*o*-OMe), 55.9 (*p*-OMe).

**MS(FAB)**: *m/z* = 523.2 $[M+H]^+$.

**HRMS(ESI)**: *m/z* calcd for = $C_{24}H_{26}O_9PS$: 521.1030 $[M-H]^-$; found: 521.1015.

***$^{(MeO)3}$(P^O)Na***; *$^{(MeO)3}$(P^O) = (2,4,6-(OMe)$_3$C$_6$H$_2$)$_2$P(2-SO$_3$C$_6$H$_4$)*

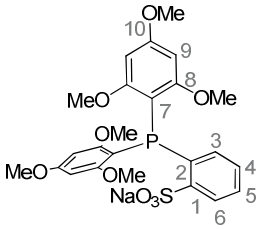


A flask was charged with **$^{(MeO)3}$(P^O)H** (490 mg, 0.94 mmol, 1.0 equiv.) and NaH (23 mg, 0.94 mmol, 1.0 equiv.), and THF (4 mL) was added. The suspension was stirred over night. The white precipitate was isolated by centrifugation, washed with THF and acetone, and dried under vacuum (200 mg, 0.37 mmol, 39%).

**$^1$H NMR** (400 MHz, $CD_3OD$): δ 7.94 (ddd, $^3J_{HH}$ = 7.8, $^4J_{PH}$ = 4.6, $^4J_{HH}$ = 1.1, 1H, 6-H), .7.39 (ddd, $^3J_{HH}$ = 7.7, $^4J_{PH}$ = 4.0, $^4J_{HH}$ = 1.0, 1H, 3-H), 7.22 (ddd, $^3J_{HH}$ = 7.7, $^3J_{HH}$ = 7.7, $^4J_{HH}$ = 1.1, 1H, 5-H), 7.14 (ddd, $^3J_{HH}$ = 7.5, $^3J_{HH}$ = 7.5, $^4J_{HH}$ = 1.2, 1H, 4-H), 6.17 (d, $^4J_{PH}$ = 2.5, 4H, 9-H), 3.77 (s, 6H, *p*-OMe), 3.43 (s, 12H, *o*-OMe).

**$^{31}$P{$^1$H} NMR** (162 MHz, $CD_3OD$): δ = -48.8.

**$^{13}$C{$^1$H} NMR** (101 MHz, $CD_3OD$): δ = 164.8 (d, $^2J_{CP}$ = 9.0, C8), 163.6 (C10), 149.0 (d, $^2J_{CP}$ = 28.0, C1), 138.9 (d, $^1J_{CP}$ = 19.9, C2), 136.3 (C3), 129.1 (C4), 128.0 (d, $^3J_{CP}$ = 4.3, C6), 127.5 (C5), 107.6 (d, $^1J_{CP}$ = 14.0, C7), 92.6 (C9), 56.2 (*o*-OMe), 55.6 (*p*-OMe).

**Anal. Calcd.** (%) for ($C_{24}H_{26}NaO_9PS$ x 1 $H_2O$): C, 52.08; H, 4.92; Found: C, 51.99; H, 5.03.

**MS(FAB)**: *m/z* = 567.1 $[M+Na]^+$, 545.1 $[M+H]^+$.

***Chlorobis(2,6-dimethoxyphenyl)phosphine***

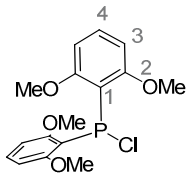


A solution of $Cl_2PNEt_2$ (1.6 g, 9 mmol, 1 equiv.) in toluene (15 mL) was added dropwise to a suspension of 2-lithium-1,3-dimethoxybenzene (2.6 g, 18 mmol, 2.1 equiv.) in toluene (100 mL). The reaction mixture was stirred for 2 h at room temperature and then ethereal HCl (2 M, 9 mL, 18 mmol, 2.0 equiv.) was added. The resulting precipitate was filtered off over celite®. The solvent was removed under vacuum to yield a white solid (2.7 g, 8 mmol, 88%). Since the chlorophosphine is not stable over time in solution only $^{1}H$ and $^{31}P$ NMR data is given.

**$^{1}H$ NMR** (400 MHz, $CDCl_3$): δ = 7.27 (td, $^{3}J_{HH}$ = 8.3, $^{5}J_{PH}$ = 1.0, 2H, 4-H), 6.52 (dd, $^{3}J_{HH}$ = 8.3, $^{4}J_{PH}$ = 2.9, 4H, 3-H), 3.70 (s, 6H, OMe).
**$^{31}P\{^{1}H\}$ NMR** (162 MHz, $CDCl_3$): δ = 60.1.

***$^{(MeO)2}$(P^O)H***; *$^{(MeO)2}$(P^O) = (2,6-(OMe)$_2$C$_6$H$_3$)$_2$P(2-SO$_3$C$_6$H$_4$)*[87]

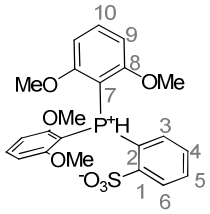


At 0 °C *n*-BuLi (10 mL, 1.6 M in hexane, 16 mmol, 2 equiv.) was added to a solution of benzene sulfonic acid (1.2 g, 8 mmol, 1 equiv.) in THF and the reaction mixture was stirred at 25 °C for 30 minutes. The suspension formed was cooled to 0 °C and a solution of chlorobis(2,6-dimethoxyphenyl)phosphine (2.6 g, 8 mmol, 1 equiv.) in THF was added. The turbid reaction mixture was stirred at 25 °C for 3 h yielding a clear solution. Volatiles were removed under vacuum to yield an off-white solid. Degassed water (40 mL) was added and the resulting suspension was acidified to pH 2 using aqueous HCl (3 M). The mixture was extracted with $CH_2Cl_2$ (3 x 20 mL) and the combined organic phase was dried over $MgSO_4$. Volatiles were removed under vacuum to yield a white solid which was purified further by washing with $CH_2Cl_2$. The product contained 0.5 equiv. of $CH_2Cl_2$, which was quantified by NMR (2.5 g, 5.0 mmol, 62%).

**$^{1}$H NMR** (400 MHz, $CDCl_3$): δ = 9.41 (d, $^{1}J_{PH}$ = 603.8, 1H, PH), 8.38–8.26 (m, 1H, 6-H), 7.69–7.62 (m, 1H, 5-H), 7.52 (t, $^{3}J_{HH}$ = 8.4, 2H, 10-H), 7.43–7.35 (m, 2H, 3- & 4-H), 6.60 (dd, $^{3}J_{HH}$ = 8.4, $^{4}J_{PH}$ = 5.2, 4H, 9-H), 3.63 (s, 12H, OMe).

**$^{31}$P NMR** (162 MHz, $CDCl_3$): δ = -29.8 (d, $^{1}J_{PH}$ = 608.5).

**$^{13}$C{$^{1}$H} NMR** (101 MHz, $CDCl_3$): δ = 162.7 (C8), 151.6 (d, $^{2}J_{PC}$ = 9.8, C1), 136.3 (C10), 133.8 (d, $^{3}J_{PC}$ = 12.1, C4), 133.4 (d, $^{4}J_{PC}$ = 3.5, C5), 129.2 (d, $^{3}J_{PC}$ = 9.9, C6), 129.0 (d, $^{2}J_{PC}$ = 13.5, C3), 115.8 ($^{1}J_{PC}$ = 103.5, C2), 104.8 (d, $^{3}J_{PC}$ = 6.2, C9), 98.2 (d, $^{1}J_{PC}$ = 102.0, C7), 56.5 (OMe).

**MS(FAB)**: *m/z* = 463 $[M+H]^+$.

**HRMS(ESI)**: *m/z* calcd for = $C_{22}H_{22}O_7PS$: 461.0818 $[M-H]^-$; found: 461.0840.

**$^{1}$H NMR** (400 MHz, $CD_3OD$): δ = 8.12 (dd, $^{3}J_{HH}$ = 7.8, $^{4}J_{PH}$ = 5.4 1H, 6-H), 7.82–7.76 (m, 1H, 5-H), 7.69–7.56 (m, 4 H, 10- & 3- & 4-H), 6.79 (dd, $^{3}J_{HH}$ = 8.5, $^{4}J_{PH}$ = 5.5, 4H, 9-H), 3.67 (s, 12H, OMe).

**$^{13}$C{$^{1}$H} NMR** (101 MHz, $CD_3OD$): δ = 164.1 (C8), 150.4 (d, $^{2}J_{PC}$ = 9.4, C1), 138.3 (C10), 136.4 (d, $^{3}J_{PC}$ = 11.2, C4), 134.7 (d, $^{4}J_{PC}$ = 3.0, C5), 131.3 (d, $^{2}J_{PC}$ = 13.3, C3), 129.2 (d, $^{3}J_{PC}$ = 9.5, C6), 118.0 (d, $^{1}J_{PC}$ = 100.9, C2), 105.9 (d, $^{3}J_{PC}$ = 6.2, C9), 97.2 (d, $^{1}J_{PC}$ = 103.3, C7), 56.9 (OMe).

***$^{(MeO)2}$(P^O)Na***; *$^{(MeO)2}$(P^O) = (2,6-(OMe)$_2$C$_6$H$_3$)$_2$P(2-SO$_3$C$_6$H$_4$)*

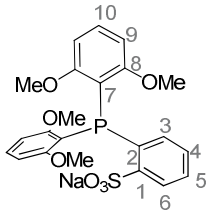


A flask was charged with **$^{(MeO)2}$(P^O)H** (1.0 g, 2.2 mmol, 1 equiv.) and NaH (62 mg, 2.6 mmol, 1.2 equiv.), and THF (10 mL) was added. The suspension was stirred over night. Phenol (31 mg, 0.3 mmol, 0.1 equiv.) was added and the reaction mixture was stirred for 1 hour. The white precipitate was isolated by filtration, washed with THF and $Et_2O$, and dried under vacuum to yield the product as a white solid (0.7 g, 1.5 mmol, 68%).

**$^{1}$H NMR** (400 MHz, $CD_3OD$): δ = 7.97 (ddd, $^{3}J_{HH}$ = 7.9, $^{3}J_{PH}$ = 3.9, $^{4}J_{HH}$ = 1.4, 1H, 6-H), 7.40 (ddd, $^{3}J_{HH}$ = 7.8, $^{3}J_{PH}$ = 3.9, $^{4}J_{HH}$ = 1.3, 1H, 3-H), 7.25 (vtd, *J* = 7.4, 1.3, 1H, 5-H), 7.21 (t, $^{3}J_{HH}$ = 8.3, 2H, 10-H), 7.13 (vtd, $^{3}J_{HH}$ = 7.5, $^{4}J_{PH}$ = 1.5, 1H, 4-H), 6.52 (dd, $^{3}J_{HH}$ = 8.3, $^{4}J_{PH}$ = 2.8, 4H, 9-H), 3.42 (s, 12H, OMe).

**$^{31}$P{$^{1}$H} NMR** (162 MHz, $CD_3OD$): δ = -45.1.

**$^{13}$C{$^{1}$H} NMR** (101 MHz, $CD_3OD$): δ = 163.8 (d, $^{2}J_{PC}$ = 8.4, C8), 149.3 (d, $^{2}J_{PC}$ = 28.7, C1), 138.1 (d, $^{1}J_{PC}$ = 19.1, C2), 136.5 (C3), 131.0 (C10), 129.2 (C4), 128.0 (d, $^{3}J_{PC}$ = 4.8, C6), 127.8 (C5), 116.4 (d, $^{1}J_{PC}$ = 17.0, C7), 105.9 (C9), 56.3 (OMe).

**Anal. Calcd.** (%) for ($C_{22}H_{22}NaO_7PS \times 2H_2O$): C, 50.77; H, 5.04; Found: C, 50.89; H, 5.01.

**MS(FAB)**: *m/z* = 507 $[M+Na]^+$, 485 $[M+H]^+$.

***Chlorobis(2-methoxy-3-isopropyl-6-methyphenyl)phosphine***

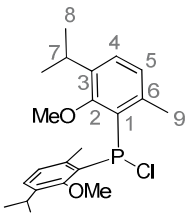


At 0 °C a solution of $Cl_2PNEt_2$ (1.5 g, 8.5 mmol, 1 equiv.) in $Et_2O$ (18 mL) was added dropwise to a suspension of *ortho*-lithium-thymol methyl ether × ½ TMEDA (4.0 g, 17.5 mmol, 2.05 equiv.) in $Et_2O$ (150 mL). The reaction mixture was stirred for 3.5 h at room temperature. Ethereal HCl (2 M, 17 mL, 35.0 mmol, 4.00 equiv.) was added at 0 °C and the resulting slurry was stirred for 1 hour. The precipitate was filtered off over celite® and rinsed with $Et_2O$ (2 x 20 mL). The solvent was removed under vacuum to yield a yellow oil (3.3 g, 8.5 mmol, 100%).

**$^1$H NMR** (400 MHz, $CDCl_3$): δ = 7.18 (d, $^3J_{HH}$ = 7.9, 2H, 4-H), 6.94 (d, $^3J_{HH}$ = 7.9, 2H, 5-H), 3.54 (s, 6H, MeO), 3.21 (m, 2H, 7-H), 2.50 (s, 6H, 9-H), 1.22 (d, $^3J_{HH}$ = 6.8, 6H, 8a-H), 1.15 (d, $^3J_{HH}$ = 6.8, 6H, 8b-H).
**$^{31}$P{$^1$H} NMR** (162 MHz, $CDCl_3$): δ = 78.6.

***$^{Thy}$(P^O)H***; *$^{Thy}$(P^O) = (2-MeO-3-(CH(CH$_3$)$_2$)-6-MeC$_6$H$_2$)$_2$P(2-SO$_3$C$_6$H$_4$)*

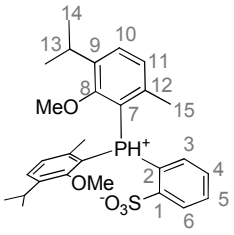


At 0 °C *n*-BuLi (11 mL, 1.6 M in hexane, 18 mmol, 2.1 equiv.) was added to a solution of benzene sulfonic acid (1.4 g, 9 mmol, 1.1 equiv.) in THF (50 mL) and the reaction mixture was stirred at 25 °C for 30 minutes. The suspension formed was cooled to 0 °C and a solution of chlorobis(2-methoxy-3-isopropyl-6-methyphenyl)phosphine (3.3 g, 8.5 mmol, 1.0 equiv.) in THF (15 mL) was added. The turbid reaction mixture was stirred at 25 °C over night yielding a dark solution. Volatiles were removed under vacuum to yield a red solid. Degassed water (40 mL) was added and the resulting white suspension was acidified to pH 2 using aqueous HCl (3 M). The mixture was extracted with $CH_2Cl_2$ (3 x 10 mL) and the combined organic phase was dried over $MgSO_4$. Volatiles were removed under vacuum to yield a white solid which was purified further by washing with $Et_2O$ and pentane (2.7 g, 4.5 mmol, 53%).

**$^{1}$H NMR** (400 MHz, $CD_2Cl_2$): δ = 9.56 (d, $^{1}J_{PH}$ = 567.8, 1H, PH), 8.20 (m, 1H, 6-H), 7.72 (m, 1H, 5-H), 7.43-7.63 (m, 4H, 4- & 3- & 10- & 10'-H), 7.01-7-24 (m, 2H, 11- & 11'-H), 3.67 (s, 3H, MeO), 3.21 (br, 2H, 13- & 13'-H), 3.01 (s, 3H, MeO'), 2.45 (br, 3H, 15- or 15'-H), 2.04 (br, 3H, 15- or 15'-H), 1.20 (m, 12H, 14- & 14'-H).

**$^{31}$P{$^{1}$H} NMR** (162 MHz, $CD_2Cl_2$): δ = -21.5.

**$^{13}$C{$^{1}$H} NMR** (101 MHz, $CD_2Cl_2$): δ = 160.3 (br, C8'), 159.7 (br, C8), 153.1 ($^{2}J_{CP}$ = 9.8, C4) 141.2 (br, C12), 141.6 (br, C12'), 141.0 (m, C9 & C9'), 136.2 (br, C3), 134.9 (C5), 134.2 (C10'), 133.5 (C10), 130.5 (d, $^{3}J_{CP}$ = 12.8, C4), 129.5 (d, $^{3}J_{CP}$ = 12.7, C11), 129.3 (br, C11'), 128.6 (br, C6), 116.8 (br, C5), 115.2 (vbr, C7 & C7'), 63.1 (MeO), 63.3(MeO'), 26.9 (m, C13 & C13'), 24.3 (m, C14 or C14'), 23.5 (m, C14 or C14'), 21.4 (m, C15 & C15').

**Anal. Calcd.** (%) for ($C_{28}H_{35}O_5PS$): C, 65.35; H, 6.86; Found: C, 65.82; H, 7.13.

**MS(FAB)**: m/z = 515.5 $[M+H]^+$.

***$^{Thy}$(P^O)Na***; *$^{Thy}$(P^O) = (2-MeO-3-(CH(CH$_3$)$_2$)-6-MeC$_6$H$_2$)$_2$P(2-SO$_3$C$_6$H$_4$)*

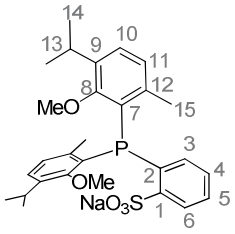


A flask was charged with **$^{Thy}$(P^O)H** (1 g, 1.9 mmol, 1.0 equiv.) and NaH (56 mg, 2.3 mmol, 1.2 equiv.), and THF (25 mL) was added. The suspension was stirred over night, concentrated to 8 mL and filtered. Volatiles were removed under vacuum. The resulting residue was washed with $Et_2O$ and dried under vacuum to yield a white solid (940 mg, 1.5 mmol, 78%).

**$^{1}$H NMR** (400 MHz, acetone-$d_6$): δ = 8.06 (m, 1H, 6-H), 7.43 (m, 1H, 3-H), 7.24 (m, 1H, 5-H), 7.17-7.15 (m, 2H, 4- 10-H), 7.11 (d, $^{3}J_{HH}$ = 7.7, 1H, 10'-H), 6.86-6.80 (m, 2H, 11- & 11'-H), 3.38 (s, 3H, MeO), 3.19 (m, 2H, 13- & 13'-H), 3.14 (s, 3H, MeO'), 2.05 (br, 3H, 15- H), 1.96 (br, 3H, 15'-H), 1.19-1.12 (m, 12H, 14- & 14'-H).

**$^{31}$P{$^{1}$H} NMR** (162 MHz, acetone-$d_6$): δ = -31.7.

**$^{13}$C{$^{1}$H} NMR** (101 MHz, acetone-$d_6$): δ = 161.1 (d, $^{2}J_{CP}$ = 11.9, C8'), 160.9 (d, $^{2}J_{CP}$ = 13.5, C8), 151.9 (d, $^{2}J_{CP}$ = 31.5, C1), 142.4 (d, $^{2}J_{CP}$ = 14.0, C12'), 142.2 (d, $^{2}J_{CP}$ = 11.1, C12), 139.7 (C9'), 139.6 (C9) , 137.5 (C3), 136.5 (d, $^{1}J_{CP}$ = 24.3. C2), 132.5 (d, $^{1}J_{CP}$ = 21.8, C7), 132.1 (d, $^{2}J_{CP}$ = 22.5, C7'), 129.0 (C4) , 128.5 (C5), 128.4 (d, $^{2}J_{CP}$ = 5.4, C6), 128.1 (C11 or C11'), 127.9 (C11 or C11'), 127.8 (C10'), 127.2 (C10) , 62.1 (d, $^{4}J_{CP}$ = 4.2, MeO), 61.9 (d, $^{4}J_{CP}$ = 2.8, MeO'), 26.9 (C13 & C13'), 24.9–23.7 (m, C14 & C14'), 23.0 (d, $^{3}J_{CP}$ = 12.7, C15), 22.8 (d, $^{3}J_{CP}$ = 15.2, C15').

**Anal. Calcd.** (%) for ($C_{28}H_{34}NaO_5PS$): C, 62.67; H, 6.39; Found: C, 60.10; H, 6.79.

**MS(FAB)**: m/z = 559.5 $[M+Na]^+$, 537.6 $[M+H]^+$.

***Chlorobis(2-methoxy-3-methyl-6-isopropylphenyl)phosphine***

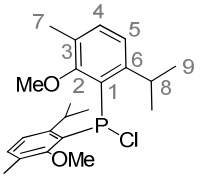


At 0 °C a solution of $Cl_2PNEt_2$ (1.5 g, 8.5 mmol, 1.00 equiv.) in $Et_2O$ (18 mL) was added dropwise to suspension of *ortho*-lithium-carvacrol methyl ether × ½ TMEDA (4.0 g, 17.5 mmol, 2.05 equiv.) in $Et_2O$ (150 mL). The reaction mixture was stirred for 3.5 h at room temperature. Ethereal HCl (2 M, 17 mL, 35.0 mmol, 4.00 equiv.) was added at 0 °C and the resulting slurry was stirred for 1 hour. The precipitate was filtered off over celite® and rinsed with $Et_2O$ (2 x 20 mL). The solvent was removed under vacuum to yield an oily white solid (3.0 g, 7.5 mmol, 88%).

**$^1$H NMR** (400 MHz, $CDCl_3$): δ = 7.14 (d, $^3J_{HH}$ = 7.6, 2H, 4-H), 7.01 (dd, $^3J_{HH}$ = 7.9, $^4J_{HH}$ = 2.6, 2H, 5-H), 3.93 (m, 2H, 8-H), 3.53 (s, 6H, MeO), 2.21 (s, 6H, 7-H), 1.14 (d, $^3J_{HH}$ = 6.8, 6H, 9a-H), 1.08 (d, $^3J_{HH}$ = 6.8, 6H, 9b-H).

**$^{13}$C{$^1$H} NMR** (101 MHz, $CDCl_3$): δ = 159.4 (d, $^2J_{PC}$ = 16.0, C2), 151.5 (d, $^2J_{PC}$ = 12.0, C6), 133.4 (C4), 132.3 (d, $^1J_{PC}$ = 54.5, C1), 127.8 (C3), 122.4 (C5), 61.0 (MeO), 29.9 (d, $^3J_{PC}$ = 14.1, C8), 24.7 (C9a), 24.1 (C9b), 16.4 (C7).

**$^{31}$P{$^1$H} NMR** (162 MHz, $CDCl_3$): δ = 75.3.

***$^{Car}$(P^O)H**; $^{Car}$(P^O) = (2-MeO-3-Me-6-(CH(CH$_3$)$_2$)C$_6$H$_2$)$_2$P(2-SO$_3$C$_6$H$_4$)*

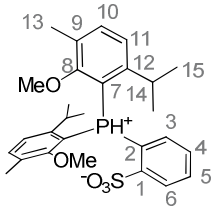


At 0 °C *n*-BuLi (14 mL, 1.6 M in hexane, 22.5 mmol, 3 equiv.) was added to a solution of benzene sulfonic acid (1.8 g, 11.3 mmol, 1.5 equiv.) in THF (50 mL) and the reaction mixture was stirred at 25 °C for 30 minutes. The suspension formed was cooled to 0 °C and a solution of chlorobis(2-methoxy-3-methyl-6-isopropylphenyl)phosphine (3.0 g, 7.5 mmol, 1.0 equiv.) in THF (15 mL) was added. The turbid reaction mixture was stirred at 25 °C for 2 hours yielding a dark solution. Volatiles were removed under vacuum to yield a red solid. Degassed water (40 mL) was added and the resulting white suspension was acidified to pH 2 using aqueous HCl (3 M). The mixture was extracted with $CH_2Cl_2$ (3 x 50 mL) and the combined organic phase was dried over $MgSO_4$. Volatiles were removed under vacuum to

yield a white solid which was purified further by washing with $Et_2O$ and pentane (3.1 g, 6.0 mmol, 80%).

**$^1$H NMR** (400 MHz, $CDCl_3$): δ = 9.71 (d, $^1J_{PH}$ = 565.4, 1H, P-H), 8.31 (br, 1H, 6-H), 7.68 (br, 1H, 5-H), 7.56-7.34 (m, 4H, 3- & 4- & 11- & 11'-H), 7.14 (br, 2H, 10- & 10'-H), 4.30-2.70 (br, 8H, MeO & MeO' & 12- & 12'-H), 2.27 (br, 6H, 13- & 13'-H), 2.04 (br, 3H, 15- or 15'-H), 1.37-0.30 (m, 12H, 14- & 14'-H).
**$^{31}$P{$^1$H} NMR** (162 MHz, $CDCl_3$): δ = -23.3 (br), -25.7 (br).
**$^{13}$C{$^1$H} NMR** (101 MHz, $CDCl_3$): δ = no assignment possible due to very broad resonances.
**Anal. Calcd.** (%) for ($C_{28}H_{35}O_5PS$): C, 65.35; H, 6.86; Found: C, 65.49; H, 7.14.
**MS(FAB)**: m/z = 515.5 $[M+H]^+$.

***$^{Car}$(P^O)Na;*** *$^{Car}$(P^O) = (2-MeO-3-Me-6-(CH(CH$_3$)$_2$)C$_6$H$_2$)$_2$P(2-SO$_3$C$_6$H$_4$)*

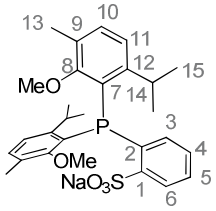


A flask was charged with **$^{Car}$(P^O)H** (1 g, 1.9 mmol, 1.0 equiv.) and NaH (56 mg, 2.3 mmol, 1.2 equiv.), and THF (20 mL) was added. The suspension was stirred over night, concentrated to 8 mL and filtered. Volatiles were removed under vacuum. The resulting residue was washed with $Et_2O$ and dried under vacuum to yield a white solid (630 mg, 1.2 mmol, 60%).

**$^1$H NMR** (400 MHz, acetone-$d_6$): δ = 8.01 (m, 1H, 6-H), 7.47 (m, 1H, 3-H), 7.24 (m, 1H, 5-H), 7.14 (m, 1H, 4-H), 7.08 (m, 2H, 11- & 11'-H), 6.94 (m, 2H, 10- & 10'-H), 3.83 (m, 14-H), 3.71 (m, 14'-H), 3.13 (s, 3H, MeO), 3.01 (s, 3H, MeO'), 2.18 (s, 6H, 13- & 13'-H), 1.12-0.78 (m, 12H, 15- & 15'-H).
**$^{31}$P{$^1$H} NMR** (162 MHz, acetone-$d_6$): δ = -38.7
**$^{13}$C{$^1$H} NMR** (101 MHz, acetone-$d_6$): δ = 162.2–161.8 (m, C8 & C8'), 153.6 (d, $^2J_{CP}$ = 18.0, C12 or C12'), 152.8 (d, $^2J_{CP}$ = 18.1, C12 or C12'), 151.9 (d, $^2J_{CP}$ = 32.6, C1), 137.4–137.1 (m, 2C, C2 & C3), 132.8 (C11 or C11'), 132.4 (C11 or C11'), 132.3 (d, $^3J_{CP}$ = 16.3, C9 or C9'), 132.1 (d, $^3J_{CP}$ = 16.1, C9 or C9'), 128.7–127.7 (m, 5C, C4 & C5 & C6 & C7 & C7'), 122.4–122.0 (m, 2C, C10 & C10'), 59.8 (d, $^4J_{CP}$ = 2.1, MeO or MeO'), 59.7 (d, $^4J_{CP}$ = 2.1, MeO or MeO'), 31.3 (m, 2C, C13 & C13'), 24.7–24.1 (m, 4C, C14 & C14'), 17.1 (d, $^3J_{CP}$ = 13.5, C15 & C15').
**Anal. Calcd.** (%) for ($C_{28}H_{34}NaO_5PS$): C, 62.67; H, 6.39; Found: C, 62.31; H, 6.74.
**MS(FAB)**: m/z = 559.5 $[M+Na]^+$, 537.6 $[M+H]^+$.

***Chlorobis(2-(cyclohexyloxy)phenyl)phosphine***

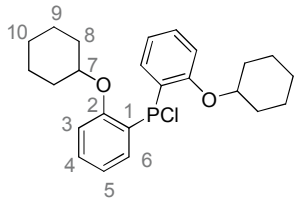


A solution of $Cl_2PNEt_2$ (0.9 g, 5.4 mmol, 1.00 equiv.) in $Et_2O$ (15 mL) was added dropwise to a suspension of 2-lithium-cyclohexyloxybenzene (2.0 g, 11.0 mmol, 2.04 equiv.) in $Et_2O$ (40 mL). The reaction mixture was stirred for 1 h at room temperature. Ethereal HCl (2 M, 5.5 mL, 11.0 mmol, 2.04 equiv.) was added and the resulting slurry was stirred for 2 hours. The precipitate was filtered off over celite® and rinsed with $Et_2O$ (20 mL). The solvent was removed under vacuum to yield a white solid (2.3 g, 5.4 mmol). NMR-analysis showed that purity was ~90%, and the product was used without further purification.

Since the chlorophosphine is not stable over time in solution only $^{1}H$ and $^{31}P$ NMR data is given.

**$^{1}$H NMR** (400 MHz, $CDCl_3$): δ = 7.43 (ddd, $^{3}J_{HH}$ = 7.6, $^{3}J_{PH}$ = 4.5, $^{4}J_{HH}$ = 1.7, 2H, 6-H), 7.33 (vtd, $^{3}J_{HH}$ = 7.9, $J$ = 1.7, 2H, 4-H), 6.93 (vt, $^{3}J_{HH}$ = 7.5, 2H, 5-H), 6.86 (dd, $^{3}J_{HH}$ = 8.2, $^{3}J_{PH}$ = 4.7, 2H, 3-H), 4.44–4.23 (m, 2H, 7-H), 1.93–1.24 (m, 12H, 9- & 10-H).

**$^{31}$P{$^{1}$H} NMR** (162 MHz, $CDCl_3$): δ = 71.6.

***$^{cHexO}$(P^O)Li***; *$^{cHexO}$(P^O) = (2-($C_6H_{11}O$)$C_6H_4$)$_2$P(2-$SO_3C_6H_4$)*

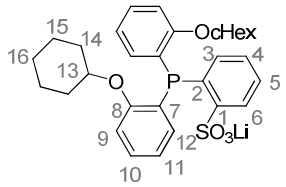


At 0 °C *n*-BuLi (6.1 mL, 1.6 M in hexane, 9.6 mmol, 2.0 equiv.) was added to a solution of benzene sulfonic acid (0.8 g, 4.8 mmol, 1.0 equiv.) in THF (20 mL) and the reaction mixture was allowed to warm to room temperature and stirred for 30 minutes. The suspension formed was cooled to 0 °C and a solution of chlorobis(2-(cyclohexyloxy)phenyl))phosphine (90%, 2.3 g, 5.4 mmol, 1.1 equiv.) in THF was added. The reaction mixture became clear within minutes and was stirred at 25 °C for 2 hours. Volatiles were removed under vacuum to afford a yellowish residue, which was suspended in $Et_2O$ (20 mL). Filtration and drying of the solid material yielded the product as a white solid (2.3 g, 4.2 mmol, 87%).

**$^1$H NMR** (400 MHz, acetone-d6): δ = 8.12 (dd, $^3J_{HH}$ = 7.8, $^4J_{PH}$ = 4.0, 1H, 6-H), 7.32–7.16 (m, 4H, 4- & 5- & 10-H), 7.12 (dd, , $^3J_{HH}$ = 7.2, $^3J_{PH}$ = 3.1, 1H, 3-H), 6.92 (dd, $^3J_{HH}$ = 8.3, $^4J_{PH}$ = 4.4, 2H, 9-H), 6.78–6.71 (m, 4H, 11- & 12-H), 4.28–4.18 (m, 2H, 13-H), 1.86–1.01 (m, 20H, 14- & 15- & 16-H).

**$^{31}$P{$^1$H} NMR** (162 MHz, acetone-d6): δ = -28.1.

**$^{13}$C{$^1$H} NMR** (101 MHz, acetone-d6): δ = 160.3 (d, $^2J_{CP}$ = 15.0, C8), 152.3 (d, $^2J_{CP}$ = 27.9, C1), 136.4 (d, $^2J_{CP}$ = 1.5, C3), 136.1 (d, $^1J_{CP}$ = 20.4, C2), 135.6–135.5 (m, C12), 130.1 (C10), 129.6 (C4), 128.8 (C5), 128.6 (d, $^3J_{CP}$ = 5.4, C6), 128.3 (d, $^1J_{CP}$ = 12.6, C7), 120.9 (C11), 113.0 (C9), 76.3 (C13), 32.2 (C14), 26.3 (C16), 24.3 (C15).

**Anal. Calcd.** (%) for ($C_{30}H_{34}LiO_5PS$*0.7 $H_2O$): C, 64.74; H, 6.40; Found: C, 64.75; H, 6.56.

**MS(FAB)**: *m/z* = 583 [$^{OcHex}$(PO)Na+Na]$^+$, 561 [$^{OcHex}$(PO)Na+H]$^+$.

**HRMS(ESI)**: *m/z* calcd for = $C_{30}H_{34}O_5PS$: 537.1859 [M-Li]$^-$; found: 537.1836.

***N,N-Diethyl-1,1-bis(2-methoxy-3,6-dimethylphenyl)phosphinamine***

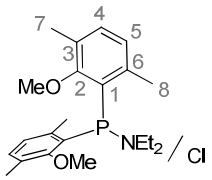


At 0 °C a solution of $Cl_2PNEt_2$ (2.1 g, 12 mmol, 1 equiv.) in toluene (10 mL) was added dropwise to a suspension of 2-lithium-3,6-dimethylanisole × ½ TMEDA (5.0 g, 25 mmol, 2 equiv.) in toluene (100 mL). The reaction mixture was stirred for 2 h at room temperature. Volatiles were removed under vacuum and the resulting waxy solid was suspended in pentane and filtered. The filtrate was concentrated to yield the product as a colorless oil (4.1 g, 11 mmol, 90 %).

**$^1$H NMR** (400 MHz, $CDCl_3$): δ = 6.97 (d, $^3J_{HH}$ = 7.6, 2H, 4-H), 6.82 (dd, $^3J_{HH}$ = 7.7, $^4J_{PH}$ = 3.6, 2H, 5-H), 3.26 (s, 6H, OMe), 3.20–3.06 (m, 4H, $NCH_2CH_3$), 2.46 (d, $^4J_{PH}$ = 1.8, 6H, 8-H), 2.20 (s, 6H, 7-H), 0.81 (br s, 6H, $NCH_2CH_3$).

**$^{31}$P{$^1$H} NMR** (162 MHz, $CDCl_3$): δ = 36.2.

**$^{13}$C{$^1$H} NMR** (101 MHz, $CDCl_3$): δ = 159.9 (d, $^2J_{CP}$ = 9.1, C2), 139.4 (d, $^2J_{CP}$ = 19.5, C6), 135.3 (m, C1), 131.0 (C4), 128.0 (C3), 126.7 (C5), 59.4 (d, $^4J_{CP}$ = 2.6, MeO), 48.0 ($NCH_2CH_3$), 21.6 (d, $^3J_{CP}$ = 18.7, C8), 16.7 (C7), 15.0 ($NCH_2CH_3$).

***Chlorobis(2-methoxy-3,6-dimethylphenyl)phosphine***

The corresponding chlorophosphine was synthesized by addition of ethereal HCl (2 M, 11 mL, 22 mmol, 2eq) to a solution of the phosphinamine (4.1 g, 11 mmol, 1 equiv.) in $Et_2O$ (100 mL). The resulting precipitate was filtered off over celite® and volatiles were removed under vacuum to yield a yellow oil (3.7 g, 11 mmol, 95%). Since the chlorophosphine is not stable over time in solution only $^1$H- and $^{31}$P NMR data is given.

**1H NMR** (400 MHz, $CDCl_3$): δ = 7.07 (d, $^3J_{HH}$ = 7.7, 2H, 4-H), 6.85 (dd, $^3J_{HH}$ = 7.7, $^4J_{PH}$ = 2.7, 2H, 5-H), 3.50 (s, 6H, OMe), 2.57 (d, $^4J_{PH}$ = 1.8, 6H, 8-H), 2.22 (s, 6H, 7-H).

**$^{31}$P{$^1$H} NMR** (162 MHz, $CDCl_3$): δ = 77.0.

***(MeO;Me2)(P^O)H***; *(MeO;Me2)(P^O) = (2-MeO-3,6-(Me)$_2$C$_6$H$_2$)$_2$P(2-SO$_3$C$_6$H$_4$)*

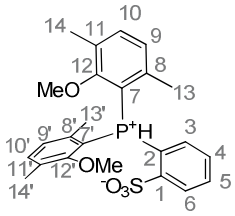


At 0 °C *n*-BuLi (14 mL, 1.6 M in hexane, 22 mmol, 2 equiv.) was added to a solution of benzene sulfonic acid (1.7 g, 11 mmol, 1 equiv.) in THF (40 mL) and the reaction mixture was stirred at 25 °C for 30 minutes. The suspension formed was cooled to 0 °C and a solution of chlorobis(2-methoxy-3,6-dimethylphenyl)phosphine (3.6 g, 11 mmol, 1 equiv.) in $Et_2O$ (10 mL) was added. The turbid reaction mixture was stirred at 25 °C for 3 hours yielding a dark solution. Volatiles were removed under vacuum to yield a red solid. Degassed water (20 mL) was added and the resulting white suspension was acidified to pH 2 using aqueous HCl (3 M). The mixture was extracted with $CH_2Cl_2$ (3 x 10 mL) and the combined organic phase was dried over $MgSO_4$. Volatiles were removed under vacuum to yield a white solid which was purified further by washing with $Et_2O$ and pentane (3.2 g, 7 mmol, 66%).

**$^1$H NMR** (400 MHz, $CD_2Cl_2$): δ = 9.49 (d, $^1J_{PH}$ = 567.7, 1H, PH), 8.19 (dd, $^3J_{HH}$ = 7.6, $^4J_{PH}$ = 5.3, 1H, 6-H), 7.76–7.68 (m, 1H, 5-H), 7.72 (vtt, 1H, *J* = 7.6, *J* = 1.5, 3-H), 7.46 (vtdd, *J* = 7.9, *J* = 2.7, *J* = 1.2, 2H, 4-H), 7.42 (d, $^3J_{HH}$ = 7.7, 2H, 10'-H), 7.37 (d, $^3J_{HH}$ = 7.7, 1H, 10-H), 7.07 (br vt, *J* = 6.8, 1H, 9'-H), 7.01 (vt, *J* = 6.8, 1H, 9-H), 3.61 (s, 3H, OMe), 3.07 (br s, 3H, OMe'), 2.44 (br s, 3H, 13'-H), 2.34 (s, 3H, 14'-H), 2.30 (s, 3H, 14-H), 2.04 (s, 3H, 13-H).

**$^{31}$P NMR** (162 MHz, $CD_2Cl_2$): δ = -21.4 ($^1J_{PH}$ = 566).

**$^{13}$C{$^1$H} NMR** (101 MHz, $CD_2Cl_2$): δ = 161.4 (C12'), 160.6 (C12), 153.1 (d, $^2J_{CP}$ = 9.8, C1), 142.4 (C8), 141.5 (C8'), 138.6 (C10'), 137.7 (C10), 136.3 (C3), 134.9 (d, $^4J_{CP}$ = 2.5, C5), 130.4 (d, *J* = 12.7, C4), 129.8 (C11'), 129.6 (C11), 128.7 (d, $^3J_{CP}$ = 12.6, C6), 128.6 (d, $^3J_{CP}$ = 8.8, C9), 128.3 (d, $^3J_{CP}$ = 10.3, C9'), 116.1 (d, $^1J_{CP}$ = 110.2, C2), 115.0 (d, $^1J_{CP}$ = 101.0, C7'), 114.5 (d, $^1J_{CP}$ = 101.5, C7'), 61.2 (OMe), 60.4 (OMe'), 21.4 (d, $^3J_{CP}$ = 9.5, C13'), 21.3 (d, $^3J_{CP}$ = 6.2, C13), 17.4 (C14'), 16.8 (C14).

**Anal. Calcd.** (%) for ($C_{24}H_{27}O_5PS$): C, 62.87; H, 5.94; Found: C, 62.56; H, 5.95.

**MS(FAB)**: m/z = 481 $[M+Na]^+$, 459 $[M+H]^+$.

**HRMS(ESI)**: *m/z* calcd for = $C_{24}H_{26}O_5PS$: 457.1244 $[M-H]^-$; found: 457.1223.

***(MeO;Me2)(P^O)Na***; *(MeO;Me2)(P^O) = (2-MeO-3,6-(Me)$_2$C$_6$H$_2$)$_2$P(2-SO$_3$C$_6$H$_4$)*

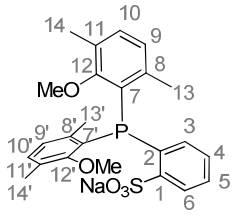


A flask was charged with **(MeO;Me2)(P^O)H** (662 mg, 1.4 mmol, 1.0 equiv.) and NaH (38 mg, 1.6 mmol, 1.1 equiv.), and THF was added (10 mL). The suspension was stirred over night, concentrated to 5 mL, and filtered. Volatiles were removed under vacuum and the resulting solid was suspended in little $Et_2O$. The solid was isolated by filtration, washed with $Et_2O$ and pentane, and dried under vacuum to yield a white solid (473 mg, 1.0 mmol, 71%).

**$^1$H NMR** (400 MHz, acetone-d6): δ = 8.06 (ddd, $^3J_{HH}$ = 7.8, $^4J_{PH}$ = 4.6, $^4J_{HH}$ = 1.5, 1H, 6-H), 7.43 (ddd, $^3J_{HH}$ = 7.7, $^3J_{PH}$ = 3.4, $^4J_{HH}$ = 1.4, 1H, 3-H), 7.24 (vtd, $^3J_{HH}$ = 7.5, $^4J_{HH}$ = 1.4, 1H, 5-H), 7.15 (vtd, $^3J_{HH}$ = 7.5, $^4J_{HH}$ = 1.5, 1H, 4-H), 7.04 (d, $^3J_{HH}$ = 7.7, 1H, 10'H), 6.99 (d, $^3J_{HH}$ = 7.6, 1H, 10-H), 6.77 (dd, $^3J_{HH}$ = 7.8, $^4J_{PH}$ = 3.2, 1H, 9'-H), 6.72 (dd, $^3J_{HH}$ = 7.7, $^4J_{PH}$ = 2.8, 1H, 9-H), 3.26 (s, 3H, OMe), 3.05 (s, 3H, OMe'), 2.16 (s, 3H, 14'-H), 2.14 (s, 3H, 14-H), 2.08 (s, 3H, 13'-H), 1.98 (s, 3H, 13-H).

**$^{31}$P{$^1$H} NMR** (162 MHz, acetone-d6): δ = -31.5.

**$^{13}$C{$^1$H} NMR** (101 MHz, acetone-d6): δ = 162.3 (d, $^2J_{CP}$ = 10.2, C12'), 161.9 (d, $^2J_{CP}$ = 11.9, C12), 151.8 (d, $^2J_{CP}$ = 31.1, C1), 142.6 (d, $^2J_{CP}$ = 13.4, C8), 142.5 (d, $^2J_{CP}$ = 16.2, C8'), 137.6 (C3), 136.3 (d, $^1J_{CP}$ = 22.1, C2), 132.5 (C10'), 132.1 (d, $^1J_{CP}$ = 21.0, C7), 132.0 (C10), 131.8 (d, $^1J_{CP}$ = 20.7, C7'), 129.0 (C4), 128.7 (C11'), 128.6 (C11), 128.5 (C5), 128.4 (d, $^3J_{CP}$ = 5.4, C6), 127.3 (d, $^3J_{CP}$ = 3.4, C9'), 127.2 (d, $^3J_{CP}$ = 2.9, C9), 60.2 (d, $^4J_{CP}$ = 2.8, OMe), 60.0 (d, $^4J_{CP}$ = 1.5, OMe'), 23.1 (d, $^4J_{CP}$ = 14.4, C13), 22.8 (d, $^4J_{CP}$ = 16.9, C13'), 17.0 (d, $^3J_{CP}$ = 1.4, C14'), 16.9 (d, $^3J_{CP}$ = 1.4, C14).

**Anal. Calcd.** (%) for ($C_{24}H_{26}NaO_5PS\times 1/2H_2O$): C, 58.89; H, 5.56; Found: C, 58.62; H, 6.02.

**MS(FAB)**: m/z = 503 $[M+Na]^+$, 481 $[M+H]^+$.

***Me*/(MeO)3(P^O)H***; *Me*/(MeO)3(P^O) = (Me)(2,4,6-(OMe)3-C6H2)P(2-SO3C6H4)*

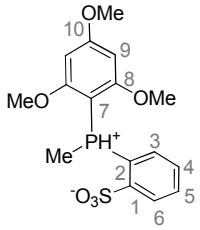


At -20 °C a solution of 1-lithium-2,4,6-trimethoxybenzene (24 mL, 0.76 M in THF, 18.2 mmol, 1.0 equiv.) was added to a solution of a $Cl_2PNEt_2$ (3.1 g, 17.7 mmol, 1.0 equiv.) in THF (15 mL). *In situ* $^{31}$P NMR analysis showed 100% conversion to $ArP(Cl)NEt_2$ (131 ppm). At 25 °C a solution of MeMgBr (18 mL, 1.0 M in THF, 18.0 mmol, 1.0 equiv.) was added and stirred for 4 hours until complete conversion to $MeArPNEt_2$ (42 ppm) was observed via *in situ* $^{31}$P NMR analysis. Ethereal HCl (2 M, 19 mL, 38.0 mmol, 2.1 equiv.) was added very slowly and the reaction mixture was stirred for 30 minutes. The volatiles were removed under vacuum.

At this stage the resulting MeArPCl could not be separated from $H_2NEt_2Cl$ formed also. The amount of salts could be reduced by extracting the residue with small amounts of THF (10 mL) and $CH_2Cl_2$ (10 mL).

At 0 °C *n*-BuLi (44 mL, 2.5 M in hexane, 110 mmol, 6.2 equiv.) was added to a solution of benzene sulfonic acid (8.5g, 53.1 mmol, 3.0 equiv.) in THF (50 mL) and the reaction mixture was allowed to warm to room temperature and stirred for 30 minutes. To the resulting suspension a solution of the MeArPCl-residue in THF and added at 0 °C. The volatiles were removed under vacuum and the resulting residue was dissolved in $H_2O$, acidified to pH 2 and extracted with $CH_2Cl_2$. The combined organic phase was dried over $MgSO_4$. Volatiles were removed under vacuum to yield a white solid. Washing with THF and drying under vacuum yielded the product as a white solid (106 mg, 0.3 mmol, 1.5%).

**$^1$H NMR** (400 MHz, $CDCl_3$): δ = 8.61 (dq, $^1J_{PH}$ = 571.4, $^3J_{HH}$ = 5.5, 1H, P-H), 8.32 (ddd, $^3J_{HH}$ = 7.6, $^4J_{PH}$ = 5.2, $^4J_{HH}$ = 1.0, 1H, 6-H), 7.68 (vtt, $^3J_{HH}$ = 7.9, $J$ = 1.6, 1H, 5-H), 7.37 (vtdd, $^3J_{HH}$ = 7.6, $^3J_{PH}$ = 2.5, $^4J_{HH}$ = 1.3, 1H, 4-H), 7.21 (ddd, $^2J_{PH}$ = 16.2, $^3J_{HH}$ = 7.8, $^4J_{HH}$ = 1.2, 1H, 3-H), 6.26 (d, $^3J_{PH}$ = 4.2, 2H, 9-H), 3.94 (s, 3H, *p*-OMe), 3.86 (s, 6H, *o*-OMe), 2.56 (dd, $^2J_{PH}$ = 16.1, $^3J_{HH}$ = 5.4, 3H, Me).

**$^{31}$P NMR** (162 MHz, $CDCl_3$): δ = -17.8 (vdt, $^1J_{PH}$ = 571.7, $^2J_{PH}$ = 16.6).

**$^{13}$C{$^1$H} NMR** (101 MHz, $CDCl_3$): δ = 168.4 (C10) , 164.5 (C8), 151.5 (d, $^2J_{CP}$ = 9.5, C1), 134.5 (d, $^4J_{CP}$ = 3.1, C5), 132.9 (d, $^2J_{CP}$ = 12.1, C3), 129.7 (d, $^3J_{CP}$ = 2.3, C6), 129.6 (d, $^3J_{CP}$ = 1.7, C4), 115.0 (d, $^1J_{CP}$ = 96.0, C2), 91.8 (d, $^3J_{CP}$ = 5.9, C9), 85.6 (d, $^1J_{CP}$ = 94.7, 7C), 56.6 (*o*-OMe), 56.1 (*p*-OMe), 9.2 (d, $^1J_{CP}$ = 61.3, Me).

**MS(FAB)**: *m/z* = 370.8 $[M+H]^+$.

**HRMS(ESI)**: *m/z* calcd for = $C_{16}H_{18}O_6PS$: 369.0556 $[M-H]^-$; found: 369.0549.

***Me*/(MeO)3(P^O)Na**; Me*/(MeO)3(P^O) = (Me)(2,4,6-(OMe)$_3$C$_6$H$_2$)P(2-SO$_3$C$_6$H$_4$)*

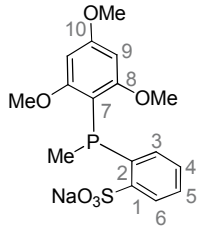


A flask was charged with **Me*/(MeO)3(P^O)H** (27 mg, 73 µmol, 1.0 equiv.) and NaH (2 mg, 83 µmol, 1.1 equiv.), and THF (2 mL) was added. The suspension was stirred over night and the resulting turbid solution was filtered. Volatiles were removed under vacuum and the resulting residue was suspended in $Et_2O$. The solid was isolated by centrifugation, washed with $Et_2O$ and dried under vacuum (25 mg, 60 µmol, 82%).

**$^1$H NMR** (400 MHz, acetone-d6): δ = 7.97 (m, 1H, 6-H), 7.50–7.41 (m, 1H, 3-H), 7.25–7.15 (m, 2H, 4- & 5-H), 6.18 (d, $^3J_{PH}$ = 2.3, 2H, 9-H), 3.80 (s, 3H, *p*-OMe), 3.64 (s, 6H,), 1.63 (d, $^2J_{PH}$ = 4.5, 3H, Me).

**$^{31}$P{$^1$H} NMR** (162 MHz, acetone-d6): δ = -40.5.

**$^{13}$C{$^1$H} NMR** (101 MHz, acetone-d6): δ = 164.7 (d, $^2J_{CP}$ = 7.7, C8), 163.7 (C10), 149.6 (d, $^2J_{CP}$ = 25.0, C1), 140.4 (d, $^1J_{CP}$ = 19.9, C2), 133.9 (C3), 129.6 (C4), 128.0 (d, $^3J_{CP}$ = 4.5, C6), 127.9 (C5), 105.8 (d, $^1J_{CP}$ = 17.2, C7), 92.4 (C9), 56.2 (*o*-OMe), 55.5(*p*-OMe), 12.6 (d, $^1J_{CP}$ = 9.4, Me).

**Anal. Calcd.** (%) for ($C_{16}H_{18}NaO_6PS$ x ½ $H_2O$): C, 47.88; H, 4.77; Found: C, 47.81; H, 4.82.

**MS(FAB)**: *m/z* = 415 $[M+Na]^+$, 393 $[M+H]^+$.

***Chlorobis(2-(trifluoromethyl)phenyl)phosphine***

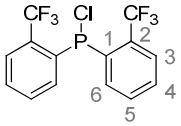


At -78 °C *n*-BuLi (10.5 mL, 2.5 M in hexane, 26 mmol, 2 equiv.) was added dropwise to a solution of 2-(trifluoromethyl)bromobenzene (5.9 g, 26 mmol, 2 equiv.) in $Et_2O$ (100 mL). The reaction mixture was allowed to warm to room temperature. The solution was cooled to -78 °C and a solution of $Cl_2PNEt_2$ (2.3 g, 13 mmol, 1 equiv.) in $Et_2O$ (15 mL) was added dropwise. The reaction mixture was allowed to warm to room temperature and stirred for 3 hours, meanwhile a white precipitate formed. The reaction mixture was cooled to 0 °C and ethereal HCl (2 M, 13 mL, 26 mmol, 2 equiv.) was added. The reaction mixture was allowed to warm to room temperature and the resulting slurry was stirred for 2 days. The precipitate was filtered off over celite® and rinsed with $Et_2O$ (50 mL). The solvent was removed under vacuum to yield an off-white solid (4.2 g, 12 mmol, 91%).

Since the chlorophosphine is not stable over time in solution only $^{1}$H-, $^{19}$F- and $^{31}$P NMR data is given.

**$^{1}$H NMR** (400 MHz, $CDCl_3$): δ = 7.81-7.74 (m, 4H, 3-H & 5-H), 7.64-7.53 (m, 4H, 4- & 6-H).

**$^{31}$P{$^{1}$H} NMR** (162 MHz, $CDCl_3$): δ = 73.7 (hept, $^{4}J_{PF}$ = 66.7).

**$^{19}$F{$^{1}$H} NMR** (376 MHz, $CDCl_3$): δ = -57.0 (d, $^{4}J_{PF}$ = 66.7).

***$^{CF3}$(P^O)Li***; *$^{CF3}$(P^O) = (2-$CF_3C_6H_4$)$_2$P(2-$SO_3C_6H_4$)*

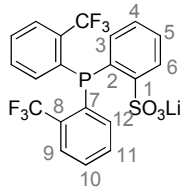


At 0 °C *n*-BuLi (5.8 mL, 1.6 M in hexane, 14.5 mmol, 2 equiv.) was added to a solution of benzene sulfonic acid (1.1 g, 7.2 mmol, 1 equiv.) in THF and the reaction mixture was stirred at 25 °C for 40 minutes. The suspension formed was cooled to 0 °C and a solution of chlorobis(2-(trifluoromethyl)phenyl)phosphine (2.6 g, 7. mmol, 1 equiv.) in THF was added. The turbid reaction mixture was stirred at 25 °C over night, yielding a clear solution. Volatiles were removed under vacuum to yield a solid. Degassed water (30 mL) was added and the resulting clear solution was acidified using aqueous HCl (3 M). The mixture was extracted with $CH_2Cl_2$ (3 x 15 mL) and the combined organic phase was dried over $MgSO_4$. The solution was concentrated under vacuum resulting in the formation of a white precipitate. The solid was isolated by filtration to yield the clean product (1.1 mmol, 15%). Volatiles of the filtrate were removed under vacuum to yield a yellow solid, which was extracted with MeOH. Solvents of the extract were removed under vacuum and the remaining residue was suspended in $Et_2O$. Filtration yielded a white solid which was rinsed with $Et_2O$ and pentane and dried under vacuum (2.4 mmol, 33%). Overall yield (1.7 g, 3.5 mmol, 48%).

**$^1$H NMR** (600 MHz, acetone-d6): δ = 8.14 (dd, $^3J_{HH}$ = 6.4, $^4J_{PH}$ = 4.6, 1H, 6-H), 7.82 (br s, 1H, 9'-H), 7.73 (br s, 1H, 9-H), 7.61–7.54 (m, 1H, 10'-H), 7.54–7.47 (m, 2H, 10- & 11'-H), 7.49–7.39 (m, 1H, 11-H), 7.32 (vt, $^3J_{HH}$ = 7.3, 1H, 5-H), 7.28 (vtd, $^3J_{HH}$ = 7.5, *J* = 1.3, 1H, 4-H), 7.01 (br s, 1H, 12-H), 6.98–7.89 (m, 1H, 12'-H), 6.73 (ddd, $^3J_{HH}$ = 7.5, $^3J_{PH}$ = 2.9, $^4J_{HH}$ = 1.1, 1H, 3-H).

**$^{31}$P{$^1$H} NMR** (162 MHz, acetone-d6): δ = -15.2 (vhept, $^4J_{PF}$ = 57.8).

**$^{19}$F{$^1$H} NMR** (376 MHz, acetone-d6): δ = -58.6 (d, $^4J_{PF}$ = -59.8, $CF_3$), 58.8 (d, $^4J_{PF}$ = -53.8, $CF_3$').

**$^{13}$C{$^1$H} NMR** (151 MHz, acetone-d6): δ = 150.9 (d, $^2J_{CP}$ = 26.3, C1), 139.5 (d, $^1J_{CP}$ = 35.8, C7'), 138.9 (d, $^1J_{CP}$ = 30.2, C7), 137.7 (C12'), 136.7 (C12), 135.6 (C3), 135.1-134.5 (m, C8'), 133.7 (d, $^1J_{CP}$ = 27.3, C2), 133.4-132.9 (m, C8), 132.7 (C11'), 132.5 (C11), 130.4 (C4), 129.9 (C10'), 129.7 (d, $^3J_{CP}$ = 3.5, C6), 129.7 (C5), 129.4 (C10), 127.5-127.0 (m, C9 & C9'), 125.6 (q, $^1J_{CF}$ = 275.0, $CF_3$), 125.5 (q, $^1J_{CF}$ = 275.0, $CF_3$').

**Anal. Calcd.** (%) for ($C_{20}H_{12}F_6LiO_3PS \times 1.25\ H_2O$): C, 47.40; H, 2.88; Found: C, 47.28; H, 2.86.

**MS(FAB)**: m/z = 523 [$^{CF3}$(PO)Na+Na]$^+$, 501 [$^{CF3}$(PO)H+Na]$^+$.

**HRMS(ESI)**: *m/z* calcd for = $C_{20}H_{12}F_6O_3PS$: 477.0143 [M-Li]$^-$; found: 477.0145.

***Chloro(2-(cyclohexyloxy)phenyl)(2,6-dimethoxyphenyl)phosphine***

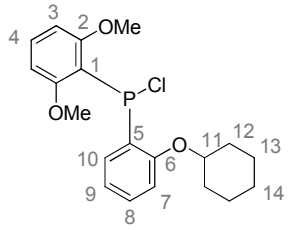


At -78 °C a suspension of 2-lithium-cyclohexyloxy benzene (538 mg, 3.0 mmol, 1.0 equiv.) in THF (10 mL) was added dropwise to a solution of $Cl_2PNEt_2$ (510 mg, 2.9 mmol, 1.0 equiv.) in $Et_2O$ (20 mL). The reaction mixture was warmed to room temperature within 20 minutes and stirred until a clear solution formed. *In situ* $^{31}$P NMR analysis showed complete conversion to $ArP(Cl)NEt_2$ (135 ppm). The reaction mixture was cooled to -20 °C and a suspension of 2-lithium-1,3-dimethoxybenzene (427 mg, 3.0 mmol, 1.0 equiv.) in $Et_2O$ (10 mL) was added dropwise. Since *in situ* $^{31}$P NMR analysis showed only 44 % conversion to $Ar^1Ar^2PNEt_2$ (36 ppm), additional 2-lithium-1,3-dimethoxybenzene (350 mg, 2.a mmol, 0.8 equiv.) in $Et_2O$ (10 mL) was added. Volatiles were removed under vacuum and the remaining brown oil was treated with pentane to afford a white precipitate, which was separated by filtration. The volatiles of the filtrate were removed under vacuum and the remaining oil was dissolved in $Et_2O$ (20 mL). Ethereal HCl (2 M, 3 mL, 6.0 mmol, 2.0 equiv.) was added and the resulting slurry was stirred for 2 hours. The precipitate was filtered off over celite® and rinsed with $Et_2O$ (20 mL). The solvent of the filtrate was removed under vacuum to yield the product as a white solid (544 mg, 1.4 mmol, 49%).

**$^1$H NMR** (400 MHz, $CDCl_3$): δ = 7.84 (ddd, $^3J_{HH}$ = 7.7, $^3J_{PH}$ = 3.7, $^4J_{HH}$ = 1.7, 1H, 10-H), 7.30 (t, $^3J_{HH}$ = 8.4, 1H, 4-H), 7.28–7.19 (m, 1H, 8-H), 7.01 (vtt, $^3J_{HH}$ = 7.4, $J$ = 1.0, 1H, 9-H), 6.74 (dd, $^3J_{HH}$ = 8.2, $^4J_{PH}$ = 5.1, 1H, 7-H), 6.47 (dd, $^3J_{HH}$ = 8.3, $^4J_{PH}$ = 2.6, 2H, 3-H), 4.23–4.15 (m, 1H, 11-H), 3.64 (s, OMe), 1.97–0.93 (m, 10H, 12- & 13- & 14H).

**$^{31}$P{$^1$H} NMR** (162 MHz, $CDCl_3$): δ = 63.4.

**$^{13}$C{$^1$H} NMR** (101 MHz, $CDCl_3$): δ = 163.2 (d, $^2J_{CP}$ = 11.7, C2), 157.3 (d, $^2J_{CP}$ = 19.4, C6), 133.4 (C4), 132.20 (d, $^2J_{CP}$ = 4.4, C10), 129.4 (C8), 127.8 (d, $^1J_{CP}$ = 35.7, C5), 120.3 (C9), 114.6 (d, $^1J_{CP}$ = 49.5, C1), 111.6 (C7), 104.5 (C3), 75.5 (C11), 55.9 (OMe), 31.3 (br, C12), 25.8 (C14), 23.4 (C13).

***cHexO/(MeO)2(P^O)Li***; *cHexO/(MeO)2(P^O) = (2-(OC$_6$H$_{11}$)C$_6$H$_4$)(2,6-(OMe)$_2$C$_6$H$_3$)P(2-SO$_3$C$_6$H$_4$)*

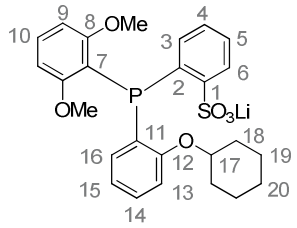


At 0 °C *n*-BuLi (1.6 mL, 1.6 M in hexane, 2.6 mmol, 2.0 equiv.) was added to a solution of benzene sulfonic acid (206 mg, 1.3 mmol, 1.0 equiv.) in THF (5 mL) and the reaction mixture was allowed to warm to room temperature and stirred for 30 minutes. The suspension formed was cooled to 0 °C and a solution of chloro(2-(cyclohexyloxy)phenyl)(2,6-dimethoxyphenyl)phosphine (493 mg, 1.3 mmol, 1.0 equiv.) in THF was added. The reaction mixture became clear within minutes and was stirred at 25 °C for 2 hours. Volatiles were removed under vacuum over night to afford a white residue, which was purified by dissolution in toluene and precipitation with pentane. Drying under vacuum yielded the product as a white solid (400 mg, 0.7 mmol, 54%). Note that the product could not be purified completely and was used as obtained, since impurities could be successfully removed in the next step on complexation to palladium.

**$^1$H NMR** (400 MHz, acetone-d6): δ = 8.02 (dd, $^3J_{HH}$ = 7.7, $^4J_{PH}$ = 4.3, 1H, 6-H), 7.50 (ddd, $^3J_{HH}$ = 7.6, $^3J_{PH}$ = 3.8, $^4J_{HH}$ = 1.2, 1H, 3-H), 7.38–7.26 (m, 2H, 5- & 10-H), 7.22 (vt, $^3J_{HH}$ = 7.4, 1H, 4-H), 7.17 (vt, $^3J_{HH}$ = 7.6, 1H, 14-H), 6.83 (dd, $^3J_{HH}$ = 8.2, $^4J_{PH}$ = 4.8, 1H, 13-H), 6.77–6.67 (m, 2H, 15- & 16-H), 6.63 (dd, $^3J_{HH}$ = 8.3, $^4J_{PH}$ = 2.6, 2H, 9-H), 4.24–4.12 (m, 1H, 17-H), 3.52 (s, 6H, OMe), 1.71–1.00 (m, 10H, 18-20-H).

**$^{31}$P{$^1$H} NMR** (162 MHz, acetone-d6): δ = -23.2.

**$^{13}$C{$^1$H} NMR** (101 MHz, acetone-d6): δ = 164.1 (d, $^2J_{CP}$ = 8.8, C8), 159.5 (d, $^2J_{CP}$ = 15.5, C12), 150.0 (d, $^2J_{CP}$ = 28.1, C1), 137.6 (C3), 135.2 (d, $^1J_{CP}$ = 19.7, C2), 133.9 (d, $^2J_{CP}$ = 3.0, C16), 132.3 (C10), 129.1 (C4), 129.0 (C14), 128.2 (C5), 127.9 (d, $^3J_{CP}$ = 5.1, C6), 127.4 (d, $^1J_{CP}$ = 9.8, C11), 120.2 (C15), 113.8 (d, $^1J_{CP}$ = 19.0, C7), 111.4 (C13), 106.3 (C9), 75.1 (C17), 56.5 (OMe), 31.9 (C18, d, *J* = 8.2), 26.1 (C20), 23.7 (C19).

**MS(FAB)**: *m/z* = 513 $[M+Li]^+$, 507 $[M+H]^+$.

**HRMS(ESI)**: *m/z* calcd for = $C_{26}H_{28}O_6PS$: 499.1339 $[M-Li]^-$; found: 499.1331.

***Chloro(2'-6'-dimethoxybiphenyl-2-yl)(2,6-dimethoxyphenyl)phosphine***

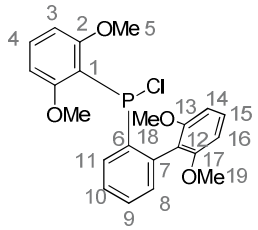


A flask was charged with 2'-bromo-2,6-dimethoxybiphenyl (2.8 g, 9.6 mmol, 1.1 equiv.) and THF (20 mL), cooled to 0 °C and *n*-BuLi (6.3 mL, 1.6 M in hexane, 10 mmol, 1.2 equiv.) was added dropwise. The suspension was cooled to -78 °C and was added dropwise to a solution of $Cl_2PNEt_2$ (1.5 g, 8.7 mmol, 1.0 equiv.) in THF (20 mL) at -78 °C. The suspension was allowed to slowly warm to room temperature and a clear solution formed. *In situ* $^{31}$P NMR analysis showed complete conversion to $Ar^1P(Cl)NEt_2$ (139 ppm). A flask was charged with 2,6-dimethoxybenzene (1.6 g, 11.6 mmol, 1.3 equiv.) and THF (20 mL), cooled to 0 °C and *n*-BuLi (7.6 mL, 1.6 M in hexane, 12 mmol, 1.4 equiv.) was added dropwise and the mixture was stirred at room temperature for 30 minutes. The freshly prepared solution of 2-lithium-1,3-dimethoxybenzene was added to the solution of $Ar^1P(Cl)NEt_2$ and the reaction mixture was stirred over night. *In situ* $^{31}$P NMR analysis showed nearly complete conversion to $Ar^1Ar^2PNEt_2$ (39 ppm). Volatiles were removed under vacuum and the remaining residue was suspended in a mixture of $Et_2O$ (200 mL) and $CH_2Cl_2$ (40 mL). Ethereal HCl (2 M, 9 mL, 18.0 mmol, 2.1 equiv.) was added very slowly and the resulting slurry was stirred over night. The precipitate was filtered off over celite® and rinsed with $Et_2O$ (20 mL). Solvents were removed under vacuum and the reaming yellow residue was suspended in pentane (20 mL). The suspension was filtered and the white solid was washed with $Et_2O$ (3 x 10 mL), and dried under vacuum (1.2 g, 2.8 mmol, 31%).

**$^1$H NMR** (400 MHz, $CD_2Cl_2$): δ = 8.10 (dd, $^3J_{HH}$ = 7.3, $^3J_{PH}$ = 2.9, 1H, 11-H), 7.44 (vt, $^3J_{HH}$ = 7.7, 1H, 10-H), 7.34 (vt, $^3J_{HH}$ = 7.3, 1H, 9-H), 7.21 (m, 2H, 4- & 15-H), 6.94 (dd, $^3J_{HH}$ = 7.4, $^4J_{PH}$ = 4.9, 1H, 8-H), 6.60 (d, $^3J_{HH}$ = 8.4, 1H, 14-H), 6.30 (dd, $^3J_{HH}$ = 8.3, $^4J_{PH}$ = 2.6, 2H, 3-H), 6.14 (d, $^3J_{HH}$ = 8.3, 1H, 16-H), 3.78 (s, 3H, 19-H), 3.42 (s, 6H, 5-H), 3.03 (s, 3H, 18-H).

**$^{31}$P{$^1$H} NMR** (162 MHz, $CD_2Cl_2$): δ = 68.9.

**$^{13}$C{$^1$H} NMR** (101 MHz, $CD_2Cl_2$): δ = 163.7 (d, $^2J_{CP}$ = 12.3, C2), 158.6 (C13), 158.0 (C17), 139.3 (d, $^1J_{CP}$ = 36.0, C6), 136.7 (d, $^2J_{CP}$ = 33.1, C7), 133.8 (C4), 131.5 (d, $^2J_{CP}$ = 5.2, C11), 130.8 (d, $^3J_{CP}$ = 2.3, C8), 130.1 (C15), 128.3 (C9), 127.0 (C10), 116.8 (d, $^3J_{CP}$ = 6.6, C12), 114.7 (d, $^1J_{CP}$ = 51.1, C1), 104.4 (C3), 104.3 (C14), 103.4 (C16), 56.5 (C19), 55.9 (C5), 55.2 (C18).

***Ar/(MeO)2(P^O)H***; *Ar/(MeO)2(P^O) = (2-(2',6'-(OMe)$_2$C$_6$H$_3$)C$_6$H$_4$)(2,6-(OMe)$_2$-C$_6$H$_3$)P(2-SO$_3$C$_6$H$_4$)*

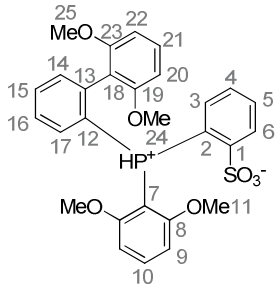


At 0 °C *n*-BuLi (3.5 mL, 1.6 M in hexane, 5.6 mmol, 2.0 equiv.) was added to a solution of benzene sulfonic acid (438 mg, 2.8 mmol, 1.1 equiv.) in THF (10 mL) and the reaction mixture was allowed to warm to room temperature and stirred for 30 minutes. The suspension formed was cooled to 0 °C and a solution of chloro(2'-6'-dimethoxybiphenyl-2-yl)(2,6-dimethoxyphenyl)phosphine (1.05 g, 2.5 mmol, 1.0 equiv.) in THF was added. The reaction mixture was stirred at 25 °C over night. Volatiles were removed under vacuum and the residue was dissolved in degassed water (50 mL). The solution was acidified to pH 2 using aqueous HCl (3 M). The mixture was extracted with $CH_2Cl_2$ (3 x 20 mL) and the combined organic phase was dried over $MgSO_4$. Volatiles were removed under vacuum to yield a yellow solid. Washing with THF and $Et_2O$ and drying under vacuum yielded the product as a white solid (512 mg, 0.9 mmol, 36%).

**$^1$H NMR** (400 MHz, $CDCl_3$): δ = 9.26 (d, $^1J_{PH}$ = 595.3, 1H, P-H), 8.29 (dd, $^3J_{HH}$ = 8.0, $^4J_{PH}$ = 5.0, 1H, 6-H), 7.68–7.35 (m, 7H, 3-5-H & 10-H & 15-17-H), 7.32 (dd, $^3J_{HH}$ = 7.7, $^4J_{PH}$ = 5.4, 1H, 14-H), 7.20 (vt, $^3J_{HH}$ = 8.4, 1H, 21-H), 6.50–6.41 (m, 3H, 9- & 22-H), 6.33 (d, $^3J_{HH}$ = 8.4, 1H, 20-H), 3.58 (s, 3H, 24/25-H), 3.57 (s, 3H, 24/25-H), 3.50 (s, 6H, 11-H).

**$^{31}$P NMR** (162 MHz, $CDCl_3$): δ = -17.7 (d, $^1J_{PH}$ = 595.2).

**$^{13}$C{$^1$H} NMR** (101 MHz, $CDCl_3$): δ = 162.2 (C8), 157.1 (C19/23), 156.9 (C19/23), 152.8 (d, $^2J_{CP}$ = 9.8, C1), 138.9 (d, $^2J_{CP}$ = 10.6, C13), 136.5 (C10), 135.1 (d, $^2J_{CP}$ = 11.0, C3), 134.4 (d, $^2J_{CP}$ = 10.6, C17), 133.8 (C5), 133.0 (d, $^3J_{CP}$ = 11.1, C14), 132.8 (d, $^4J_{CP}$ = 2.8, C15), 130.8 (C21), 129.0 (d, $^3J_{CP}$ = 9.5, C6), 128.9 (d, $^3J_{CP}$ = 13.0, C4), 127.6 (d, $^3J_{CP}$ = 13.4, C16), 121.1 (d, $^1J_{CP}$ = 97.1, C12), 114.7 (d, $^3J_{CP}$ = 5.2, C18), 114.0 (d, $^1J_{CP}$ = 98.4, C2), 104.9 (d, $^3J_{CP}$ = 5.9, C9), 103.7 (C20/22), 103.7 (C20/22), 97.9 (d, $^1J_{CP}$ = 96.8, C7), 56.3 (C11), 55.7 (C24/25), 55.4 (C24/25).

**MS(FAB)**: *m/z* = 539 $[M+H]^+$.

**HRMS(ESI)**: *m/z* calcd for = $C_{28}H_{26}O_7PS$: 537.1131 $[M-H]^-$; found: 537.1114.

***$^{Ar/(MeO)2}$(P^O)Na***; *$^{Ar/(MeO)2}$(P^O) = (2-(2',6'-(OMe)$_2$C$_6$H$_3$)C$_6$H$_4$)(2,6-(OMe)$_2$-C$_6$H$_3$)P(2-SO$_3$C$_6$H$_4$)*

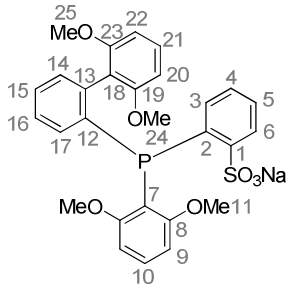


A flask was charged with **$^{Ar/(MeO)2}$(P^O)H** (208 mg, 0.4 mmol, 1.0 equiv.) and NaH (15 mg, 0.6 mmol, 1.6 equiv.), and THF (8 mL) was added. The suspension was stirred over night and the resulting turbid solution was filtered. Volatiles were removed under vacuum and the resulting residue was suspended in $Et_2O$. The solid was isolated by centrifugation, washed with $Et_2O$ and dried under vacuum (171 mg, 0.3 mmol, 79%).

**$^1$H NMR** (400 MHz, acetone-d6): δ = 8.06 (dd, $^3J_{HH}$ = 7.1, $^4J_{PH}$ = 4.1, 1H, 6-H), 7.55 (ddd, $^3J_{HH}$ = 7.7, $^3J_{PH}$ = 3.8, $^4J_{HH}$ = 1.4, 1H, 3-H), 7.30 (vt, $^3J_{HH}$ = 7.1, 1H, 5-H), 7.27–7.05 (m, 6H, 4-H & 10-H & 15-17-H & 21-H), 7.00 (ddd, $^3J_{HH}$ = 7.3, $^4J_{PH}$ = 4.3, $^4J_{HH}$ = 1.4, 1H, 14-H), 6.59 (d, $^3J_{HH}$ = 8.2, 1H, 22-H), 6.40 (dd, $^3J_{HH}$ = 8.3, $^4J_{PH}$ = 2.7, 2H, 9-H), 6.35 (d, $^3J_{HH}$ = 8.4, 1H, 20-H), 3.42 (s, 3H, 24-H), 3.32 (s, 3H, 25-H), 3.31 (s, 6H, 11-H).

**$^{31}$P{$^1$H} NMR** (162 MHz, acetone-d6): δ = -31.4.

**$^{13}$C{$^1$H} NMR** (101 MHz, acetone-d6): δ = 164.2 (d, $^2J_{CP}$ = 8.7, C8), 158.5 (C19), 158.3 (C23), 151.6 (d, $^2J_{CP}$ = 27.8, C1), 141.0 (d, $^1J_{CP}$ = 6.8, C12), 138.3 (d, $^2J_{CP}$ = 30.7, C13), 137.1 (C3), 134.9 (C17), 134.5 (d, $^1J_{CP}$ = 20.9, C2), 132.2 (C10), 131.7 (d, $^3J_{CP}$ = 5.3, C14), 129.6 (C21), 129.4 (C4), 128.5 (C6), 128.4 (C5), 127.3 (C15), 126.8 (C16), 121.8 (d, $^3J_{CP}$ = 5.8, C18), 114.3 (d, $^1J_{CP}$ = 16.9, C7), 109.3 (C22), 105.8 (C20), 105.7 (C9), 59.2 (C25), 56.0 (C11), 55.8 (C24).

**Anal. Calcd.** (%) for ($C_{28}H_{26}NaO_7PS \times 1.5H_2O$): C, 57.24; H, 4.97; Found: C, 57.11; H, 5.26.

**MS(FAB)**: *m/z* = 539 [$^{(Ar/MeO2)}$(PO)H+H]$^+$.

***Chlorobis(2,6-diisopropoxyphenyl)phosphine***

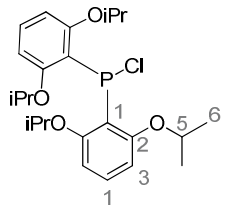


At 0 °C *n*-BuLi (17.5 mL, 1.6 M in hexane, 28 mmol, 2.1 equiv.) was added dropwise to a solution of 1,3-diisopropoxybenzene (5.2 g, 26 mmol, 2.0 equiv.) in THF (50 mL). The reaction mixture was stirred at 0 °C for 2.5 hours and at 25 °C for 1 hour. The solution was cooled to 0 °C, and a solution of $Cl_2PNEt_2$ (2.3 g, 13 mmol, 1.0 equiv.) in $Et_2O$ (15 mL) was added dropwise. The reaction mixture was allowed to warm to room temperature and stirred for 1 hour, meanwhile a white precipitate formed. Volatiles were removed under vacuum and the residue was suspended in $Et_2O$ (125 mL). Ethereal HCl (2 M, 13.5 mL, 27 mmol, 2.1 equiv.) was added. The reaction mixture was allowed to warm to room temperature and the resulting slurry was stirred over night. The precipitate was filtered off over celite® and rinsed with $Et_2O$ (50 mL). The solvent was removed under vacuum to yield an off-white solid, which was washed with pentane and $Et_2O$ and dried under vacuum to yield a white solid (3.4 g, 8 mmol, 57%). NMR-analysis showed that the product was obtained in ~70% purity. The product was used as obtained as purification is performed in the next step.

**$^1$H NMR** (400 MHz, $CDCl_3$): 7.15 (td, $^3J_{HH}$ = 8.3, $^5J_{PH}$ = 1.3, 2H, 4-H), 6.40 (dd, $^3J_{HH}$ = 8.3, $^4J_{PH}$ = 2.8, 4H, 3-H), 4.44 (hept, $^3J_{HH}$ = 6.1, 4H, 5-H), 1.14 (d, $^3J_{HH}$ = 6.0, 24H, 6-H).
**$^{31}$P{$^1$H} NMR** (162 MHz, $CDCl_3$): δ = 65.6.

***(iPrO)2(P^O)H***; *(iPrO)2(P^O) = (2,6-(iPrO)$_2$C$_6$H$_3$)$_2$P(2-SO$_3$C$_6$H$_4$)*

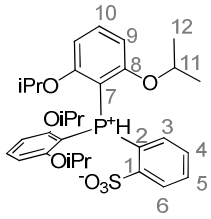


At 0 °C *n*-BuLi (6.5 mL, 1.6 M in hexane, 10.4 mmol, 2 equiv.) was added to a solution of benzene sulfonic acid (826 mg, 5.2 mmol, 1 equiv.) in THF (30 mL) and the reaction mixture was stirred at 25 °C for 30 minutes. The suspension formed was cooled to 0 °C and a solution of chlorobis(2,6-diisopropoxyphenyl)phosphine (2.4 g, 5.3 mmol, 1 equiv.) in THF (20 mL) was added. The turbid reaction mixture was stirred at 25 °C for 3 hours yielding a clear solution. Volatiles were removed under vacuum to yield an off-white residue. The residue was dissolved in $CH_2Cl_2$ (30 mL) and ethereal HCl (2 M, 2.6 mL, 5.4 mmol, 1 equiv.) was added. Volatiles were removed under vacuum and the residue was suspended in water (50 mL). The mixture was extracted with $CH_2Cl_2$ (3 x 30 mL) and the combined organic phase was dried over $MgSO_4$. Volatiles were removed under vacuum and the residue was suspended in $Et_2O$ (50 mL), isolated by filtration, and dried under vacuum (2.2 g, 4.0 mmol, 77%).

**$^1$H NMR** (400 MHz, $CD_2Cl_2$/acetone-d6): δ = 9.32 (d, $^1J_{PH}$ = 602.8, 1H, PH), 8.08 (ddd, $^3J_{HH}$ = 7.9, $^4J_{PH}$ = 5.2, $^4J_{HH}$ = 1.3, 1H, 6-H), 7.68–7.59 (m, 2H, 5- & 3-H), 7.52 (t, $^3J_{HH}$ = 8.4, 2H, 10-H), 7.40 (vtdd, $^3J_{HH}$ = 7.6, $^4J_{PH}$ = 2.6, $^4J_{HH}$ = 1.3, 1H, 4-H), 6.65 (dd, $^3J_{HH}$ = 8.5, $^4J_{PH}$ = 5.2, 4H, 9-H), 4.59 (hept, $^3J_{HH}$ = 6.0, 4H, 11-H), 1.05 (d, $^3J_{HH}$ = 6.0, 12H, 12a-H), 0.89 (d, $^3J_{HH}$ = 6.0, 12H, 12b-H).

**$^{31}$P NMR** (162 MHz, $CDCl_3$): δ = -28.7 (d, $^1J_{PH}$ = 615.7).

**$^{13}$C{$^1$H} NMR** (101 MHz, $CD_2Cl_2$/acetone-d6): δ = 161.8 (C8), 153.6 (d, $^2J_{CP}$ = 10.3, C1), 136.0 (C10), 135.5 (d, $^2J_{CP}$ = 11.8, C3), 133.2 (d, $^4J_{CP}$ = 3.1, C5), 129.2 (d, $^3J_{CP}$ = 13.4, C4), 128.0 (d, $^3J_{CP}$ = 9.8, C6), 118.8 (d, $^1J_{CP}$ = 102.1, C2), 105.7 (d, $^3J_{CP}$ = 6.5, C9), 100.0 (d, $^1J_{CP}$ = 119.3, C7), 71.6 (C11), 21.4 (C12b), 21.3 (C12a).

**MS(FAB)**: *m/z* = 575 $[M+H]^+$.

**HRMS(ESI)**: *m/z* calcd for = $C_{30}H_{38}O_7PS$: 573.2070 $[M-H]^-$; found: 573.2044.

***$^{(iPrO)2}$(P^O)Na***; *$^{(iPrO)2}$(P^O) = (2,6-(iPrO)$_2$C$_6$H$_3$)$_2$P(2-SO$_3$C$_6$H$_4$)*

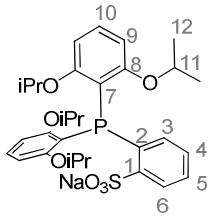


A flask was charged with **$^{(iPrO)2}$(P^O)H** (1.3 g, 2.2 mmol, 1.0 equiv.) and NaH (67 mg, 2.7 mmol, 1.2 equiv.), and THF (20 mL) was added. The mixture was stirred over night and the resulting turbid solution was filtered. Volatiles were removed under vacuum and the resulting residue was dissolved in pentane (50 mL), filtered, and concentrated to 5 mL to yield a white precipitate. The precipitate was isolated by centrifugation and dried under vacuum (991 mg, 1.7 mmol, 71%).

**$^1$H NMR** (400 MHz, acetone-d6): δ = 7.99 (ddd, $^3J_{HH}$ = 7.8, $^4J_{PH}$ = 4.7, $^4J_{HH}$ = 1.4, 1H, 6-H), 7.69 (ddd, $^3J_{HH}$ = 7.8, $^3J_{PH}$ = 4.2, $^4J_{HH}$ = 1.3, 1H, 3-H), 7.20 (vtd, $^3J_{HH}$ = 7.5, $^4J_{HH}$ = 1.4, 1H, 4-H), 7.13 (t, $^3J_{HH}$ = 8.3, 2H, 10-H), 7.06 (td, $^3J_{HH}$ = 7.5, $^4J_{HH}$ = 1.5, 1H, 5-H), 6.45 (dd, $^3J_{HH}$ = 8.3, $^4J_{PH}$= 2.8, 4H, 9-H), 4.39 (hept, $^3J_{HH}$ = 6.2, 4H, 11-H), 0.96 (d, $^3J_{HH}$ = 6.0, 12H, 12a-H), 0.84 (d, $^3J_{HH}$ = 6.1, 12H).

**$^{31}$P{$^1$H} NMR** (162 MHz, acetone-d6): δ = -45.7.

**$^{13}$C{$^1$H} NMR** (101 MHz, acetone-d6): δ = 161.7 (d, $^2J_{PC}$ = 8.2, C8), 151.8 (d, $^2J_{PC}$ = 31.4, C1), 138.0 (d, $^2J_{PC}$ = 2.0, C3), 137.2 (d, $^1J_{PC}$ = 13.3, C2), 129.9 (C10), 128.0 (C4), 127.8 (d, $^3J_{PC}$ = 6.5, C6), 127.4 (C5), 117.2 (d, $^1J_{PC}$ = 13.2, C7), 106.0 (C9), 70.3 (C11), 21.9 (C12b), 21.7 (C12a).

**Anal. Calcd.** (%) for ($C_{30}H_{38}NaO_7PS \times 3\ H_2O$): C, 55.37; H, 6.82; Found: C, 55.28; H, 6.51.

**MS(FAB)**: *m/z* = 613 $[M+Na]^+$, 597 $[M+H]^+$, 575 $[^{(iPrO)2}(PO)H+H]^+$.

***6-Chloro-6H-dibenz[c,e][1,2]oxaphosphorin***[163]

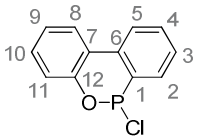


A three neck round bottom flask was charged with 2-phenylphenol (85 g, 0.50 mol, 1.0 equiv.) and $PCl_3$ (82 g, 0.59 mol, 1.2 equiv.) and heated to 150 °C for 6 hours during which HCl evolved. Anhydrous zinc chloride (0.5 g, 3.7 mmol, 0.01 equiv.) was added and the reaction mixture was heated to 180 °C for 2 hours. The reaction mixture was cooled and the excess $PCl_3$ was distilled off under ambient pressure. The residue was distilled under line vacuum (~5 $\times 10^{-2}$ bar) to give the product as a colorless oil which solidified upon cooling (60 g, 0.25 mol, 50%).

**$^{1}$H NMR** (400 MHz, $CDCl_3$): δ = 7.96–7.86 (m, 2H, 5- & 8-H), 7.65–7.53 (m, 2H, 2- & 4-H), 7.42–7.36 (m, 1H, 3-H), 7.34–7.28 (m, 1H, 10-H), 7.25–7.13 (m, 2H, 9- & 11-H).

**$^{31}$P{$^{1}$H} NMR** (162 MHz, $CDCl_3$): 133.3.

**$^{13}$C{$^{1}$H} NMR** (101 MHz, $CDCl_3$): δ = 148.3 (d, $^{2}J_{CP}$ = 9.6, C12), 133.1 (d, $^{1}J_{CP}$ = 36.4, C1), 133.0 (C4), 131.6 (d, $^{2}J_{CP}$ = 3.6, C6), 130.3 (C10), 129.9 (d, $^{2}J_{CP}$ = 52.1, C2), 128.1 (d, $^{3}J_{CP}$ = 13.8, C3), 125.1 (C8), 124.9 (C9), 124.2 (C5), 122.4 (d, $^{3}J_{CP}$ = 6.7, C7), 121.3 (d, $^{3}J_{CP}$ = 2.1, C11).

***oxa*(P^O)H**; *oxa*(P^O) = *cyclo*(2-(2-$OC_6H_4$)$C_6H_4$)P(2-$SO_3C_6H_4$)

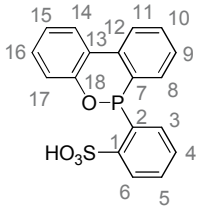


At 0 °C *n*-BuLi (17 mL, 2.5 M in hexane, 42.5 mmol, 2.0 equiv.) was added to a solution of benzene sulfonic acid (3.4 g, 21.0 mmol, 1.0 equiv.) in THF (50 ml) and the reaction mixture was stirred at 25 °C for 1 hour. The suspension formed was cooled to 0 °C and added to a solution of 6-chloro-6H-dibenz[c,e][1,2]oxaphosphorin (5.0 g, 21.0 mmol, 1.0 equiv.) in THF (50 ml). The reaction mixture was stirred over night at 25 °C. The solution was concentrated to 1/3 of its volume and trifluoroacetic acid (1.72 mL, 22.0 mmol, 1.0 equiv.) was added at 0 °C. The reaction mixture was stirred at room temperature for 1 hour. A white precipitate formed which was isolated by filtration, rinsed with THF and $Et_2O$ and dried under vacuum to yield the product as a white solid (1.4 g, 3.9 mmol, 18%).

**$^1$H NMR** (400 MHz, DMSO-$d_6$): δ = 14.50 (s, 1H, -$SO_3$H), 8.32 (dd, $^3J_{PH}$ = 14.1, $^3J_{HH}$ = 7.7, 1H, 3-H), 8.22–8.12 (m, 2H, 11- & 14-H), 7.96 (vt, *J* = 6.6, 1H, 6-H), 7.72–7.55 (m, 3H, 4- & 5- & 6-H), 7.47–7.33 (m, 3H, 8- & 9- & 16-H), 7.25 (vt, $^3J_{HH}$ = 7.6, 1H, 15-H), 7.17 (d, $^3J_{HH}$ = 8.2, 1H, 17-H).

**$^{31}$P NMR** (162 MHz, DMSO-$d_6$): δ = 22.7.

**$^{13}$C{$^1$H} NMR** (101 MHz, DMSO-$d_6$): δ = 151.7 (d, $^2J_{CP}$ = 9.1, C1), 149.8 (d, $^2J_{CP}$ = 8.5, C18), 135.4 (d, $^2J_{CP}$ = 10.3, C3), 134.6 (d, $^2J_{CP}$ = 4.9, C12), 132.9 (d, $^4J_{CP}$ = 2.9, C5), 131.6 (d, $^4J_{CP}$ = 1.9, C10), 129.7 (C16), 129.70 (d, $^2J_{CP}$ = 12.5, C8), 129.1 (d, $^3J_{CP}$ = 10.9, C6), 128.3 (d, $^3J_{CP}$ = 12.6, C4), 127.4 (d, $^3J_{CP}$ = 14.8, C9), 127.2 (d, $^1J_{CP}$ = 134.9, C7), 124.9 (C14), 124.9 (d, $^1J_{CP}$ = 141.8, C2), 123.5 (C15), 122.9 (d, $^3J_{CP}$ = 9.7, C11), 122.0 (d, $^3J_{CP}$ = 11.8, C13), 120.3 (d, $^3J_{CP}$ = 6.8, C17).

**MS(FAB)**: *m/z* = 357 $[M+H]^+$.

**Anal. Calcd.** (%) for ($C_{18}H_{13}O_4PS$): C, 60.67; H, 3.68; Found: C, 60.63; H, 3.83.

## 7.2.5 Syntheses of Complexes

### 7.2.5.1 Syntheses of Phosphine Oxide Complexes

***1-OPBu$_3$***; *[$^{MeO}$(P^O)PdMe(OPBu$_3$)]; $^{MeO}$(P^O) = (2-MeOC$_6$H$_4$)$_2$P(2-SO$_3$C$_6$H$_4$)*

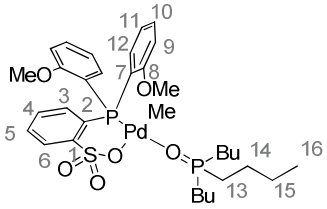


A suspension of [{(**1-Cl**)-μ-Na}$_2$] (99 mg, 0.08 mmol, 1 equiv.), $AgBF_4$ (33 mg, 0.17 mmol, 1.1 equiv.), and $OPBu_3$ (35 mg, 0.16 mmol, 1.0 equiv.) in $CH_2Cl_2$ (5 mL) was stirred for 30 minutes in the dark. The resulting precipitate was filtered off to afford a yellow solution. The filtrate was evaporated. The resulting residue was washed with pentane and dried under vacuum to yield **1-OPBu$_3$** as a beige solid (100 mg, 0.14 mmol, 88 %).

Crystals suitable for X-Ray diffraction analysis were obtained from a saturated toluene solution at -20 °C.

**$^1$H NMR** (400 MHz, $CD_2Cl_2$): δ = 8.02 (dd, $^3J_{HH}$ = 7.1, $^4J_{PH}$ = 4.9, 1H, 6-H), 7.66 (br, 2H, 12-H), 7.52 (vt, *J* = 7.8, 2H, 10-H), 7.43 (vt, *J* = 7.4, 1H, 5-H), 7.32-7.25 (m, 2H, 4-H & 3-H), 7.01 (vt, *J* = 7.4, 2H, 11-H), 6.93 (dd, $^3J_{HH}$ = 7.8, $^4J_{PH}$ = 4.8, 2H, 9-H), 3.60 (s, 6H, OMe), 1.95-1.85 (m, 6H, 13-H), 1.66-1.58 (m, 6H, 14-H), 1.51-1.43 (m, 6H, 15-H), 0.94 (t, $^3J_{HH}$ = 7.3, 9H, 16-H), 0.14 (s, 3H, Pd−$CH_3$).

**$^{31}$P{$^1$H} NMR** (162 MHz, $CD_2Cl_2$): δ = 66.4 (br, $OPBu_3$), 27.2 ($P_{Ar}$).

**$^{13}$C{$^1$H} NMR** (101 MHz, $CD_2Cl_2$): δ = 160.9 (d, $^2J_{PC}$ = 1.4, C8), 148.9 (d, $^2J_{PC}$ = 15.7, C1), 138.4 (br, C12), 135.0 (d, $^2J_{PC}$ = 2.5, C3), 133.7 (C10), 130.5 (C5), 128.6 (br d, $^3J_{PC}$ = 6.0, C4), 128.1 (d, $^1J_{PC}$ = 52.9, C2), 127.9 (d, $^3J_{PC}$ = 8.0, C6), 120.8 (d, $^3J_{PC}$ = 12.4, C11), 117.1 (d, $^1J_{PC}$ = 59.4, C7), 111.9 (d, $^3J_{PC}$ = 4.5, C9), 55.7 (OMe), 27.5 (d, $^1J_{PC}$ = 64.8, C13), 24.7 (d, $^3J_{PC}$ = 14.7, C15), 24.3 (d, $^2J_{PC}$ = 3.8, C14), 14.0 (C16), 0.9 (br, Pd−$CH_3$).

**Anal. Calcd.** (%) for ($C_{33}H_{48}O_6P_2PdS$): C, 53.48; H, 6.53; Found: C, 53.53; H, 6.53.

**MS(FAB):** *m/z* = 740 $[M]^+$, 725 $[M\text{-}Me]^+$, 522 $[M\text{-}OPBu_3]^+$, 507 $[M\text{-}OPBu_3\text{-}Me]^+$, 216 $[OPBu_3+H]^+$.

**ATR-IR:** 1/λ [$cm^{-1}$] = 2956 (m), 2869 (m), 1588 (m), 1575 (m), 1476 (m), 1427 (m), 1248 (s), 1159 (s, $\nu_{asym}(SO_3)$), 1113 (ss, $\nu$(P=O)), 988 (s, $\nu_{sym}(SO_3)$), 747 (s), 669 (m).

***1-OPOct$_3$;*** *[$^{MeO}$(P^O)PdMe(OPOct$_3$)];* $^{MeO}$*(P^O) = (2-MeOC$_6$H$_4$)$_2$P(2-SO$_3$C$_6$H$_4$)*

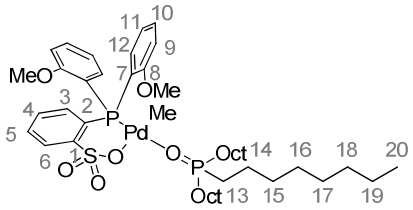


A suspension of [{(**1-Cl**)-μ-Na}$_2$] (92 mg, 0.08 mmol, 1 equiv.), $AgBF_4$ (32 mg, 0.16 mmol, 1.0 equiv.), and $OPOct_3$ (64 mg, 0.16 mmol, 1.0 equiv.) in $CH_2Cl_2$ (5 mL) was stirred for 30 minutes in the dark. The resulting precipitate was filtered off to afford a yellow solution. The filtrate was evaporated. The resulting residue was washed with pentane and dried under vacuum to yield **1-OPOct$_3$** as a beige solid (122 mg, 0.13 mmol, 81 %).

**$^1$H NMR** (400 MHz, $CD_2Cl_2$): δ = 8.03 (dd, $^3J_{HH}$ = 7.6, $^4J_{PH}$ = 4.7, 1H, 6-H), 7.67 (br, 2H, 12-H), 7.51 (vt, *J* = 7.8, 2H, 10-H), 7.42 (vt, *J* = 7.2, 1H, 5-H), 7.35-7.21 (m, 2H, 4-H & 3-H), 7.01 (vt, *J* = 7.5, 2H, 11-H), 6.93 (dd, $^3J_{HH}$ = 8.2, $^4J_{PH}$ = 4.7, 2H, 9-H) , 3.60 (s, 6H, OMe), 1.96-1.84 (m, 6H, 13-H), 1.69-1.56 (m, 6H, 14-H), 1.49-1.40 (m, 6H, 15-H), 1.38-1.21 (m, 24H, 16-H & 17-H & 18-H & 19-H), 0.88 (t, $^3J_{HH}$ = 6.7, 9H, 20-H), 0.14 (s, 3H, Pd−$CH_3$).

**$^{31}$P{$^1$H} NMR** (162 MHz, $CD_2Cl_2$): δ = 65.3 (br, $OPOct_3$), 26.1 ($P_{Ar}$).

**$^{13}$C{$^1$H} NMR** (101 MHz, $CD_2Cl_2$): δ = 160.9 (d, $^2J_{PC}$ = 1.7, C8), 149.2 (br, C1), 138.4 (br, C12), 135.0 (d, $^2J_{PC}$ = 2.7, C3), 133.6 (C10), 130.5 (C5), 128.5 (br d, $^3J_{PC}$ = 8.5, C4), 128.2 (d, $^1J_{PC}$ = 52.8, C2), 128.0 (d, $^3J_{PC}$ = 8.9, C6), 120.8 (d, $^3J_{PC}$ = 12.5, C11), 117.2 (d, $^1J_{PC}$ = 59.7, C7), 111.9 (d, $^3J_{PC}$ = 4.6, C9), 55.7 (OMe), 32.4 (C18), 31.7 (d, $^3J_{CP}$ = 14.3, C15), 29.7 (C16 & C17), 27.8 (d, $^1J_{PC}$ = 64.5, C13), 23.2 (C19), 22.3 (d, $^2J_{PC}$ = 3.8, C14), 14.4 (C20) , 0.9 (br, Pd−$CH_3$).

**Anal. Calcd.** (%) for ($C_{45}H_{72}O_6P_2PdS$): C, 59.43; H, 7.98; Found: C, 58.18; H, 7.87.

**MS(FAB):** *m/z* = 908 $[M]^+$, 893 $[M\text{-}Me]^+$, 773 $[H(OPOct_3)_2]^+$, 522 $[M\text{-}OPOct_3]^+$, 507 $[M\text{-}OPOct_3\text{-}Me]^+$, 387 $[OPOct_3+H]^+$.

**ATR-IR:** 1/$\lambda$ [$cm^{-1}$] = 2923(m), 2853 (m), 1588 (w), 1574 (w), 1476(m), 1464 (m), 1430 (m), 1262 (s), 1251 (s), 1159 (s, $\nu_{asym}(SO_3)$), 1107 (ss, $\nu$(P=O)), 1001 (s, $\nu_{sym}(SO_3)$), 755 (s), 669 (m).

***1-OPPh$_3$;*** *[$^{MeO}$(P^O)PdMe(OPPh$_3$)];* $^{MeO}$*(P^O) = (2-MeOC$_6$H$_4$)$_2$P(2-SO$_3$C$_6$H$_4$)*

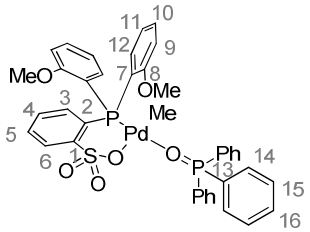


A suspension of [{(**1-Cl**)-μ-Na}$_2$] (131 mg, 0.10 mmol, 1 equiv.), $OPPh_3$ (57 mg, 0.20 mmol, 1.0 equiv.), and $AgBF_4$ (40 mg, 0.21 mmol, 1.0 equiv.) in $CH_2Cl_2$ (20 mL) was stirred for 12 hours in the dark. The resulting precipitate was filtered off to give a yellow solution. The filtrate was evaporated. The resulting residue was suspended in 20 mL pentane and stirred for 3 hours. The precipitate was collected by filtration and dried under vacuum to yield **1-OPPh$_3$** as a slightly yellow solid (125 mg, 0.16 mmol, 80 %).

Crystals suitable for X-Ray diffraction analysis were obtained from a $CHCl_3$ solution after layering with pentane.

**$^1$H NMR** (600 MHz, $CD_2Cl_2$): δ = 8.04-8.00 (m, 1H, 6-H), 7.82-7.75 (m, 6H, 14-H), 7.63-7.48 (m, 13H, 10-H & 12-H & 15-H & 16-H), 7.44-7.40 (m, 1H, 5-H), 7.31-7.24 (m, 2H, 3-H & 4-H), 6.98 (vt, $J$ = 7.2, 2H, 11-H), 6.92 (dd, $^3J_{HH}$ = 7.5, $^4J_{PH}$ = 4.7, 2H, 9-H) , 3.57 (s, 6H, OMe), 0.13 (br s, 3H, Pd−$CH_3$). Note that the Pd-Me shift is very sensitive towards small amounts of impurities, e.g. $H_2O$.

**$^{31}$P{$^1$H} NMR** (162 MHz, $CD_2Cl_2$): δ = 34.9 (br, $OPPh_3$), 27.0 ($P_{Ar}$).

**$^{13}$C{$^1$H} NMR** (151 MHz, $CD_2Cl_2$): δ = 160.9 (C8), 148.9 (br, C1), 138.4 (br, C12), 135.0 (C3), 133.7 (C10), 133.0 (d, $^2J_{PC}$ = 10.2, C14), 132.9 (C16), 131.8 (d, $^1J_{PC}$,= 110.9, C13), 130.5 (C5), 129.1 (d, $^3J_{CP}$ = 12.6, C15), 128.7 (br, C4), 128.1 (br, C6), 128.0 (d, $^1J_{CP}$ = 53.7, C2), 120.9 (d, $^3J_{PC}$ = 12.3, C11), 117.0 (d, $^1J_{PC}$ = 59.3, C7), 111.9 (d, $^3J_{PC}$ = 4.3, C9), 55.7 (OMe), 1.1 (br, Pd−$CH_3$).

**Anal. Calcd.** (%) for ($C_{39}H_{36}O_6P_2PdS$): C, 58.47; H, 4.53; Found: C, 58.47; H, 4.81.

**MS(FAB):** *m/z* = 802 $[M]^+$, 785 $[M\text{-}Me]^+$, 522 $[M\text{-}OPPh_3]^+$, 507 $[M\text{-}OPPh_3\text{-}Me]^+$, 278 $[OPPh_3+H]^+$.

**ATR-IR:** 1/$\lambda$ [$cm^{-1}$] = 3062 (w), 1587 (m), 1574 (m), 1476 (m), 1434 (m), 1253 (s), 1162 (s, $\nu_{asym}(SO_3)$), 1150 (s, $\nu$(P=O)), 1115 (s), 998 (s, $\nu_{sym}(SO_3)$), 755 (s), 723 (ss), 694 (s), 670 (s).

### 7.2.5.2 Syntheses of [{($^{X}$1-Cl)-μ-M}$_n$] Complexes

*[{($^{MeO}$**1-Cl**)-μ-Na}$_2$]; [{($^{MeO}$(P^O)Pd(Me)Cl)-μ-Na}$_2$]; $^{MeO}$(P^O) = (2-MeOC$_6$H$_4$)$_2$P(2-SO$_3$C$_6$H$_4$)*[61]

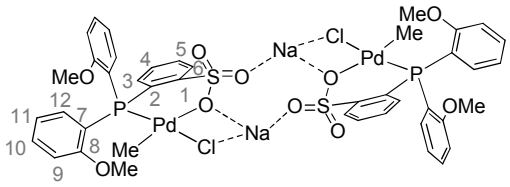


A flask was charged with $^{MeO}$**(P^O)Na** (164 mg, 0.39 mmol, 1.0 equiv.) and [(cod)PdMeCl] (101 mg, 0.38 mmol, 1.0 equiv.). Acetone (4 mL) was added and the reaction mixture was stirred for one hour. The precipitate was isolated by centrifugation and washed with little acetone and $Et_2O$. After drying under vacuum the product was obtained as a white solid (190 mg, 0.32 mmol, 84%).

**$^1$H NMR** (400 MHz, $CD_3OD$, 25 °C): δ = 8.04–7.98 (m, 1H, 6-H), 7.66–7.55 (br m, 1H, 12H), 7.59–7.54 (m, 2H, 10-H), 7.54–7.49 (m, 1H. 5-H), 7.43–7.34 (m, 2H, 4- & 3-H), 7.09–7.00 (m, 4H, 9- & 11-H), 3.64 (s, 6H, OMe), 0.17 (d, J = 1.2, 3H, Pd-Me).

**$^{31}$P{$^1$H} NMR** (162 MHz, $CD_3OD$): δ = 26.8.

**$^{13}$C{$^1$H} NMR** (101 MHz, $CD_3OD$): δ = 161.9 (d, $^2J_{CP}$ = 1.8, C8), 148.3 (d, $^2J_{CP}$ = 14.7, C1), 138.8 (br, C12) , 136.3 (d, $^2J_{CP}$ = 2.9, C3), 134.9 (d, $^4J_{CP}$ = 2.1, C10), 131.4 (d, $^4J_{CP}$ = 2.5, C5), 130.1 (d, $^3J_{CP}$ = 7.6, C4), 129.3 (d, $^1J_{CP}$ = 53.2, C2), 128.2 (d, $^3J_{CP}$ = 8.4, C6), 121.6 (d, $^3J_{CP}$ = 12.6, C11), 116.8 (d, $^1J_{CP}$ = 62.0, C7), 112.7 (d, $^3J_{CP}$ = 4.8, C9), 55.7 (OMe), 0.8 (d, $^2J_{CP}$ = 2.2, Pd-Me).

*[{($^{Ar}$**1-Cl**)-μ-Na}$_n$]; [{($^{Ar}$(P^O)Pd(Me)Cl)-μ-Na}$_n$] $^{Ar}$(P^O) = (2-(2',6'-(MeO)$_2$C$_6$H$_3$)C$_6$H$_4$)$_2$P(2-SO$_3$C$_6$H$_4$))*

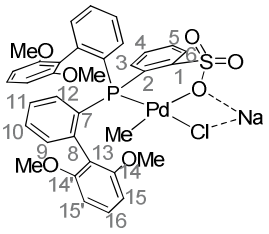


A suspension of $^{Ar}$**(P^O)Na** (80 mg, 0.13 mmol, 1 equiv.) and [(cod)PdMeCl] (34 mg, 0.13 mmol, 1 equiv.) in acetone (5 mL) was stirred for 3 hours. The solvent was removed under vacuum. The remaining residue was washed with $Et_2O$ (3 x 6 mL) and dried under vacuum. A yellow solid was obtained (78 mg, 0.10 mmol, 77%).

**$^1$H NMR** (600 MHz, $CD_3OD$): δ = 7.78 (br s, 2H, 12-H), 7.66 (dd, $^3J_{HH}$ = 7.4, $^3J_{PH}$ = 4.8, 1H, 6-H), 7.40 (vt, $^3J_{HH}$ = 7.5, 2H, 10-H), 7.37–7.30 (m, 1H, 3-H), 7.30 (vt, $^3J_{HH}$ = 7.7, 2H, 11-H), 7.14 (br s, 1H, 5-H), 7.05 (vt, $^3J_{HH}$ = 7.4, 2H, 16-H), 7.02 (dd, $^3J_{HH}$ = 6.8, $^4J_{PH}$ = 4.7, 2H, 9-H), 6.89 (br s, 1H, 4-H), 6.41–6.28 (m, 4H, 15-&15'-H), 3.56 (s, 6H, OMe'), 3.41 (s, 6H, OMe), 0.12 (s, 3H, Pd-Me).

**$^{31}$P{$^1$H} NMR** (162 MHz, $CD_3OD$): δ = 29.7.

**$^{13}$C{$^1$H} NMR** (151 MHz, $CD_3OD$): δ = 158.6 (s, C14), 158.6 (s, C14'), 148.2 (d, $^2J_{CP}$ = 14.1, C1), 141.8 (br s, C8), 138.3 (br s, C12), 136.9 (s, C3), 135.3 (d, $^3J_{CP}$ = 8.9, C9), 132.6 (d, $^1J_{CP}$ = 57.5, C7), 130.9 (s, C10), 130.6 (s, C5), 130.3 (s, C16), 129.4 (s, C4), 128.1 (s, C6), 126.8 (d, $^3J_{CP}$ = 11.1, C11), 119.8 (s, C13), 104.5 (s, C15'), 104.1 (s, C15), 55.5 (s, OMe'), 55.3 (s, OMe), 4.7 (s, Pd-Me). C2 could not be detected.

**Anal. Calcd.** (%) for ($C_{35}H_{33}ClNaO_7PPdS$ × 0.25 $C_5H_{12}$): C, 53.65; H, 4.49; Found: C, 54.04; H, 4.58.

**MS(FAB):** *m/z* = 777 [(P^O)PdCl+Na]$^+$, 756 [(P^O)PdMe+Na]$^+$, 742 [(P^O)Pd+Na]$^+$, 719 [(P^O)Pd]$^+$.

*[{($^{Ph}$**1-Cl**)-μ-Na}$_n$]; [{($^{Ph}$(P^O)Pd(Me)Cl)-μ-Na}$_n$]; $^{Ph}$(P^O) = (2-PhC$_6$H$_4$)$_2$P(2-SO$_3$C$_6$H$_4$)*

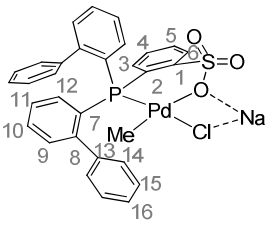


A flask was charged with $^{Ph}$**(P^O)Na** (303 mg, 0.57 mmol, 1.0 equiv.) and [(cod)PdMeCl] (150 mg, 0.57 mmol, 1.0 equiv.). Benzene (2 mL) was added and the reaction mixture was stirred for 1 hour, meanwhile a white precipitate formed. The precipitate was isolated by centrifugation, washed with benzene (2 mL) and $Et_2O$ (8 mL), and dried under vacuum to yield the product as a white solid (280 mg, 0.42 mmol, 74%).

The corresponding lutidine complex was obtained by reaction of [{($^{Ph}$**1-Cl**)-μ-Na}$_n$] with 2,6-lutidine in $CH_2Cl_2$. The solution was filtered and volatiles were removed under vacuum. Crystals for X-ray diffraction were grown from layering a solution of $^{Ph}$**1-lut** in acetone with pentane.

**$^1$H NMR** (600 MHz, acetone-d6): δ = 8.22–8.10 (m, 1H, C12'), 7.95–7.87 (m, 2H, 14-H), 7.71 (dd, $^3J_{HH}$ = 7.6, $^4J_{PH}$ = 5.1, 1H, 6-H), 7.60–7.55 (m, 1H, 10-H), 7.55–7.52 (m, 1H, 10'-H), 7.51–7.45 (m, 1H, 11'-H), 7.39 (vt, $^3J_{HH}$ = 7.5, 1H, 11-H), 7.35–7.32 (m, 1H, 1H, 9-H), 7.27–7.07 (m, 8H, 5- & 9'- & 12- & 15- & 16- 14'-H), 6.98 (t, $^3J_{HH}$ = 7.4, 1H, 16'-H), 6.87 (vt, $^3J_{HH}$ = 7.4, 2H, 15'-H), 6.75 (vt, $^3J_{HH}$ = 7.7, 1H, 4-H), 6.60 (vt, *J* = 9.0, 1H, 3-H), 0.20 (s, 3H, Pd-Me).

**$^{31}$P{$^1$H} NMR** (162 MHz, acetone-d6): δ = 26.2.

**$^{13}$C{$^1$H} NMR** (151 MHz, acetone-d6): δ = 148.4 (d, $^2J_{CP}$ = 14.6, C1), 147.7 (d, $^2J_{CP}$ = 12.8, C8), 146.7 (C8'), 142.5 (C13), 142.3 (C13'), 139.8 (d, $^2J_{CP}$ = 22.7, C12'), 137.0 (C3), 135.4 (d, $^2J_{CP}$ = 2.6, C12), 133.8–133.4 (m, 9 & C9'), 131.4 (C10), 131.3 (C10'), 131.0 (C14), 130.4–129.6 (m, 7 & C7'), 130.2 (C14'), 130.1 (C5), 129.4 (d, $^3J_{CP}$ = 6.8, C4), 128.7 (C15), 128.2–127.5 (m, C2), 128.0 (C15'), 127.9 (C11' & C16'), 127.7–127.6 (m, C11 & C16), 127.4 (d, $^3J_{CP}$ = 8.3, C6), 1.2 (br, Pd-Me).

**Anal. Calcd.** (%) for ($C_{31}H_{25}ClNaO_3PPdS$): C, 55.29; H, 3.74; Found: C, 55.27; H, 4.10.

**MS(FAB):** *m/z* = 657 [(P^O)PdCl+Na]$^+$, 621 [(P^O)PdMe+Li]$^+$, 615 [(P^O)PdMe+H]$^+$, 599 [(P^O)Pd]$^+$.

*[{($^{(MeO)3}$**1-Cl**)-μ-Na}$_n$]; [{($^{(MeO)3}$(P^O)Pd(Me)Cl)-μ-Na}$_n$]; $^{(MeO)3}$(P^O) = (2,4,6-(OMe)$_3$C$_6$H$_2$)$_2$P(2-SO$_3$C$_6$H$_4$)*

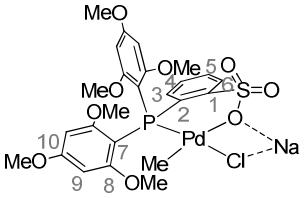


A flask was charged with $^{(MeO)3}$**(P^O)Na** (108 mg, 0.20 mmol, 1.0 equiv.) and [(cod)PdMeCl] (53 mg, 0.20 mmol, 1.0 equiv.). Acetone (3 mL) was added and the reaction mixture was stirred for 30 minutes. The resulting precipitate was isolated by centrifugation, washed with pentane and dried under vacuum to yield the desired product as a white solid (100 mg, 0.15 mmol, 73%).

The corresponding lutidine complex was obtained by reaction of [{($^{(MeO)3}$**1-Cl**)-μ-Na}$_n$] with 2,6-lutidine in $CH_2Cl_2$. The solution was filtered and volatiles were removed under vacuum. Crystals for X-ray diffraction were grown by layering a solution of $^{(MeO)3}$**1-lut** in $CH_2Cl_2$ with pentane.

**$^1$H NMR** (600 MHz, $CD_3OD$): δ = 7.94 (ddd, $^3J_{HH}$ = 7.8, $^4J_{PH}$ = 4.7, $^4J_{HH}$ = 1.2, 1H, 6-H), 7.52 (ddd, $^3J_{PH}$ = 11.8, $^3J_{HH}$ = 7.9, $^4J_{HH}$ = 1.4, 1H, 3-H), 7.37 (vtt, $^3J_{HH}$ = 7.6, $J$ = 1.5, 1H, 5-H), 7.30 (vt, $^3J_{HH}$ = 7.6, 1H, 4-H), 6.16 (d, $^4J_{PH}$ = 3.8, 4H, 9-H), 3.82 (s, 6H, *p*-OMe), 3.55 (s, 12H, *o*-OMe), 0.24 (s, 3H, PdMe).

**$^{31}$P{$^1$H} NMR** (162 MHz, $CD_3OD$): δ = -9.8.

**$^{13}$C{$^1$H} NMR** (151 MHz, $CD_3OD$): δ = 165.5 (C10), 164.3 (d, $^2J_{CP}$ = 1.6, C8), 147.0 (d, $^2J_{CP}$ = 15.5, C1), 136.0 (C3), 133.6 (d, $^1J_{CP}$ = 55.2, C2), 129.7 (C5), 128.9 (d, $^3J_{CP}$ = 7.3, C4), 128.1 (d, $^3J_{CP}$ = 8.6, C6), 99.4 (d, $^1J_{CP}$ = 66.6, C7), 92.1 (d, $^3J_{CP}$ = 5.1, C9), 55.9 (*o*-OMe), 55.8 (*p*-OMe), -0.2 (br, PdMe).

**Anal. Calcd.** (%) for ($C_{25}H_{29}ClNaO_9PPdS$): C, 42.81; H, 4.17; Found: C, 42.39; H, 4.21.

**MS(FAB):** *m/z* = $[(P^O)PdCl+Na]^+$, $[(P^O)PdMe+Na]^+$, $[(P^O)PdMe+H]^+$, $[(P^O)Pd]^+$.

*[{(**(MeO)2**1-Cl)-μ-Na}n]; [{(*(MeO)2*(P^O)Pd(Me)Cl)-μ-Na}n]; *(MeO)2*(P^O) = (2,6-(OMe)2C6H3)2P(2-SO3C6H4)*

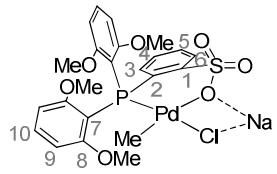


A flask was charged with **(MeO)2(P^O)Na** × 0.75 THF (58 mg, 0.11 mmol, 1.1 equiv.) and [(cod)PdMeCl] (26 mg, 0.10 mmol, 1.0 equiv.). Acetone (4 mL) was added and the reaction mixture was stirred for 5 minutes. The slightly turbid solution was filtered and volatiles were removed under vacuum. The remaining solid was washed twice with $Et_2O$ and pentane and dried under vacuum to yield the desired product as a white solid (50 mg, 0.08 mmol, 80%).

The corresponding pyridine complex was obtained by reaction of [{(**(MeO)2**1-Cl)-μ-Na}n] with pyridine in $CH_2Cl_2$. The solution was filtered and volatiles were removed under vacuum. Crystals for X-ray diffraction were grown by layering a solution of **(MeO)2**1-py in acetone with pentane.

**$^1$H NMR** (400 MHz, acetone-d6): δ = 7.92 (ddd, $^3J_{HH}$ = 7.9, $^4J_{PH}$ = 4.8, $^4J_{HH}$ = 1.4, 1H, 6-H), 7.48 (ddd, $^3J_{PH}$ = 11.2, $^3J_{HH}$ = 7.8, $^4J_{HH}$ = 1.4, 1H, 3-H), 7.34 (t, $^3J_{HH}$ = 8.3, 2H, 10-H), 7.37–7.30 (m, 1H, 5-H), 7.26 (vt, $^3J_{HH}$ = 7.7, 1H, 4-H), 6.59 (dd, $^3J_{HH}$ = 8.3, $^4J_{PH}$ = 4.1, 4H, 9-H), 3.54 (s, 12H, OMe), 0.32 (d, $^3J_{PH}$ = 2.7, 3H, PdMe).

**$^{31}$P{$^1$H} NMR** (162 MHz, acetone-d6): δ = -11.6.

**$^{13}$C{$^1$H} NMR** (151 MHz, acetone-d6): δ = 162.9 (C8), 148.5 (d, $^2J_{CP}$ = 16.5, C1), 135.6 (C3), 132.7 (C10), 132.3 (d, $^1J_{CP}$ = 54.1, C2), 129.0 (C5), 127.9 (d, $^3J_{CP}$ = 8.7, C6), 127.7 (d, $^3J_{CP}$ = 6.7, C4), 108.6 (d, $^1J_{CP}$ = 55.6, C7), 105.2 (d, $^3J_{CP}$ = 4.5, C9), 55.9 (OMe), -2.6 (br, PdMe).

**Anal. Calcd.** (%) for ($C_{23}H_{25}O_7PPdS$ × ½NaCl): C, 45.13; H, 4.12; Found: C, 44.95; H, 4.39.

**MS(FAB):** *m/z* = 625 [(P^O)PdCl+Na]$^+$, 605 [(P^O)PdMe+Na]$^+$, 590 [(P^O)Pd+Na]$^+$, 567 [(P^O)Pd]$^+$.

*[{(**cHexO1-Cl**)-μ-Li}]$_n$; [{($^{cHexO}$(P^O)Pd(Me)Cl)-μ-Li}$_n$]; $^{cHexO}$ (P^O) = (2-($C_6H_{11}O$)$C_6H_4$)$_2$P(2-$SO_3C_6H_4$)*

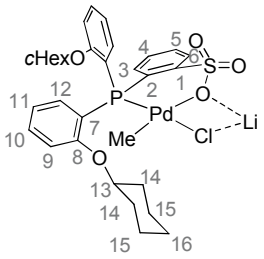


A flask was charged with **$^{cHexO}$(P^O)Li** (214 mg, 0.39 mmol, 1.1 equiv.) and [(cod)PdMeCl] (95 mg, 0.36 mmol, 1.0 equiv.). Acetone (6 mL) was added and the reaction mixture was stirred for 5 minutes, filtered, and volatiles were removed under vacuum. The remaining residue was washed with $Et_2O$ (4 mL) and pentane (8 mL). After drying under vacuum the product was obtained as a white solid (160 mg, 0.23 mmol, 64%).

**$^1$H NMR** (600 MHz, acetone-d6): δ = 9.14–8.83 (m, 1H, 12-H), 7.95 (s, 1H, 6-H), 7.60 (dd, $^3J_{PH}$ = 11.5, $^3J_{HH}$ = 7.8, 1H, 3-H), 7.49–7.40 (m, 3H, 10- & 10'- & 5-H), 7.36 (vt, $^3J_{HH}$ = 7.7, 1H, 4-H), 7.13–7.00 (m, 3H, 9'-, 11- & 12'-H), 6.97 (s, 1H, 9-H), 6.88 (s, 1H, 11'-H), 4.43 (s, 1H, 13-H), 4.26 (s, 1H, 13'-H), 2.00–0.75 (m, 20H, 14-16-H & 14'-16'-H), 0.23 (s, 3H, Pd-Me).

**$^{31}$P{$^1$H} NMR** (162 MHz, acetone-d6): δ = 25.8.

**$^{13}$C{$^1$H} NMR** (151 MHz, acetone-d6): δ = 160.0 (C8), 159.0 (C8'), 149.1 (d, $^2J_{CP}$ = 11.1, C1), 145.4 (d, $^2J_{CP}$ = 22.8, C12), 137.4 (C3), 135.7 (C12'), 134.3 (C10/10'), 133.0 (C10/10'), 130.1 (C5), 129.45 (d, $^1J_{CP}$ = 78.1, C2), 128.9 (d, $^3J_{CP}$ = 7.2, C4), 127.4 (d, $^3J_{CP}$ = 8.3, C6), 120.4 (C11), 119.4 (C11'), 117.9 (d, $^1J_{CP}$ = 59.9, 7/7'), 116.3 (d, $^1J_{CP}$ = 54.3, 7/7'), 112.4 (C9'), 112.1 (C9), 76.6 (C13'), 75.6 (C13), 32.6 (C14/14'), 32.2 (C14/14'), 32.1 (C14/14'), 31.8 (C14/14'), 26.2 (C16 & C16'), 25.1 (C15/15'), 24.9 (C15/15'), 23.6 (C15/15'), 23.5 (C15/15'), -2.0 (Pd-Me).

**Anal. Calcd.** (%) for ($C_{31}H_{37}ClLiO_5PPdS$): C, 53.08; H, 5.32; Found: C, 52.96 H, 5.58.

**MS(FAB):** *m/z* = 678 [(P^O)PdCl+H]$^+$, 659 [(P^O)PdMe+H]$^+$, 643 [(P^O)Pd]$^+$.

*[{(^(MeO;Me2)1-Cl)-μ-Li}$_n$]; [{(^(MeO;Me2) (P^O)Pd(Me)Cl)-μ-Na}$_n$]; ^(MeO;Me2)(P^O) = (2-MeO-3,6-(Me)$_2$C$_6$H$_2$)$_2$P(2-SO$_3$C$_6$H$_4$))*

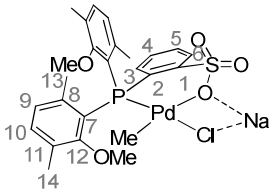


A flask was charged with **^(MeO;Me2)(P^O)Na** (197 mg, 0.41 mmol, 1.0 equiv.) and [(cod)PdMeCl] (109 mg, 0.41 mmol, 1.0 equiv.). Acetone (4 mL) was added and the reaction mixture was stirred for 10 minutes to yield a yellow solution. Volatiles were removed under vacuum. The remaining yellow solid was washed with pentane (3 x 8 mL). Removal of solvents under vacuum yielded a white solid (188 mg, 0.29 mmol, 71%).

The corresponding lutidine complex was obtained by reaction of [{(^(MeO;Me2)**1-Cl**)-μ-Na}$_n$] with 2,6-lutidine in $CH_2Cl_2$. The solution was filtered and volatiles were removed under vacuum. Crystals for X-ray diffraction were grown by layering a solution of ^(MeO;Me2)**1-lut** in $CH_2Cl_2$ with pentane.

**$^1$H NMR** (600 MHz, acetone-d6): δ = 7.93 (ddd, $^3J_{HH}$ = 7.7, $^4J_{PH}$ = 4.7, $^4J_{HH}$ = 1.4, 1H, 6-H), 7.52 (ddd, $^3J_{PH}$ = 10.8, $^3J_{HH}$ = 7.9, $^4J_{HH}$ = 1.3, 1H, 3-H), 7.43 (vtt, $^3J_{HH}$ = 7.4, *J* = 1.4, 1H, 5-H), 7.31 (vtt, $^3J_{HH}$ = 7.6, *J* = 1.3, 1H, 4-H), 7.25 (d, $^3J_{HH}$ = 7.6, 1H, 10'-H), 7.12 (d, $^3J_{HH}$ = 7.7, 1H, 10-H), 6.96 (dd, $^3J_{HH}$ = 7.7, $^4J_{PH}$ = 4.5, 1H, 9'-H), 6.89 (dd, $^3J_{HH}$ = 7.8, $^4J_{HH}$ = 5.6, 1H, 9-H), 3.39 (s, 3H, 13-H), 3.28 (s, 3H, OMe), 3.14 (s, 3H, OMe'), 2.65 (s, 3H, 13'-H), 2.20 (s, 3H, 14'-H), 2.10 (s, 3H, 14-H), 0.41 (d, $^3J_{PH}$ = 3.4, 3H, Pd-Me).

**$^{31}$P{$^1$H} NMR** (162 MHz, acetone-d6): δ = -0.9.

**$^{13}$C{$^1$H} NMR** (151 MHz, acetone-d6): δ = 162.9 (C12), 162.4 (C12'), 148.8 (d, $^2J_{CP}$ = 15.3, C1), 142.9 (d, $^2J_{CP}$ = 16.3, C8), 141.9 (d, $^2J_{CP}$ = 10.8, C8'), 137.0 (C3), 135.0 (C10), 134.1 (C10'), 131.9 (d, $^1J_{CP}$ = 48.8, C2), 130.0 (d, $^4J_{CP}$ = 2.3, C5), 129.5 (d, $^3J_{CP}$ = 4.1, C11'), 128.6 (d, $^3J_{CP}$ = 5.4, C4), 128.6 (d, $^3J_{CP}$ = 10.9, C9'), 128.1 (d, $^3J_{CP}$ = 8.7, C6), 127.1 (d, $^3J_{CP}$ = 11.0, C9), 126.3 (d, $^3J_{CP}$ = 4.3, C11'), 124.4 (d, $^1J_{CP}$ = 49.0, C7), 124.0 (d, $^1J_{CP}$ = 50.6, C7'), 60.4 (OMe'), 59.8 (OMe), 27.1 (d, $^3J_{CP}$ = 14.2, C13), 25.3 (d, $^3J_{CP}$ = 13.2, C13'), 18.0 (C14), 16.9 (C14'), 1.9 (br, Pd-Me).

**Anal. Calcd.** (%) for ($C_{25}H_{29}ClNaO_5PPdS$): C, 47.11; H, 4.59; Found: C, 47.16; H, 5.03.

**MS(FAB)**: m/z = 643 $[M+Li]^+$, 621 $[(P^O)PdCl+Na]^+$, 601 $[(P^O)PdMe+Na]^+$, 585 $[(P^O)PdMe+Li]^+$, 563 $[(P^O)Pd]^+$.

*[{($^{Thy}$**1-Cl**)-μ-Na}$_n$]; [{($^{Thy}$(P^O)Pd(Me)Cl)-μ-Na}$_n$]; $^{Thy}$(P^O) = (2-MeO-3-iPr-6-MeC$_6$H$_2$)$_2$P(2-SO$_3$C$_6$H$_4$)*

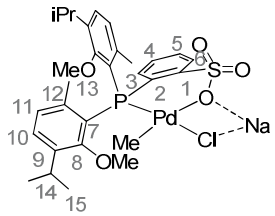


A flask was charged with $^{Thy}$**(P^O)Na** (500 mg, 0.8 mmol, 1.0 equiv.) and [(cod)PdMeCl] (215 mg, 0.8 mmol, 1.0 equiv.). Acetone (20 mL) was added and the reaction mixture was treated in an ultrasonic bath for 15 minutes. Volatiles were removed under vacuum and the residue was dissolved in $Et_2O$ (5 mL) and filtered. Volatiles were removed under vacuum to yield an orange solid which was washed with pentane (2 x 8 mL) and dried under vacuum (543 mg, 0.78 mmol, 97%).

**$^1$H NMR** (400 MHz, acetone-d6): δ = 7.95 (m, 1H, 6-H), 7.52-7.44 (m, 2H, 3- & 5-H), 7.38-7.29 (m, 3H, 4- & 10- & 10'-H), 7.01 (m, 2H, 11- & 11'-H), 3.34 (s, 3H, 13-H), 3.08 (s, 3H, MeO'), 3.06 (s, 3H, MeO), 2.64 (s, 3H, 13'-H), 1.23-1.11 (m, 12H, 15- & 15'-H), 0.43 (d, $^3J_{HP}$ = 3.1, Pd-Me).

**$^{31}$P{$^1$H} NMR** (162 MHz, acetone-d6): δ = 0.32.

**$^{13}$C{$^1$H} NMR** (101 MHz, acetone-d6): δ = 162.4 (d, $^2J_{CP}$ = 2.1, C8), 161.6 (C8'), 149.2 (d, $^2J_{CP}$ = 15.0, C1), 142.9 (d, $^2J_{CP}$ = 15.9, C12), 141.8 (d, $^2J_{CP}$ = 10.2, C12'), 140.4 (d, $^3J_{CP}$ = 3.8, C9'), 138.3 (d, $^4J_{CP}$ = 3.7, C9), 136.9 (d, $^2J_{CP}$ = 1.8, C3), 132.2 (d, $^1J_{CP}$ = 49.2, C2), 130.4 (C10), 130.1 (d, $^4J_{CP}$ = 1.8, C5), 129.8 (C10'), 129.3–129.0 (m, 2C, C4 & C11'), 128.3–128.0 (m, 2C, C6 & C11), 124.4 (d, $^1J_{CP}$ = 47.4, C7), 123.7 (d, $^1J_{CP}$ = 50.8, C7), 62.2 (MeO'), 61.9 (MeO), 27.3 (C14), 27.0 (C14'), 27.0 (d, $^3J_{CP}$ = 13.9, C13), 25.4 (d, $^3J_{CP}$ = 13.2, C13'), 24.5 (C9'a), 24.4 (C9a , 23.7 (C9'b), 23.5 (C9b), 2.6 (br, Pd-Me).

**Anal. Calcd.** (%) for ($C_{29}H_{37}ClNaO_5PPdS$): C, 50.22; H, 5.38; Found: C, 51.58; H, 5.84.

**MS(ESI,neg):** *m/z* = 671.1 [M-Na]$^-$.

*[{(**[Car]1-Cl**)-μ-Na}$_n$]; [{([Car](P^O)Pd(Me)Cl)-μ-Na}$_n$]; [Car](P^O) = (2-MeO-3-Me-6-iPrC$_6$H$_2$)$_2$P(2-SO$_3$C$_6$H$_4$)*

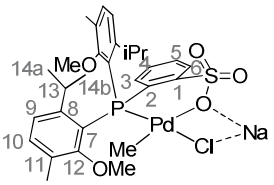


A flask was charged with **[Car](P^O)Na** (142 mg, 0.26 mmol, 1.0 equiv.) and [(cod)PdMeCl] (70 mg, 0.26 mmol, 1.0 equiv.). Acetone (7 mL) was added and the reaction mixture was treated in an ultrasonic bath for 5 minutes. Volatiles were removed under vacuum. The remaining yellow solid was dissolved in $Et_2O$ (5 mL) to yield a clear solution from which a white solid precipitated. The precipitate was isolated by centrifugation, washed with pentane (8 mL) and dried under vacuum to yield the product as a white solid (106 mg, 0.15 mmol, 57%).

**$^1$H NMR** (600 MHz, acetone-d6): δ = 7.93 (ddd, $^3J_{HH}$ = 7.7, $^4J_{PH}$ = 4.6, $^4J_{HH}$ = 1.6, 1H, 6-H), 7.57 (ddd, $^3J_{PH}$ = 10.9, $^3J_{HH}$ = 7.8, , $^4J_{HH}$ = 1.4, 1H, 3-H), 7.41 (vtt, $^3J_{HH}$ = 7.6, *J* = 1.6, 1H, 5-H), 7.35 (vtt, $^3J_{HH}$ = 7.4, *J* = 1.3, 1H, 4-H), 7.28 (d, $^3J_{HH}$ = 8.0, 1H, 10'-H), 7.22 (d, $^3J_{HH}$ = 8.0, 1H, 10-H), 7.13–7.08 (m, 2H, 11- & 11'-H), 5.37 (br m, 1H, 13-H), 4.48 (br m, 1H, 13'-H), 3.40 (s, 3H, OMe), 3.24 (s, 3H, OMe'), 2.22 (s, 3H, Ar-Me'), 2.12 (s, 3H, Ar-Me), 1.34 (d, $^3J_{HH}$ = 6.5, 3H, 14a-H), 1.20 (d, $^3J_{HH}$ = 6.7, 3H, 14b-H), 1.13 (d, $^3J_{HH}$ = 6.5, 3H, 14a'-H), 0.92 (d, $^3J_{HH}$ = 6.5, 3H, 14b'-H), 0.57 (d, $^3J_{PH}$ = 3.5, 3H, Pd-Me).

**$^{31}$P{$^1$H} NMR** (162 MHz, acetone-d6): δ = -2.1.

**$^{13}$C{$^1$H} NMR** (151 MHz, acetone-d6): δ = 161.9 (C12), 161.5 (C12'), 154.1 (d, $^2J_{CP}$ = 13.2, C8), 152.8 (d, $^2J_{CP}$ = 10.3, C8'), 148.5 (d, $^2J_{CP}$ = 16.9, C1), 138.8 (C3), 135.2 (C10), 134.9 (C10'), 129.7 (C5), 128.7 (d, $^3J_{CP}$ = 6.8, C4), 128.3 (d, $^3J_{CP}$ = 4.4, C11'), 127.6 (d, $^3J_{CP}$ = 8.2, C6), 126.0 (d, $^3J_{CP}$ = 4.2, C11'), 124.8 (d, $^1J_{CP}$ = 53.8, C7), 123.9 (d, $^3J_{CP}$ = 9.3, C9'), 123.9 (d, $^1J_{CP}$ = 48.9, C7'), 122.9 (d, $^3J_{CP}$ = 10.2, C9), 60.7 (OMe), 60.3 (OMe'), 32.4 (d, $^3J_{CP}$ = 12.9, C13'), 31.5 (d, $^3J_{CP}$ = 13.9, C13), 26.3 (C14b), 25.9 (C14a'), 25.7 (C14a), 24.3 (C14b`), 18.1 (Ar-Me), 17.8 (Ar-Me'), 1.7 (vbr, Pd-Me). C2 could not be detected.

**Anal. Calcd.** (%) for ($C_{29}H_{37}O_5PPdS$×½NaCl): C, 52.43; H, 5.61; Found: C, 52.45; H, 5.83.

*[{(**$^{H}$1-Cl**)-μ-Li}$_n$]; [{($^{H}$(P^O)Pd(Me)Cl)-μ-Na}$_n$]; (P^O) = $Ph_2P(2\text{-}SO_3C_6H_4)$*

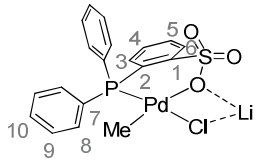


A flask was charged with **$^{H}$(P^O)Li** (308 mg, 0.88 mmol, 1.03 equiv.) and [(cod)PdMeCl] (225 mg, 0.85 mmol, 1.00 equiv.). Acetone (15 mL) was added and the suspension was stirred for 3 hours. The precipitate was isolated by filtration, rinsed with acetone and $Et_2O$, and dried under vacuum. The product contained 1 equiv. of acetone which was quantified by NMR-spectroscopy (443 mg, 0.78 mmol, 92%).

**$^{1}$H NMR** (600 MHz, $CD_3OD$): δ = 8.09 (ddd, $^{3}J_{HH}$ = 7.8, $^{4}J_{PH}$ = 4.1, $^{4}J_{HH}$ = 1.3, 1H, 6-H), 7.61 (vtt, $^{3}J_{PH}$ = 7.7, *J* = 1.4, 1H, 5-H), 7.59–7.51 (m, 6H, 8- & 10-H), 7.50–7.44 (m, 5H, 4- & 9-H), 7.10 (ddd, $^{3}J_{PH}$ = 10.1, $^{3}J_{HH}$ = 7.8, $^{4}J_{HH}$ = 1.2, 1H, 3-H), 0.51 (d, $^{3}J_{PH}$ = 2.1, 3H, Pd-Me).

**$^{31}$P{$^{1}$H} NMR** (162 MHz, $CD_3OD$): δ = 30.4.

**$^{13}$C{$^{1}$H} NMR** (151 MHz, $CD_3OD$): δ = 149.4 (d, $^{2}J_{CP}$ = 13.6, C1), 136.4 (d, $^{3}J_{CP}$ = 2.3, C3), 135.3 (d, $^{2}J_{CP}$ = 12.3, C8), 132.3 (C5), 132.3 (d, $^{4}J_{CP}$ = 2.6, C10), 131.7 (d, $^{4}J_{CP}$ = 6.6, C4), 131.2 (d, $^{1}J_{CP}$ = 57.1, C7), 130.5 (d, $^{1}J_{CP}$ = 44.5, C2), 129.8 (d, $^{3}J_{CP}$ = 11.1, C9), 128.8 (d, $^{2}J_{CP}$ = 7.6, C6), -0.3 (Pd-Me).

**Anal. Calcd.** (%) for ($C_{19}H_{17}ClLiO_3PPdS\times H_2O$): C, 43.62; H, 3.66; Found: C, 43.68 H, 3.83.

**MS(ESI):** *m/z* = 500.8 [(PO)PdMe + K]$^{+}$; 574.9 [(PO)PdMe + Na]$^{+}$; 464.9 [(PO)PdMe + H]$^{+}$.

*[{($^{Me*/(MeO)3}$**1-Cl**)-μ-Na}$_n$]; [{($^{Me*/(MeO)3}$(P^O)Pd(Me)Cl)-μ-Na}$_n$]; $^{Me*/(MeO)3}$(P^O) = (Me)(2,4,6-(OMe)$_2$C$_6$H$_2$)P(2-SO$_3$C$_6$H$_4$)*

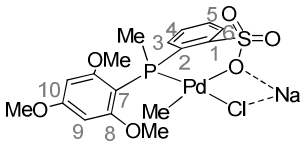


A flask was charged with $^{Me*/(MeO)3}$**(P^O)Na** (25 mg, 60 μmol, 1.0 equiv.) and [(cod)PdMeCl] (16 mg, 60 μmol, 1.0 equiv.). Acetone (0.6 mL) was added and the reaction mixture was stirred for 5 minutes. The slightly turbid solution was filtered and volatiles were removed under vacuum. The remaining solid was washed twice with $Et_2O$ and pentane and dried under vacuum to yield the desired product as a white solid (18 mg, 0.32 μmol, 53%).

**$^1$H NMR** (400 MHz, $CD_3OD$): δ = 8.07-7.98 (m, 1H, 6-H), 7.55-7.46 (m, 1H, 5-H), 7.43-7.33 (m, 1H, 4-H), 7.31-7.22 (m, 1H. 3-H), 6.27 (d, $^4J_{HP}$ = 3.7, 2H, 9-H), 3.86 (s, 3H, p-MeO), 3.72 (s, 6H, o-MeO), 2.11 (d, $^2J_{HP}$ = 11.9, 3H, Me-P), 0.27 (d, $^3J_{HP}$ = 1.6, 3H, Pd-Me).

**$^{31}$P{$^1$H} NMR** (162 MHz, $CD_3OD$): δ = 11.0.

**$^{13}$C{$^1$H} NMR** (101 MHz, $CD_3OD$): δ = 166.5 (C10), 164.3 (d, $^2J_{CP}$ = 1.4, C8), 147.2 (C1), 135.4 (d, $^1J_{CP}$ = 63.0, C2), 132.7 (d, $^2J_{CP}$ = 2.3, C3), 131.7 (d, $^3J_{CP}$ = 7.4, C4), 131.1 (d, $^4J_{CP}$ = 2.1, C5), 128.2 (d, $^3J_{CP}$ = 8.0, C6), 99.5 (d, $^1J_{CP}$ = 71.4 ,C7), 92.7 (d, $^2J_{CP}$ = 5.0, C9), 56.3 (*o*-MeO), 56.1 (*p*-MeO), 18.4 (d, $^1J_{CP}$ = 36.0, Me-P), -3.6 (br, Pd-Me).

**Anal. Calcd.** (%) for ($C_{17}H_{21}ClNaO_6PPdS$ x ¼ $OC(CH_3)_2$, ⅛ $Et_2O$)[a]: C, 38.25; H, 4.18; Found: C, 38.63; H, 4.56.

**MS(FAB):** *m/z* = 432.9 [(P^O)PdCl+Na]$^+$, 517.9 [(P^O)PdMe+Na]$^+$, 490.9 [(P^O)PdMe+H]$^+$, 474.8 [(P^O)Pd]$^+$.

[a]in agreement with $^1$H NMR.

*[{(**CF3**1-Cl)-μ-Li}$_n$]; [{(*$^{CF3}$*(P^O)Pd(Me)Cl)-μ-Li}$_n$]; $^{CF3}$(P^O) = (2-CF$_3$C$_6$H$_4$)$_2$P(2-SO$_3$C$_6$H$_4$)*

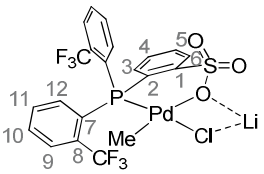


A flask was charged with **$^{CF3}$(P^O)Li** (184 mg, 0.38 mmol, 1.0 equiv.) and [(cod)PdMeCl] (100 mg, 0.38 mmol, 1.0 equiv.). Acetone (5 mL) was added and a clear solution formed within minutes. Volatiles were removed under vacuum and the residue was washed with $Et_2O$ (2 x 5 mL) and pentane (8 mL). After drying under vacuum the product was obtained as a white solid (179 mg, 0.28 mmol, 74%).

The corresponding lutidine complex was obtained by reaction of [{(**$^{CF3}$1-Cl**)-μ-Li}$_n$] with 2,6-lutidine in $CH_2Cl_2$. The solution was filtered and volatiles were removed under vacuum. Crystals for X-ray diffraction were grown by layering a solution of **$^{CF3}$1-lut** in acetone with $Et_2O$.

**$^1$H NMR** (600 MHz, acetone-d6): δ = 9.11–8.77 (m, 1H, 12'-H), 8.07–8.03 (m, 1H, 6-H), 8.01 (dd, $^3J_{HH}$ = 7.9, $^4J_{PH}$ = 4.6, 1H, 9-H), 7.90–7.86 (m, 1H, 9'-H), 7.86–7.77 (m, 3H, 10- & 10'- & 11'-H), 7.62 (m, 2H, 5- & 11-H), 7.49 (vt, $^3J_{HH}$ = 7.7, 1H, 4-H), 7.29 (vt, *J* = 9.5, 1H, 3-H), 7.02 (dd, $^3J_{PH}$ = 12.1, $^3J_{HH}$ = 8.0, 1H, 12-H), 0.48 (d, $^3J_{HP}$ = 3.4, 3H, Pd-Me).

**$^{31}$P{$^1$H} NMR** (162 MHz, acetone-d6): δ = 41.4 (br).

**$^{19}$F{$^1$H} NMR** (376 MHz, acetone-d6): δ = 125.1 (d, $^4J_{FP}$ = 21.8, $CF_3$), 122.1 (br s, $CF_3$).

**$^{13}$C{$^1$H} NMR** (151 MHz, acetone-d6): δ = 149.6 (d, $^2J_{PH}$ = 15.3, C1), 144.0 (br d, $^2J_{PH}$ = 28.2, C12'), 136.9 (d, $^2J_{PH}$ = 4.6, C12), 135.6 (C3), 134.0 (qd, $^2J_{FH}$ = 31.9, $^2J_{PH}$ = 9.5, C8), 133.2 (d, $^3J_{PH}$ = 15.0, C11'), 133.0–132.4 (m, C8'), 132.7 (C10'), 132.7 (d, $^3J_{PH}$ = 8.1, C11), 132.4 (C10), 132.0 (C5), 130.2 (vt, *J* = 5.8, C9), 130.0 (d, $^1J_{PH}$ = 40.2, C7'), 129.9 (d, $^3J_{PH}$ = 7.3, C4), 129.1 (vt, *J* = 6.0, C9'), 128.8 (d, $^3J_{PH}$ = 7.5, C6), 128.5–128.1 (m, C2 & C7), 125.3 (q, $^1J_{CF}$ = 275.6, $CF_3$), 124.5 (q, $^1J_{CF}$ = 274.5, $CF_3$').

**Anal. Calcd.** (%) for ($C_{21}H_{15}ClF_6LiO_3PPdS$): C, 39.34; H, 2.82; Found: C, 39.13 H, 2.82.

**MS(FAB):** *m/z* = 641 [(P^O)PdCl+Na]$^+$, 621 [(P^O)PdMe+Na]$^+$, 599 [(P^O)PdMe+H]$^+$, 583 [(P^O)Pd]$^+$.

*[{(**cHex/(MeO)2**1-Cl)-μ-Li}n]; [{(cHexO/(MeO)2(P^O)Pd(Me)Cl)-μ-Li}n]; cHexO/(MeO)2(P^O) = (2-(C6H11O)C6H4)(2,6-(OMe)2C6H3)P(2-SO3C6H4)):*

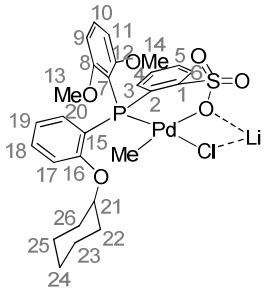


A flask was charged with crude **cHexO/(MeO)2(P^O)Li** (142 mg, 0.28 mmol, 1.0 equiv.) and [(cod)PdMeCl] (81 mg, 0.31 mmol, 1.1 equiv.). Acetone (2.5 mL) was added and the solution was stirred for 5 minutes. Upon standing a precipitate formed. The precipitate was isolated by centrifugation and dried under vacuum. The product was obtained containing 0.5 equiv. of acetone (85 mg, 0.12 mmol, 43%).

The corresponding lutidine complex was obtained by reaction of [{(**cHexO/(MeO)2****1-Cl**)-μ-Li}n] with 2,6-lutidine in $CH_2Cl_2$. The solution was filtered and volatiles were removed under vacuum. Crystals for X-ray diffraction were obtained from a saturated solution of **cHex/(MeO)2****1-lut** in toluene.

**$^1$H NMR** (600 MHz, $CD_3OD$): δ = 7.95 (ddd, $^3J_{HH}$ = 7.9, $^4J_{PH}$ = 4.5, $^4J_{HH}$ = 1.3, 1H, 6-H), 7.54 (dd, $^3J_{PH}$ = 11.5, $^3J_{HH}$ = 8.2, 1H, 3-H), 7.50–7.41 (m, 4H, 5- & 10- & 18- & 20-H), 7.34 (vt, $^3J_{HH}$ = 7.7, 1H, 4-H), 6.94 (dd, $^3J_{HH}$ = 8.3, $^4J_{PH}$ = 5.2, 1H, 17-H), 6.89 (vtd, $^3J_{HH}$ = 7.5, $^4J_{HH}$ = 1.5, 1H, 19-H), 6.79–6.74 (m, 1H, 9/11-H), 6.57–6.52 (m, 1H, 9/11-H), 4.41–4.35 (m, 1H, 21-H), 3.87 (s, 3H, 14-H), 3.30 (s, 3H, 13-H), 1.88–1.19 (m, 10H, 22-26H), 0.19 (s, 1H, Pd-Me).

**$^{31}$P{$^1$H} NMR** (162 MHz, $CD_3OD$): δ = 5.4.

**$^{13}$C{$^1$H} NMR** (151 MHz, $CD_3OD$): δ = 164.2 (C12), 163.4 (C8), 160.2 (d, $^2J_{CP}$ = 2.9, C16), 147.7 (d, $^2J_{CP}$ = 15.2, C1), 137.4 (br, C20), 137.2 (d, $^2J_{CP}$ = 2.4, C3), 135.1 (C10), 133.6 (C18), 131.3 (d, $^1J_{CP}$ = 53.3, C2), 130.3 (C5), 129.3 (d, $^3J_{CP}$ = 7.6, C4), 127.8 (d, $^3J_{CP}$ = 8.6, C6), 120.0 (d, $^3J_{CP}$ = 12.2, C19), 118.0 (d, $^1J_{CP}$ = 67.1, C7), 112.1 (d, $^3J_{CP}$ = 5.1, C17), 106.4 (C9/11), 105.1 (C9/11), 76.2 (C21), 56.3 (C14), 55.1 (C13), 32.5 (C22/26), 32.5 (C22/26), 26.7 (C24), 24.2 (C23/25), 24.1 (C23/C25), 0.6 (Pd-Me). (Note that C15 could not be detected in the $^{13}$C NMR spectrum).

**Anal. Calcd.** (%) for ($C_{27}H_{31}ClLiO_6PPdS \times 0.5\ OC(CH_3)_2$): C, 49.44; H, 4.95; Found: C, 49.51 H, 5.29.

**MS(FAB):** *m/z* = 647 $[(P^O)PdCl+Li]^+$, 627 $[(P^O)PdMe+Li]^+$, 612 $[(P^O)Pd+Li]^+$, 605$[(P^O)Pd]^+$.

*[{($^{Ar/(MeO)2}$**1-Cl**)-μ-Na}$_n$]; [{($^{Ar/(MeO)2}$(P^O)Pd(Me)Cl)-μ-Na}$_n$]; $^{Ar/(MeO)2}$(P^O) = (2-(2',6'-(OMe)$_2$C$_6$H$_3$)C$_6$H$_4$)(2,6-(OMe)$_2$C$_6$H$_3$)P(2-SO$_3$C$_6$H$_4$)*

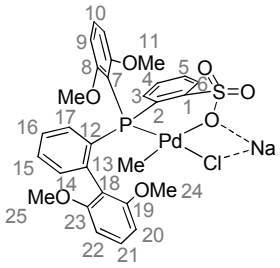


A flask was charged with $^{Ar/(MeO)2}$**(P^O)Na** (270 mg, 0.48 mmol, 1.0 equiv.) and [(cod)PdMeCl] (128 mg, 0.48 mmol, 1.0 equiv.). Benzene (4 mL) was added and a clear dark yellow solution formed. Within 5 minutes a white precipitate formed and the reaction mixture was stirred for additional 30 minutes. The precipitate was isolated by centrifugation and washed with benzene (2 mL) and $Et_2O$ (2 x 7 mL). After drying under vacuum the product was obtained as a white solid (194 mg, 0.27 mmol, 59%).

The corresponding pyridine complex was obtained by reaction of [{($^{Ar/(MeO)2}$**1-Cl**)-μ-Na}$_n$] with pyridine in $CH_2Cl_2$. The solution was filtered and volatiles were removed under vacuum. Crystals for X-ray diffraction were grown by layering a solution of $^{Ar/(MeO)2}$**1-py** in acetone with pentane.

**$^1$H NMR** (600 MHz, $CD_3OD$): δ = 8.05–7.91 (m, 2H, 6-H & 14/17-H), 7.46–7.03 (m, 7H, 3-5 & 10-& 15-16 & 21-H), 7.01 (dd, $^3J_{HH}$ = 7.8, *J* = 6.4, 1H, 14/17-H), 6.67–6.39 (m, 3H, 9- & 20/22-H), 6.36 (d, $^3J_{HH}$ = 8.4, 1H, 20/22H), 3.93–2.85 (br m, 12H, 11- & 24- & 25-H), 0.24 (vbr s, 1H, Pd-Me).

**$^{31}$P{$^1$H} NMR** (162 MHz, $CD_3OD$): δ = 15.1.

**$^{13}$C{$^1$H} NMR** (151 MHz, $CD_3OD$): δ = 163.1 (br, C8), 159.1 (C23 & C19), 148.1 (d, $^3J_{CP}$ = 14.2, C6), 141.5, 137.6 (vbr), 134.5, 134.3 (br), 130.4, 130.4, 130.2 (br), 129.7 (br), 128.7 (br), 126.6, 126.5, 119.8 (vbr), 106.6 (br d, *J* = 39.0), 105.1 (C9), 103.9 (C20 & C22), 55.5 (br, all MeO), 0.8 (Pd-Me). (Note that a more exact assignment was not possible due to broadness and overlapping of the resonances).

**Anal. Calcd.** (%) for ($C_{29}H_{29}ClNaO_7PPdS$): C, 48.55; H, 4.07; Found: C, 48.04, 4.07.

**MS(FAB):** *m/z* = 701 [(P^O)PdCl+Na]$^+$, 681 [(P^O)PdMe+Na]$^+$, 666 [(P^O)Pd+Na]$^+$, 643 [(P^O)Pd]$^+$.

***[{(($^{(iPrO)2}$1-Cl)-μ-Na}$_n$]; [{($^{(iPrO)2}$(P^O)Pd(Me)Cl)-μ-Na}$_n$]; $^{(iPrO)2}$(P^O) = (2,6-(iPrO)$_2$C$_6$H$_3$)$_2$P(2-SO$_3$C$_6$H$_4$))***

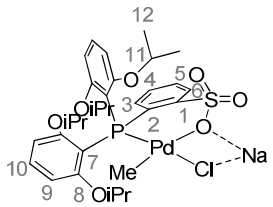


A flask was charged with **$^{(iPrO)2}$(P^O)Na** (531 mg, 0.89 mmol, 1.05 equiv.) and [(cod)PdMeCl] (223 mg, 0.84 mmol, 1.00 equiv.). Acetone (8 mL) was added and a slightly turbid solution formed. The solution was filtered and volatiles were removed under vacuum. The residue was washed with pentane and dried under vacuum (601 mg, 0.27 mmol, 95%).

The corresponding lutidine complex was obtained by reaction of [{($^{(iPrO)2}$**1-Cl**)-μ-Na}$_n$] with 2,6-lutidine in $CH_2Cl_2$. The solution was filtered and volatiles were removed under vacuum. Crystals for X-ray diffraction were grown by layering a solution of $^{(iPrO)}$**1-lut** in acetone with pentane.

**$^1$H NMR** (400 MHz, acetone-d6): δ = 7.87 (dd, $^3J_{HH}$ = 7.7, $^4J_{PH}$ 5.2, 1H, 6-H), 7.78 (ddd, $^3J_{PH}$ = 11.1, $^3J_{HH}$ = 7.9, $^4J_{HH}$ = 1.4, 1H, 3-H), 7.31 (vt, $^3J_{HH}$ = 7.3, 1H, 5-H), 7.28–7.17 (m, 3H, 4- & 10-H), 6.44 (dd, $^3J_{HH}$ = 8.3, $^4J_{PH}$ = 4.0, 4H, 9-H), 4.51 (hept, $^3J_{HH}$ = 6.1, 4H, 11-H), 1.11 (d, $^3J_{HH}$ = 6.0, 12H, 12a-H), 1.10 (d, $^3J_{HH}$ = 6.0, 12b-H), 0.36 (d, $^3J_{PH}$ = 3.4, 3H, Pd-Me).

**$^{31}$P{$^1$H} NMR** (162 MHz, acetone-d6): δ = -14.3.

**$^{13}$C{$^1$H} NMR** (101 MHz, acetone-d6): δ = 161.5 (C8), 148.0 (d, $^2J_{CP}$ = 15.1, C1), 138.3 (C3), 133.0 (d, $^1J_{CP}$ = 52.1, C2), 131.9 (C10), 128.4 (C5), 127.5 (d, $^3J_{CP}$ = 6.0, C6), 127.1 (d, $^3J_{CP}$ = 6.8, C4), 108.4 (d, $^1J_{CP}$ = 51.7, C7), 104.0 (d, $^3J_{CP}$ = 4.5, C9), 70.1 (C11), 22.3 (C12b), 21.9 (C12a), -2.1 (Pd-Me).

**Anal. Calcd.** (%) for ($C_{31}H_{41}ClNaO_7PPdS$): C, 49.41; H, 5.48; Found: C, 49.60; H, 5.70.

**MS(FAB):** *m/z* = 737 [(P^O)PdCl+Na]$^+$, 717 [(P^O)PdMe+Na]$^+$, 679 [(P^O)Pd]$^+$.

### 7.2.5.3 Synthesis of [$^{oxa}$($^{O}$P^O)PdMe(tmeda)]

[***$^{oxa}$($^{O}$P^O)PdMe(tmeda)***; *$^{oxa}$($^{O}$P^O) = (cyclo(2-(2-OC$_6$H$_4$)C$_6$H$_4$)P(2-SO$_3$C$_6$H$_4$))*

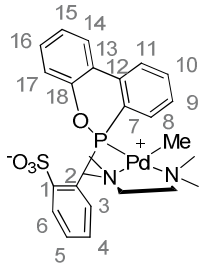


To a suspension of **$^{oxa}$(P^O)H** (131 mg, 0.4 mmol, 1 equiv.) in THF (3 mL) a solution of (tmeda)PdMe$_2$ in THF was added at 0 °C. The reaction mixture was stirred for 3 hours at 25 °C and the resulting precipitate was isolated by centrifugation, washed with THF and $Et_2O$, and dried under vacuum to yield a white solid (139 mg, 0.23 mmol, 62%).

**$^1$H NMR** (400 MHz, $CD_2Cl_2$): δ = 8.11 (dd, $^3J_{HH}$ = 7.9, $^4J_{PH}$ = 4.5, 1H, 6-H), 8.02 (dd, $^3J_{PH}$ = 13.5, $^3J_{HH}$ = 7.6, 1H, 8-H), 7.94 (dd, $^3J_{HH}$ = 8.0, $^4J_{PH}$ = 2.6, 1H, 11-H), 7.78 (dd, $^3J_{HH}$ = 7.8, $^4J_{PH}$ = 1.6, 1H, 14-H), 7.71 (vt, $^3J_{HH}$ = 7.7, 1H, 10-H), 7.54 (vtd, $^3J_{HH}$ = 7.5, $^4J_{PH}$ = 2.2, 1H, 9-H), 7.41–7.32 (m, 2H, 5- & 17-H), 7.26 (vt, $^3J_{HH}$ = 7.8, 1H, 16-H), 7.14 (vt, $^3J_{HH}$ = 7.5, 1H, 15-H), 7.05 (vt, $^3J_{HH}$ = 7.6, 1H, 4-H), 6.84 (vt, *J* = 9.5, 1H, 3-H), 2.81 (d, $^3J_{HH}$ = 10.3, 2H, $CH_{2\text{-tmeda}}$), 2.59 (s, 12H, $CH_{3\text{-tmeda}}$), 2.52 (d, $^3J_{HH}$ = 9.7, 2H, $CH_{2\text{-tmeda'}}$), 0.21 (d, $^3J_{PH}$ = 3.8, 3H, Pd-Me).

**$^{31}$P{$^1$H} NMR** (162 MHz, $CD_2Cl_2$): δ = 105.1.

**$^{13}$C{$^1$H} NMR** (101 MHz, $CD_2Cl_2$): δ = 151.8 (d, $^2J_{CP}$ = 13.5, C1), 150.8 (d, $^2J_{CP}$ = 12.5, C18), 135.9 (d, $^2J_{CP}$ = 2.8; C12), 135.3 (d, $^2J_{CP}$ = 24.1, C8), 133.1 (d, $^4J_{CP}$ = 2.4, C10), 132.2 (d, $^4J_{CP}$ = 2.1, C5), 132.1 (d, $^2J_{CP}$ = 6.8, C3), 130.9 (C16), 130.2 (d, $^3J_{CP}$ = 7.8, C6), 128.6 (d, $^3J_{CP}$ = 13.8, C9), 128.1 (d, $^3J_{CP}$ = 8.2, C4), 128.0 (d, $^1J_{CP}$ = 46.3, C7), 127.5 (d, $^1J_{CP}$ = 50.7, C2), 125.3 (m, C18), 125.3 (C14), 125.2 (d, $^3J_{CP}$ = 5.6, C11), 125.0 (C15), 122.3 (d, $^3J_{CP}$ = 4.2, C17), 61.2 ($CH_{2\text{-TMEDA}}$), 49.9 ($CH_{3\text{-TMEDA}}$), 2.7 (d, $^2J_{CP}$ = 10.7, Pd-Me).

**Anal. Calcd.** (%) for ($C_{25}H_{31}N_2O_4PPdS$): C, 50.64; H, 5.27; N, 4.72; Found: C, 50.00; H, 5.34; N, 4.74.

**MS(ESI):** *m/z* = 615.2 $[M+Na]^+$, 499.1 $[M\text{-TMEDA+Na}]^+$.

## 7.2.6 Syntheses of Insertion Products

General Procedure: To a mixture of [{($^{X}$**1-Cl**)-μ-M}$_2$] (M = Na, Li) and 1.2 equiv. $AgBF_4$ was added $C_2D_2Cl_4$ or $CD_2Cl_2$ ([Pd] ~0.02 mol $L^{-1}$) and the suspension was shaken for 1 minute. The NMR tube was sealed with a septum and MA (~15 equiv.) was added by a micro syringe at the corresponding temperature.

For most of the insertion products and intermediates a full analysis is not possible due to the high reactivity. The analysis is focused on the Pd*(MA)$_x$Me* spin systems which in all cases have similar resonances. Spin systems are assigned by $^1$H $^1$H zTOCSY and by $^1$H $^1$H gCOSY; $^1$H $^{13}$C gHSQC; $^1$H $^{13}$C gHMBC analysis where applicable. The insertion products of the first insertion $^{X}$**2** were analyzed either *in situ* during the insertion process or after completion of the first insertion and removal of additional monomer at temperatures between -40 °C to 25 °C.

### Characterization of insertion products

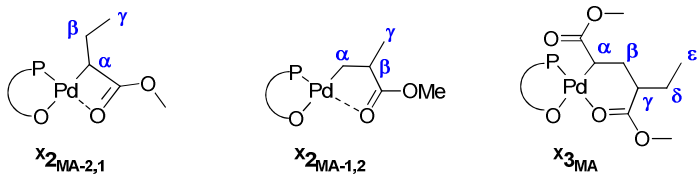


**Figure 7-5.** Numbering of the relevant spin systems of the insertion products $^{X}$**2**$_{MA}$ and $^{X}$**3**$_{MA}$ for NMR assignment.

**Table 7-1.** Comparative overview of the $^1$H NMR shifts of the insertion products $^{X}$**2**$_{MA-2,1}$.

| compound | α-H | β-H | β-H | γ-H |
|---|---|---|---|---|
| $^{MeO}$**1** | 1.83 | 1.62 | 0.98 | 0.33 |
| $^{CF3}$**1** | 1.79 | 1.44 | 0.84 | 0.27 |
| $^{CF3}$**1** | 1.87 | 1.66 | 1.02 | 0.61 |
| $^{(MeO)2}$**1** | 2.11 | 1.75 | 1.30 | 0.29 |
| $^{(iPrO)2}$**1** | 1.60 | 1.40 | 1.14 | 0.51 |
| $^{(MeO)3}$**1** | 2.12 | 1.75 | 1.22 | 0.26 |
| $^{(MeO;Me2)}$**1** | 1.73 | 1.57 | 1.17 | 0.39 |
| $^{(MeO;Me2)}$**1'** | 1.73 | 1.73 | 1.47 | 0.51 |
| $^{Ar}$**1** | 1.86 | 1.27 | 0.25 | 0.25 |
| $^{Ar}$**1'** | 2.26 | 1.34 | -0.11 | 0.15 |
| $^{Ar/(MeO)2}$**1** | 2.02 | 1.59 | 1.32 | 0.60 |
| $^{Ar/(MeO)2}$**1'** | 2.19 | 1.41 | 0.82 | 0.30 |
| $^{(cHexO/(MeO)2)}$**1** | 1.84 | 1.62 | 1.30 | 0.61 |
| $^{(cHexO/(MeO)2)}$**1'** | 2.40 | 1.63 | 0.77 | 0.15 |
| $^{Me*/(MeO)3}$**1** | 2.22 | 1.39 | 1.03 | 0.51 |
| $^{Me*/(MeO)3}$**1'** | 2.21 | 1.71 | 1.54 | 0.99 |
| $^{cHexO}$**1** | 1.61 | 1.33 | 0.55 | 0.11 |
| $^{H}$**1** | 2.16 | 1.51 | 1.01 | 0.34 |

**Table 7-2.** Comparative overview of the $^{1}$H NMR shifts of the insertion products $^{X}\mathbf{2}_{\mathbf{MA\text{-}1,2}}$.

| compound | α-H | α-H | β-H | γ-H |
|---|---|---|---|---|
| $^{MeO}\mathbf{1}$ | 1.55 | 1.26 | 2.84 | 1.09 |
| $^{CF3}\mathbf{1}$ | 1.37 | 1.27 | 3.16 | 1.04 |
| $^{CF3}\mathbf{1}$ | 1.67 | 1.26 | 2.93 | 1.12 |
| $^{(i\mathrm{PrO})2}\mathbf{1}$ | 1.38 | 0.99 | 2.77 | 0.92 |
| $^{Ar}\mathbf{1}$ | 1.23 | 1.05 | 2.80 | 0.87 |
| $^{Ar/(MeO)2}\mathbf{1}$ | 1.92 | 1.09 | 2.91 | 1.01 |
| $^{(c\mathrm{HexO}/(MeO)2)}\mathbf{1}$ | 1.31 | 0.85 | 2.97 | 1.01 |
| $^{(MeO;Me2)}\mathbf{1}$ | 1.45 | 0.91 | 2.79 | 1.03 |
| $^{(MeO;Me2)}\mathbf{1'}$ | 1.29 | 0.74 | 2.89 | 0.99 |
| $^{c\mathrm{HexO}}\mathbf{1}$ | n.d. | n.d. | 3.18 | 0.93 |
| $^{H}\mathbf{1}$ | 1.66 | 1.59 | 2.83 | 1.13 |

**Table 7-3.** Comparative overview of the $^{1}$H NMR shifts of the insertion products $^{X}\mathbf{3}_{\mathbf{MA}}$.

| compound | α-H | β-H | β-H | γ-H | δ-H | δ-H | ε-H |
|---|---|---|---|---|---|---|---|
| $^{MeO}\mathbf{1}$ | 2.07 | 1.24 | 0.90 | 3.16 | 1.81 | 1.39 | 0.93 |
| $^{MeO}\mathbf{1'}$ | 1.94 | 1.26 | 1.25 | 2.98 | 2.06 | 1.76 | 0.93 |
| $^{CF3}\mathbf{1}$ | 2.11 | 1.41 | 0.97 | 3.01 | 1.80 | 1.41 | 0.90 |
| $^{CF3}\mathbf{1}$ | 1.97 | 1.51 | 1.07 | 3.18 | 1.81 | 1.69 | 0.90 |
| $^{(MeO)2}\mathbf{1}$ | 2.24 | 1.42 | 1.20 | 3.07 | 1.80 | 1.42 | 0.92 |
| $^{(MeO)2}\mathbf{1}$ | 2.01 | 1.50 | 1.27 | 3.11 | 1.93 | 1.71 | 0.89 |
| $^{(i\mathrm{PrO})2}\mathbf{1}$ | 2.10 | 1.29 | 0.96 | 3.22 | 1.74 | 1.34 | 0.88 |
| $^{(i\mathrm{PrO})2}\mathbf{1}$ | 2.11 | 1.69 | 1.11 | 2.94 | 1.80 | 1.61 | 0.92 |
| $^{(MeO)3}\mathbf{1}$ | 1.99 | 1.50 | 1.31 | 3.11 | 1.95 | 1.71 | 0.90 |
| $^{(MeO)3}\mathbf{1'}$ | 2.17 | 1.79 | 1.41 | 3.03 | 1.42 | 1.26 | 0.91 |
| $^{Ar/(MeO)2}\mathbf{1}$ | 2.34 | 1.22 | 0.94 | 3.18 | 1.75 | 1.36 | 0.86 |
| $^{Ar/(MeO)2}\mathbf{1'}$ | 2.73 | 2.17 | 1.20 | 3.34 | 1.89 | 1.56 | 1.05 |
| $^{Ar/(MeO)2}\mathbf{1''}$ | 2.67 | 1.87 | 1.40 | 2.88 | 2.15 | 1.87 | 1.01 |
| $^{(c\mathrm{HexO}/(MeO)2)}\mathbf{1}$ | 2.39 | 1.70 | 1.21 | 3.20 | 1.86 | 1.49 | 0.99 |
| $^{(c\mathrm{HexO}/(MeO)2)}\mathbf{1'}$ | 2.30 | 1.17 | 1.05 | 2.84 | 2.04 | 1.70 | 0.87 |
| $^{(c\mathrm{HexO}/(MeO)2)}\mathbf{1''}$ | 1.86 | 1.60 | 1.08 | 3.28 | 1.80 | 1.71 | 0.88 |
| $^{(c\mathrm{HexO}/(MeO)2)}\mathbf{1'''}$ | 2.49 | 0.81 | 0.81 | 3.00 | 1.75 | 1.30 | 0.81 |
| $^{Me*/(MeO)3}\mathbf{1}$ | 2.20 | 1.38 | 1.07 | 2.96 | 2.15 | 1.72 | 0.87 |
| $^{Me*/(MeO)3}\mathbf{1'}$ | 2.27 | 1.20 | 1.11 | 2.93 | 1.79 | 1.37 | 0.88 |
| $^{Me*/(MeO)3}\mathbf{1''}$ | 2.52 | 2.01 | 1.34 | 3.23 | 1.85 | 1.52 | 1.01 |
| $^{Me*/(MeO)3}\mathbf{1'''}$ | 2.48 | 1.69 | 1.69 | 2.94 | 2.47 | 1.93 | 1.00 |
| $^{H}\mathbf{1}$ | 2.43 | 1.43 | 1.36 | 2.96 | 2.10 | 1.81 | 0.93 |
| $^{H}\mathbf{1'}$ | 2.57 | 1.54 | 1.05 | 3.18 | 1.83 | 11.48 | 0.92 |

**Table 7-4.** Comparative overview of selected $^{13}$C NMR shifts of the insertion products $^{X}\mathbf{2}_{\mathbf{MA\text{-}2,1}}$.

| compound | α-H | β-H | γ-H |
|---|---|---|---|
| $^{Ar}\mathbf{1}$ | 34.5 | 22.3 | 13.2 |
| $^{Ar}\mathbf{1'}$ | 32.6 | 20.7 | 13.0 |
| $^{Ar/(MeO)2}\mathbf{1}$ | 31.5 | 25.6 | 14.7 |
| $^{Me*/(MeO)3}\mathbf{1}$ | 32.1 | 23.4 | 14.5 |
| $^{Me*/(MeO)3}\mathbf{1'}$ | 32.1 | 24.8 | 15.5 |

**Table 7-5.** Comparative overview of selected $^{13}$C NMR shifts of the insertion products $^{X}\mathbf{2}_{\mathbf{MA\text{-}1,2}}$.

| compound | α-H | β-H | γ-H |
|---|---|---|---|
| $^{MeO}\mathbf{1}$ | 23.9 | 45.2 | 18.9 |
| $^{Ar}\mathbf{1}$ | 25.5 | 44 | 17.8 |
| $^{Ar/(MeO)2}\mathbf{1}$ | 24.2 | 45.8 | 18.3 |

**Table 7-6.** Comparative overview of selected $^{13}C$ NMR shifts of the insertion products $^{X}\mathbf{3}_{\mathbf{MA}}$.

| compound | α-H | β-H | γ-H | δ-H | ε-H | Stereo |
|---|---|---|---|---|---|---|
| $^{MeO}\mathbf{1}$ | 27.2 | 32.4 | 52.1 | 24.3 | 12.4 | rac |
| $^{MeO}\mathbf{1}$' | 28.1 | 29.5 | 44.7 | 27.6 | 12.0 | meso |
| $^{CF3}\mathbf{1}$ | 31.0 | 28.6 | 43.7 | 26.0 | 11.9 | meso |
| $^{CF3}\mathbf{1}$ | 28.8 | 31.3 | 50.2 | 23.4 | 11.9 | rac |
| $^{(MeO)2}\mathbf{1}$ | 27.9 | 32.5 | 50.9 | 23.9 | 12.2 | rac |
| $^{(MeO)2}\mathbf{1}$ | 29.1 | 29.4 | 44.3 | 26.5 | 11.7 | meso |
| $^{(i\mathrm{PrO})2}\mathbf{1}$ | 28.2 | 33.5 | 50.7 | 24.3 | 12.0 | rac |
| $^{(i\mathrm{PrO})2}\mathbf{1}$ | 27.4 | 30.4 | 44.1 | 26.9 | 12.0 | meso |
| $^{(MeO)3}\mathbf{1}$ | 29.7 | 29.7 | 44.5 | 26.9 | 11.8 | meso |
| $^{(MeO)3}\mathbf{1}$' | 29.1 | 32.7 | 51.0 | 23.9 | 13.4 | rac |
| $^{Ar/(MeO)2}\mathbf{1}$ | 28.5 | 33.0 | 51.1 | 24.3 | 12.4 | rac |
| $^{Ar/(MeO)2}\mathbf{1}$' | 24.7 | 34.4 | 51.6 | 24.7 | 12.9 | rac |
| $^{Ar/(MeO)2}\mathbf{1}$'' | 25.2 | 31.2 | 45.1 | 27.9 | 12.8 | meso |
| $^{(c\mathrm{HexO}/(MeO)2)}\mathbf{1}$ | 24.8 | 33.1 | 51.3 | 24.2 | 12.1 | rac |
| $^{(c\mathrm{HexO}/(MeO)2)}\mathbf{1}$' | 26.6 | 29.2 | 44.9 | 27.8 | 11.5 | meso |
| $^{(c\mathrm{HexO}/(MeO)2)}\mathbf{1}$'' | 28.0 | 29.9 | 43.8 | 26.5 | 11.4 | meso |
| $^{(c\mathrm{HexO}/(MeO)2)}\mathbf{1}$''' | 24.9 | 31.6 | 51.4 | 24.0 | 12.3 | rac |
| $^{Me^*/(MeO)3}\mathbf{1}$ | 26.3 | 28.8 | 44.7 | 27.7 | 11.7 | meso |
| $^{Me^*/(MeO)3}\mathbf{1}$' | 25.7 | 31.8 | 51.4 | 23.7 | 11.7 | rac |
| $^{Me^*/(MeO)3}\mathbf{1}$'' | 23.1 | 32.9 | 51.2 | 24.1 | 11.9 | rac |
| $^{Me^*/(MeO)3}\mathbf{1}$''' | 23.1 | 30.0 | 44.7 | 27.8 | 11.9 | meso |
| $^{H}\mathbf{1}$ | 27.7 | 30.9 | 50.8 | 23.1 | 11.2 | rac |
| $^{H}\mathbf{1}$' | 28.9 | 28.5 | 43.8 | 26.7 | 11.2 | meso |

**Decomposition Products**

trans-Methyl crotonate, (*E*)-methyl but-2-enoate

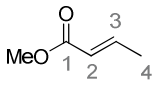


**$^1$H NMR** (400 MHz, $CD_2Cl_2$): δ 7.02–6.85 (m, 1H, 3-H), 5.95–5.74 (m, 1H, 2-H), 3.67 (s, 3H, OMe), 1.86 (d, *J* = 7.0, 3H, 4-H).

cis-Methyl crotonate, (*Z*)-methyl but-2-enoate[190]

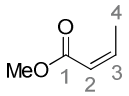


**$^1$H NMR** (400 MHz, $CD_2Cl_2$): δ 6.34 (m), 5.82 (m), 3.60 (s, MeO), 2.11 (d, *J* = 7.4).
**$^1$H NMR**[190] (60 MHz, $CCl_4$): δ 6.28 (dd, $^3J_{HH}$ = 7.0, $^3J_{HH}$ = 11.4, 3-H), 5.72 (dd, $^3J_{HH}$ = 11.4, $^4J_{HH}$ = -1.6, 2-H), 3.64 (s, MeO), 2.14 (dd, $^3J_{HH}$ = 7.0, $^4J_{HH}$ = -1.6, 4-H).

Methyl but-3-enoate

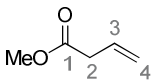


**$^1$H NMR** (400 MHz, $CD_2Cl_2$): δ 5.98-5.85 (m, 1H, 3-H), 5.19–5.14 (m, 1H, 4-H), 5.13 (vt, *J* = 1.4, 1H, 4-H), 3.66 (s, 3H, MeO), 3.08 (vdt, *J* = 6.9, 1.4, 2H, 2-H).

Methyl methacrylate

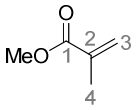


$^1$H NMR (400 MHz, $CD_2Cl_2$): δ 6.06 (d, *J* = 0.9, 1H, 3-H), 5.57–5.54 (m, 1H, 3-H), 3.72 (s, 3H, OMe), 1.93 (s, 3H, 4-H).

(E)-Dimethyl 4-ethylpent-2-enedioate[44]

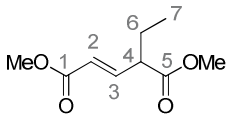


**$^1$H NMR** (400 MHz, $CD_2Cl_2$): δ 6.89 (dd, *J* = 15.7, 8.9, 1H, 3-H), 5.89 (d, *J* = 15.7, 1H, 2-H), 3.10 (td, *J* = 8.5, 7.6, 1H, 4-H), 1.85–1.79 (m, 1H, 6-H), 1.69–1.60 (m, 1H, 6-H), 0.91 (t, *J* = 7.5, 3H, 7-H).

(E)-Dimethyl 4-methylpent-2-enedioate

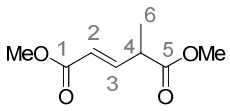


**$^1$H NMR** (400 MHz, $CD_2Cl_2$): δ 7.00-6.92 (m, 1H, 3-H), 5-87-5.82 (m, 1H, 2-H), 3.32 (m, 1H, 4-H), 1.31 (d, *J* = 7.1, 1H, 6-H), 0.91 (t, *J* = 7.5, 3H, 7-H).

Methyl butyrate

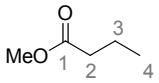


**$^1$H NMR** (400 MHz, $CDCl_3$): δ 3.63 (s, 3H, MeO), 2.26 (t, *J* = 7.4, 2H, 2-H), 1.62 (h, *J* = 7.5, 2H, 3-H), 0.93 (t, *J* = 7.4, 3H, 4-H).

Methyl propionate

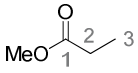


**$^1$H NMR** (400 MHz, $CD_2Cl_2$): δ 3.63 (s, 3H, OMe), 2.30 (q, *J* = 7.6, 2H, 2-H), 1.10 (t, *J* = 7.6, 3H, 3-H).

Methyl isobutyrate

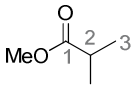


**$^1$H NMR** (400 MHz, $CD_2Cl_2$): δ 3.63 (s, 3H, OMe), 2.53 (hept, *J* = 7.0, 1H, 2-H), 1.14 (d, *J* = 7.0, 6H, 3-H).

# 8. Crystallographic Appendix

**Table 8-1.** Crystallographic Data of Complex $^{MeO}3_{MA\text{-}rac/meso}$.

Structure solution and refinement: I. Göttker-Schnetmann

| | |
|---|---|
| **CCDC deposit no** | **759055** |
| Crystal description | colorless prism |
| Formula | $C_{38}H_{42}O_9PPdS$ ($C_{29}H_{33}O_9PPdS$, 1.5 $C_6H_6$); pentane squeezed out by Platon |
| Crystal Size [$mm^3$] | 0.45 × 0.317 × 0.1 |
| Crystal System | triclinic |
| Space group | $P_{-1}$ (2) |
| *a* [Å] | 11.2956(11) |
| *b* [Å] | 11.9428(10) |
| *c* [Å] | 17.5109(16) |
| α [°] | 77.449(7) |
| β [°] | 76.951(7) |
| γ [°] | 77.429(7) |
| *V* [$Å^3$] | 2210.7(3) |
| *Z* | 2 |
| $M_r$ [$g \cdot mol^{-1}$] | 812.15 (squeezed pentane not considered) |
| $\rho_{calc}$ [$g \cdot cm^{-3}$] | 1.220 (squeezed pentane not considered) |
| $\mu$ (Mo-Kα) [$mm^{-1}$] | 0.548 |
| *F*(000) [e] | 838 (squeezed pentane not considered) |
| T [K] | 100 |
| Wavelenght [Å] | 0.71073 (Mo-$K_\alpha$) |
| Diffractometer | STOE IPDS 2T |
| Scan | ω-scan |
| $\theta_{min\text{-}max}$ [°] | 1.78-25.77 |
| (sin$\theta$/λ)max [$Å^{-1}$] | 0.59 |
| Data total / unique | 27509/ 8369 |
| $R_{int}$ | 0.0760 |
| $R_{sigma}$ | 0.0576 |
| Data obs ($F^2 \geq 4\sigma(F^2)$) | 5638 |
| *hkl*-range | -13/13, -14/14, -21/21 |
| Absorption correction | numerical Integration; (two molecules of Pentane per unit cell considered) |
| Structure Solution | SHELXS-97 |
| Structure Refinement | SHELXL-97 |
| H atoms | mixed |
| Number Parameters | 488 |
| R(F) obs. / all | 0.0488/ 0.0656 |
| wR($F^2$) all | 0.1393 |
| w (*a*, *b*)[a] | 0.0748, 0.7133 |
| GoF ($F^2$) | 1.057 |
| $dU_{max}$ | 0.000 |
| $\Delta\rho_{fin}$ (min./max.) [$e \cdot Å^{-3}$] | 0.74/-1.05 |
| remarks | Disordered pentane at 0.0, 0.0, 0.0 was removed by the PLATON SQUEEZE[191] routine; further disorder was modeled anisotropically |

[a] weighting scheme: $w = 1/[\sigma^2(Fo^2) + (a \cdot P)^2 + b \cdot P)$, $P = [max(Fo^2,0) + 2\,Fc^2]/3$.

**Table 8-2.** Crystallographic Data of Complex $^{MeO}$**1-OPBu$_3$**.

Structure solution and refinement: I. Göttker-Schnetmann

| | |
|---|---|
| **CCDC deposit no** | **862044** |
| Crystal description | colorless fragment |
| Formula | C33 H48 O6 P2 Pd S |
| Formula weight | 741.11 |
| Crystal Size [mm$^3$] | 0.50 x 0.28 x 0.05 |
| Crystal System | Triclinic |
| Space group | $P_{-1}$ (2) |
| a [Å] | 12.0993(8) |
| b [Å] | 12.0348(8) |
| c [Å] | 13.4363(8) |
| α [°] | 77.079(5) |
| β [°] | 69.231(5) |
| γ [°] | 75.256(5) |
| V [Å$^3$] | 1749.78(19) |
| Z | 2 |
| $\rho_{calc}$ [g·cm-3] | 1.407 |
| μ (Mo-Kα) [mm$^{-1}$] | 0.722 |
| F(000) | 772 |
| T [K] | 100 |
| Wavelenght [Å] | 0.71073 (Mo-$K_\alpha$) |
| Diffractometer | STOE IPDS 2T |
| Scan | ω-scan |
| θmin-max [°] | 1.77-27.94 |
| (sinθ/λ)max [Å$^{-1}$] | 0.63 |
| Data total / unique | 28093/8347 |
| $R_{int}$ | 0.0914 |
| $R_{sigma}$ | 0.0752 |
| Data obs ($F^2 \geq 4\sigma(F^2)$) | 6679 |
| hkl-range | -15/15, -15/15, -17/17 |
| Absorption correction | numerical Integration |
| Structure Solution | SHELXS-97 |
| Structure Refinement | SHELXL-97 |
| H atoms | constrained |
| Number Parameters | 397 |
| R(F) obs. / all | 0.0394/ 0.0581 |
| wR($F^2$) all | 0.0811 |
| w (a, b)[a] | 0.0344, 0.000 |
| GoF ($F^2$) | 0.986 |
| $dU_{max}$ | 0.000 |
| $\Delta\rho_{fin}$ (min./max.) [e·Å$^{-3}$] | 0.679/-1.004 |

[a] weighting scheme: $w = 1/[\sigma^2(Fo^2) + (a \cdot P)^2 + b \cdot P)$, $P = [\max(Fo^2,0) + 2\,Fc^2]/3$.

**Table 8-3.** Crystallographic Data of Complex $^{MeO}$**1-OPPh$_3$**.

Structure solution and refinement: I. Göttker-Schnetmann

| | |
|---|---|
| **CCDC deposit no** | **862045** |
| Crystal description | colorless cube |
| Formula | C39 H36 O6 P2 Pd S * C H Cl3 |
| Formula weight | 920.45 |
| Crystal Size [mm$^3$] | 0.20 x 0.20 x 0.20 |
| Crystal System | Monoclinic |
| Space group | P21/c (14) |
| a [Å] | 14.2186(5) |
| b [Å] | 10.6220(5) |
| c [Å] | 29.5485(12) |
| α [°] | 90 |
| β [°] | 115.328(3) |
| γ [°] | 90 |
| V [Å$^3$] | 4033.7(3) |
| Z | 4 |
| $\rho_{calc}$ [g·cm-3] | 1.516 |
| μ (Mo-Kα) [mm$^{-1}$] | 0.711 |
| F(000) | 1872 |
| T [K] | 100(2) |
| Wavelenght [Å] | 0.71073 (Mo-K$_\alpha$) |
| Diffractometer | STOE IPDS 2T |
| Scan | ω-scan |
| θmin-max [°] | 2.06-26.87 |
| (sinθ/λ)max [Å$^{-1}$] | 0.67 |
| Data total / unique | 56509/8624 |
| $R_{int}$ | 0.0784 |
| $R_{sigma}$ | 0.0432 |
| Data obs ($F^2 \geq 4\sigma(F^2)$) | 6928 |
| hkl-range | -17/18, -13/13, -37/37 |
| Absorption correction | numerical Integration |
| Structure Solution | SHELXS-97 |
| Structure Refinement | SHELXL-97 |
| H atoms | constrained |
| Number Parameters | 481 |
| R(F) obs. / all | 0.0459/ 0.0647 |
| wR($F^2$) all | 0.1036 |
| w (a, b)[a] | 0.043, 9.46 |
| GoF ($F^2$) | 1.033 |
| $dU_{max}$ | 0.000 |
| $\Delta\rho_{fin}$ (min./max.) [e·Å$^{-3}$] | 2.750/-1.678 |

[a] weighting scheme: $w = 1/[\sigma^2(Fo^2) + (a \cdot P)^2 + b \cdot P)$, $P = [\max(Fo^2,0) + 2\,Fc^2]/3$.

**Table 8-4.** Crystallographic Data of Complex $^{(i\text{PrO})2}$**1-lut**.

| | |
|---|---|
| **CCDC deposit no** | not submitted |
| Crystal description | yellow cube |
| Formula | C38 H50 N O7 P Pd S |
| Formula weight | 802.22 |
| Crystal Size [$mm^3$] | 0.40 x 0.28 x 0.20 |
| Crystal System | Monoclinic |
| Space group | P21/c (14) |
| a [Å] | 10.7062(6) |
| b [Å] | 18.8381(11) |
| c [Å] | 18.7634(11) |
| α [°] | 90 |
| β [°] | 97.247(5) |
| γ [°] | 90 |
| V [$Å^3$] | 3754.1(4) |
| Z | 4 |
| $\rho_{calc}$ [$g \cdot cm^{-3}$] | 1.419 |
| μ (Mo-Kα) [$mm^{-1}$] | 0.641 |
| F(000) | 1672 |
| T [K] | 100(2) |
| Wavelenght [Å] | 0.71073 (Mo-$K_\alpha$) |
| Diffractometer | STOE IPDS 2T |
| Scan | ω-scan |
| θmin-max [°] | 1.92-28.05 |
| (sinθ/λ)max [$Å^{-1}$] | 0.64 |
| Data total / unique | 50338/8966 |
| $R_{int}$ | 0.0497 |
| $R_{sigma}$ | 0.0402 |
| Data obs ($F^2 \geq 4\sigma(F^2)$) | 7133 |
| hkl-range | -14/14, -24/24, -24/24 |
| Absorption correction | numerical Integration |
| Structure Solution | SHELXS-97 |
| Structure Refinement | SHELXL-97 |
| H atoms | constrained |
| Number Parameters | 453 |
| R(F) obs. / all | 0.0306/ 0.0485 |
| wR($F^2$) all | 0.0553 |
| w (a, b)[a] | 0.0304, 0 |
| GoF ($F^2$) | 0.998 |
| $dU_{max}$ | 0.001 |
| $\Delta\rho_{fin}$ (min./max.) [$e \cdot Å^{-3}$] | 0.406/-0.522 |

[a] weighting scheme: $w = 1/[\sigma^2(Fo^2) + (a \cdot P)^2 + b \cdot P)$, $P = [\max(Fo^2,0) + 2\,Fc^2]/3$.

**Table 8-5.** Crystallographic Data of Complex $^{(MeO;Me2)}$**1-lut**.

| | |
|---|---|
| **CCDC deposit no** | not submitted |
| Crystal description | colorless cube |
| Formula | C32 H38 N O5 P Pd S |
| Formula weight | 686.09 |
| Crystal Size [$mm^3$] | 0.25 x 0.20 x 0.10 |
| Crystal System | Triclinic |
| Space group | P -1(2) |
| a [Å] | 9.2493(8) |
| b [Å] | 11.1666(10) |
| c [Å] | 15.8107(14) |
| α [°] | 76.750(7) |
| β [°] | 75.034(7) |
| γ [°] | 80.670(7) |
| V [$Å^3$] | 1526.4(2) |
| Z | 2 |
| $\rho_{calc}$ [$g \cdot cm^{-3}$] | 1.493 |
| μ (Mo-Kα) [$mm^{-1}$] | 0.770 |
| F(000) | 708 |
| T [K] | 100(2) |
| Wavelenght [Å] | 0.71073 (Mo-$K_\alpha$) |
| Diffractometer | STOE IPDS 2T |
| Scan | ω-scan |
| θmin-max [°] | 1.36-26.81 |
| (sinθ/λ)max [$Å^{-1}$] | 0.61 |
| Data total / unique | 19956/6450 |
| $R_{int}$ | 0.0649 |
| $R_{sigma}$ | 0.0643 |
| Data obs ($F^2 \geq 4\sigma(F^2)$) | 4865 |
| hkl-range | -11/11, -24/24, -19/19 |
| Absorption correction | numerical Integration |
| Structure Solution | SHELXS-97 |
| Structure Refinement | SHELXL-97 |
| H atoms | constrained |
| Number Parameters | 379 |
| R(F) obs. / all | 0.0370/ 0.0599 |
| wR($F^2$) all | 0.0828 |
| w (a, b)[a] | 0.0416, 0 |
| GoF ($F^2$) | 0.945 |
| $dU_{max}$ | 0.001 |
| $\Delta\rho_{fin}$ (min./max.) [$e \cdot Å^{-3}$] | 0.817/-0.931 |

[a] weighting scheme: $w = 1/[\sigma^2(Fo^2) + (a \cdot P)^2 + b \cdot P)$, $P = [max(Fo^2,0) + 2\,Fc^2]/3$.

**Table 8-6.** Crystallographic Data of Complex $^{Ph}$**1-lut**.

| | |
|---|---|
| **CCDC deposit no** | not submitted |
| Crystal description | colorless cube |
| Formula | C38 H34 N O3 P Pd S |
| Formula weight | 722.09 |
| Crystal Size [$mm^3$] | 0.50 x 0.40 x 0.20 |
| Crystal System | Orthorhombic |
| Space group | P 21 21 21 (19) |
| a [Å] | 9.4337(3) |
| b [Å] | 10.9480(3) |
| c [Å] | 31.5433(11) |
| α [°] | 90 |
| β [°] | 90 |
| γ [°] | 90 |
| V [$Å^3$] | 3257.8(2) |
| Z | 4 |
| $\rho_{calc}$ [$g \cdot cm^{-3}$] | 1.472 |
| μ (Mo-Kα) [$mm^{-1}$] | 0.722 |
| F(000) | 1480 |
| T [K] | 100(2) |
| Wavelenght [Å] | 0.71073 (Mo-$K_\alpha$) |
| Diffractometer | STOE IPDS 2T |
| Scan | ω-scan |
| θmin-max [°] | 1.97-27.98 |
| (sinθ/λ)max [$Å^{-1}$] | 0.63 |
| Data total / unique | 53124/7792 |
| $R_{int}$ | 0.0866 |
| $R_{sigma}$ | 0.0399 |
| Data obs ($F^2 \geq 4\sigma(F^2)$) | 7529 |
| hkl-range | -12/12, -14/14, -41/41 |
| Absorption correction | numerical Integration |
| Structure Solution | SHELXS-97 |
| Structure Refinement | SHELXL-97 |
| H atoms | constrained |
| Number Parameters | 409 |
| R(F) obs. / all | 0.0427/ 0.0445 |
| wR($F^2$) all | 0.0952 |
| w (a, b)[a] | 0, 7.7 |
| GoF ($F^2$) | 1.195 |
| $dU_{max}$ | 0.000 |
| $\Delta\rho_{fin}$ (min./max.) [$e \cdot Å^{-3}$] | 0.666/-1.478 |

[a] weighting scheme: $w = 1/[\sigma^2(Fo^2) + (a \cdot P)^2 + b \cdot P)$, $P = [max(Fo^2,0) + 2\ Fc^2]/3$.

**Table 8-7.** Crystallographic Data of Complex $^{(MeO)2}$**1-py**.

| | |
|---|---|
| **CCDC deposit no** | not submitted |
| Crystal description | yellow cube |
| Formula | C28 H30 N O7 P Pd S |
| Formula weight | 661.96 |
| Crystal Size [$mm^3$] | 0.50 x 0.27 x 0.15 |
| Crystal System | Monoclinic |
| Space group | P21/c (14) |
| a [Å] | 11.8322(4) |
| b [Å] | 14.9891(7) |
| c [Å] | 15.3343(5) |
| α [°] | 90 |
| β [°] | 96.380(3) |
| γ [°] | 90 |
| V [$Å^3$] | 2702.76(18) |
| Z | 4 |
| $\rho_{calc}$ [$g \cdot cm^{-3}$] | 1.6127 |
| μ (Mo-Kα) [$mm^{-1}$] | 0.872 |
| F(000) | 1352 |
| T [K] | 100(2) |
| Wavelenght [Å] | 0.71073 (Mo-$K_\alpha$) |
| Diffractometer | STOE IPDS 2T |
| Scan | ω-scan |
| θmin-max [°] | 1.73-28.02 |
| sin(θ/λ)max [$Å^{-1}$] | 0.64 |
| Data total / unique | 44680/6474 |
| $R_{int}$ | 0.0676 |
| $R_{sigma}$ | 0.0320 |
| Data obs ($F^2 \geq 4\sigma(F^2)$) | 5696 |
| hkl-range | -15/15, -19/19, -20/20 |
| Absorption correction | numerical Integration |
| Structure Solution | SHELXS-97 |
| Structure Refinement | SHELXL-97 |
| H atoms | constrained |
| Number Parameters | 357 |
| R(F) obs. / all | 0.0239/ 0.0305 |
| wR($F^2$) all | 0.0557 |
| w (a, b)[a] | 0.0252, 1.1086 |
| GoF ($F^2$) | 1.041 |
| $dU_{max}$ | 0.001 |
| $\Delta\rho_{fin}$ (min./max.) [$e \cdot Å^{-3}$] | 0.443/-0.739 |

[a] weighting scheme: $w = 1/[\sigma^2(Fo^2) + (a \cdot P)^2 + b \cdot P)$, $P = [max(Fo^2,0) + 2\ Fc^2]/3$.

**Table 8-8.** Crystallographic Data of Complex $\{(^{(MeO)2}\mathbf{1})_6\text{-}\mathbf{Cl_4}\}\mathbf{Na_4}$.

| | |
|---|---|
| **CCDC deposit no** | not submitted |
| Crystal description | yellow cube |
| Formula | C69 H75 Cl2 Na2 O22 P3 Pd3 S3 (pentane and part of one acetone molecule were removed by the squeeze routine) |
| Formula weight | 1881.46 |
| Crystal Size [$mm^3$] | 0.60 x 0.40 x 0.20 |
| Crystal System | P-1/c (2) |
| a [Å] | 15.7392(9) |
| b [Å] | 17.2312(11) |
| c [Å] | 18.1978(11) |
| α [°] | 79.341(5) |
| β [°] | 88.843(5) |
| γ [°] | 67.146(5) |
| V [$Å^3$] | 4462.2(5) |
| Z | 2 |
| $\rho_{calc}$ [$g \cdot cm^{-3}$] | 1.400 |
| μ (Mo-Kα) [$mm^{-1}$] | 0.854 |
| F(000) | 1904 |
| T [K] | 100(2) |
| Wavelenght [Å] | 0.71073 (Mo-$K_\alpha$) |
| Diffractometer | STOE IPDS 2T |
| Scan | ω-scan |
| θmin-max [°] | 1.76-26.24 |
| sin(θ/λ)max [$Å^{-1}$] | 0.60 |
| Data total / unique | 17601/17601 |
| $R_{int}$ | 0 (after squeezing) |
| $R_{sigma}$ | 0.1321 |
| Data obs ($F^2 \geq 4\sigma(F^2)$) | 10083 |
| hkl-range | -19/19, -20/21, 0/22 |
| Absorption correction | numerical Integration |
| Structure Solution | SHELXS-97 |
| Structure Refinement | SHELXL-97 |
| H atoms | constrained |
| Number Parameters | 947 |
| R(F) obs. / all | 0.0588/ 0 |
| wR($F^2$) all | 0.1306 |
| w (a, b)[a] | 0.0252, 1.1086 |
| GoF ($F^2$) | 0.880 |
| $dU_{max}$ | 0.002 |
| $\Delta\rho_{fin}$ (min./max.) [$e \cdot Å^{-3}$] | 2.242/-0.997 |
| Remarks | The quality of the structure is low and but the connectivity can be derived from the data. Disordered pentane and the $C(CH_3)_2$ moiety of a disordered acetone molecule coordinated to one sodium atom had to be removed for stabilization of the structure in the refinement. By the SQUEEZE routine 221 $e^-$ (2 $C(CH_3)_2$ + 2 pentane) were removed from a 923 $Å^3$ solvent accessible void from the reflection data. |

[a] weighting scheme: $w = 1/[\sigma^2(Fo^2) + (a \cdot P)^2 + b \cdot P)$, $P = [\max(Fo^2,0) + 2\,Fc^2]/3$.

**Table 8-9.** Crystallographic Data of Complex $^{(MeO)3}$**1-lut**.

| | |
|---|---|
| **CCDC deposit no** | not submitted |
| Crystal description | yellow cube |
| Formula | C64 H76 N2 O18 P2 Pd2 S2 × $CH_2Cl_2$ |
| Formula weight | 1584.05 |
| Crystal Size [$mm^3$] | 0.50 x 0.33 x 0.20 |
| Crystal System | Monoclinic |
| Space group | P21/c (14) |
| a [Å] | 21.2396(6) |
| b [Å] | 18.4034(7) |
| c [Å] | 18.3510(6) |
| α [°] | 90 |
| β [°] | 98.848(2) |
| γ [°] | 90 |
| V [$Å^3$] | 7087.7(4) |
| Z | 4 |
| $\rho_{calc}$ [$g \cdot cm^{-3}$] | 1.485 |
| μ (Mo-Kα) [$mm^{-1}$] | 0.755 |
| F(000) | 3256 |
| T [K] | 100(2) |
| Wavelenght [Å] | 0.71073 (Mo-$K_\alpha$) |
| Diffractometer | STOE IPDS 2T |
| Scan | ω-scan |
| θmin-max [°] | 1.94-26.92 |
| sin(θ/λ)max [$Å^{-1}$] | 0.61 |
| Data total / unique | 80317/15090 |
| $R_{int}$ | 0.0967 |
| $R_{sigma}$ | 0.0677 |
| Data obs ($F^2 \geq 4\sigma(F^2)$) | 10802 |
| hkl-range | -27/27, -23/23, -23/23 |
| Absorption correction | numerical Integration |
| Structure Solution | SHELXS-97 |
| Structure Refinement | SHELXL-97 |
| H atoms | constrained |
| Number Parameters | 879 |
| R(F) obs. / all | 0.0587/ 0.0918 |
| wR($F^2$) all | 0.1515 |
| w (a, b)[a] | 0.0852, 1.4794 |
| GoF ($F^2$) | 1.033 |
| $dU_{max}$ | 0.008 |
| $\Delta\rho_{fin}$ (min./max.) [$e \cdot Å^{-3}$] | 2.761/-1.277 |
| Remarks | The high R values can be explained with a strongly disordered $CH_2Cl_2$ molecule in the unit cell: The structure contains at least one molecule $CH_2Cl_2$ per asymmetric unit (4 per cell) which is disordered over at least three positions. However, disorder could only be solved for two positions. For the position with the lower occupancy the carbon atom could not be modeled anisotropically. |

[a] weighting scheme: $w = 1/[\sigma^2(Fo^2) + (a \cdot P)^2 + b \cdot P)$, $P = [\max(Fo^2,0) + 2\,Fc^2]/3$.

**Table 8-10.** Crystallographic Data of Complex $^{CF3}$**1-lut**.

| | |
|---|---|
| **CCDC deposit no** | not submitted |
| Crystal description | colorless plate |
| Formula | C28 H24 F6 N O3 P Pd S |
| Formula weight | 705.91 |
| Crystal Size [$mm^3$] | 0.50 x 0.340 x 0.20 |
| Crystal System | Triclinic |
| Space group | P -1 (2) |
| a [Å] | 9.0726(11) |
| b [Å] | 9.3430(12) |
| c [Å] | 16.604(2) |
| α [°] | 76.153(10) |
| β [°] | 83.610(10) |
| γ [°] | 87.256(10) |
| V [$Å^3$] | 1357.8(3) |
| Z | 2 |
| ρcalc [$g \cdot cm^{-3}$] | 1.727 |
| μ (Mo-Kα) [$mm^{-1}$] | 0.893 |
| F(000) | 708 |
| T [K] | 100(2) |
| Wavelenght [Å] | 0.71073 (Mo-Kα) |
| Diffractometer | STOE IPDS 2T |
| Scan | ω-scan |
| θmin-max [°] | 2.25-27.96 |
| (sinθ/λ)max [$Å^{-1}$] | 0.63 |
| Data total / unique | 19017 / 6438 |
| Rint | 0.1024 |
| Rsigma | 0.0801 |
| Data obs ($F^2 \geq 4\sigma(F^2)$) | 4990 |
| hkl-range | -11/11, -12/12, -21/21 |
| Absorption correction | numerical Integration |
| Structure Solution | SHELXS-97 |
| Structure Refinement | SHELXL-97 |
| H atoms | constrained |
| Number Parameters | 373 |
| R(F) obs. / all | 0.0400/ 0.0632 |
| wR(F2) all | 0.0934 |
| w (a, b)[a] | 0.0242, 2.6585 |
| GoF ($F^2$) | 1.053 |
| dUmax | 0.001 |
| Δρfin (min./max.) [$e \cdot Å^{-3}$] | 0.790/-1.421 |

[a] weighting scheme: $w = 1/[\sigma^2(Fo^2) + (a \cdot P)^2 + b \cdot P)$, $P = [\max(Fo^2,0) + 2\,Fc^2]/3$.

**Table 8-11.** Crystallographic Data of Complex $^{Ar/(MeO)2}$**1-py**.

| | |
|---|---|
| **CCDC deposit no** | **896035** |
| Crystal description | colorless plate |
| Formula | C34 H34 N O7 P Pd S |
| Formula weight | 738.05 |
| Crystal Size [$mm^3$] | 0.20 x 0.13 x 0.10 |
| Crystal System | Monoclinic |
| Space group | P 21/c (14) |
| a [Å] | 9.7288(6) |
| b [Å] | 37.6675(15) |
| c [Å] | 9.6351(5) |
| α [°] | 90 |
| β [°] | 116.530(4) |
| γ [°] | 90 |
| V [$Å^3$] | 3159.1(3) |
| Z | 4 |
| ρcalc [$g \cdot cm^{-3}$] | 1.552 |
| μ (Mo-Kα) [$mm^{-1}$] | 0.755 |
| F(000) | 1512 |
| T [K] | 100(2) |
| Wavelenght [Å] | 0.71073 (Mo-Kα) |
| Diffractometer | STOE IPDS 2T |
| Scan | ω-scan |
| θmin-max [°] | 2.16-25.73 |
| (sinθ/λ)max [$Å^{-1}$] | 0.59 |
| Data total / unique | 41389/5969 |
| Rint | 0.0920 |
| Rsigma | 0.0491 |
| Data obs ($F^2 \geq 4\sigma(F^2)$) | 4490 |
| hkl-range | -11/11, -45/43, -11/11 |
| Absorption correction | numerical Integration |
| Structure Solution | SHELXS-97 |
| Structure Refinement | SHELXL-97 |
| H atoms | constrained |
| Number Parameters | 411 |
| R(F) obs. / all | 0.0486/ 0.0667 |
| wR(F2) all | 0.1215 |
| w (a, b)[a] | 0.0673, 0.3066 |
| GoF ($F^2$) | 1.072 |
| dUmax | 0.003 |
| Δρfin (min./max.) [$e \cdot Å^{-3}$] | 0.437/-1.068 |

[a] weighting scheme: $w = 1/[\sigma^2(Fo^2) + (a \cdot P)^2 + b \cdot P)$, $P = [\max(Fo^2,0) + 2\,Fc^2]/3$.

**Table 8-12.** Crystallographic Data of Complex $^{cHexO/(MeO)2}$**1-lut**.

| | |
|---|---|
| **CCDC deposit no** | **896036** |
| Crystal description | colorless plate |
| Formula | C34 H40 N O6 P Pd S<br>toluene squeezed out by Platon |
| Formula weight | 728.10 (squeezed toluene not considered) |
| Crystal Size [$mm^3$] | 0.30 x 0.18 x 0.05 |
| Crystal System | Triclinic |
| Space group | P -1 (2) |
| a [Å] | 14.9093(6) |
| b [Å] | 15.1538(7) |
| c [Å] | 18.8836(8) |
| α [°] | 83.646(3) |
| β [°] | 72.284(3) |
| γ [°] | 80.759(3) |
| V [$Å^3$] | 4002.7(3) |
| Z | 4 |
| ρcalc [$g \cdot cm^{-3}$] | 1.208 (squeezed toluene not considered) |
| μ (Mo-Kα) [$mm^{-1}$] | 0.593 |
| F(000) | 1504 (squeezed toluene not considered) |
| T [K] | 100(2) |
| Wavelenght [Å] | 0.71073 (Mo-Kα) |
| Diffractometer | STOE IPDS 2T |
| Scan | ω-scan |
| θmin-max [°] | 2.08-26.84 |
| (sinθ/λ)max [$Å^{-1}$] | 0.61 |
| Data total / unique | 58103/16949 |
| Rint | 0.0752 |
| Rsigma | 0.0722 |
| Data obs ($F^2 \geq 4\sigma(F^2)$) | 12227 |
| hkl-range | -18/18, -19/19, -23/23 |
| Absorption correction | numerical Integration<br>(four molecules of toluene per unit cell considered) |
| Structure Solution | SHELXS-97 |
| Structure Refinement | SHELXL-97 |
| H atoms | constrained |
| Number Parameters | 803 |
| R(F) obs. / all | 0.0389/ 0.0653 |
| wR(F2) all | 0.0823 |
| w (a, b)[a] | 0.0421, 0 |
| GoF ($F^2$) | 0.927 |
| dUmax | 0.002 |
| Δρfin (min./max.) [$e \cdot Å^{-3}$] | 0.447/-0.477 |
| remarks | Toluene was detected in at least three independent positions in the asymmetric unit close to the center of symmetry and could not be satisfactorily modeled due to disorder. Further improvement was achieved using the SQUEEZE routine by which 323 $e^-$ (four molecules of toluene) were removed from a 998 $Å^3$ solvent accessible void from the reflection data. |

[a] weighting scheme: $w = 1/[\sigma^2(Fo^2) + (a \cdot P)^2 + b \cdot P)$, $P = [\max(Fo^2,0) + 2\,Fc^2]/3$.

**Table 8-13.** Crystallographic Data of Complex **[{(O^P^O)Ni(py)}$_2$]**.

| | |
|---|---|
| **CCDC deposit no** | not submitted |
| Crystal description | cubic |
| Formula | C60 H52 N2 Ni2 O8 P2 S2 |
| Formula weight | 1172.52 |
| Crystal Size [mm$^3$] | 0.10 x 0.10 x 0.10 |
| Crystal System | Monoclinic |
| Space group | P 21/c (14) |
| a [Å] | 10.0838(9) |
| b [Å] | 24.4106(17) |
| c [Å] | 13.1546(12) |
| α [°] | 90 |
| β [°] | 95.433(8) |
| γ [°] | 90 |
| V [Å$^3$] | 2695.3(4) |
| Z | 2 |
| ρcalc [g·cm$^{-3}$] | 1.445 |
| μ (Mo-Kα) [mm$^{-1}$] | 0.894 |
| F(000) | 1216 |
| T [K] | 100(2) |
| Wavelenght [Å] | 0.71073 (Mo-Kα) |
| Diffractometer | STOE IPDS 2T |
| Scan | ω-scan |
| θmin-max [°] | 1.85-25.25 |
| (sinθ/λ)max [Å$^{-1}$] | 0.58 |
| Data total / unique | 26684/4813 |
| Rint | 0.0876 |
| Rsigma | 0.0708 |
| Data obs ($F^2 \geq 4\sigma(F^2)$) | 3543 |
| hkl-range | -12/11, -24/24, -15/15 |
| Absorption correction | numerical Integration |
| Structure Solution | SHELXS-97 |
| Structure Refinement | SHELXL-97 |
| H atoms | constrained |
| Number Parameters | 344 |
| R(F) obs. / all | 0.0435/ 0.0728 |
| wR(F2) all | 0.0737 |
| w (a, b)[a] | 0.0348, 0.1191 |
| GoF ($F^2$) | 1.017 |
| dUmax | 0.000 |
| Δρfin (min./max.) [e·Å$^{-3}$] | 0.406/-0.451 |

[a] weighting scheme: $w = 1/[\sigma^2(Fo^2) + (a \cdot P)^2 + b \cdot P)$, $P = [\max(Fo^2,0) + 2\,Fc^2]/3$.

**Table 8-14.** Crystallographic Data of Complex **[(O^P^O)Ni(tmeda)]**.

| | |
|---|---|
| **CCDC deposit no** | not submitted |
| Crystal description | plate |
| Formula | C25 H31 N2 Ni2 O4 P S |
| Formula weight | 542.26 |
| Crystal Size [$mm^3$] | 0.5 x 0.28 x 0.05 |
| Crystal System | Monoclinic |
| Space group | P 21/c (14) |
| a [Å] | 10.3447(5) |
| b [Å] | 12.4855(4) |
| c [Å] | 19.1959(10) |
| α [°] | 90 |
| β [°] | 104.977(4) |
| γ [°] | 90 |
| V [$Å^3$] | 2395.09 |
| Z | 4 |
| ρcalc [$g \cdot cm^{-3}$] | 1.512 |
| μ (Mo-Kα) [$mm^{-1}$] | 1.000 |
| F(000) | 1144 |
| T [K] | 100(2) |
| Wavelenght [Å] | 0.71073 (Mo-Kα) |
| Diffractometer | STOE IPDS 2T |
| Scan | ω-scan |
| θmin-max [°] | 1.97-28.08 |
| (sinθ/λ)max [$Å^{-1}$] | 0.64 |
| Data total / unique | 37687/5745 |
| Rint | 0.0577 |
| Rsigma | 0.0314 |
| Data obs ($F^2 \geq 4\sigma(F^2)$) | 4834 |
| hkl-range | -13/13, -16/15, -25/25 |
| Absorption correction | numerical Integration |
| Structure Solution | SHELXS-97 |
| Structure Refinement | SHELXL-97 |
| H atoms | constrained |
| Number Parameters | 312 |
| R(F) obs. / all | 0.0286/ 0.0396 |
| wR(F2) all | 0.0641 |
| w (a, b)[a] | 0.0326, 0.6494 |
| GoF ($F^2$) | 1.021 |
| dUmax | 0.001 |
| Δρfin (min./max.) [$e \cdot Å^{-3}$] | 0.338/-0.349 |

[a] weighting scheme: $w = 1/[\sigma^2(Fo^2) + (a \cdot P)^2 + b \cdot P)$, $P = [\max(Fo^2,0) + 2\,Fc^2]/3$.

# 9. References


1) Mülhaupt, R. *Macromol. Chem. Phys.* **2003**, *204*, 289-327.
2) Boffa, L. S.; Novak, B. M. *Chem. Rev.* **2000**, *100*, 1479-1494.
3) Ittel, S. D.; Johnson, L. K.; Brookhart, M. *Chem. Rev.* **2000**, *100*, 1169-1204.
4) Doak, K. W. In *Encyclopedia of Polymer Science and Engineering*; Mark, H. F., Ed.; John Wiley & Sons: New York, 1986; Vol.6, p 386.
5) Hagman, J. F.; Crary, J. W. In *Encyclopedia of Polymer Science and Engineering;* Mark, H. F., Bikales, N. M., Overberger, C. G., Menges, G., Kroschwitz, J. I., Eds.; Wiley-Interscience: New York, 1985; Vol. 1, p 325.
6) Boaen, N. K.; Hillmyer, M. A. *Chem. Soc. Rev.* **2005**, *34*, 267-275.
7) Lehman, S. E.; Wagener, K. B.; Baugh, L. S.; Rucker, S. P.; Schulz, D. N.; Varma-Nair, M.; Berluche, E., *Macromolecules* **2007**, *40*, 2643-2656.
8) Mutlu, H.; de Espinosa, L. M.; Meier, M. A. R., *Chem. Soc. Rev.* **2011**, *40*, 1404-1445.
9) Ziegler, K.; Holzkamp, E.; Breil, H.; Martin, H. *Angew. Chem.* **1955**, *67*, 541-547.
10) Natta, G. *Angew. Chem.* **1956**, *68*, 393-403.
11) Yasuda, H.; Furo, M.; Yamamoto, H.; Nakamura, A.; Miyake, S.; Kibino, N. *Macromolecules* **1992**, *25*, 5115-5116.
12) Glockner, P. W.; Keim, W.; Mason, R. F. US 3,647,914, 1972.
13) Keim, W.; Kowaldt, F. H.; Goddard, R.; Krüger, C. *Angew. Chem., Int. Ed.* **1978**, *17*, 466-467.
14) Mecking, S. *Angew. Chem.* **2001**, *113*, 550-557.
15) Johnson, L. K.; Killian, C. M.; Brookhart, M. *J. Am. Chem. Soc.* **1995**, *117*, 6414-6415.
16) Johnson, L. K.; Mecking, S.; Brookhart, M. *J. Am. Chem. Soc.* **1996**, *118*, 267-268.
17) Luo, S.; Jordan, R. F. *J. Am. Chem. Soc.* **2006**, *128*, 12072-12073.
18) Mecking, S.; Johnson, L. K.; Wang, L.; Brookhart, M. *J. Am. Chem. Soc.* **1998**, *120*, 888-899.
19) Drent, E.; Dijk, R. v.; Ginkel, R. v.; Oort, B. v.; Pugh, R. I. *Chem. Commun.* **2002**, 744-745.
20) Hearley, A. K.; Nowack, R. J.; Rieger, B. *Organometallics* **2005**, *24*, 2755-2763.
21) Kochi, T.; Yoshimura, K.; Nozaki, K. *Dalton Trans.* **2006**, 25-27.
22) Nakamura, A.; Ito, S.; Nozaki, K. *Chem. Rev.* **2009**, *109*, 5215-5244.

23) Drent, E.; Dijk, R. v.; Ginkel, R. v.; Oort, B. v.; Pugh, R. I. *Chem. Commun.* **2002**, 964-965.

24) Skupov, K. M.; Marella, P. R.; Simard, M.; Yap, G. P. A.; Allen, N.; Conner, D.; Goodall, B. L.; Claverie, J. P. *Macromol. Rapid Commun.* **2007**, *28*, 2033-2038.

25) Vela, J.; Lief, G. R.; Shen, Z.; Jordan, R. F. *Organometallics* **2007**, *26*, 6624-6635.

26) Weng, W.; Shen, Z.; Jordan, R. F. *J. Am. Chem. Soc.* **2007**, *129*, 15450-15451.

27) Nagai, Y.; Kochi, T.; Nozaki, K. *Organometallics* **2009**, *28*, 6131-6134.

28) Piche, L.; Daigle, J.-C.; Poli, R.; Claverie, J. P. *Eur. J. Inorg. Chem.* **2010**, 4595-4601.

29) Shen, Z.; Jordan, R. F. *J. Am. Chem. Soc.* **2010**, *132*, 52-53.

30) Anselment, T. M. J.; Anderson, C. E.; Rieger, B.; Boeddinghaus, M. B.; Fassler, T. F. *Dalton Trans.* **2011**, *40*, 8304-8313.

31) Anselment, T. M. J.; Wichmann, C.; Anderson, C. E.; Herdtweck, E.; Rieger, B. *Organometallics* **2011**, *30*, 6602-6611.

32) Chen, C.; Anselment, T. M. J.; Fröhlich, R.; Rieger, B.; Kehr, G.; Erker, G. *Organometallics* **2011**, *30*, 5248-5257.

33) Gott, A. L.; Piers, W. E.; Dutton, J. L.; McDonald, R.; Parvez, M. *Organometallics* **2011**, *30*, 4236-4249.

34) Kim, Y.; Jordan, R. F. *Organometallics* **2011**, *30*, 4250-4256.

35) Sauca, S. N.; Asua, J. M. *Chem. Eng. J.* **2011**, *168*, 1319-1330.

36) Zhou, X.; Jordan, R. F. *Organometallics* **2011**, *30*, 4632-4642.

37) Piche, L.; Daigle, J.-C.; Rehse, G.; Claverie, J. P. *Chem. Eur. J.* **2012**, *18*, 3277-3285.

38) Allen, N. T.; Goodall, B. L.; McIntosh, L. H. Europ. Patent Appl. EP1760086A2, 2007.

39) Perrotin, P.; McCahill, J. S. J.; Wu, G.; Scott, S. L. *Chem. Commun.* **2011**, *47*, 6948-6950.

40) Nakamura, A.; Kageyama, T.; Goto, H.; Carrow, B. P.; Ito, S.; Nozaki, K. *J. Am. Chem. Soc.* **2012**, *134*, 12366-12369.

41) Wucher, P.; Caporaso, L.; Roesle, P.; Ragone, F.; Cavallo, L.; Mecking, S.; Göttker-Schnetmann, I. *Proc. Natl. Acad. Sci. U.S.A.* **2011**, *108*, 8955-8959.

42) Wucher, P.; Roesle, P.; Falivene, L.; Cavallo, L.; Caporaso, L.; Göttker-Schnetmann, I.; Mecking, S. *Organometallics* **2012**, *31*, 8505-8515.

43) Guironnet, D.; Roesle, P.; Rünzi, T.; Göttker-Schnetmann, I.; Mecking, S. *J. Am. Chem. Soc.* **2009**, *131*, 422-423.

44) Guironnet, D., PhD. Thesis, University of Konstanz, 2009.

45) Kochi, T.; Noda, S.; Yoshimura, K.; Nozaki, K. *J. Am. Chem. Soc.* **2007**, *129*, 8948-8949.

46) Borkar, S.; Newsham, D. K.; Sen, A. *Organometallics* **2008**, *27*, 3331-3334.

47) Nakamura, A.; Munakata, K.; Kochi, T.; Nozaki, K. *J. Am. Chem. Soc.* **2008**, *130*, 8128-8129.

48) Skupov, K. M.; Marella, P. R.; Hobbs, J. L.; McIntosh, L. H.; Goodall, B. L.; Claverie, J. P. *Macromolecules* **2006**, *39*, 4279-4281.

49) Luo, S.; Vela, J.; Lief, G. R.; Jordan, R. F. *J. Am. Chem. Soc.* **2007**, *129*, 8946-8947.

50) Skupov, K. M.; Piche, L.; Claverie, J. P. *Macromolecules* **2008**, *41*, 2309-2310.

51) Ito, S.; Munakata, K.; Nakamura, A.; Nozaki, K. *J. Am. Chem. Soc.* **2009**, *131*, 14606-14607.

52) Bouilhac, C.; Rünzi, T.; Mecking, S. *Macromolecules* **2010**, *43*, 3589-3590.

53) Ito, S.; Nozaki, K. *Chem. Rec.* **2010**, *10*, 315-325.

54) Rünzi, T.; Fröhlich, D.; Mecking, S. *J. Am. Chem. Soc.* **2010**, *132*, 17690-17691.

55) Daigle, J.-C.; Piche, L.; Claverie, J. P. *Macromolecules* **2011**, *44*, 1760-1762.

56) Friedberger, T.; Wucher, P.; Mecking, S. *J. Am. Chem. Soc.* **2011**, *134*, 1010-1018.

57) Ito, S.; Kanazawa, M.; Munakata, K.; Kuroda, J.-i.; Okumura, Y.; Nozaki, K. *J. Am. Chem. Soc.* **2011**.

58) Ravasio, A.; Boggioni, L.; Tritto, I. *Macromolecules* **2011**, *44*, 4180-4186.

59) Daigle, J.-C.; Piche, L.; Arnold, A.; Claverie, J. P. *ACS Macro Lett.* **2012**, *1*, 343-346.

60) Shen, Z.; Jordan, R. F. *Macromolecules* **2010**, *43*, 8706-8708.

61) Rünzi, T.; Guironnet, D.; Göttker-Schnetmann, I.; Mecking, S. *J. Am. Chem. Soc.* **2010**, *132*, 16623-16630.

62) Newsham, D. K.; Borkar, S.; Sen, A.; Conner, D. M.; Goodall, B. L. *Organometallics* **2007**, *26*, 3636-3638.

63) Bettucci, L.; Bianchini, C.; Claver, C.; Suarez, E. J. G.; Ruiz, A.; Meli, A.; Oberhauser, W. *Dalton Trans.* **2007**, 5590-5602.

64) Haras, A.; Michalak, A.; Rieger, B.; Ziegler, T. *J. Am. Chem. Soc.* **2005**, *127*, 8765-8774.

65) Kochi, T.; Nakamura, A.; Ida, H.; Nozaki, K. *J. Am. Chem. Soc.* **2007**, *129*, 7770-7771.

66) Nakamura, A.; Munakata, K.; Ito, S.; Kochi, T.; Chung, L. W.; Morokuma, K.; Nozaki, K. *J. Am. Chem. Soc.* **2011**, *133*, 6761-6779.

67) Noda, S.; Nakamura, A.; Kochi, T.; Chung, L. W.; Morokuma, K.; Nozaki, K. *J. Am. Chem. Soc.* **2009**, *131*, 14088-14100.

68) Nozaki, K.; Kusumoto, S.; Noda, S.; Kochi, T.; Chung, L. W.; Morokuma, K. *J. Am. Chem. Soc.* **2010**, *132*, 16030-16042.

69) Haras, A.; Anderson, G. D. W.; Michalak, A.; Rieger, B.; Ziegler, T. *Organometallics* **2006**, *25*, 4491-4497.

70) Skupov, K. M.; Hobbs, J.; Marella, P.; Conner, D.; Golisz, S.; Goodall, B. L.; Claverie, J. P. *Macromolecules* **2009**, *42*, 6953-6963.

71) Kanazawa, M.; Ito, S.; Nozaki, K. *Organometallics* **2011**, *30*, 6049-6052.

72) Berkefeld, A.; Mecking, S. *Angew. Chem., Int. Ed.* **2008**, *47*, 2538-2542.

73) von Schenck, H.; Åkermark, B.; Svensson, M. *J. Am. Chem. Soc.* **2003**, *125*, 3503-3508.

74) von Schenck, H.; Strömberg, S.; Zetterberg, K.; Ludwig, M.; Åkermark, B.; Svensson, M. *Organometallics* **2001**, *20*, 2813-2819.

75) Michalak, A.; Ziegler, T. *Organometallics* **1999**, *18*, 3998-4004.

76) Michalak, A.; Ziegler, T., *J. Am. Chem. Soc.* **2001**, *123*, 12266-12278.

77) Szabo, M. J.; Jordan, R. F.; Michalak, A.; Piers, W. E.; Weiss, T.; Yang, S.-Y.; Ziegler, T. *Organometallics* **2004**, *23*, 5565-5572.

78) Johnson L.; Bennett, A.; Dobbs, K.; Hauptman, E.; Ionkin, A.; Ittel, S. D; McCord, E.; McLain, S.; Radzewich, C.; Yin, Z.; Wang, L.; Wang, Y.; Brookhart, M. *Polym. Mater. Sci. Eng.* **2002**, *86*, 319.

79) Johnson, L.; Wang, L.; McLain, S.; Bennett, A.; Dobbs, K.; Hauptman, E.; Ionkin, A.; Ittel, S.; Kunitsky, K.; Marshall, W.; McCord, E.; Radzewich, C.; Rinehart, A.; Sweetman, K. J.; Wang, Y.; Yin, Z.; Brookhart, M., in *Beyond Metallocenes*, American Chemical Society: 2003; Vol. 857, 131-142.

80) Wang, L.; Hauptman, E.; Johnson L.; Marshall, W.; McCord, E.; Wang, Y.; Ittel, S.; Radzewich, C. E.; Kunitsky, K.; Ionkin, A. S. *Polym. Mater. Sci. Eng.* **2002**, *86*, 322.

81) Brasse, M.; Cámpora, J.; Palma, P.; Álvarez, E.; Cruz, V.; Ramos, J.; Reyes, M. L. *Organometallics* **2008**, *27*, 4711-4723.

82) Gibson, V. C.; Tomov, A. *Chem. Commun.* **2001**, 1964-1965.

83) Younkin, T. R.; Connor, E. F.; Henderson, J. I.; Friedrich, S. K.; Grubbs, R. H.; Bansleben, D. A. *Science* **2000**, *287*, 460-462.

84) Connor, E. F.; Younkin, T. R.; Henderson, J. I.; Hwang, S.; Grubbs, R. H.; Roberts, W. P.; Litzau, J. J. *J. Polym. Sci. A-1* **2002**, *40*, 2842-2854.

85) Carrow, B. P.; Nozaki, K. *J. Am. Chem. Soc.* **2012**, *134*, 8802-8805.

86) Zhang, D.; Guironnet, D.; Göttker-Schnetmann, I.; Mecking, S. *Organometallics* **2009**, *28*, 4072–4078.

87) Liu, S.; Borkar, S.; Newsham, D.; Yennawar, H.; Sen, A. *Organometallics* **2007**, *26*, 210–216.

88) Downing, J. H.; Smith, M. B. In *Comprehensive Coordination Chemistry II*; McCleverty, J. A., Meyer, T. J., Eds.; Pergamon: Oxford, 2003, p 253–296.

89) Grushin, V. V. *Chem. Rev.* **2004**, *104*, 1629–1662.

90) Slone, C. S.; Weinberger, D. A.; Mirkin, C. A. In *Progress in Inorganic Chemistry*; John Wiley & Sons, Inc.: 2007, p 233–350.

91) Keim, W.; Maas, H.; Mecking, S. *Z. Naturforsch. B* **1995**, *50*, 430-438.

92) Brassat, I.; Keim, W.; Killat, S.; Mothrath, M.; Mastrorilli, P.; Nobile, C. F.; Suranna, G. P. *J. Mol. Catal. A* **2000**, *157*, 41-58.

93) Mecking, S.; Keim, W. *Organometallics* **1996**, *15*, 2650-2656.

94) Denmark, S. E.; Smith, R. C.; Tymonko, S. A. *Tetrahedron* **2007**, *63*, 5730–5738.

95) Xiaozhong, L.; Hongmei, L.; Fanzhi, K. *J. Organomet. Chem.* **2002**, *664*, 1–4.

96) Billington, D. C.; Malcolm Helps, I.; Pauson, P. L.; Thomson, W.; Willison, D. *J. Organomet. Chem.* **1988**, *354*, 233–242.

97) Starzewski, K. A. O.; Witte, J. *Angew. Chem., Int. Ed.* **1987**, *26*, 63–64.

98) Beach, D. l.; Harrison, J. J. US4293727, 1981.

99) Wilkinson, G., Gillard, R. D., McCleverty, J. A., *Comprehensive Coordination Chemistry*, Pergamon: Oxford, 1987.

100) Tolman, C. A. *Chem. Rev.* **1977**, *77*, 313–348.

101) Wilson, M. R.; Woska, D. C.; Prock, A.; Giering, W. P. *Organometallics* **1993**, *12*, 1742–1752.

102) Derencsenyi, T. T. *Inorg. Chem.* **1981**, *20*, 665–670.

103) Ullrich, M.; Lough, A. J.; Stephan, D. W. *Organometallics* **2010**, *29*, 3647–3654.

104) Burford, N. *Coord. Chem. Rev.* **1992**, *112*, 1–18.

105) Deacon, G. B.; Fallon, G. D.; Forsyth, C. M.; Gatehouse, B. M.; Junk, P. C.; Philosof, A.; White, P. A. *J. Organomet. Chem*. **1998**, *565*, 201–210.

106) Cotton, F. A.; Barnes, R. D.; Bannister, E. *J. Chem. Soc.* **1960**, 2199–2203.

107) Jones, C. J.; McCleverty, J. A.; Rothin, A. S.; Adams, H.; Bailey, N. A. *J. Chem. Soc., Dalton Trans.* **1986**, 2055–2061.

108) Brock, C. P.; Schweizer, W. B.; Dunitz, J. D. *J. Am. Chem. Soc.* **1985**, *107*, 6964–6970.

109) Bandoli, G.; Bortolozzo, G.; Clemente, D. A.; Croatto, U.; Panattoni, C. *J. Chem. Soc. A* **1970**, 2778–2780; Speck, A. L. *Acta Crystallogr., Sect. C: Cryst. Struct. Commun*. **1987**, *43*, 1233–1235; Al-Farhan, K. A. J. *Chem. Crystallogr.* **1992**, *22*, 687–689; Thomas, J. A.; Hamor, T. A. *Acta Crystallogr., Sect. C: Cryst. Struct. Commun.* **1993**, *49*, 355–357.

110) Coles, S. J.; Edwards, P. G.; Hursthouse, M. B.; Abdul Malik, K. M.; Thick, J. L.; Tooze, R. P. *J. Chem. Soc., Dalton Trans.* **1997**, 1821–1830.

111) Braunstein, P.; Agostinho, M. *Chem. Commun.* **2007**, 58–60.

112) Braunstein, P.; Frison, C.; Morise, X. *Angew. Chem. Int. Ed.* **2000**, *39*, 2867–9870.

113) Williams, B. S.; Leatherman, M. D.; White, P. S.; Brookhart, M. J. *Am. Chem. Soc.* **2005**, *127*, 5132–5146.

114) Chou, W. N.; Pomerantz, M. *J. Org. Chem.* **1991**, *56*, 2762-2769.

115) Rünzi, T.; Tritschler, U.; Roesle, P.; Göttker-Schnetmann, I.; Möller, H. M.; Caporaso, L.; Poater, A.; Cavallo, L.; Mecking, S. *Organometallics* **2012**, *31*, 8388-8406.

116) Berkefeld, A.; Mecking, S. *J. Am. Chem. Soc.* **2009**, *131*, 1565-1574.

117) Albeniz, A. C.; Espinet, P.; Lopez-Fernandez, R. *Organometallics* **2003**, *22*, 4206-4212.

118) Nagel, M.; Sen, A. *Organometallics* **2006**, *25*, 4722-4724.

119) Meyers, A. I.; Himmelsbach, R. J. *J. Am. Chem. Soc.* **1985**, *107*, 682-685.

120) Gates, D. P.; Svejda, S. A.; Oñate, E.; Killian, C. M.; Johnson, L. K.; White, P. S.; Brookhart, M. *Macromolecules* **2000**, *33*, 2320-2334.

121) Popeney, C.; Guan, Z. *Organometallics* **2005**, *24*, 1145-1155.

122) Popeney, C. S.; Guan, Z. *Macromolecules* **2010**, *43*, 4091-4097.

123) Popeney, C. S.; Levins, C. M.; Guan, Z. *Organometallics* **2011**, *30*, 2432-2452.

124) Göttker-Schnetmann, I.; Wehrmann, P.; Röhr, C.; Mecking, S. *Organometallics* **2007**, *26*, 2348-2362.

125) Baugh, L. S.; Canich, J. M. *Stereoselective Polymerization with Single-Site Catalysts*; CRC Press: London, 2008.

126) Matsuzaki, K.; Uryu, T.; Ishida, A.; Ohki, T.; Takeuchi, M. *J. Polym. Sci. A-1* **1967**, *5*, 2167-2177.

127) Liu, W.; Nakano, T.; Okamoto, Y. *Polymer Journal* **1999**, *31*, 479-481.

128) Deng, H.; Soga, K. *Macromolecules* **1996**, *29*, 1847-1848.

129) Porter, N. A.; Allen, T. R.; Breyer, R. A. *J. Am. Chem. Soc.* **1992**, *114*, 7676-7683.

130) Liu, W.; Nakano, T.; Okamoto, Y. *Polymer* **2000**, *41*, 4467-4472.

131) Matsuzaki, K.; Uryu, T.; Kanai, T.; Hosonuma, K.; Matsubara, T.; Tachikawa, H.; Yamada, M.; Okuzono, S. *Makromol. Chem.* **1977**, *178*, 11-17.

132) Brintzinger, H.-H.; Fischer, D.; Mülhaupt, R.; Rieger, B.; Waymouth, R. *Angew. Chem. Int. Ed.* **1995**, *34*, 1143-1170.

133) Resconi, L.; Cavallo, L.; Fait, A.; Piemontesi, F. *Chem. Rev.* **2000**, *100*, 1253-1346.

134) Byers, J. A.; Bercaw, J. E. *Proc. Natl. Acad. Sci. U.S.A.* **2006**, *103*, 15303-15308.

135) Milano, G.; Guerra, G.; Pellecchia, C.; Cavallo, L. *Organometallics* **2000**, *19*, 1343-1349.

136) Tshuva, E. Y.; Goldberg, I.; Kol, M. *J. Am. Chem. Soc.* **2000**, *122*, 10706-10707.

137) Mitani, M.; Saito, J.; Ishii, S.-I.; Nakayama, Y.; Makio, H.; Matsukawa, N.; Matsui, S.; Mohri, J.-i.; Furuyama, R.; Terao, H.; Bando, H.; Tanaka, H.; Fujita, T. *Chem. Rec.* **2004**, *4*, 137-158.

138) Makio, H.; Terao, H.; Iwashita, A.; Fujita, T. *Chem. Rev.* **2011**, *111*, 2363-2449.

139) Corradini, P.; Guerra, G.; Cavallo, L. *Acc. Chem. Res.* **2004**, *37*, 231-241.

140) Brookhart, M.; Wagner, M. I.; Balavoine, G. G. A.; Haddou, H. A. *J. Am. Chem. Soc.* **1994**, *116*, 3641-3642.

141) Aeby, A.; Consiglio, G. *Inorg. Chim. Acta.* **1999**, *296*, 45-51.

142) Bianchini, C.; Meli, A. *Coord. Chem. Rev.* **2002**, *225*, 35-66.

143) Nozaki, K.; Sato, N.; Tonomura, Y.; Yasutomi, M.; Takaya, H.; Hiyama, T.; Matsubara, T.; Koga, N. *J. Am. Chem. Soc.* **1997**, *119*, 12779-12795.

144) Sesto, B.; Consiglio, G. *Chem. Commun.* **2000**, 1011-1012.

145) Sesto, B.; Consiglio, G. *J. Am. Chem. Soc.* **2001**, *123*, 4097-4098.

146) Pappalardo, D.; Mazzeo, M.; Antinucci, S.; Pellecchia, C. *Macromolecules* **2000**, *33*, 9483-9487.

147) Conley, M. P.; Jordan, R. F. *Angew. Chem. Int. Ed.* **2011**, *50*, 3744-3746.

148) Mislow, K. *Acc. Chem. Res.* **1976**, *9*, 26-33.

149) Bettucci, L.; Bianchini, C.; Meli, A.; Oberhauser, W. *J. Mol. Catal. A: Chem.* **2008**, *291*, 57-65.

150) Howell, J. A. S.; Fey, N.; Lovatt, J. D.; Yates, P. C.; McArdle, P.; Cunningham, D.; Sadeh, E.; Gottlieb, H. E.; Goldschmidt, Z.; Hursthouse, M. B.; Light, M. E. *J. Chem. Soc., Dalton Trans.* **1999**, 3015-3028.

151) Howell, J. A. S.; Palin, M. G.; Yates, P. C.; McArdle, P.; Cunningham, D.; Goldschmidt, Z.; Gottlieb, H. E.; Hezroni-Langerman, D. *J. Chem. Soc., Perkin Trans.2* **1992**, 1769-1775.

152) Widenhoefer, R. A.; Zhong, H. A.; Buchwald, S. L. *Organometallics* **1996**, *15*, 2745-2754.

153) Miller, R. G.; Stauffer, R. D.; Fahey, D. R.; Parnell, D. R. *J. Am. Chem. Soc.* **1970**, *92*, 1511-1521.

154) Friebolin, H. *Basic one- and two-dimensional NMR spectroscopy*; 4th enl. ed.; Wiley-VCH: Weinheim, Germany, 2005.

155) Fey, N.; Howell, J. A. S.; Lovatt, J. D.; Yates, P. C.; Cunningham, D.; McArdle, P.; Gottlieb, H. E.; Coles, S. J. *Dalton Trans.* **2006**, 5464-5475.

156) Howell, J. A. S.; Palin, M. G.; McArdle, P.; Cunningham, D.; Goldschmidt, Z.; Gottlieb, H. E.; Hezroni-Langerman, D. *Inorg. Chem.* **1993**, *32*, 3493-3500.

157) Howell, J. A. S.; Yates, P. C.; Palin, M. G.; McArdle, P.; Cunningham, D.; Goldschmidt, Z.; Gottlieb, H. E.; Hezroni-Langerman, D. *J. Chem. Soc., Dalton Trans.* **1993**, 2775-2780.

158) Baber, R. A.; Orpen, A. G.; Pringle, P. G.; Wilkinson, M. J.; Wingad, R. L. *Dalton Trans.* **2005**, 659-667.

159) Forniés, J.; Martín, A.; Navarro, R.; Sicilia, V.; Villarroya, P. *Organometallics* **1996**, *15*, 1826-1833.

160) Claridge, T. D. W., *High-Resolution NMR Techniques in Organic Chemistry*. In *Tetrahedron Organic Chemistry Series*, Elsevier: 2009; Vol. 27, p 281.

161) Lopez-Fernandez, R.; Carrera, N.; Albeniz, A. C.; Espinet, P. *Organometallics* **2009**, *28*, 4996–5001.

162) Ziegler, T., Autschbach, J. *Chem. Rev*. **2005**, *105*, 2695.

163) Pastor, S. D.; Spivack, J. D.; Steinhuebel, L. P. *Phosphorus, Sulfur Silicon Relat. Elem.* **1987**, *31*, 71-76.

164) Agostinho, M.; Braunstein, P.; Welter, R. *Dalton Trans.* **2007**, 759-770.

165) Kermagoret, A.; Braunstein, P. *Organometallics* **2008**, *27*, 88-99.

166) Lv, X.; Bao, W. *J. Org. Chem.* **2007**, *72*, 3863-3867.

167) Armarego, W. L.; Perrin, D. D., *Purification of laboratory chemicals*. 4th ed.; Elsevier: Burlington, 1996.

168) Stone, M. T.; Moore, J. S. *Org. Lett.* **2004**, *6*, 469-472.

169) De Graaf, W.; Boersma, J.; Smeets, W. J. J.; Spek, A. L.; Van Koten, G. *Organometallics* **1989**, *8*, 2907-2917.

170) Salo, E. V.; Guan, Z. *Organometallics* **2003**, *22*, 5033-5046.

171) Stoe, *X-RED version 1.3, Data Reduction Program,* Darmstadt, Germany, 2005.

172) Sheldrick, G. M. *SHELXS-97, Program for Crystal Structure Analysis*; Universität Göttingen: Göttingen, 1986.

173) Sheldrick, G. M. *SHELXL-97, Program for Crystal Structure Refinement*; Universität Göttingen: Göttingen, 1997.

174) Brandenburg, K. *Diamond Ver. 3.0a,*; Crystal Impact GbR: Bonn, 2005.

175) Luft, G.; Dorn M. *Angew. Makromol. Chem.* **1991**, *188*, 177-188.

176) Lee, L.; Ou, H.; Hsu, H. *Fluid Phase Equilib.* **2005**, *231*, 221-230.

177) Reich, H. J., *WINDNMR Ver. 7.1.13*,. Madison, 2008.

178) Savitzky, A.; Golay, M. J. E. *Analyt. Chem.* **1964**, *36*, 1627-1639.

179) Frisch, M. J.; Trucks, G. W.; Schlegel, H. B.; Scuseria, G. E.; Robb, M. A.; Cheeseman, J. R.; Scalmani, G.; Barone, V.; Mennucci, B.; Petersson, G. A.; Nakatsuji, H.; Caricato, M.; Li, X.; Hratchian, H. P.; Izmaylov, A. F.; Bloino, J.; Zheng, G.; Sonnenberg, J. L.; Hada, M.; Ehara, M.; Toyota, K.; Fukuda, R.; Hasegawa, J.; Ishida, M.; Nakajima, T.; Honda, Y.; Kitao, O.; Nakai, H.; Vreven, T.; Montgomery, Jr., J. A.; Peralta, J. E.; Ogliaro, F.; Bearpark, M.; Heyd, J. J.; Brothers, E.; Kudin, K. N.; Staroverov, V. N.; Kobayashi, R.; Normand, J.; Raghavachari, K.; Rendell, A.; Burant, J. C.; Iyengar, S. S.; Tomasi, J.; Cossi, M.; Rega, N.; Millam, J. M.; Klene, M.; Knox, J. E.; Cross, J. B.; Bakken, V.; Adamo, C.; Jaramillo, J.; Gomperts, R.; Stratmann, R. E.; Yazyev, O.; Austin, A. J.; Cammi, R.; Pomelli, C.; Ochterski, J. W.; Martin, R. L.; Morokuma, K.; Zakrzewski, V. G.; Voth, G. A.; Salvador, P.; Dannenberg, J. J.; Dapprich, S.; Daniels, A. D.; Farkas, Ö.; Foresman, J. B.; Ortiz, J. V.; Cioslowski, J.; Fox, D. J. Gaussian, Inc., Wallingford CT, 2009.

180) Becke, A. D. *Phys. Rev. A* **1988**, *38*, 3098.

181) Perdew, J. P. *Phys. Rev. B* **1986**, *34*, 7406.

182) Perdew, J. P. *Phys. Rev. B* **1986**, *33*, 8822.

183) T. H. Dunning Jr. and P. J. Hay, in *Modern Theoretical Chemistry*, Ed. H. F. Schaefer III, Vol. 3 (Plenum, New York, 1976) 1-28. P. J. Hay and W. R. Wadt, *J. Chem. Phys.* **1985**, *82* 270-83.

184) Wu, H.-C.; Yu, J.-Q.; Spencer, J. B. *Org. Lett.* **2004**, *6*, 4675-4678.

185) Eapen, K. C.; Tamborski, C., *J. Fluorine Chem.* **1980**, *15*, 239-243.

186) Cameron, T. S.; Dahlen, B. *J. Chem. Soc., Perkin Trans. 2* **1975**, 1737-1751.

187) Mingos, D. M. P.; Müller, T. E. *J. Organomet. Chem.* **1995**, *500*, 251-259.

188) Paptchikhine, A.; Itto, K.; Andersson, P. G. *Chem. Commun.* **2011**, *47*, 3989-3991.

189) Jackman, L. M.; Scarmoutzos, L. M.; DeBrosse, C. W. *J. Am. Chem. Soc.* **1987**, *109*, 5355-5361.

190) Fraser, R. R.; McGreer, D. E. *Can. J. Chem.* **1961**, *39*, 505-509.

191) Speck, A. L., *Platon*. Universiteit Utrecht: Utrecht, 1997.